

MEMS BASED ELECTROCHEMICAL DNA SENSOR TO DETECT METHICILLIN RESISTANT
Staphylococcus aureus AND VANCOMYCIN RESISTANT *Enterococcus* SPECIES

A THESIS SUBMITTED TO
THE GRADUATE SCHOOL OF NATURAL AND APPLIED SCIENCES
OF
MIDDLE EAST TECHNICAL UNIVERSITY

BY

HATİCE CEYLAN KOYDEMİR

IN PARTIAL FULFILLMENT OF THE REQUIREMENTS
FOR
THE DEGREE OF DOCTOR OF PHILOSOPHY
IN
CHEMICAL ENGINEERING

JANUARY 2013

Approval of the thesis:

**MEMS BASED ELECTROCHEMICAL DNA SENSOR TO DETECT METHICILLIN
RESISTANT *Staphylococcus aureus* AND VANCOMYCIN RESISTANT *Enterococcus* SPECIES**

submitted by **HATİCE CEYLAN KOYDEMİR** in partial fulfillment of the requirements for the degree
of **Doctor of Philosophy in Chemical Engineering Department, Middle East Technical University**
by,

Prof. Dr. Canan Özgen
Dean, Graduate School of **Natural and Applied Sciences** -----

Prof. Dr. Deniz Üner
Head of Department, **Chemical Engineering** -----

Prof. Dr. Canan Özgen
Supervisor, **Chemical Engineering Dept., METU** -----

Assoc. Prof. Dr. Haluk Külah
Co-Supervisor, **Electrical and Electronics Eng. Dept., METU** -----

Examining Committee Members:

Prof. Dr. Hayrettin Yücel
Chemical Engineering Dept., METU -----

Prof. Dr. Canan Özgen
Chemical Engineering Dept., METU -----

Prof. Dr. Ayşegül Üner
Pathology Dept., Hacettepe University -----

Prof. Dr. Tayfun Akın
Electrical and Electronics Eng. Dept., METU -----

Prof. Dr. İsmail Tosun
Chemical Engineering Dept., METU -----

Date: 30 January 2013

I hereby declare that all information in this document has been obtained and presented in accordance with academic rules and ethical conduct. I also declare that, as required by these rules and conduct, I have fully cited and referenced all material and results that are not original to this work.

Name, Last name: Hatice, Ceylan Koydemir
Signature:

ABSTRACT

MEMS BASED ELECTROCHEMICAL DNA SENSOR TO DETECT METHICILLIN RESISTANT *Staphylococcus aureus* AND VANCOMYCIN RESISTANT *Enterococcus* SPECIES

Ceylan Koydemir, Hatice

Ph.D., Department of Chemical Engineering
Supervisor: Prof.Dr. Canan Özgen
Co-Supervisor: Assoc.Prof.Dr. Haluk Külah

January 2013, 145 pages

Methicillin Resistant *Staphylococcus aureus* (MRSA) is one of the most important threats of nosocomial infections in many regions of the world and Vancomycin Resistant *Enterococcus* (VRE) is an emerging pathogen that develops full resistance against third-generation glycopeptide antibiotics. Conventional methods for identification of MRSA and VRE generally depend on culturing, which requires incubation of biological samples at least 24-72 hours to get accurate results. These methods are time consuming and necessitate optical devices and experts for evaluation of the results. On the other hand, early diagnosis and initiation of appropriate treatment are necessary to decrease morbidity and mortality rates. Thus, new diagnostic systems are essential for rapid and accurate detection of biological analytes at the point of care.

This study presents design, fabrication, and implementation of MEMS based micro electrochemical sensor (μ ECS) to detect the methicillin resistance in *Staphylococcus aureus* and vancomycin resistance in *Enterococcus* species. To the best of our knowledge, the developed sensor is the first μ ECS which utilizes on-chip reference (Ag), working (Au), and counter (Pt) electrodes together with a microchannel to detect MRSA and VRE.

The characterization of the designed sensor was achieved analyzing the interactions of the buffer solutions and solvents with the electrodes and Parylene C film layer by using optical and electrochemical methods. Specific parts of genes that are indicators of antimicrobial resistances were used in order to detect the resistances with high selectivity and sensitivity. Thus, synthetic DNA and bacterial PCR product were used as target probes in redox marker based detection and enzyme based detection, respectively. In order to enhance the hybridization, folding structures of the capture probe were investigated by using mfold Web Server. In redox marker based detection, the hybridization of DNA was indirectly detected by using Hoechst 33258 as redox marker with differential pulse voltammetry. The cross reactivity of the tests were performed by using different target probes of *femA* genes of *S. aureus* and *S. epidermis*, which are the major genes detected in methicillin detection assays. Consequently, amplification of signal by using horseradish peroxidase and TMB/H₂O₂ as substrate was achieved in order to enhance detection sensitivity. The sensor could detect 0.01 nM 23-mer specific part of *mecA* gene with redox marker based detection and 10 times diluted PCR product with enzyme-based detection in about six hours including the steps of sample preparation from whole blood. This sensor with its compatibility to MEMS fabrication processes and IC technology has a promising potential for a hand-held device for POC through the integration of micropotentiostat.

Keywords: biosensor, electrochemical detection, nucleic acid, MEMS, MRSA, VRE, and point of care diagnostic.

ÖZ

METİSİLİN DİRENÇLİ *Staphylococcus aureus* VE VANKOMİSİN DİRENÇLİ *Enterococcus* SUŞLARININ TANISI İÇİN MEMS TABANLI ELEKTROKİMYASAL SENSÖR

Ceylan Koydemir, Hatice

Doktora, Kimya Mühendisliği Bölümü
Tez Yöneticisi: Prof.Dr. Canan Özgen
Ortak Tez Yöneticisi: Doç.Dr. Haluk Külah

Ocak 2013, 145 sayfa

Metisilin Dirençli *Staphylococcus aureus* (MRSA) dünyanın bir çok yerinde hastane kaynaklı enfeksiyonların en önemli tehditlerinden biridir ve Vankomisin Dirençli *Enterococcus* (VRE) üçüncü nesil glikopeptit antibiyotiklere karşı tam direnç geliştiren yeni ortaya çıkan patojendir. Bu patojenlerin tanısında kullanılan geleneksel metotlar genellikle, doğru sonucun alınması için biyolojik örneklerin en az 24-72 saat inkübasyonunu gerektiren, kültüre dayanmaktadır. Bu metotlar zaman kaybettiricidir ve optik yöntemlerin kullanılmasını ve sonuçların değerlendirilmesi için uzman personel gerektirmektedir. Bununla birlikte, hastalığa yakalananların sayısını ve ölüm oranını azaltmak için erken tanı ve uygun tedavinin başlatılması gereklidir. Bu nedenle, nokta analizinde biyolojik ajanların doğru ve hızlı tanısı için yeni tanı sistemleri gereklidir.

Bu çalışmada, MEMS tabanlı mikroelektrokimyasal sensörün tasarımı, mikroüretimi, ve MRSA ve VRE'nin tanısında uygulanması sunulmuştur. Bildiğimiz kadarıyla, bu sensör, MRSA ve VRE tanısında kullanılan, çip üzerinde mikrokannalları ile birlikte (Ag) referans, (Au) çalışma, ve (Pt) yardımcı elektrotlara sahip ilk mikroelektrokimyasal sensör (μ ECS)'dür.

Tasarımı yapılan sensörün karakterizasyonunda elektrotların ve Parilen C film tabakasının kullanılan tampon çözeltilerle ve çözücülerle etkileşimi analiz edilmiştir. Antimikrobiyal direncin yüksek hassasiyetle ve seçicilikle tanısı için bu dirençlerin belirteçleri olan genlerin belirli bölümleri kullanılmıştır. Bu nedenle, sentetik DNA ve bakteriyel PCR ürünü, sırasıyla, redoks işaretçi dayalı ve enzyeme dayalı elektrokimyasal tanı metotlarında hedef prob olarak kullanılmıştır. Hibridizasyonu arttırmak için, kaptür probun katlanma yapıları mfold Web Server kullanılarak araştırılmıştır. Redoks işaretçi dayalı tanıda, Hoechst 33258 redoks işaretçi olarak kullanılarak diferensiyel puls voltammetrisi ile DNA hibridizasyonunun dolaylı olarak tanısı yapılmıştır. Çapraz reaktivite testlerinde metisilin tanı testlerinde sıklıkla kullanılan temel genlerden olan *S.aureus*'un ve *S.epidermis*'in *femA* genlerinin farklı problemleri kullanılmıştır. Ayrıca, tanı hassasiyetini arttırmak için horseradish peroksidaz ve TMB/H₂O₂ kullanılarak sinyal arttırımı sağlanmıştır. Redoks işaretçi kullanılarak 0.01 nM *mecA* geninin belirli 23-bazlık zincirinin tanısının ve enzyeme dayalı tanı metodu kullanılarak 10 kez seyreltilmiş PCR ürünün tanısının tam kandan örnek hazırlama aşamalarını da dahil ederek yaklaşık altı saat içerisinde mümkün olduğu gösterilmiştir. MEMS üretim prosesleri ve entegre devre teknolojileri ile uyumlu bu sensör, mikropotentiostat ile entegre edilerek nokta analizinde kullanılmak üzere elde taşınabilir sistemlerin bir parçası olabilir.

Anahtar kelimeler: biyosensör, elektrokimyasal tanı, nükleik asit, MEMS, MRSA, VRE, ve nokta analizi.

To my husband, Ferit Koydemir

and

To Recep Ali Ceylan and Emel Gül

ACKNOWLEDGMENTS

I would like to thank to my supervisor Prof. Dr. Canan Özgen for her guidance, support, and valuable comments throughout the thesis study. Although I am one of her graduate students, her support has not limited with the research. She has leaded me as being a model with her knowledge, wisdom, and leadership. I believe that I will move traces of her impression in every corner of my life.

I am grateful to my co-supervisor Assoc. Prof. Dr. Haluk K ulah for his endless trust, support, and guidance to make this study real, and envisioned my perspective. One of the most important things he taught me was that it is important to do your best for perfection, even while doing small tasks.

I am also grateful to Prof. Dr. Tayfun Akın for his support and his geniality.

I would like to thank to Prof. Dr. G l sen Haşcelik, Assoc. Prof. Dr. Alpaslan Alp, and my thesis committee members, Prof. Dr. Ayşeg l  ner and Prof. Dr. Hayrettin Y cel, for their valuable discussions throughout the thesis study.

I am also grateful to all staff of METU-MEMS Research and Application Center, especially to Orhan Akar for his endless support during the microfabrication and testing steps of the sensor. I would also like to thank to  zgecan Dervişođlu, Akın Aydemir, Sel uk Keskin, Kaan Demirel, İlker Comart, Eren Canga, Ebru Topallı, Evren Erdil, Evrim  z akır, Mert Torunbalcı, Osman Aydın, Murat  nal, Mehmet Kargı, Celalettin İmer, Ali Aytekin, Aykut Bakırcı, Levent Abat, and Yusuf Murat for their help in the fabrication steps and their friendship.

I would also thank to METU-BioMEMS Group for their valuable discussions, help, and friendship. I would especially like to thank to Ekrem Bayraktar, G rkan Yılmaz, Deniz Erođlu, Deniz Ert rkan, Dr. İbrahim Sarı, Dr. Ender Yıldırım, Levent Beker, Bilge Akbıyık, Dr.Yekbun Adıg zel, and Aziz Koyuncuođlu for their kind friendships.

I am also grateful to all staff of Graduate School of Natural and Applied Sciences for their valuable friendship and their support. My special thanks go to Hamdi K m rc , Ali Şahin, M nevver G n, G lhal G r, Cemalettin Ayyıldız, Derya Korkmazer, and Esra T z n for their support and politeness.

I am grateful to my friends Arzu Kanca and Işık Haykır for their endless support and friendship. Without their support, this study would never end.

I would like to thank to my dear husband Ferit Koydemir for his support, guidance, and love.

I would also like to thank to my nieces, Emirhan and Yađızhan G l for their love and joy of living.

Last but certainly not least, I would like to thank to my family, who always supported me whatever I do, taught me how to face challenges, and were felt near to me even we were apart.

Financial support of The Scientific and Technological Research Council of Turkey (TUBITAK) is also acknowledged.

TABLE OF CONTENTS

ABSTRACT.....	v
ÖZ	vi
ACKNOWLEDGMENTS.....	ix
TABLE OF CONTENTS.....	xi
LIST OF TABLES	xiii
LIST OF FIGURES.....	xv
CHAPTERS	
1. INTRODUCTION.....	1
2. LITERATURE SURVEY	5
2.1. <i>Staphylococcus aureus</i> and <i>Enterococcus</i> Species	5
2.1.1. <i>Staphylococcus aureus</i>	5
2.1.2. <i>Enterococcus</i> Species.....	6
2.2. Antibiotic Resistance, MRSA and VRE	6
2.3. Clinical Importance and Prevalence	9
2.4. Methods for Detection	12
2.4.1. Conventional Methods for the Detection of MRSA.....	12
2.4.2. Conventional Methods for the Detection of VRE	12
2.4.3 MEMS Based Methods for Detection	13
2.4.3.1 Use of MEMS Based Methods for the Detection of MRSA	15
2.4.3.2 Use of MEMS Based Methods for the Detection of VRE	20
2.5. Commercialized Products.....	20
2.6. Discussion of Detection Methods for MRSA and VRE	24
3. THEORY OF ELECTROCHEMICAL DETECTION.....	25
3.1. Rate Determining Reactions in Electrochemical Analysis	25
3.2. Modeling Studies	28
4. DESIGN AND FABRICATION OF MICRO ELECTROCHEMICAL SENSOR.....	31
4.1. Design of Micro Electrochemical Sensor	31
4.2. Mask Layouts	33
4.3.1. Ag Layer Deposition	35
4.3.2. Details of Fabrication Steps of the Electrochemical Sensor.....	44
5. EXPERIMENTAL STUDIES.....	53
5.1. Redox Marker Based Detection.....	53
5.1.1. Materials	55
5.1.2. Methods.....	55
5.1.2.1. Selection of Capture Probe	55
5.1.2.2. Self Assembled Monolayer (SAM) Formation.....	55
5.1.2.3. dsDNA Hybridization and Adsorption of Hoechst 33258.....	56
5.1.2.4. Electrochemical Detection.....	56
5.2. Enzyme Based Detection	56
5.2.1. Materials	57
5.2.2. Methods.....	59
5.2.2.1. Selection of PCR Primers and Probe Design	59
5.2.2.2. Streptavidin-HRP Enzyme Conjugation	59
5.2.2.3. Surface Modification	61
5.2.2.4. Electrochemical Detection.....	61
5.3. Solvent Compatibility of Parylene C Film Layer	62
5.3.1. Materials	63
5.3.2. Measurements	63

5.4. Effects of Solvents on Dissolution of Photo Resist Encapsulated in Parylene Microchannels	65
5.4.1.Theory for Dissolution of Photoresist inside the Microchannels.....	65
5.4.2. Fabrication of Test Structure and Measurements	66
6. RESULTS AND DISCUSSION.....	69
6.1. Characterization of the Sensor	69
6.1.1. Ag Electrode.....	69
6.1.2. Au Electrode.....	69
6.2. Redox Marker Based Detection	73
6.2.1. Capture Probe Selection	73
6.2.2 Detection of Hybridization	73
6.2.3. Cross-reactivity Tests	77
6.3. Enzyme Based Detection	78
6.3.1. Capture Probe Selection	78
6.3.2. Cyclic Voltammetry	81
6.3.3. Microdisk Chronoamperometry.....	81
6.3.4. Optimization of Detection Method.....	82
6.3.5. Analysis of Effect of Scan Rate on Peak Current.....	87
6.3.6. Different concentrations of target DNA	88
6.3.7. Analysis of Effect of Addition of Acid.....	89
6.4. Comparison with Other Studies in Literature.....	90
6.5 Solvent Compatibility of Parylene C Film Layer.....	92
6.5.1. Swelling of Parylene C in Solvents	92
6.5.2. Prediction of Solvent Compatibility	95
6.5.3. Deswelling of Parylene C.....	101
6.5.4. Surface Roughness Measurements	101
6.5.5. Comparison with Swelling of PDMS	101
6.5.6. Application	102
6.6 Effects of Solvents on Dissolution of Photo Resist Encapsulated in Parylene Microchannels	104
7. CONCLUSIONS AND RECOMMENDATIONS	107
REFERENCES	111
APPENDICES	
A. SIMULATION CODE.....	119
B. PROCESS FLOW	131
C. ALGORITHMS AND CALCULATIONS	137
C.1. Algorithms.....	137
C.2. Calculations	138
C.2.1. Curve Fit to Find Effective Surface Area of Gold Electrode	138
C.2.2. Curve Fit to Find D and C.....	139
C.2.3.Polymer Preparation and Characterization.....	139
C.2.3.1.Polymer Preparation.....	139
C.2.3.2. Characterization	140
CURRICULUM VITAE.....	143

LIST OF TABLES

TABLES

Table 2.1. Commercial FDA approved products as a clinical aid to identify MRSA.	21
Table 4.1. Materials used in the fabrication of the sensor.	32
Table 4.2. Dimensions of structures of different micro electrochemical sensors.	32
Table 4.3. Layers used, their trade names and numbers.	33
Table 4.4. Pillar numbers and area increase.	35
Table 4.5. Ag and Au etchants (Microchemicals, 2007).	39
Table 4.6. Process conditions for Ag layer formation (Sant et al., 1999).	41
Table 4.7. Different etchants and etch times for Ag etch.	43
Table 5.1. List of the some studies related to DNA detection by using HRP as non-electroactive marker.	58
Table 5.2. Solvents and their physical properties.	67
Table 6.1. Data for surface roughness measurement.	71
Table 6.2. Folding structures and thermodynamic details of the capture probe (0.01M Na ⁺ , 37 °C).	75
Table 6.3. Peak current values for a set of measurements for the electrochemical detection of <i>mecA</i> gene using Hoechst 33258 as redox marker.	76
Table 6.4. Peak current values for cross reactivity tests of 1 μM DNA samples.	78
Table 6.5. Oligonucleotide primers used for <i>mecA</i> amplification.	78
Table 6.6. The thermodynamic details of folding structures of amplified product.	79
Table 6.7. The thermodynamic details of folding structures of capture probe DNA.	81
Table 6.8. The data of TMB oxidation peak for each scan rate.	88
Table 6.9. The concentration of TMB for each scan rate.	88
Table 6.10. Concentrations of prepared solutions for the analysis of change in concentration of target DNA.	89
Table 6.11. A summary of some reported MEMS biosensors in the literature and their comparison with this work.	91
Table 6.12. Parylene C swelling ratios in different solvents.	93
Table 6.13 Molar volumes, values of Ra, and RED numbers of each specified solvent with their Parylene C swelling ranks.	100
Table B.1. Details of the steps for the fabrication of the sensor.	133

LIST OF FIGURES

FIGURES

Figure 2.1. Schematic diagram of <i>S. aureus</i>	5
Figure 2.2. SEM image of <i>Enterococcus faecium</i> (Solutions, 2012)	6
Figure 2.3. Schematic representation of mechanism of resistance (Nordberg et al., 2005).	7
Figure 2.4. Schematic representation of structure of peptidoglycan layer for bacteria (Bugg and Walsh, 1992).	8
Figure 2.5. (A) General structure of β -lactam antibiotics. N-Acyl Group of (B) benzylpenicillin (Penicillin G) (C) methicillin (Madigan et al., 2000).	8
Figure 2.6. Mechanism of <i>S. aureus</i> resistance to (a) penicillin (b) methicillin (Lowy, 2003).	9
Figure 2.7. Schematic diagram for the mechanism of vancomycin resistance (Salminen et al., 1998).....	10
Figure 2.8. Prevalence of MRSA by country in 2009 in Europe (ECDC, 2010).....	11
Figure 2.9. Prevalence of VRE by country in 2009 in Europe (ECDC, 2010).....	11
Figure 2.10. Main steps of diagnosis with μ TAS.	13
Figure 2.11. Magnetic, electrical, and optical detection strategies (Bhattacharya et al., 2007).....	14
Figure 2.12. A picture demonstrating microfluidic cartridge and its control instrument developed by (Sista et al., 2008).....	16
Figure 2.13. A picture demonstrating lab-on-a-disc cartridge developed by (Lutz et al., 2010).	17
Figure 2.14. A picture demonstrating lab-on-a-disc system developed by (Focke et al., 2010a).....	18
Figure 2.15. A picture demonstrating lab-on-a-disc cartridge developed by (Focke et al., 2010b).	18
Figure 2.16. A picture demonstrating portable PCR-CE analysis system developed by (Lagally et al., 2004).	19
Figure 2.17. A picture demonstrating the dipstick type microelectrode array and its detection mechanism (Gebala et al., 2011).	20
Figure 3.1. Concentration profile and resulting voltammogram for a linear potential scan (Wang, 2006).	26
Figure 3.2. Schematic diagrams of (A) potential time waveform in CV (B) cyclic voltammogram for a reversible system (Wang, 2006).	27
Figure 3.3. Schematic diagram of potential time waveform in DPV (Aoki et al., 1984; Wang, 2006).	28
Figure 3.4. Graphical user interface (GUI) for current vs. potential diagram with the parameters taken from the study of (Fan et al., 2000) for DPV.	29
Figure 4.1. A schematic view of micro electrochemical sensor	31
Figure 4.2. The structures of micro electrochemical sensor with electrodes and channel with 15 μ m in height.....	32
Figure 4.3. Ag electroplating region of the sensor.	33
Figure 4.4. Titanium circles in the reservoir.	34
Figure 4.5. Upside view of detection zone.	34
Figure 4.6. Pillars on Au electrode and their dimensions.	34

Figure 4.7. Mask layout for a device whose working electrode has the radius of 500 μm .	35
Figure 4.8. Overall view of mask layouts for the whole wafer.	36
Figure 4.9. Distribution of devices on wafer.	36
Figure 4.10. 50 μm x 50 μm regions on Au seed layer after Ag electroplating.	37
Figure 4.11. Surface profile of electrical connections of diamond structure at quarter one of wafer (A) 3-D view (B) 2-D analysis.	38
Figure 4.12. (a) Before (b) during (c) after silver deposition.	39
Figure 4.13. Silver mirror on Au coated wafer.	39
Figure 4.14. Glass slide (A) before (B) after etching.	39
Figure 4.15. Photograph of the wafer after Ag etching process.	40
Figure 4.16. 3D surface profile of electroless Ag deposited wafer.	40
Figure 4.17. Ag layer thickness profile as a function of time [300 W, 10 mTorr, and 100 Ar % (23 sccm)].	41
Figure 4.18. (A) Before (B) After Ag etching.	42
Figure 4.19. $\text{HNO}_3:\text{H}_2\text{O}$ (1:1, 6 s) (A) Before (B) After (with no pr strip) (C) After (with pr strip)	44
Figure 4.20. $\text{HNO}_3:\text{H}_2\text{O}$ (1:1, 13+3 s) (A) Before (B) After (with no pr strip) (C) After (with pr strip)	44
Figure 4. 21. A picture demonstrating detection zone after lithography step for Au etch.	45
Figure 4.22. A picture demonstrating a Crystalbond TM bonded wafer.	45
Figure 4.23. A photograph demonstrating electrodes before Pt etch.	46
Figure 4.24. A photograph demonstrating electrodes after Pt etch on metal RIE (2 min + 1 min 5 s).	46
Figure 4.25. A photograph demonstrating detection zone after Pt etch on metal RIE (2 min + 2 min).	47
Figure 4. 26. The corners of Pt electrode.	47
(Pt etch at metal RIE (2 min + 1 min + 10 s+ 10 s)).	47
Figure 4.27. SEM pictures taken from the #8 wafer.	47
(Pt etch at metal RIE (2min + 2min)).	47
Figure 4.28. Thickness profile of electrode layers.	49
Figure 4.29. Process flow of the micro electrochemical sensor (A) Insulation layer deposition (B) Metallization (C) Formation of working electrode (Au patterning) (D) Formation of counter electrode (Pt patterning) (E) Isolation of electrodes and formation of alignment marks (Ti patterning) (F) Protective layer deposition to prevent non specific adsorption (Parylene C deposition) (G) Formation of reference electrode (Ag sputtering and patterning) (H) Formation of micro channels and micro reservoirs (Parylene C deposition).	50
Figure 4.30. A photograph demonstrating fabricated prototype integrated with microchannels (r = 500 μm).	50
Figure 4.31. A photograph demonstrating fabricated prototypes (a) r = 100 μm , (b) r = 150 μm , (c) r = 200 μm , (d) r = 300 μm .	51
Figure 5.1. Chemical structure of Hoechst 33258.	54
Figure 5.2. The binding of Hoechst 33258 to minor grooves of dsDNA (Sufen et al., 2002).	54
Figure 5.3. Schematic view of mechanism for modification of Au electrode surface (McEwen et al., 2009).	54
Figure 5.4. Schematic view of mechanism for modification of Au electrode surface.	55
Figure 5.5 Experimental set-up for electrochemical detection.	56
Figure 5.6. Enzymatic cycle of TMB in the presence of H_2O_2 .	57

Figure 5.7. Redox reactions of TMB with HRP in the presence of less than equimolar and equimolar concentrations of H ₂ O ₂ (Baldrich et al., 2009; Josephy et al., 1982).	58
Figure 5.8. Isolation and amplification of DNA.....	59
Figure 5.9. A schematic illustration of sandwich-enzyme immunoassay.....	60
Figure 5.10. A schematic illustration of protein-enzyme conjugation (Adapted from the study of (Greg T, 2008)).....	61
Figure 5.11. (A) Illustration of the process flow for fabrication of the test structures used in the experiments of Parylene C swelling: (a.1) Parylene C deposition, (a.2) Photo resist coating and patterning, (a.3) Parylene C etching and photo resist stripping. (B) A photograph of the fabricated test structure for the Parylene C swelling experiments. (C) Illustration of the process flow for the fabrication of the test structures used in the solvent diffusion experiments: (c.1) Parylene C deposition, (c.2) Photo resist coating and patterning, (c.3) Parylene C layer deposition and dicing. (D) A photograph of fabricated prototype for the solvent diffusion experiments and SEM picture of encapsulated photo resist structures.	64
Figure 5.12. Schematic view of dissolution of photo resist in Parylene C microchannel.	66
Figure 5.13. Fabrication flow: (a) Wafer cleaning, (b) Parylene C deposition, (c) Patterning with photo resist, (d) Parylene C deposition and dicing.	67
Figure 6.1. Cyclic voltammograms for different KCl concentrations.	70
Figure 6.2. Cyclic voltammograms for different PBS concentrations.....	70
Figure 6.3. 3D plot of a bare gold surface.	71
Figure 6.4. Cyclic voltammograms of Au oxidation (a) for the first and the last crossings of cyclic voltammetry (b) for each crossings of cyclic voltammetry (r = 300 μm).	72
Figure 6.5. Cyclic voltammograms of Au redox cycle (r = 100 μm).	73
Figure 6.6. Electrochemical detection of methicillin resistance with different concentrations of mecA gene (A) The maximum peak currents obtained by DPV (B) The mean of the peak current values demonstrating the monolayer adsorption isotherm.	76
Figure 6.7. C/Y vs. C graph to determine adsorption constants.	77
Figure 6.8. Cross reactivity test results for the specificity of the chip.	77
Figure 6.9. NCBI Blast results for the primer sequences (a) MR1 and (b) MR2 (Medicine, 2012).....	78
Figure 6.10. Nucleotide sequence of mecA gene indicating the primers selected (Medicine, 2012).	79
Figure 6.11 Circular diagram for the reverse complement of amplified product.	80
Figure 6.12. Cyclic voltammogram for TMB solution on HRP activated gold microdisc electrode.	81
Figure 6.13. Current-time response curve of TMB solution on HRP activated gold microdisc electrode.	83
Figure 6.14. Current-time (i-t) response curves for working electrodes in the absence (blue line) and in the presence (red line) of target DNA (hybridized for one hour at room temperature) in the TMB substrate solution. E = 0.15 V.	83
Figure 6.15. Experimental (circles) and fitted (red line) chronoamperometric curve for the two-electron reduction of TMB on a 300-μm gold microdisc electrode for a fixed potential of 0.15 V. Fitting was performed by MATLAB software and Diffusion coefficient, D was determined as 9.43±0.74 x 10 ⁻⁶ cm ² /s.	83
Figure 6.16. Cyclic voltammograms for the optimization of hybridization time for 100 μm working electrode (black line (30 min), blue line (1 hour), red line (2 hours), green line (3 hours)).	84
Figure 6.17. Optimization of hybridization time. Operating conditions: capture probe, 10 μM; target probe, 10 times diluted PCR product; capture probe immobilization time, 24 hrs; streptavidin conjugated HRP incubation time, 15 min; TMB/H ₂ O ₂ incubation time, 15 min. Other conditions: wait time, 5s; lower vertex potential, 0 V; upper vertex potential, 0.9 V; step potential, 2.44 mV; scan rate, 0.1 V/s.	84

Figure 6.19 Cyclic voltammograms showing TMB oxidation with different incubation times (black line, no HRP; blue line, 5 min; red line, 15min; green line, 30 min). Operating conditions: capture probe, 10 μ M; target probe, 10 times diluted PCR product; capture probe immobilization time, 24 hrs; target probe incubation time, 2 hrs; streptavidin conjugated HRP incubation time 5 min. Other conditions: wait time, 5s; lower vertex potential, 0 V; upper vertex potential, 0.9 V; step potential, 2.44 mV; scan rate, 0.1 V/s.	86
Figure 6.20 Peak current vs incubation time graph for TMB oxidation reaction.	86
Figure 6.21. Cyclic voltammograms of TMB oxidation for different scan rates (blue line: 1 V/s, green line: 0.5625 V/s, red line: 0.25 V/s, purple line: 0.1 V/s, orange line: 0.0625 V/s).	87
Figure 6.22. Cyclic voltammograms of TMB oxidation for different scan rates. Inset: Linear proportionality of peak current to the square root of scan rate.	88
Figure 6.23. Concentration dependence for biotinylated PCR product: (blue line) 28.7 ng/ μ l, (red line) 20.8 ng/ μ l, (green line) 18.1 ng/ μ l, (black line) no target DNA. Operating conditions: capture probe, 10 μ M; capture probe immobilization time, 24 hrs; target probe incubation time, 2 hrs; streptavidin conjugated HRP incubation time 5 min. TMB incubation time, 15 min; Other conditions: wait time, 5s; lower vertex potential, 0 V; upper vertex potential, 0.9 V; step potential, 2.44 mV; scan rate, 0.1 V/s.	89
Figure 6.24 A photo demonstrating the color change due to enzymatic activity of HRP.	90
Figure 6.25 Time course of enzymatic activity and the effect of addition of acid.	90
Figure 6.26. The change of the swelling ratio of Parylene C (SParylene) with the solubility parameter (δ). Error bars demonstrate an error of $\pm 0.5\%$ standard deviation (number of samples = 9). The line () designates the place of solubility parameter of Parylene C ($\delta = 9.6$ (cal/cm ³) ^{1/2}), calculated from the study of Miller et al. (Miller and Leighton, 1990) while the line () indicates the place of solubility parameter of Parylene C ($\delta = 9.2$ (cal/cm ³) ^{1/2}) proposed in this study.	94
Figure 6.27. 3D solubility sphere of Parylene C created in MATLAB.	96
Figure 6.31 Percent changes in the average roughness (Ra) and root mean square roughness (Rq) of Parylene C surfaces after being immersed into the specified solvents for 24 hours at room temperature. The dashed lines are used to group the solvents as hydrocarbons, acyl and halogenated compounds, alcohols, and the others.	102
Figure 6.32. The change of the swelling ratios of Parylene C (SParylene) and PDMS (SPDMS)(Lee et al., 2003) with solubility parameter (δ). Ranking of solvents was made with respect to the degree of swelling ratio of Parylene C.	103
Figure 6.33. Time course of solvent penetration through 4 μ m-thick Parylene C film layer. Solvents: (a) DMSO, (b) DMF, (c) acetone, (d) n-butyl acetate (e) NMP, and (f) MEK	104
Figure 6.34. Dissolution data for dipolar aprotic solvents.	105
Figure 6.35. Dissolution data for different UV exposure values.	105
Figure 6.36. Dissolution data for DMSO at different temperatures and percentages [v/v] with acetone.	106
Figure C.1. Algorithm for Nova 1.5 to characterize Au layer using cyclic voltammetry.	137
Figure C. 2. Chronoamperometry algorithm for determination of HRP activity.	138
Figure C.3 Experimental (dots) and fitted (red line) cyclic voltammogram for the gold layer characterization in the acid solution for 300 μ m electrode.	139

CHAPTER 1

INTRODUCTION

Since the early 1990s, there have been many efforts and, as a result, success towards the development of micro total analysis systems (μ TAS or lab-on-a-chip) in an extended platform from health to biosecurity by using microfluidics and Micro Electro Mechanical Systems (MEMS) technology. Lab-on-a-chip systems have the ability of integrating complex laboratory processes with biological analyte detection to realize point of care diagnosis (Focke et al., 2010a). The advantages of micro scale structures in clinical diagnostics are numerous as portability, high sensitivity, and low cost with the use of small volumes of samples and reagents. With these advantages, the interest in developing new methods for detection of bacteria, virus, etc. has increased [cancer cases, sexually transmitted diseases and infectious diseases (Deisingh and Thompson, 2002)]. Among the many diseases, the control of infectious ones is becoming an overhanging danger due to continuous rise in the number of pathogens with antibiotic resistance (Okeke et al., 2005).

Antimicrobial resistance, which is the ability of an organism to resist the antibiotics due to misuse and overuse of drugs, is one of the most rapid growing problems all over the world that necessitates immediate action. These organisms decrease the chance of effective treatment of infectious diseases and increase the rates of morbidity and mortality for patients. Actually, it is hard to tell precisely the exact impact of resistance on morbidity and mortality since it is an extra problem for an infected patient. However, it is evident that, patients infected with an antibiotic resistant organism will be ill for longer time compared to other patients, need more expensive treatments and stay longer in hospitals, which increase the financial burden not only on clinics but also on patients (ETAG, 2006). In a recent report of World Health Organization (WHO) on *Antibacterial Drug Resistance*, it is stated that, infectious diseases accounts for 20% of all deaths, also the expected cost of treatment of resistant infections to USA for each year is over 20 billion US dollars, representing a huge economic burden to healthcare units (WHO, 2012).

One of the most important threats of nosocomial infections in many regions of the world, including Europe, North Africa, USA, and Far East (Klonoski et al., 2010) is Methicillin Resistant *Staphylococcus aureus* (MRSA), the indicator of which is *mecA* gene. *Staphylococcus aureus* is naturally found in skin and nose flora and it is of greatest importance because of its ability to adapt to different living conditions, intrinsic virulence, and ability to cause a range of illnesses from minor skin infections to life threatening infections (Lowy, 2003). Its resistance to a great number of bactericidal antibiotics increases day by day due to its flourishing mechanisms in making drugs passive. The prevalence of MRSA, which has increased very rapidly in the last two decades, can differ between nations, age groups, and specimens taken from blood, wound, and nose (Bordon et al., 2010). For example, in Japan, although the first isolation for MRSA was done in 1980, the prevalence of MRSA in the last decade has been 40-70%, which is the highest prevalence of MRSA in the world (Kunishima et al., 2010). On the other hand, Enterococci has been reported as an emerging pathogen for healthcare associated infections since 1970s and they are the first prominent nosocomial pathogens to develop full resistance against third-generation glycopeptide antibiotics (vancomycin and teicoplanin) (Nordberg et al., 2005). Vancomycin-resistant enterococci (VRE), the indicators of which are *vanA* and *vanB* genes, are one of the most important groups of these pathogens due to their antimicrobial resistance mechanism (Nordberg et al., 2005).

Early diagnosis and initiation of appropriate treatment are necessary to decrease morbidity and mortality rates related to antimicrobial resistance based infections (Lindsey et al., 2008). At the same time, reducing diagnosis time can also reduce duration of a patient's hospital stay, and increase hospital cost savings. In clinics, conventional culture based methods are mostly used due to their ease of use and low

cost. However, they are time consuming since it is necessary to incubate the samples at least 24 to 72 hours to ensure resistance to methicillin after detection of bacterial growth by an automated continuous-monitoring blood culture system (Klonoski et al., 2010). Therefore, use of molecular methods is becoming important for diagnosis not only for its high sensitivity, but also for its rapidity. To meet this clinical demand, commercialized products have been introduced into clinical use in which the use of polymerase chain reaction (PCR) based assay is preferred commonly for detection of indicator genes to increase sensitivity and reduce time to result. However, these assays require expensive devices and trained personnel for analysis, and they are used in clinics as clinical aid with the other clinical analysis. Therefore, they have not been accepted in the clinical community, yet.

In order to overcome all of these drawbacks, MEMS based biosensors have been developed to form complete lab-on-a-chip systems. By using this novel technology, it is possible to fabricate wells, reactors, channels, detectors, and electrodes in micro scale to perform biological operations like growing cultures, amplification of nucleic acids, detection of biological analytes, and work with each of the analytes individually in small-size, low-cost, multifunctional micro laboratories. Fabricated surfaces can be activated by using surface chemistry (especially by using Self Assembled Monolayers (SAMs)) for adsorption of biological samples, and responses can be converted into mechanical, optical, or electronic signals by using detection markers that will amplify the signal. It is also possible to detect multiple biological analytes in the same device by forming parallel units, which will increase the advantages of cost and efficiency.

In the literature, there are different methods to detect the presence of MRSA in a specimen while there is not enough study related to the detection of VRE by using MEMS based biosensors. The method of detection can be optical, mechanical, magnetic, electrochemical, or combinations of them (Boedicker et al., 2008; Dutta et al., 2005; Focke et al., 2010a; Focke et al., 2010b; Guntupalli et al., 2008; Lutz et al., 2010; Shen et al., 2010; Sista et al., 2008). Among them, electrochemical detection, which includes amperometric, potentiometric, and conductometric detection, allows one to transfer electronic output signal of biological reaction to macroscopic environment, and the magnitude of this signal depends on the electrode surface area and the reaction on the surface rather than the reaction volume as in the optical detection. Moreover, it is possible to fabricate the microelectrodes directly in the micro channels by using micro fabrication technology. Therefore, electrochemical detection for integration of microfluidic chips is the most appropriate detection strategy (Verpoorte and De Rooij, 2003). Although this is the case, the electrochemical studies in the literature are based mainly on the concept of thin film biosensor and there is no study, which represents a full system with its micro reservoirs, microelectrodes, and micro channels to detect MRSA and VRE electrochemically.

The main aim of this study is to design, fabricate, and test MEMS based electrochemical DNA biosensor to detect *mecA*, *vanA*, and *vanB* genes. In electrochemical detection, cyclic voltammetry and differential pulse voltammetry are considered to be used in the study. This biosensor is aimed to be a complete system with its micro reservoirs (inlet and outlet ports, and detection zone), microelectrodes, and micro channels. In the detection zone, self-assembled monolayer can be formed on working electrode and DNA based probes adsorbed on the microelectrode can target DNA sequence of specified part of *mecA*, *vanA* and *vanB* genes, and sensitivity can be increased by using redox marker and enzyme based detections to amplify electronic signal.

In order to achieve this objective, the following methods and steps are considered:

- Design of complementary and target DNA probes,
- Design and fabrication of electrochemical sensor,
- Characterization of the sensor,
- Redox labeled electrochemical detection of genes by using Hoechst 33258,
- Enzyme based electrochemical detection of genes by using horseradish peroxidase.

In the following chapters, literature on the current state of the conventional methods and MEMS based biosensors, which are currently available for detections of MRSA and VRE, will be given together with

the basic properties of *S.aureus*. Also, bacterial function and emergence of antibiotic resistances in *S.aureus* and Enterococcus species will be introduced together with clinical importance of MRSA. Current detection strategies such as culturing, immunological approaches, and MEMS based biosensors will also be given in detail. Finally, detection principles of some commercialized products for in vitro research/clinical use will be illustrated. In the third chapter, the theory of electrochemical detection and adsorption, in the fourth chapter, the design and details of micro fabrication of the MEMS biosensor will be discussed. In the fifth chapter, surface characterization, protocols for redox and enzyme based detection and experimental setup and in the sixth chapter, results and discussions will be given, including characterization of the sensor, redox marker based detection, enzyme based detection and studies on Parylene C film layer and encapsulated photoresist. Finally, future work will be recommended together with conclusions.

CHAPTER 2

LITERATURE SURVEY

In this chapter, literature survey about the importance of methicillin resistant *Staphylococcus aureus* and vancomycin resistant *Enterococcus* species will be given by introducing the organisms, antibiotic resistance, and their clinical importance and prevalence. The research studies performed in the field of MEMS based biosensors will be given in comparison with conventional methods and commercialized products approved by US Food and Drug Administration (FDA) will be explained finally (Ceylan Koydemir et al., 2011).

2.1. *Staphylococcus aureus* and *Enterococcus* Species

Infections caused by antimicrobial resistant Gram-positive bacteria present a global burden to the community, especially in terms of increased hospital stays of patients and implementation of disease control measures (Woodford and Livermore, 2009). *Staphylococcus aureus* and *Enterococcus* species are two major gram-positive bacteria that cause hospital-acquired infections around the world and the acquired antimicrobial resistances in these bacteria play a vital role in appropriate treatment since they are normal components of human flora.

2.1.1. *Staphylococcus aureus*

Staphylococcus aureus (*S.aureus*), which is one of the 32 species in *Staphylococcus* genus and naturally found in skin and nose flora, is the leading cause of health care associated infections (Ceylan Koydemir et al., 2011). This pathogen has the greatest importance because of its ability to adapt to different living conditions, intrinsic virulence, and ability to cause a range of illnesses from minor skin infections to life threatening infections (Freeman-Cook and Freeman-Cook, 2006; Lowy, 2003). The origin of *S. aureus* is not known but it was first discovered in 1884 by Anton Rosenbach (Deurenberg and Stobberingh, 2008). In Greek language, “Staphyle” and “cocci” mean “bunch of grapes” and “spherical bacteria”, respectively. The name “aureus” means “gold” in Latin since bacteria grow in large yellow colonies. Its size is about 1 μ m. *S.aureus* is a prokaryote and it has a typical bacterial structure without flagella (Figure 2.1).

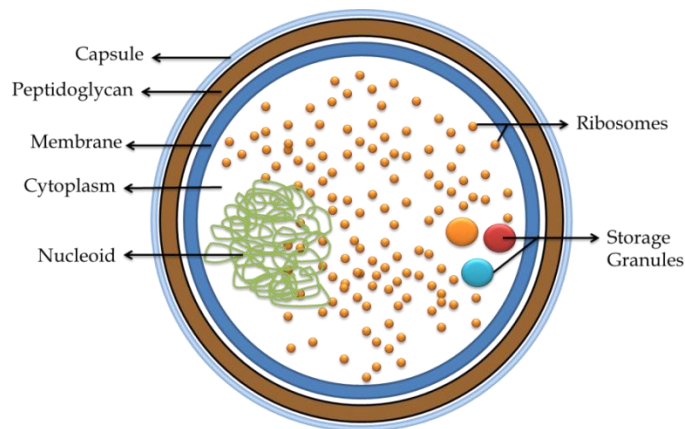


Figure 2.1. Schematic diagram of *S. aureus*.

The outermost layer (capsule) contains polysaccharides, which play an important role in the attachment of *S. aureus* to inert surfaces or to their hosts. Peptidoglycan layer is comprised of two sugar derivatives (N-acetylglucosamine and N-acetylmuramic acid) and amino acids (L-alanine, D-alanine, D-glutamic acid, glycine and lysine). Its thickness determines the strength of the cell wall (Garcia-Lara et al., 2005; Madigan et al., 2000). In peptidoglycan structure of *S. aureus*, there are about 15 repeating units and chain length of 30 peptide units (Dworkin et al., 2006). Since it is involved in bacterial cell division, the prevention of its formation can be bactericidal. The cytoplasmic membrane, a section for energy conservation in the cell prevents the leakage of nutrients into or out of the cells. The membrane is also the site of proteins and enzymes, which are involved in transport of constituents in or out of the cell. Lastly, the cytoplasm consists of ribosomes, nucleic acids, and storage granules.

2.1.2. *Enterococcus* Species

Enterococci as a group was first discovered by Thiercelin in 1899 and the genus *Enterococcus* was introduced by Thiercelin and Jouhad in 1903. Most of the *Enterococcus* species have the ability to grow between 283.15 K and 318.15 K and in 6.5% NaCl, at pH 9.6 and can live at temperatures up to 333.15 K (Franz et al., 1999).

Enterococcus species are gram positive and live in the digestive and genital tracts of humans. Only two of several *Enterococcus* species identified are the cause of infections: *E. faecalis* (about 80% of clinical isolates) and *E. faecium* (about 15% of clinical isolates) (Figure 2.2) (Çetinkaya et al., 2000; Solutions, 2012). The reason for the focus of attention on Enterococci is not only their cause to nosocomial infections, but also their ascending intrinsic or acquired resistance to commonly used antibiotics. The presence of intrinsic and acquired antimicrobial resistance, which will be explained in the next section, in the same bacteria is leading to difficulties in the treatment of patients.

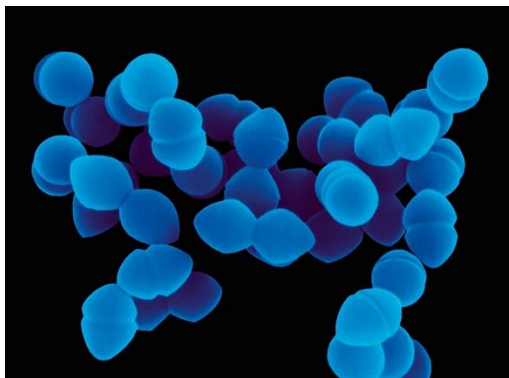


Figure 2.2. SEM image of *Enterococcus faecium* (Solutions, 2012)

2.2. Antibiotic Resistance, MRSA and VRE

Antibiotic resistance is the ability of an organism to resist the effects of an antimicrobial. The antimicrobial resistance can be in two ways: intrinsic or acquired. In intrinsic resistance, bacteria may not have the structure that antibiotic inhibits, impermeable to the antibiotic and able to inactivate the antibiotic (Taylor-Robinson and Bebear, 1997) while acquired resistance is encoded at either the chromosomal or the plasmid level (Madigan et al., 2000; Taylor-Robinson and Bebear, 1997). In chromosomal basis, the resistance is due to the mutations in the chromosome. In the plasmid basis, bacteria inactivate the drug by the genes encoding new enzymes (Madigan et al., 2000). Moreover, the bacterial colony can have the multi resistant properties due to accumulation of genetic elements with newly developed antibiotics (Nordberg et al., 2005). There are four different mechanisms of resistance in principal (Figure 2.3)

antibiotics can be altered by the enzymes to passive form, can be kept out from cell entry, can be inactivated by enzymatic degradation and can be ejected from the cell.

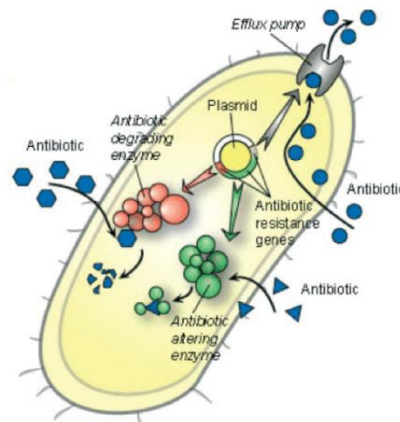


Figure 2.3. Schematic representation of mechanism of resistance (Nordberg et al., 2005).

Antimicrobial drugs can inhibit cell wall formation (β -lactams and glycopeptides (vancomycin)), cell membrane (polymyxins), protein synthesis (tetracyclines) or nucleic acid metabolism (rifampin) of an organism (Figure 2.4) (Bugg and Walsh, 1992; Madigan et al., 2000). Since bacteria die with cell lysis, it is essential to inhibit the peptidoglycan layer of bacterial cell wall that provides strength and rigidity in bacteria. Therefore, β -lactams and glycopeptides are extensively used in the treatment of patients due to their specificity and non-toxicity to host cells, which results in the rise of bacterial resistance (Bugg and Walsh, 1992).

Penicillin G (Figure 2.5) is one of the β -lactam antibiotics and it is produced by fungus *Penicillium chrysogenum*. Its action is on infections related with gram-positive bacteria. Although it was introduced in 1941, the recognition of penicillin resistant *staphylococci* was as early as 1942 (Lowy, 2003; Smith and Jarvis, 1999). This resistance was due to the production of penicillinase (about 80%), which is responsible for hydrolysis of β -lactam ring, in penicillin-resistant staphylococcal isolates. Two adjacent regulatory genes, the repressor *blaI* and antirepressor *blaR1* control the activation of *blaZ*, which encodes penicillinase. This enzyme is produced when the regulatory genes are cleaved sequentially. In the presence of β -lactams, penicillin, *blaR1* cleaves itself and activates *blaI* with the cleaved proteins, which leads to penicillinase production (Figure 2.6) (Lowy, 2003; Pantosti et al., 2007).

After the discovery of penicillin resistance, the β -lactam ring was changed in 1960 by the introduction of semisynthetic penicillin, methicillin, in clinical use (Figure 2.5) (Jeljaszewicz et al., 2000; Madigan et al., 2000). After one year, in 1961, the first resistance was reported, and this type of *S. aureus* has been named as Methicillin Resistance *Staphylococcus aureus* (MRSA) (Berger-Bächi and Rohrer, 2002). This acronym is also used for oxacillin resistant *S.aureus* since the mechanism of resistance in both antibiotics (i.e., oxacillin and methicillin) is based on the production of penicillin binding protein (PBP2a or PBP2'), which is encoded by chromosomal *mecA* gene, with low affinity to β -lactams (Prere et al., 2006). PBP2a has the weight of 78 kDa.

Production of peptidoglycan layer is catalyzed by PBPs membrane bound enzymes. PBP2a replaces with PBPs and enables the bacteria to survive in the presence of antibiotic due to its low affinity to β -lactams (Lowy, 2003). Therefore, methicillin resistance spreads out all β -lactams and their derivatives. Similar to the penicillin resistance, two adjacent regulatory genes, the repressor *mecI* and antirepressor *mecR1* control the activation of *mecA*, which encodes PBP2a. The response of *mecA* to β -lactams is similar to the regulation of *blaZ* (Figure 2.6) (Lowy, 2003; Pantosti et al., 2007). The methicillin resistance determinant, *mecA* gene is a part of the genomic island and placed on *Staphylococcus* cassette chromosome

mec (*SCCmec*). The resistance levels are based on the “genetic background of the strain into which *SCCmec* has entered” (Berger-Bächi, 2002). In healthcare-associated MRSA (HA-MRSA), *mecA* gene is placed on Type I-III *SCCmec* whereas it is placed on Type IV *SCCmec* (a and b, AB063172 and AB063173, respectively) in community-acquired MRSA (CA-MRSA) (Graves et al., 2010; Hiramatsu et al., 2001). Type IV element is more mobile and shorter than the other types of element and it does not have any other antimicrobial resistance (Hiramatsu et al., 2001; Lowy, 2003).

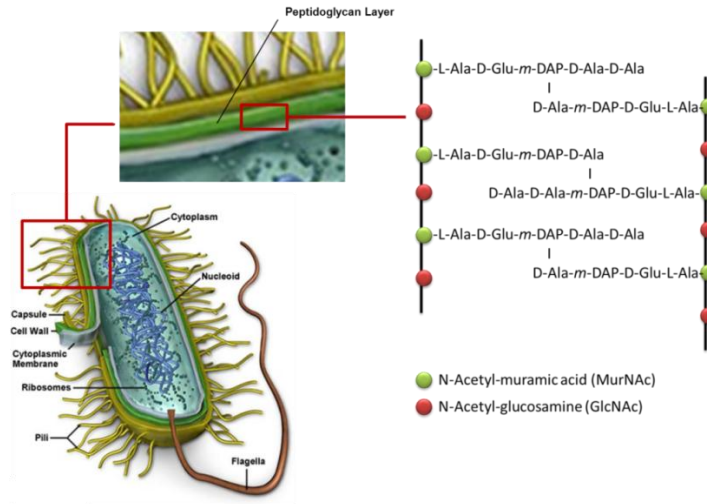


Figure 2.4. Schematic representation of structure of peptidoglycan layer for bacteria (Bugg and Walsh, 1992).

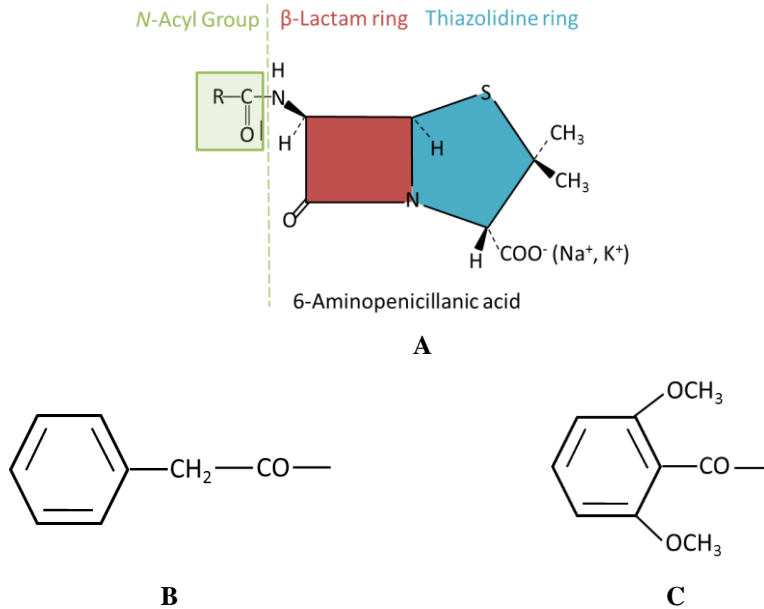


Figure 2.5. (A) General structure of β -lactam antibiotics. N-Acyl Group of (B) benzylpenicillin (Penicillin G) (C) methicillin (Madigan et al., 2000).

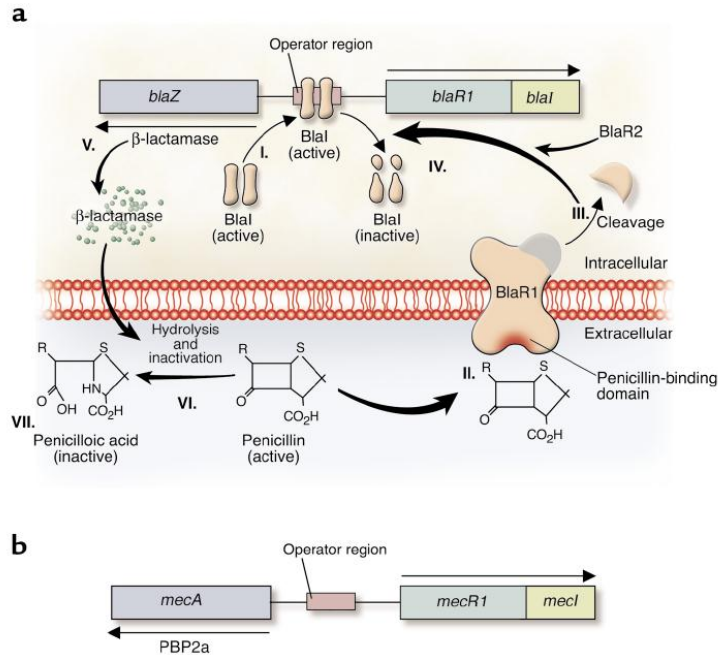


Figure 2.6. Mechanism of *S. aureus* resistance to (a) penicillin (b) methicillin (Lowy, 2003).

On the other hand, Enterococci species are highly resistant to aminoglycoside antibiotics due to their aminoglycoside-modifying enzymes, and to β -lactams due to their penicillin binding proteins (PBP) with low affinity. Therefore, vancomycin, which is a narrow-spectrum antibiotic obtained from *Streptomyces orientalis*, has been used in clinical use since 1980s, due to its activity against MRSA and other Gram-positive bacteria (Çetinkaya et al., 2000). Vancomycin is also used in penicillin-allergic patients to treat Gram-positive infections. However, after vancomycin resistance enterococci (VRE) were firstly reported in England in 1988, the same resistance was detected in United Kingdom, France and in the eastern half of the United States (Çetinkaya et al., 2000; Uttley et al., 1993). Afterwards, VRE has spread at a great speed all over the world. Vancomycin acts by binding to the β -lactam-sensitive transglycosylase/transpeptidase, namely lipid-PP-disaccharide-pentapeptide, by five hydrogen bonds. This binding prevents the further activity of transglycosylase/transpeptidase, which leads to a lower strength of peptidoglycan layer and lysis due to the change in osmotic pressure (Walsh et al., 2001). There are two major types of mechanisms of vancomycin resistance in enterococci: VanA (resistance to vancomycin and teicoplanin) and VanB (resistance to vancomycin only) (Figure 2.7) (Salminen et al., 1998). In the VanA resistance, expression of *vanA*, *vanR*, *vanS*, *vanH*, *vanX*, and *vanZ* genes leads to synthesis of abnormal peptidoglycan precursors terminating in D-Ala-D-Lac instead of D-Ala-D-Ala (Çetinkaya et al., 2000). The binding of vancomycin to D-Ala-D-Lac is weaker than the one to D-Ala-D-Ala. VanB resistance is distinguished from VanA resistance with its regulatory genes (*vanZ* gene is replaced by the gene *vanW*) and the structure of VanY-type carboxypeptidase (Salminen et al., 1998).

2.3. Clinical Importance and Prevalence

S. aureus belong to the normal bacterial flora of the skin and nose. However, it can cause illnesses from skin infections to sepsis and the severity of illness increases with its methicillin resistant form. Treatment failure due to inappropriate antibiotic usage and the lack of efficacy of anti-MRSA drugs increase morbidity and mortality. Therefore, it is important to prevent transmission of MRSA. Controlling actions like patient isolation, use of disposable gloves etc. are necessary and they increase the burden on patients and healthcare units (Gould, 2005).

According to the European Antimicrobial Resistance Surveillance System Report in 2009 (ECDC, 2010), 30,680 nosocomial isolates were collected from 28 countries (Figure 2.8) and 5965 of them were methicillin resistant. The prevalence of MRSA is different in various parts of the world. It is <1% in northern countries and it increases to 50% in southern countries of Europe. Between 2006 and 2009, the trend of prevalence significantly decreases in eight countries (like France, Austria, Latvia, Bulgaria, and United Kingdom) while the prevalence in Czech Republic increases to 15% (Figure 2.8). Although a decrease is observed in the collected data of some countries, the MRSA is still a serious cause of health problem all over the world. In USA, the MRSA rate was higher than 50% in 2008 (Bordon et al., 2010). On the other hand, in Asian countries like Australia, Singapore, and Pakistan the prevalence is 20%, while it is higher than 50% in China, India, and Korea (Reinert et al., 2007).

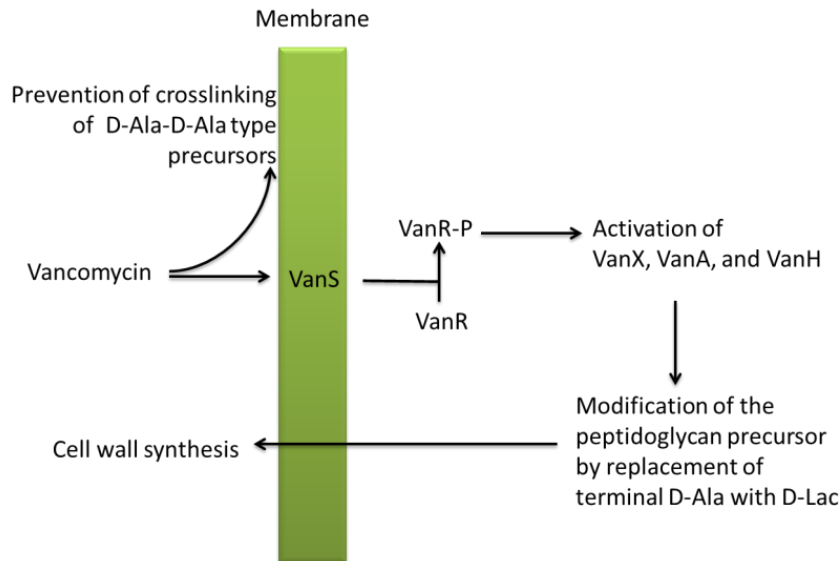


Figure 2.7. Schematic diagram for the mechanism of vancomycin resistance (Salminen et al., 1998).

Although Enterococci are found in the normal flora of the gastrointestinal tract and the female genital tract, it can cause serious enterococcal infections like endocarditis and bacteremia. In the treatment of patients antibiotics are used which isolate the Enterococcus without having high level of resistance and is susceptible. Among the antibiotics, vancomycin is used in the treatment. However, the acquired resistance of Enterococci lowers its bactericidal activity and makes the treatment of infections difficult.

The prevalence of VRE is different in many parts of the world. According to the European Antimicrobial Resistance Surveillance System Report in 2009 (ECDC, 2010), 4945 nosocomial isolates were collected from 28 countries (Figure 2.9) and 451 of them were vancomycin resistant. The prevalence of VRE is above 25% in Greece, Ireland, and Luxemburg while it is below 10% in most of the European countries (including Turkey) (Schouten et al., 2000). Between 2006 and 2009, the highest increase in proportion to resistance is observed in Austria (from <1% to 4%). On the other hand, in Korea, the prevalence of resistance of *Enterococcus faecium* to vancomycin increased from 2.9% to 16% between 1997 and 2006 (Yoon et al., 2009). In Canada, the prevalence of VRE was below <1% in 2006. The highest resistance to vancomycin for *Enterococcus faecium* specie is 60% in USA (Nichol et al., 2006). The difference in the prevalence rates between Europe and USA may be related to the use of avoparcin (similar to vancomycin) in the farm animals up to year of 1997, different nosocomial strains of the same species, overuse of vancomycin in USA compared to the European countries (Tacconelli and Cataldo, 2008). Thus, it is important to detect methicillin and vancomycin resistances in species.

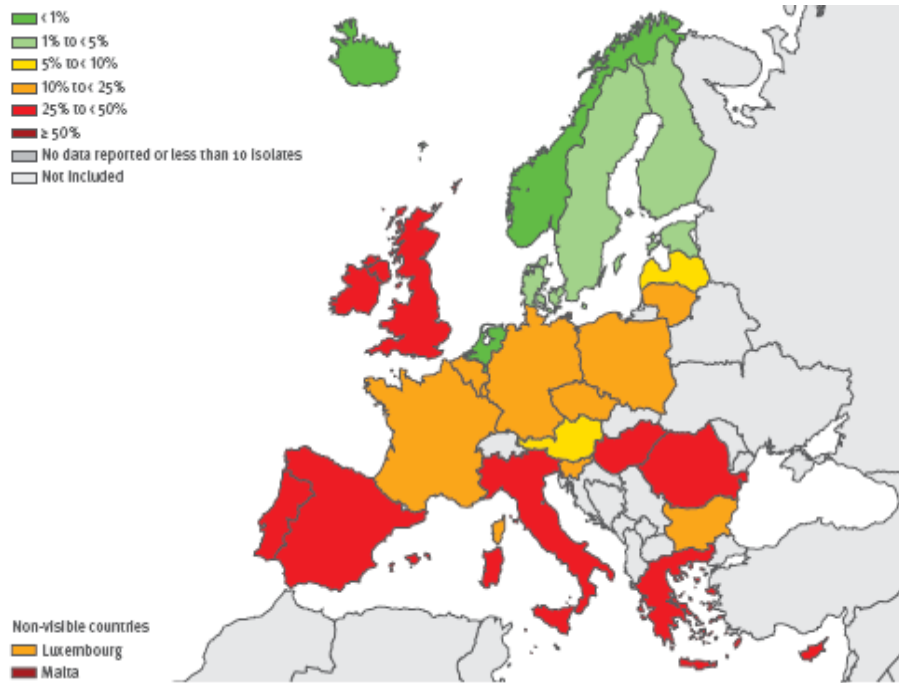


Figure 2.8. Prevalence of MRSA by country in 2009 in Europe (ECDC, 2010).

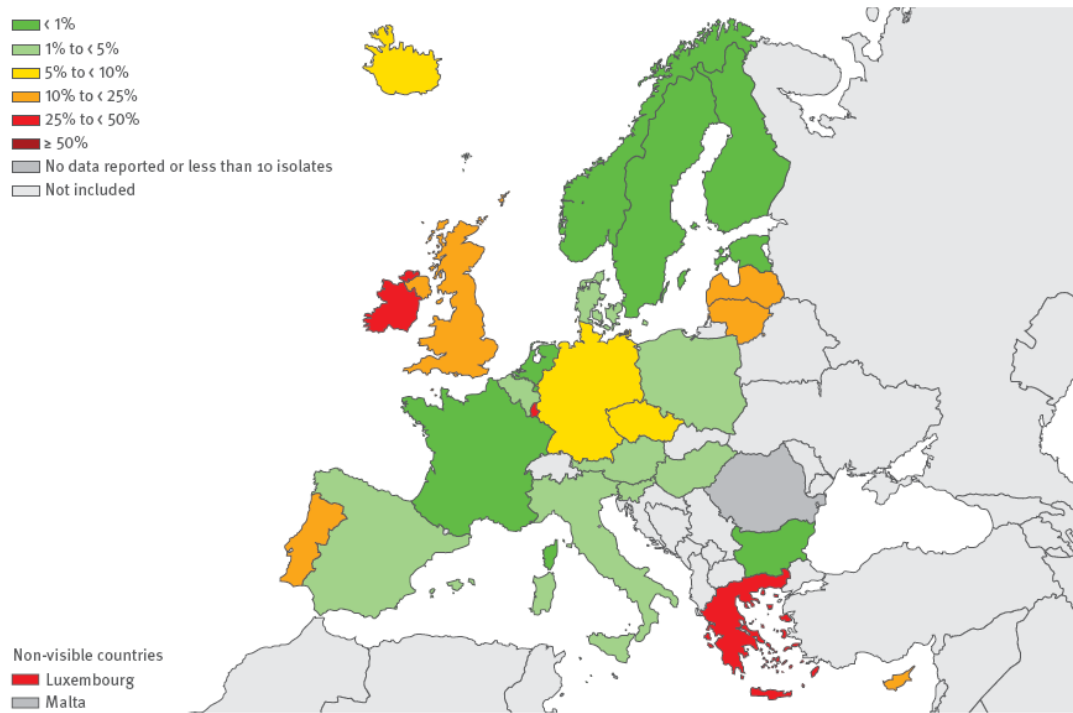


Figure 2.9. Prevalence of VRE by country in 2009 in Europe (ECDC, 2010).

2.4. Methods for Detection

Conventional and MEMS based methods to detect MRSA and VRE will be explained below. Most of the current methods are based on enhancing the expression of resistance in modified cultures while MEMS based approaches are based on the amplification of signal to enhance detection limits.

2.4.1. Conventional Methods for the Detection of MRSA

There are different methods to distinguish methicillin resistance from susceptible strains: agar dilution, E-test (AB Biodisk, Solna, Sweden), breakpoint methods, disk diffusion tests (e.g. cefoxitin, and oxacillin), latex agglutination test which depends on detection of PBP2a, and molecular methods (e.g. use of radiolabelled DNA probes, and PCR to detect *mecA* gene) (Brown et al., 2005). The expression of resistance in the detection of MRSA is strongly based on the selective test agent, NaCl concentration, culture medium, inoculum, incubation temperature, and minimum inhibitory concentration (MIC) breakpoint (Brown, 2001). The selective test agent is oxacillin in almost all culture-based methods since methicillin is no longer being produced. As an alternative to oxacillin, cefoxitin is also used in disk diffusion tests and provides more reliable results. Although addition of NaCl increases the expression of resistance in some mediums such as Mueller – Hilton, some strains are adversely affected from the high concentration of NaCl. However, addition of 2% NaCl into the medium is sufficient to have good results. It is inhibitory to add more than 5% NaCl to the test medium. Temperatures about 303.15 – 308.15 K are commonly used in incubation. Except the molecular methods, it is necessary to incubate samples at least 24 hours. Since resistant sub-populations of some strains grow slowly, it may be necessary to incubate samples for 48 hours to ensure the resistance although further culturing increases costs and retards the results (Struelens et al., 2009). MIC breakpoint for oxacillin > 2 mg/l indicates resistance for dilution and breakpoint methods, while in disk diffusion methods MIC is determined with reduced zones or rings of inhibition around the antibiotic disk. However, optimal conditions for detecting resistance changes with the type of the strains that will also affect the methicillin MIC values. Therefore, a reference, which is determined by using a dilution method, is used for comparison in evaluating the performance of the test. The reference method is now being replaced by molecular methods that are regarded as gold standard due to their high sensitivity and specificity. The molecular methods generally rely on polymerase chain reaction (PCR) to detect *S. aureus* (*fem* genes) and *mecA* gene, whose presence directly indicates methicillin resistance after primary culturing. Moreover, heterogeneous MRSA populations and strains with extremely low-level methicillin resistance are susceptible to most of the non- β -lactam antibiotics, and routine oxacillin tests lead to false positive results (Berger-Bächi and Rohrer, 2002; Felten et al., 2002). Therefore, it is important to detect the presence of the *mecA* gene.

2.4.2. Conventional Methods for the Detection of VRE

Use of cultures to determine the VRE status of the patient is a conventional method in healthcare units. There are different media that can be used for culturing such as Columbia blood agar, brain heart infusion (BHI) blood agar or any blood agar base containing 5% animal blood. Among the agars, yeasts and some microorganisms cannot grow on bile-esculin-azide (BEA) agar containing vancomycin. The concentration of vancomycin in most of these agars is 6 μ g/ml. MIC can be determined by using the methods such as agar dilution, agar gradient dilution, broth macrodilution, or manual broth microdilution. The MIC breakpoint is ≤ 4 μ g/ml for susceptible isolates and ≥ 32 μ g/ml for resistant isolates. These cultures have a limit of detection approximately 10^4 CFU/ml, which may result to false negative results. On the other hand, susceptibility testing can be done by using The Etest (AB BioDisk, Solna, Sweden) for vancomycin, micro dilution plate assays, disk diffusion, and Mueller-Hinton and BHI agars with 6 μ g/ml of vancomycin. These methods are good in specificity and sensitivity for detection of resistance to vancomycin. However, the difference between the types of VRE (e.g. VanA, or VanB) could not be done by using the mentioned methods (Dodgson, 2004). To overcome with this drawback, the use of PCR is preferred to detect a few copies of a gene as in most clinical applications.

2.4.3 MEMS Based Methods for Detection

Lab on a chip, which is also known as micro total analysis system (μ TAS), is an integrated small-scale device performing the conventional laboratory operations by combining microfluidics and micro electromechanical systems (MEMS). The laboratory operations are mainly: sample preparation, detection, culturing, amplification, or cell lysis (Lee and Lee, 2004). There are numerous advantages of these chips, low weight, portability, rapidity, fabrication in mass production, high sensitivity, and necessity of low volume samples, which make them applicable in various biological research areas.

In fact, the main steps for clinical diagnostic in conventional methods (Lee and Lee, 2004) are almost the same in μ TAS devices except with the number of manual handling steps (Figure 2.10). However, some of these steps (e.g. grow/culture cells, or amplification of nucleic acid) may not be necessary in μ TAS devices, since the specificity and selectivity in these devices can be higher than the one in conventional methods.

Among the MEMS based methods for the detection of biological analytes, there are mainly four different methods: optical, mechanical, magnetic, and electrochemical and their combinations (Figure 2.11) (Bhattacharya et al., 2007).

Optical detection: In this method, detection can be done by labeling or label-free. In labeling strategies, fluorescent dye molecules, quantum dot labels, metal colloid labels are generally used. The working principle for label based optical detection is such that, DNA molecule is conjugated with a dye molecule with a specific excitation and emission wave length and then monitoring this excitation by using optic devices like fluorescence microscope, surface plasmon resonance enhanced fluorescence, fiber optic sensor arrays etc. On the other hand, in label free detection, imaging surface plasmon resonance (SPR) and imaging ellipsometry are commonly used. The major disadvantages in optical detection are the necessity of expensive optical devices and the necessity of experts to analyze the results. Although the resolutions of these devices are relatively low, they are preferred due to rapid reach of the results (Bally et al., 2006).

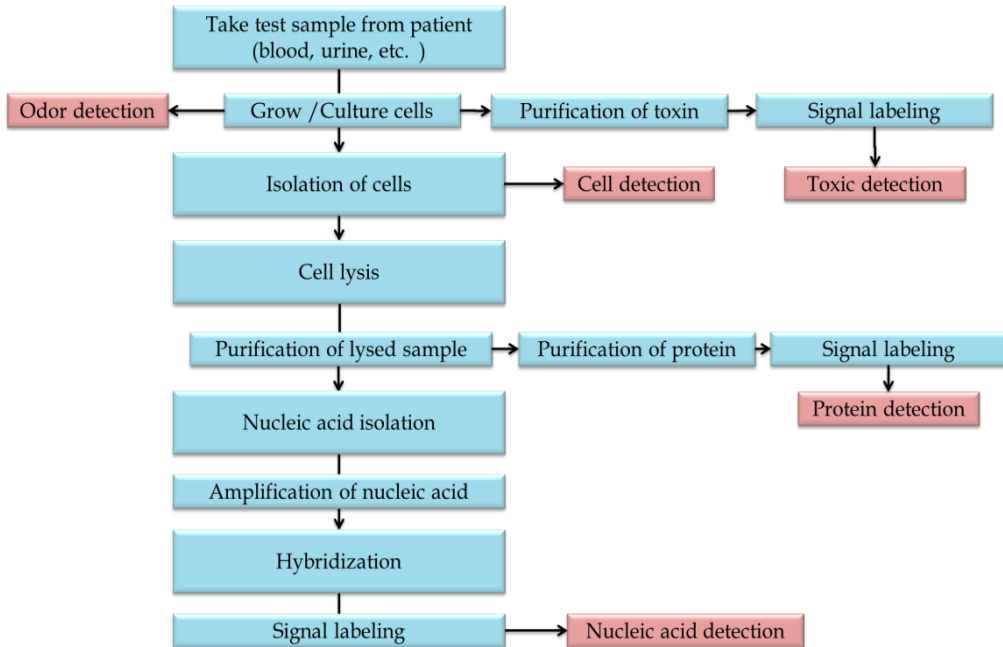


Figure 2.10. Main steps of diagnosis with μ TAS.

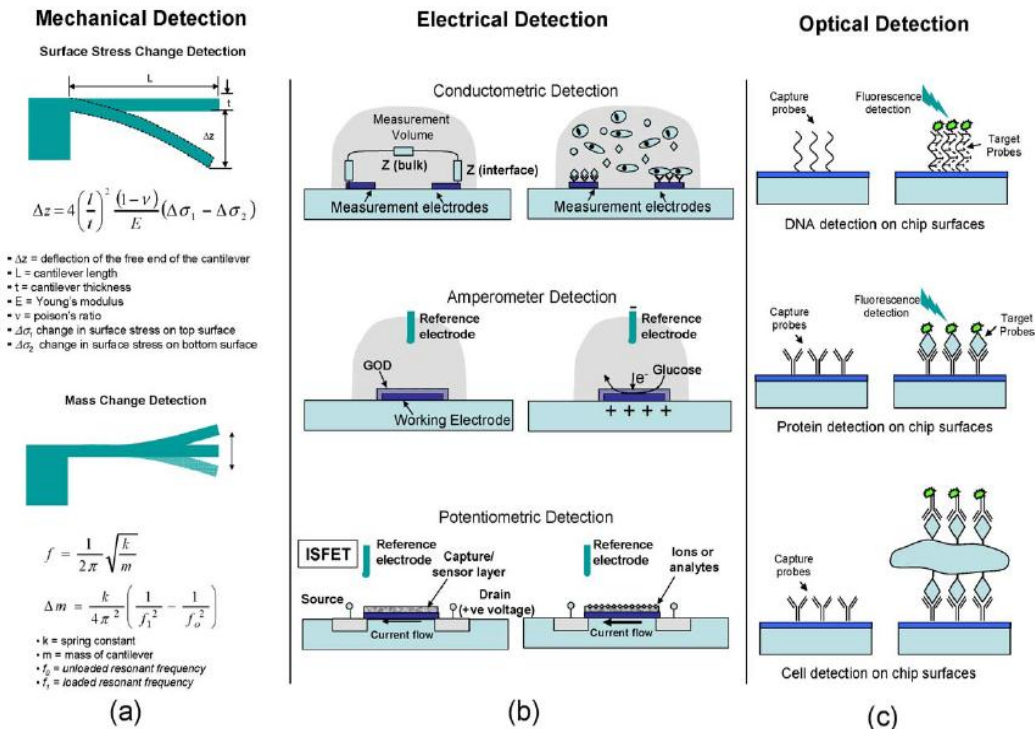


Figure 2.11. Magnetic, electrical, and optical detection strategies (Bhattacharya et al., 2007).

Magnetic detection: It is based on conjugation of paramagnetic and ferromagnetic nanoparticles to biological analytes. The dimensions of these particles change between 0.5 μm to 10 μm and can be produced by using different methods. For example, ferrum oxide nanoparticles can be produced by covering polymer particles with ferrum oxide. Although producing magnetic nanoparticles is easy and its application is wide, the use of magnetic nanoparticles does not give reproducible results at every point of sensor and does not offer high sensitivity, which is required for mutation detections. Moreover, magnetic sensors do not have multiple detections of biological analytes with one sensor and magnetic particles have the possibility of reacting with buffer solutions used in experiments (Palecek and Fojta, 2007).

Mechanical detection: Mechanical sensors have two different sensing strategies: (1) determination of change of surface stress, (2) determination of mass change. Biochemical reaction on the cantilever surface results in a change of stress. Adsorbed biological analytes causes the cantilever move down and results in stress change. Spring constant, which is one of the design parameters, can be decreased to increase stress sensitivity. In determining mass change, cantilever surface is activated by using complementary of biological analyte. When the fluid is passed over microcantilever, active sites adsorb biological analytes and results to a change in resonance frequency of cantilever. Although there is still research going on cantilevers, the sensitivity of cantilever is questionable since its resonance frequency is affected from environment, fluid velocity, etc. (Fritz et al., 2000).

Electrochemical detection: It includes amperometric, potentiometric and conductometric detection. It allows one to transfer electronic output signal of biological reaction to macroscopic environment, and the magnitude of this signal depends on the electrode surface area and the reaction on the surface rather than the reaction volume as it is in the optical detection. Moreover, it is possible to fabricate the microelectrodes directly in the micro channels by using micro fabrication technology. Therefore, electrochemical detection for integration of microfluidic chips is the most appropriate detection strategy (Verpoorte and De Rooij, 2003).

2.4.3.1 Use of MEMS Based Methods for the Detection of MRSA

The classification of the developed biosensors for the identification of MRSA can be done either by the type of detection or by the biological analytes used in the detection. In this study, the classification is made according to the biological analytes for elucidating the sensitivity and specificity of the biosensors in relation to the selected agents. There are five different biological analytes studied by researchers to detect MRSA by using MEMS based devices: odor, cell, modified bacteriophage, toxin gene, and *mecA* gene.

In the detection of volatile organic compounds (odor) produced by MRSA, methicillin sensitive *Staphylococcus aureus* (MSSA), and *S. aureus*, an electronic nose which has an array of 32 carbon black polymer composite resistive sensors is used for analyzing the specimens taken from the infected parts of patients' ear, nose, and throat (Dutta et al., 2005). The electronic nose consists of two parts: A detection system and an analyzing system. Detection is based on the decrease in conductance between carbon sensors, which increases the total resistance, due to the expansion of carbon surfaces when odor is sniffed by the device. Without necessitating culturing before sniffing, the analysis of the signals taken from the array is done by using exploratory techniques like principal component analysis, self-organizing map network, and Fuzzy C Means. Then, three different types of bacteria are analyzed by using artificial neural network (NN) classifiers to evaluate the classification performance. Among the NN classifiers, Radial Basis Function Network (RBF) gives an accuracy of the system, which is above 99%. However, it is very hard to differentiate species, since the acquired data is very complex and requires detailed analysis. In the recent study of (Boedicker et al., 2008), a PDMS based microfluidic chip is developed to form nanoliter droplets to determine MRSA susceptibility to antibiotics (ampicillin, oxacillin, cefoxitin, vancomycin, and erythromycin) and to differentiate MRSA and MSSA from the specimens of human blood plasma. Detection principle is based on the confinement of a single cell, fluorescent dye, and antibiotics into a plug. The increase in fluorescence intensity in these plugs presents the resistance of the bacteria to the antibiotic in the plugs. This "stochastic confinement" based detection allows rapid MRSA detection and antibiotic susceptibility testing without prior incubation of samples. The time to reach the result is directly proportional to the size of the plugs and independent from the initial concentration of the sample and it takes about two hours for 1 nL plugs with bacterium. The limit of detection is about 10^5 CFU/ml. In the study of Guntupalli et al. (Guntupalli et al., 2008), a bacteriophage, which has specific lytic activity to *S. aureus* and MRSA, was used as a bio selective agent. This bacteriophage was adsorbed on the glass surfaces using Langmuir–Blodgett (LB) technique with a sensitivity of 10^6 CFU/ml to form a monolayer. The advantage of the immobilization technique, which is the reduced non-specific binding, was merged with quantification capability of a light microscope system to accelerate the detection of MRSA. The detection was performed in the aqueous samples with concentrations ranging from 10^6 to 10^9 CFU/ml without labeling and preincubation of bacteria. However, the authors stated that it is necessary to analyze one more analyte (e.g., PBP2a, or *mecA* gene) other than the bacteriophage to ensure the specificity of the test.

In detection of genes, it is necessary to lyse the cells, purify the sample and, if the amount of biological analyte in the sample is too low to be detected, it is necessary to amplify either the nucleic acid or the output signal or both of them to have more accurate results. Nucleic acid amplification can be done by using PCR, one cycle of which is composed of template denaturation, primer annealing, and primer extension in a thermal cycler. At each cycle, the amount of the target sequence is doubled. When the fluorescently labeled oligonucleotide probes or DNA stains are used during PCR process, the product of PCR allows quantitative results that can be analyzed in real time (real time PCR). There are also different isothermal nucleic acid amplification techniques like loop mediated amplification (LAMP) (Aryan et al., 2010), transcription mediated amplification (TMA) (Moller et al., 2008), nucleic acid based amplification (NASBA) for selective amplification of RNA (Compton, 1991), rolling circle amplification (RCA) driven by DNA polymerase (Lizardi et al., 1998) and recombinase polymerase amplification (RPA) (Piepenburg et al., 2006).

In the study of House et al. (House et al., 2010), a four well PDMS based PCR chip was used in the detection of MRSA for three different samples, which are purified DNA, crude DNA, and boiled culture.

Amplification of DNA concentrations as low as 3.73 pg/ μ l was shown possible with the chip, which was made of PDMS, parylene, and a glass plate to reduce the cost. On the other hand, in the study of (Sista et al., 2008), the development of electro wetting-based digital microfluidic platform was presented for rapid immunoassays, DNA amplification by using real time PCR, and sample preparation for MRSA detection from whole blood samples. A cartridge with its chip and cover plate was used in the immunoassays, DNA amplification, and DNA sample preparation. The cartridge had inlet and outlet ports, droplet-dividing units, and an electrode array for moving droplets inside the package, while the cover plate was used to have parallel configuration (Figure 2.12). It was shown possible to perform on-chip immunoassay protocols in less than 10 min and to amplify 400 bp genomic DNA of MRSA in 12 min for 40 cycle by using real time PCR technique with the cartridge.

Integration of microfluidic device with RPA was successfully performed by using a lab on a foil cartridge (Lutz et al., 2010). This cartridge was a product of simple fabrication of a cyclic olefin polymer (COP) and at each cartridge; six identical fluidic devices were fabricated with 30 different reaction chambers (Figure 2.13). It was shown possible to perform different microfluidic unit operations like storage, mixing, and dividing the sample into different fragments. The reagents for RPA were prestored and their delivery to reaction zones is controlled by centrifugal forces, which were generated by a modified type of commercially available thermal cycler for RT-PCR (Rotor-Gene 2000, Corbett Life Sciences, Australia). The analyzed DNA sample had the size of 420 bp as a part of *mecA* gene of *S. aureus* and all reactions are performed at 310.15 K. The detection was performed optically by measuring real time fluorescence intensity at the reaction chambers. The detection limit of the cartridge was less than 10 copies with no cross contamination between the reaction zones. Detection time was less than 20 min including the time necessary for loading samples to the cartridge and placing the cartridge into the Rotor-Gene 2000.

The integration of magnetic bead based detection with LAMP process was studied recently by (Wang et al., 2011a). A microfluidic chip, which consists of three structural layers made of glass, PDMS, and metals, was presented for the specific detection of MRSA directly from three types of specimens, which are sputum, serum, and milk. Protein A (*spa*) gene was used for identification of *S. aureus*, and *mecA* gene was used for the detection of methicillin resistance in the identification of MRSA.

Hybridization was conducted by using magnetic bead conjugated complementary probes. Cell lysis, DNA isolation, and amplification by using LAMP technique were performed totally in the microfluidic device. The amplified products were analyzed by using either gel electrophoresis or spectrophotometer, which implies the integration ability of the device with automatic systems. The high specificity of the detection procedure was confirmed by analyzing ten different strains of MRSA and MSSA, and seven types of Gram-negative and Gram-positive bacteria. The limit of detection is determined as 10 fg/ μ l of DNA with a turnaround time of approximately 60 min.

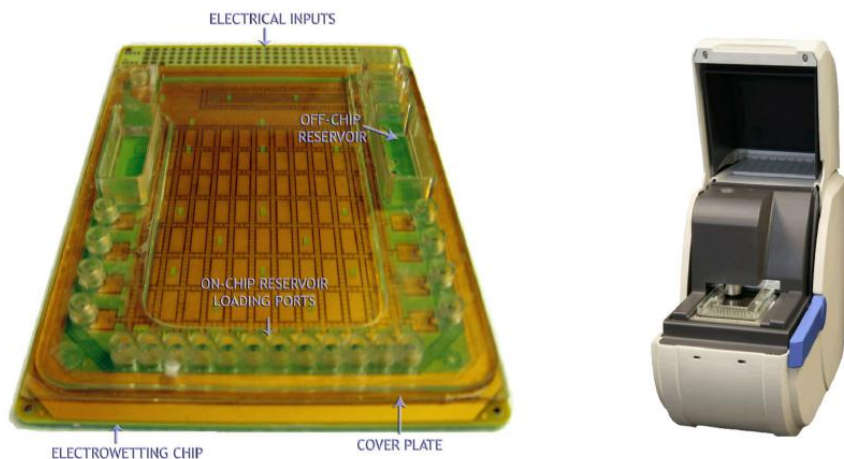


Figure 2.12. A picture demonstrating microfluidic cartridge and its control instrument developed (Sista et al., 2008).

In a latter study, the suitability of microfluidic foil cartridges for real time PCR was demonstrated by Focke et al. (Focke et al., 2010a). Micro thermoforming by soft lithography (μ TSL) was used in the fabrication of microfluidic cartridges. The design of the cartridge was different from the one used in the study of (Lutz et al., 2010), to distribute sample evenly to the reaction chambers, to facilitate efficient heating during real time PCR, and to align it in the Rotor-Gene 2000. The cartridge had four identical microfluidic devices with 32 reaction chambers (Figure 2.14). In the system, Exfoliatin Toxin A (*ExfA*) gene of MRSA was studied with pre-stored dry reagents and probes and the microfluidic flow was controlled by centrifugal forces. The limit of detection was less than 10 copies of DNA and process time for detection was 110 min with a high specificity, which was controlled by using seven different genetic subtypes of MRSA.

Preamplification can be done to increase sensitivity of real time PCR for low quantity genes. In the study of Focke et al. (Focke et al., 2010b), primary amplification and secondary real time PCR were integrated with a centrifugal lab on a foil disk to detect *ExfA* gene. The disk contained two identical devices with 14 different reaction chambers, mixing chambers and valves at each device (Figure 2.15). The efficiency of amplification was found as 85% with no cross contamination over the wells for 10 set of thermocycles. The limit of detection was as low as seven copies of DNA with great reproducibility. Moreover, the applicability of the microfluidic foil cartridge for the preamplification of multiplex PCR, in which amplifications of different nucleic acid targets were conducted by using multiple primers and reagents, was demonstrated by using four target genes. In the study of (Shen et al., 2010), multiplex PCR was performed for 20 different genes of four species (MRSA, MSSA, *Candida albicans*, *P. aeruginosa*, and *E. Coli*) by using SlipChip platforms which had either 40 or 384 wells. The dry reagents were prestored in each well without cross contamination avoiding any need of pumps to divide the reagents. The fluid was controlled by sliding two plates, the well geometries of which were different, relative to each other with the help of a program.

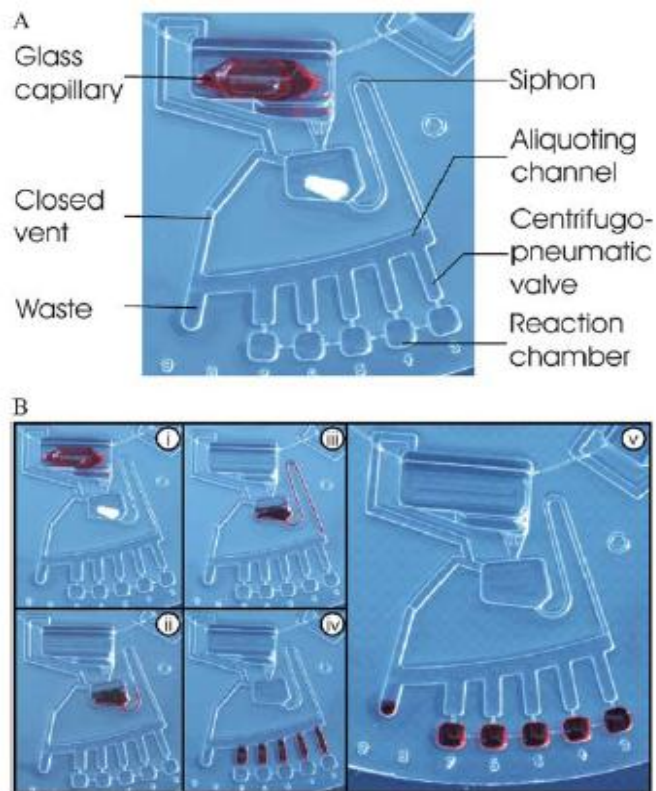


Figure 2.13. A picture demonstrating lab-on-a-disc cartridge developed (Lutz et al., 2010).

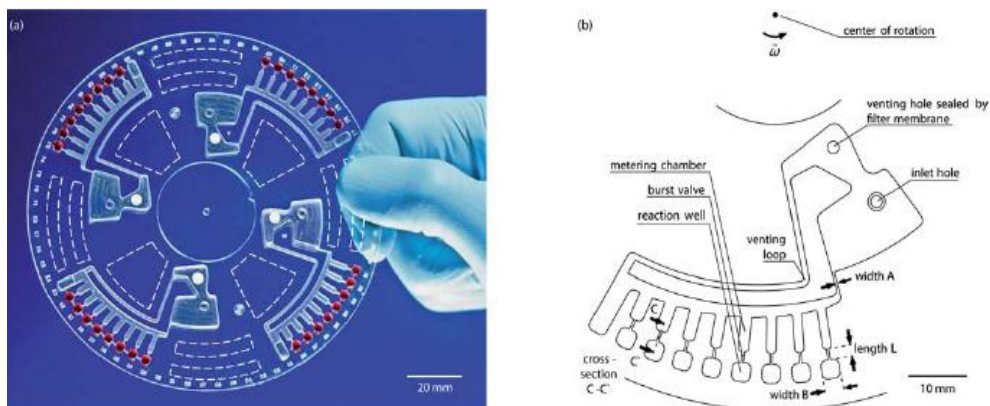


Figure 2.14. A picture demonstrating lab-on-a-disc system developed (Focke et al., 2010a).

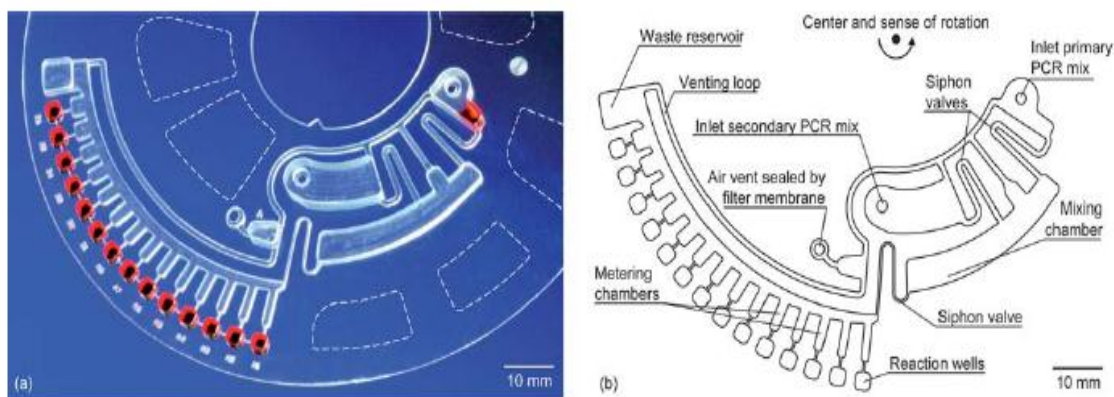


Figure 2.15. A picture demonstrating lab-on-a-disc cartridge developed (Focke et al., 2010b).

The detection of amplified samples can also be done by using capillary electrophoresis. The integration of PCR amplification with capillary electrophoresis and MRSA detection in a portable device was performed in 2004 (Figure 2.16) (Lagally et al., 2004). The presence of MRSA in blood samples was analyzed by detecting 219 bp part of *femA*, whose presence indicates the specie of *S.aureus*, and 310 bp part of *mecA* genes. The system consisted of portable PCR-CE microchip, detection unit and a computer to analyze results. Precultured and diluted samples with a concentration of 10000 cells/ μ l were used for 30 cycle of PCR amplification in less than 20 minutes. In the study of Naikare et al. (Naikare et al., 2009), multiplexed isothermal amplification of products of bacterial cell lysis was followed with detection of *femA* and *mecA* genes by using cycling probe reaction and capillary electrophoresis without necessity of purification of lysed cell sample. The limit of detection was $\sim 10^4$ CFU/ml with a time to result of three hours without culturing of bacteria.

In the above techniques, the hybridization reaction was carried out in micro reactors. On the other hand, it is also possible to detect biological analytes on modified surfaces such as thin film biosensors. In the study of (Tombelli et al., 2006), two different immobilization techniques (usage of either biotinylated or thiol derivatised synthetic probes) were studied on active surface of piezoelectric device for detection of 27-mer specific region of *mecA* gene of methicillin resistant strain *S.aureus* subspecies *aureus* Rosenbach (ATCC 700699) for piezoelectric biosensor. It was observed that the frequency change for the biotinylated surface was six times higher than the change for thiol modified surface. In the study of (Lindsey et al., 2008), a thin film biosensor was developed to detect visually *mecA*, *femB*, and *tuf* genes

of *S. aureus* directly from positive blood culture with a detection limit of 10 fM in 90 minutes. The detection strategy was based on the surface activation by using capture probes and hybridization with target sequence.

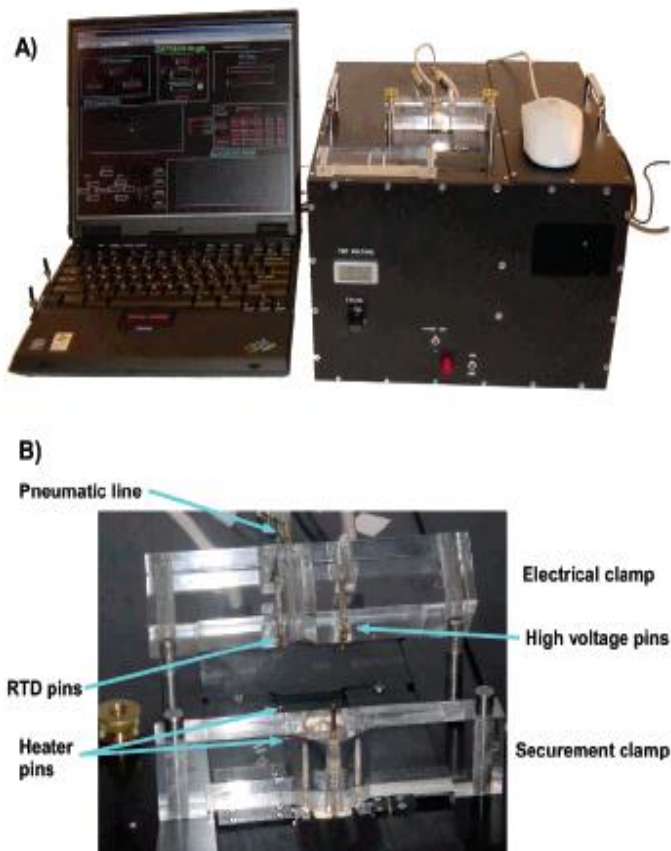


Figure 2.16. A picture demonstrating portable PCR-CE analysis system developed (Lagally et al., 2004).

After that detector probe was hybridized to the target sequence and antibody/horseradish peroxidase (HRP) conjugate adsorbed to the probe for signal amplification. The substrate, 3,3',5,5'-tetramethylbenzidine (TMB) was reacted by HRP to produce precipitate, whose color is visually detectable when its thickness increases at least 20 Å and the limit of detection by charge-coupled device is 10 fM (Jenison et al., 2001). This method is advantageous since it does not necessitate to amplifying nucleic acid. Therefore it eliminates the cross contamination due to amplification samples and it does not necessitate optical instrument for detection. Although the limit of detection is good enough, the detection limits and time to result can be lowered to have more rapid and accurate detection. In the study of (Klonoski et al., 2010), the fastest signal amplification method was presented to detect *mecA*, *femB*, and *tuf* genes of *S. aureus* directly from positive blood culture. The activation of surfaces by immobilizing 5'-I modified capture probes was done and after that, target sequences were hybridized to capture biotin modified signal probe. Two signal detection protocols were compared: standard detection and polymer enhanced detection (PED) protocol. In standard detection strategy, biotin labeled probe was detected directly by anti-biotin antibody/HRP that was used to enhance signal by TMB reaction. On the other hand, in PED, the probe was detected by streptavidin/polymer complex, which increased the adsorbed number of HRP molecules. The detection limit in standard detection was enhanced by 25-fold in PED protocol (detection limit is 1 fM) in 25 minutes. In another study, researchers (Gebala et al., 2011) used a self-assembled monolayer modified microelectrode array, which was composed of 32 individually

addressable gold electrodes to detect MRSA for electrochemical detection (Figure 2.17). Gold electrodes ($70\ \mu\text{m} \times 70\ \mu\text{m}$) were modified by using thiolated capture probe DNA and 11-mercapto-1-undecanol and, hybridization occurred with the complementary target strand, which was pre-modified with ferrocene units at its 5' end. Intercalation of biotinylated intercalator and avidin/alkaline phosphatase (AP) conjugate was done with further modification. With the enzyme amplification, the limit of detection was as low as 10 pM. In a recent study (Wang et al., 2011b), label free detection of 30-mer DNA of specific part of MRSA on graphene oxide modified glassy carbon electrode with a diameter of 3 mm was studied. Electrochemical impedance spectroscopy (EIS) was used to analyze the electron transfer and diffusion processes during DNA adsorption on the modified surface with different concentrations of target DNA. Although it is label free detection, the achieved detection limit is 100 fM, which is quite good.

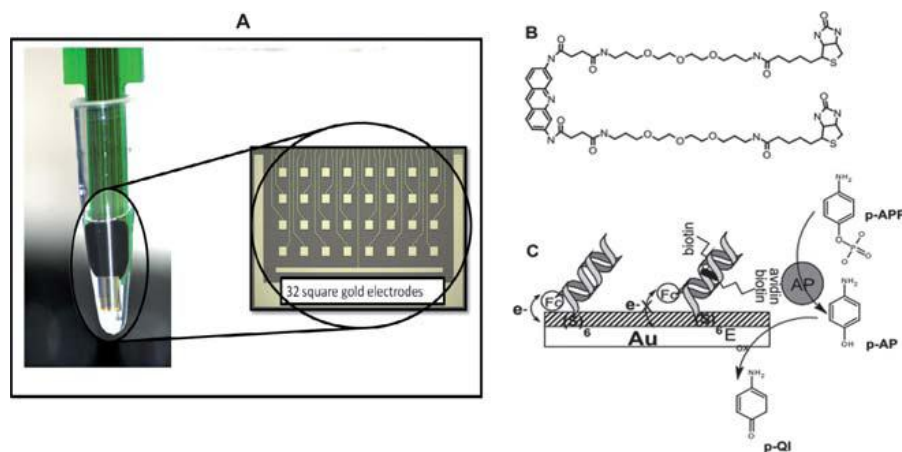


Figure 2.17. A picture demonstrating the dipstick type microelectrode array and its detection mechanism (Gebala et al., 2011).

2.4.3.2 Use of MEMS Based Methods for the Detection of VRE

In the literature, a study related to the detecting VRE by MEMS based sensor could not be found. However, the detection of vancomycin resistance genes by using cyclic probe technology was studied by Modrusan et al. (Modrusan et al., 1999). The time to result was three hours for identification of 40 enterococcal isolates and it was possible to differentiate the resistant types by using this technology. On the other hand, the detection of VRE was also performed by using FePt magnetic nanoparticles (3-4 nm in diameter) with a limit of detection $<10^2$ CFU/ml in less than one hour (Gu et al., 2003).

2.5. Commercialized Products

There are several products approved by U.S. Food and Drug Administration (FDA) for *in vitro* diagnostics of MRSA (Table 2.1) (FDA, 2011). The products are allowed for use in clinics as a clinical aid in conjunction with other laboratory tests that are used in the identification and diagnosis of MRSA from infected patients' samples. These products can be classified in four categories: Culture media, nucleic acid amplification test systems, test kits/assays, and antimicrobial susceptibility test systems. In the identification of MRSA, the most frequently used target specimens are nasal swab, and skin-and-soft tissue wounds. In the list of culture media products, the mediums are selective chromogenic for qualitative detection of MRSA. The medium contains selective antibiotics (e.g., ceftiofime) and antifungal substrates to impair the growth of yeasts, Gram-negative and Gram-positive bacteria (especially *Staphylococcus epidermidis*) other than MRSA.

Table 2.1. Commercial FDA approved products as a clinical aid to identify MRSA.

Device Name (Company)	Target Specimen	Inoculation	Test Methodology	Target Sequence	Turnaround Time	Special Instrument Requirement	Clinical Sensitivity /Specificity	LoD	510 (k) Number
Culture Media									
MRSASelect (BIO-RAD)	Skin and soft-tissue wound	Direct from specimen collection devices	Selective chromogenic agar	NA	18 - 28 hours	NA	91.7% / 99.4%	10 ³ CFU/mL	K100589
Remel Spectra™ MRSA (REMEL, INC. as a part of THERMO FISHER SCIENTIFIC)	Nasal swab	Positive blood culture	Selective and differential chromogenic prepared culture medium	NA	24 hours	NA	NA / NA	NA	K092407
Remel Spectra™ MRSA (REMEL, INC. as a part of THERMO FISHER SCIENTIFIC)	Nasal swab	Anterior nares swab	Selective and differential chromogenic prepared culture medium	NA	24 hours	NA	NA / NA	NA	K073027
BBL™CHROMagar™ MRSA II (BECTON DICKINSON & CO.)	Anterior nares	Direct from specimen collection devices	Selective and differential culture media	NA	18 - 28 hours	NA	NA / NA	NA	K092767
BBL™ CHROMagar™ MRSA (BECTON DICKINSON & CO.)	Anterior nares swab	Direct anterior nares specimens	Selective chromogenic agar	NA	24-48 hours	NA	NA / NA	NA	K042812
chromID™ MRSA Agar (BIOMERIEUX, INC.)	Anterior nares swab	Direct from specimen collection devices	Selective and differential chromogenic prepared culture medium	NA	24 hours	NA	NA / NA	NA	K091024
MRSA SCREEN AGAR (MUELLER HINTON W/NACL & OXACIL.) (HARDY MEDIA)									K870649
Nucleic acid amplification test systems									
Xpert® MRSA/SA Blood Culture Assay (CEPHEID)		Positive blood culture	Real-time PCR	Sequence incorporating the insertion site (attBsse) of Staphylococcal mec (SCCmec) for detection of MRSA. Sequence specific to methicillin/Oxacillin resistance (mecA gene)	50 minutes	GeneXpert® Dx System (GX-4 or GX-16 instruments, and the GeneXpert® Dx System Software 1.6b)		250 CFU/test	K101879
Xpert® MRSA/SA Nasal Assay (CEPHEID)									K100822
LightCycler® MRSA Advanced Test (ROCHE MOLECULAR SYSTEMS, INC.)	Nasal swab	Direct from specimen collection devices	Real-time PCR and melting peak analysis	Sequence incorporating the insertion site of the <i>SCCmec</i> in the <i>S. aureus orfX</i> gene	2 hours	LightCycler 2.0 Instrument	NA / NA	240 CFU/swab	K091409
IDI-MRSA™ Assay (INFECTIO DIAGNOSTIC (I.D.I.) INC)	Nasal swab	Direct from specimen	PCR	Presence of SCCmec cassette (genetic element that carries the mecA gene) at orfIX junction (specific to <i>S. aureus</i>).	60 - 75 minutes	Smart Cycler® Instrument	NA / NA	325 CFU/swab	K042357

Table 2.1. Commercial FDA approved products as a clinical aid to identify MRSA (Continued).

Device Name (Company)	Target Specimen	Inoculation	Test Methodology	Target Sequence	Turnaround Time	Special Instrument Requirement	Clinical Sensitivity /Specificity	LoD	510 (k) Number
BD GeneOhm™ MRSA ACP Assay (BD DIAGNOSTICS (GENEOHM SCIENCES, INC.))	Nasal swab	Direct from specimen collection devices	Real-time PCR and molecular beacon technology	Mec Right Extremity Junction genotypes i, ii, iii, iv, v and vii	60-75 minutes	Cepheid SmartCycler II System with Dx Software version 1.7b.	95% / 95%	Approximately 1,250 CFU/swab for Type i, ii, iii, iv, and vii, approximately 625 CFU/swab for Type v	K093346
Xpert™ MRSA/SA SSTI Assay (CEPHEID)	Skin and soft tissue infection swabs	Direct from skin and soft tissue infection swabs	Real-time PCR	Staphylococcal protein A (spa), for methicillin/oxacillin resistance (mecA), and for the staphylococcal chromosomal cassette (SCCmec) insertion event into the staphylococcus aureus chromosomal attB site	Approximately 50 minutes	GeneXpert® Dx System (GX-4 or GX-16 instruments, and the GeneXpert® Dx System Software 1.6b)	NA / NA		K080837
Xpert™ MRSA (CEPHEID)	Nasal swab	Direct from specimen collection devices	Real-time PCR	Sequence incorporating the insertion site (attBsc) of Staphylococcal Chromosome Cassette mec (SCC mec)	75 minutes	Gene Xpert® Dx System	NA / NA	80 CFU/swab	K070462
Test Kits									
MASTALEX™- MRSA RST 501 (MAST GROUP LTD.)			Slide latex agglutination	PBP2' (penicillin binding protein 2')					K062864
MRSA-Screen (DENKA SEIKEN'S)			Slide latex agglutination	PBP2' (penicillin binding protein 2')					K011400
Velogene™ Genomic Identification Assay For MRSA With One-Step Detection (ID BIOMEDICAL CORP.)			Cycling Probe Technology	mecA gene	90 minutes after primary isolation				K010858
Velogene™ Rapid Mrsa Identification Assay (ID BIOMEDICAL CORP.)			Cycling Probe Technology	mecA gene	90 minutes after primary isolation				K990640
Antimicrobial Susceptibility Test Systems									
BBL CRYSTAL MRSA ID SYSTEM (BECTON DICKINSON MICROBIOLOGY SYSTEMS)									K941997
BBL CRYSTAL MRSA ID SYSTEM (BECTON DICKINSON MICROBIOLOGY SYSTEMS)									K926294

LoD = Limit of Detection, NA = Not Applicable

The differentiation of MRSA from the other colonies are done by the split of a chromogenic agent, which results in the growth of colored colonies, in the presence of a specific enzyme of *S. aureus*. The growth of colored (e.g., strong pink, blue, denim-blue, mauve, and green) colonies on the agar plate is the indication of MRSA. There is no need of any special instrument in the analysis since it is done manually. Time to result in the usage of culture media for identification of MRSA is ranging from 18 hours to 48 hours. (Malhotra-Kumar et al., 2010) compared five chromogenic media (Brilliance MRSA (REMEL Inc.), ChromID (BIOMERIEUX), MRSA>Select (Bio-Rad), CHROMagar (CHROMagar Microbiology), BBL™-CHROMagar™ (BD Diagnostics)) for 24 h incubation period of pure isolates and pre-enriched nasal and groin swabs. It is stated that, BBL™-CHROMagar™ (BD Diagnostics) gave the best results for specificity, sensitivity, and positive predictive value among the five types of media. However, cross reactivity with other staphylococcal species were observed on the chromogenic media. Therefore, it is necessary to incubate the media for further 24 hours to increase the sensitivity of all types of the media and an accurate identification method is necessary to confirm the results. The use of nucleic acid detection systems may be useful to settle any query (Rajan et al., 2007).

The basic detection principle of nucleic acid amplification test systems is based on four main steps: isolation of nucleic acid, amplification, hybridization, and detection. RT-PCR or PCR is used to amplify the target sequence(s) of the specimen. After completion of amplification, a melting curve analysis or analysis of molecular beacons with different fluorescence properties is performed to detect hybridization. *mecA* gene, which is the indication of methicillin/oxacillin resistance, *orfX* gene, which is specific to *S. aureus* staphylococcal protein A (*spa*), and chromosomal *attB* site for the staphylococcal chromosomal cassette (SCC*mec*) insertion event into the *S. aureus* are used as target sequences to detect MRSA. The specified turnaround time for nucleic acid amplification systems ranges from 50 min to two hours although the tests are performed from the direct specimen collection devices. The analyses of results are performed automatically by using special instruments and software specific to these instruments and a report of the results can be generated. The limit of detection is also different for the products. Xpert™ MRSA (CEPHEID) has 80CFU/swab, while BD GeneOhm™ MRSA ACP Assay (BD Diagnostics (GENEOHM Sciences, Inc.)) has approximately 1250 CFU/swab for Mec Right Extremity Junction Genotypes i, ii, iii, iv, and vii, and approximately 625 CFU/swab for Type v with a clinical sensitivity and specificity, of both 95%. In the aspect of test kits/assays, target analytes for identification of MRSA are PBP2' and *mecA* gene. Slide latex agglutination or cyclic probe technology are used in different products as a test methodology. Moreover, there are antimicrobial susceptibility test systems, in which the analysis of the results is done manually. The identification principle of BBL Crystal MRSA ID system depends on the fluorescence detection of a fluorescent indicator, which becomes active when dissolved oxygen in the medium is consumed by bacteria. The resistance to methicillin/oxacillin can be detected by adding oxacillin into the medium (Knapp et al., 1994).

HainLifescience (Germany) developed four different products for MRSA detection on swabs taken from nose, throat, skin, and wounds for clinical and research use in Europe. The products require different times to get result from the specimen depending on the use of cultured or noncultured specimen. Times to result for GeneQuick® MRSA and GenoType® MRSA Direct are 2.5 hours and 4 hours, respectively, and these products do not necessitate culturing of the specimen. The other two products, GenoType® MRSA and GenoType®*Staphylococcus* require primary culture and the time to result is 4 hours for both. The principle of detection for all products is based on the DNA-STRIP® technology, except GeneQuick® MRSA that is based on GenoQuick® technology. In both technologies, three steps are necessary for detection of *mecA* gene: DNA isolation, DNA amplification, and hybridization (Prere et al., 2006). Following DNA isolation with enzymatic lysis, amplification is performed by using PCR. In DNA-STRIP® technology, hybridization is done on strips, which are further modified with a streptavidin conjugated AP and its substrate. Then, hybridization is made visible with a colorimetric reaction, which can be observed manually other than automatically. On the other hand, in GenoQuick® technology, hybridization is performed with specific probes that have a gold binding site. After hybridization, gold particles are adsorbed from the test strip and gold particle conjugated hybrid is adsorbed to the specific sites on the strip while moving in a lateral flow of buffer. This results in a specific visible band for the specimen. It was stated that the IDI-MRSA™ Assay (Infectio Diagnostic (I.D.I.) Inc.) is the most sensitive product when it is compared with CHROMagar MRSA (BD Diagnostics, Sparks, MD), GenoType® MRSA Direct PCR assay (HainLifescience (Germany)), MRSA ID (Biomerieux Inc.), and MRSA>Select (Bio-

Rad) (Bischof et al., 2009; van Hal et al., 2007). The sensitivities for the target specimens of nasal, groin and axilla, and overall are 94%, 80%, and 90%, respectively. Consequently, LightCycler® MRSA Advanced Test demonstrated equivalent sensitivity and specificity with BD GeneOhm™ MRSA Assay (Peterson et al., 2010).

2.6. Discussion of Detection Methods for MRSA and VRE

In conclusion, high sensitivity and specificity, and short turnaround time are mainly desired properties of *in vitro* diagnostics for the identification of MRSA and VRE since the aim is rapid identification of target analyte with accurate positive test results for early and appropriate treatment. Conventional and MEMS based methods, and commercial products for the detection of MRSA and VRE have been considered above for specimens taken from infected patients' samples (e.g., blood, wound, nose, and throat). Present conventional methods are mostly limited by the incubation time of media to grow culture for at least 24 hours to increase the specificity and sensitivity (Brown et al., 2005). Therefore, there is a potential that the lab-on-a-chip devices will replace the conventional methods by which patients are diagnosed. Thus, the use of integration of molecular methods and MEMS, detect genes which indicate methicillin and vancomycin resistances, can be a common approach in identification of MRSA and VRE.

There are different micro devices for micro culturing, cell lysis, PCR, capillary electrophoresis, etc. which are used individually or in combination. However, in the literature, there is not yet a compact micro device reported to handle sample directly taken from the patient and analyze it on a chip to identify the MRSA and VRE without the need of any macro device. This is because the novel technology to combine all of the advantages of MEMS into a device is not yet fully developed. Currently, knowledge of theory behind the microfluidics and nanofluidics, the surface chemistry, and transport of the samples in the microfluidic channels and reservoirs affect the detection limits. The design limitations of the MEMS based devices can be numerous and it is essential to take care of them at the beginning stages of the development. Therefore, it is necessary to work in collaboration with different disciplines to tackle challenges in the field of clinical diagnosis and to meet the demands of clinicians.

CHAPTER 3

THEORY OF ELECTROCHEMICAL DETECTION

In this chapter, the theory related to electrochemical detection will be given in detail. Also a model study will be presented for which a simulation code was prepared to realize current - potential relationship by using differential pulse voltammetry with the help of MATLAB programming language.

3.1. Rate Determining Reactions in Electrochemical Analysis

The three steps for electrode reactions are simply mass transport of the electroactive species to the surface, the reaction at the interface, and desorption of the product back to the bulk solution. The overall rate of the reactions depends on the slowest step, which can be either mass transport or the reaction itself. The slowest step is determined by considering both the type of the electro active specie and the experimental conditions (Wang, 2006).

The mass transport of species for electrochemical analysis can be in three ways: diffusion, convection, and migration. In voltammetric analysis of species, it is assumed that mass transport of the species occurs only by diffusion. Thus, convection can be assumed negligible by using non-flow solution (Heinze, 1984). Due to size of the electrodes and the ratio of the volume of the electrolyte solution to the area of the electrode, there are three limiting cases in diffusion. In the first limit, the ratio of volume to the area can be very low, which results in negligible mass transport of species and no diffusion gradient. In the second, for an increase in the ratio of V/A, the semi-infinite planar diffusion of the species can be obtained. In the third limiting case, the ratio of V/A is increased by ultra microelectrodes, which reverses the situation and the diffusion is based on the size and geometry of the electrodes (Heinze, 1993).

A redox reaction on the surface is as follows:



and oxidation of electro active specie with a linear potential scan in a static solution is analyzed by scanning the potential from an initial potential to final potential. When the potential is close to the standard potential (E^0) from negative side, the concentration of the specie rapidly decrease by obeying the Nernst Equation as given below:

$$E = E^0 + \frac{2.3RT}{nF} \log \frac{C_O(0,t)}{C_R(0,t)} \quad (3.2)$$

Decrease in the concentration results in an increase of the diffusion-layer thickness. This increase determines the shape of the voltammogram after the concentration reaches zero. The potential is further applied positively and the peak shaped voltammogram is obtained (Figure 3.1).

The rates of the forward and reverse reactions are presented as:

$$V_f = k_f C_R(0,t) \quad (3.3)$$

$$V_b = k_b C_O(0,t) \quad (3.4)$$

where k_f and k_b are heterogenous rate constants which rely on operating potential as follows:

$$k_f = k^0 \exp[-\alpha nF(E-E^0)/RT] \quad (3.5)$$

$$k_b = k^0 \exp[(1-\alpha)nF(E-E^0)/RT] \quad (3.6)$$

where k^0 is standard rate constant and α is the transfer coefficient. The value of k^0 indicates the type of the reaction between the electroactive specie and the electrode material. The value of the transfer coefficient demonstrates the shape of the voltammogram. If it is near to 0.5, the shape will be symmetric.

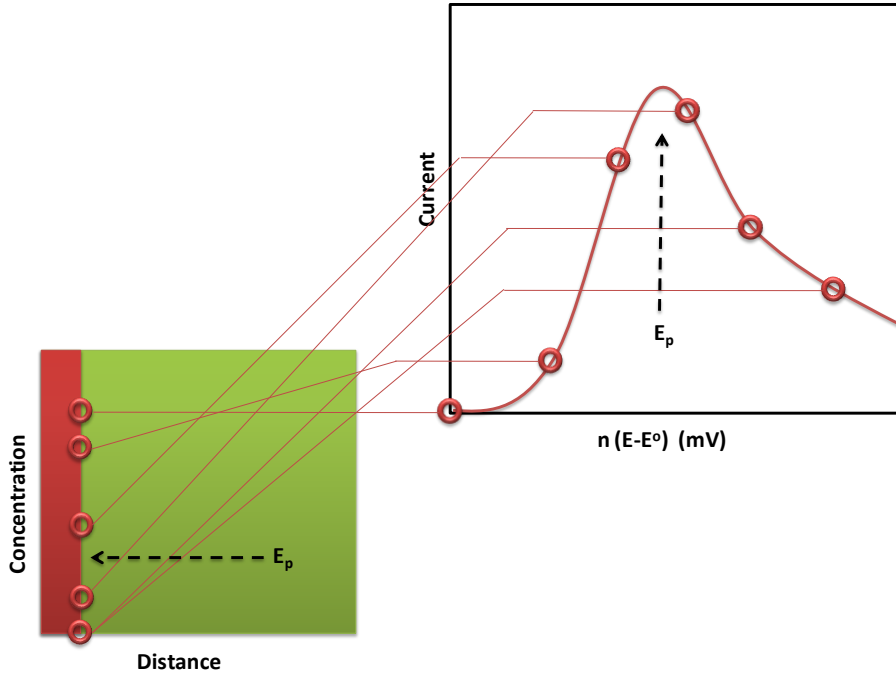


Figure 3.1. Concentration profile and resulting voltammogram for a linear potential scan (Wang, 2006).

The forward and backward currents are proportional to the rates of reactions and the net current is calculated as follows:

$$i_{\text{net}} = i_f - i_b = nFA[k_f C_R(0,t) - k_b C_O(0,t)] \quad (3.7)$$

The substitution of the expressions for rate constants leads to *Butler-Volmer* Equation:

$$i = nFAk^0 \left\{ C_R(0,t) \exp \left[-\frac{\alpha nF(E-E^0)}{RT} \right] - C_O(0,t) \exp \left[\frac{(1-\alpha)nF(E-E^0)}{RT} \right] \right\} \quad (3.8)$$

The concentrations of R and O on the electrode surface at any time is as follows (Aoki et al., 1984):

$$C_R(0,t) = C_R^* (\pi D)^{-1/2} \int_0^t (i/nFA)(t-u)^{-1/2} du \quad (3.9)$$

$$C_O(0,t) = (\pi D)^{-1/2} \int_0^t (i/nFA)(t-u)^{-1/2} du \quad (3.10)$$

Where C_R^* is the bulk concentration of R, t is time, A is for the area of the electrode, and i is the total current. The sign of current is positive for anodic processes. Equations 3.9 and 3.10 are valid with the following assumptions:

- The redox reaction occurs on the surface only.
- The semi infinite linear diffusion is applicable for the mass transport of electroactive species and the diffusion coefficient, D , is same for each specie.
- Initially there is only R on the surface.

By substitution of Equations 3.9 and 3.10 into Butler Volmer Equation (Equation 3.8) and with some algebraic manipulations, the following equation is obtained (Aoki et al., 1984):

$$\frac{i}{i_d} = \sqrt{\pi} \Lambda \exp(\alpha \xi) \left[1 - \pi^{-1} (1 + e^{-\xi}) \int_0^x \left(\frac{i}{i_d} \right) (x-u)^{-1/2} du \right] \quad (3.11)$$

where

$$i_d = nFA C_R^* \left(\frac{D}{\pi \delta} \right)^{1/2} \quad (3.12)$$

$$\Lambda = k^0 \left(\frac{\delta}{D} \right)^{1/2} \quad (3.13)$$

$$\xi = nF(E-E^0)/RT \quad (3.14)$$

$$x = t/\delta \quad (3.15)$$

The developed equations above are valid for any potential time wave form.

The aim of the electrochemical detection is to get a current response which is proportional to the concentration of the target analyte on the working electrode. Therefore, the redox reaction on the electrochemical cell is monitored by using potential techniques. There are different controlled potential techniques with different detection limits and shape of responses (Wang, 2006). Among them, Cyclic Voltammetry (CV) and Differential Pulse Voltammetry (DPV) are commonly used in the detection of biological analytes. CV with its 10^{-6} M (1 nmol/ml) detection limit is widely used for the analysis of electrochemical reactions due to its ability to reveal thermodynamics of redox processes and the kinetics of electron transfer reactions (Wang, 2006). In electrochemical analysis of redox reactions, CV is used firstly to find the locations of redox potentials of species. In the analysis, the potential is applied to the working electrode linearly using a triangular potential waveform in quiet solution (Figure 3.2). While applying potential to the electrode, the resultant current is measured, and a graph of potential vs. current is obtained, which is known as cyclic voltammogram. In the analysis of current and potential on the working electrode by potentiostat, a nonpolarized reference electrode (generally Ag and AgCl) is used with a counter or auxiliary electrode. The current flows through the working and the auxiliary electrodes while no current is passed through reference electrode due to its high impedance.

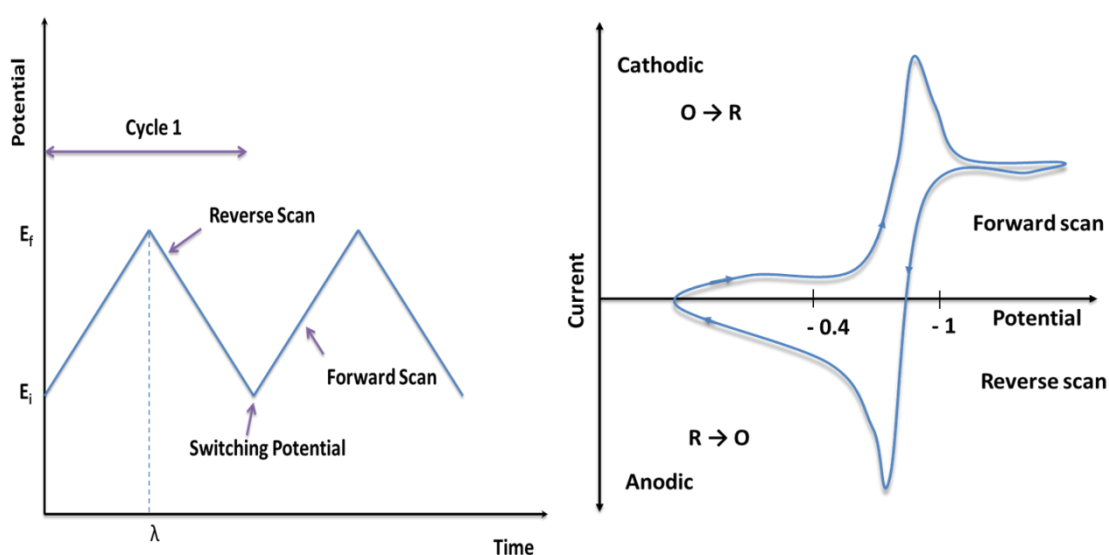


Figure 3.2. Schematic diagrams of (A) potential time waveform in CV (B) cyclic voltammogram for a reversible system (Wang, 2006).

On the other hand, Differential Pulse Voltammetry (DPV) is used for electrochemical analysis of organic and inorganic substances with 10^{-8} M (10 pmol/ml) detection limit. The potential is applied to the working electrode as a step functional change with pulses in DPV. In Figure 3.3, ΔE is the pulse height, τ is the interval between two pulses, δ is the pulse width, and v is the potential sweep rate. The current on the working electrode is sampled twice: before the pulse and after the decay of current charge (after ~ 40 ms) (Wang, 2006). The current is calculated by subtracting the first reading on the current from the second one, and the resulting current peaks are plotted against applied potential interval.

The Equations 3.11 – 3.15 can be arranged further for differential pulse voltammetry by adding equations related to applied potential waveform (Equations 3.16 and 3.17) (Aoki et al., 1984):

$$E = E_i + (m-1)v\tau' \quad \text{for } (m-1)\tau' < t < (m-1)\tau' + \tau \quad (3.16)$$

$$E = E_i + (m-1)v\tau' + \Delta E \quad \text{for } (m-1)\tau' + \tau < t < m\tau' \quad (3.17)$$

where $\tau' = \tau + \delta$ and $m = 1, 2, \dots$

Equations 3.16 and 3.17 are arranged as follows:

$$\xi = nF(E_i - E^0)/RT + (m-1)w(1+r) \quad \text{for } (m-1)\tau' < t < (m-1)\tau' + \tau \quad (3.18)$$

$$\xi = nF(E_i - E^0)/RT + (m-1)w(1+r) + \Delta\xi \quad \text{for } (m-1)\tau' + \tau < t < m\tau' \quad (3.19)$$

where

$$w = (nFv/RT)\delta \quad (3.20)$$

$$r = \tau/\delta \quad (3.21)$$

The Equations 3.11 – 3.15 can be arranged further for cyclic voltammetry by adding equations related to applied potential waveform.

$$E = E_i + (m-1)v\delta \quad \text{for forward scan} \quad (3.22)$$

$$E = E_r - (m-1)v\delta \quad \text{for reverse scan} \quad (3.23)$$

where $m = 1, 2, \dots, N$

These equations are arranged as follows:

$$\xi = nF(E_i - E^0)/RT + (m-1)w\delta^2 \quad \text{for forward scan} \quad (3.24)$$

$$\xi = nF(E_r - E^0)/RT - (m-1)w\delta^2 \quad \text{for reverse scan} \quad (3.25)$$

The Equation (3.11) together with Equations 3.18 and 3.19 are named as Volterra Equation of the second kind. The numerical solution can be done by using product integration method with Trapezoid rule with a constant step length h (Delves and Mohamed, 1992) as,

$$\int_0^{x_i} \left(\frac{i}{i_d}\right) (x-u)^{-1/2} du \approx h \sum_{j=0}^i w_{ij} k(x_i, u_j, f_j) \quad (3.26)$$

$$= h \sum_{j=0}^i w_{ij} k(x_i, u_j) f(u_j) \quad (3.27)$$

$$h = (b-a)/N \quad a \leq x \leq b \quad (3.28)$$

where $x_i = u_i = ih$, $i = 0, 1, \dots, N$ has weights defined by

$$w_{i0} = \frac{2h^{1/2}}{3} \{3i^{1/2} + 2[(i-1)^{3/2} - i^{3/2}]\} \quad (3.29)$$

$$w_{ij} = \frac{4h^{1/2}}{3} \{(i-j-1)^{3/2} + (i-j+1)^{3/2} - 2(i-j)^{3/2}\} \quad j=1, 2, \dots, i-1 \quad (3.30)$$

$$w_{ii} = \frac{4h^{1/2}}{3} \quad (3.31)$$

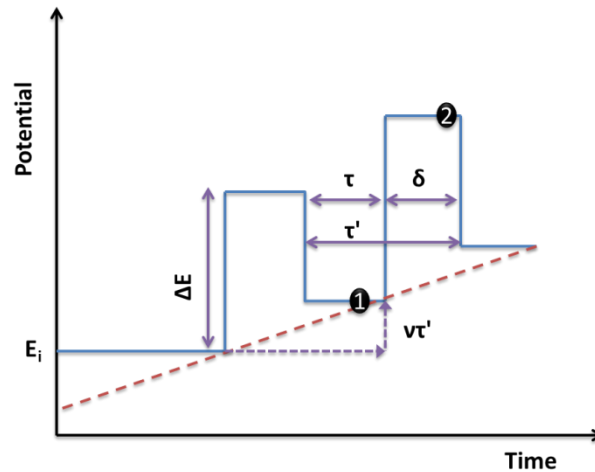


Figure 3.3. Schematic diagram of potential time waveform in DPV (Aoki et al., 1984; Wang, 2006).

3.2. Modeling Studies

A simulation code and its user interface (Figure 3.4) were prepared by using MATLAB programming language for above-mentioned equations of differential pulse voltammetry to determine current versus potential relationship with user-defined parameters. The prepared simulation code is given in

Appendix A. Thus, one can enter the parameters to the opened window at MATLAB for macro electrodes and obtain the result in a dialog box. The limitations of the code are given below:

- The geometries of the electrodes are not included in the model.
- It is assumed that all reactions occur at the surface of the working electrode, i.e., there is no self-assembled monolayer formation on the surface. The formation of SAM on the surface will reduce obtained current when the length of the SAM from the surface becomes higher.

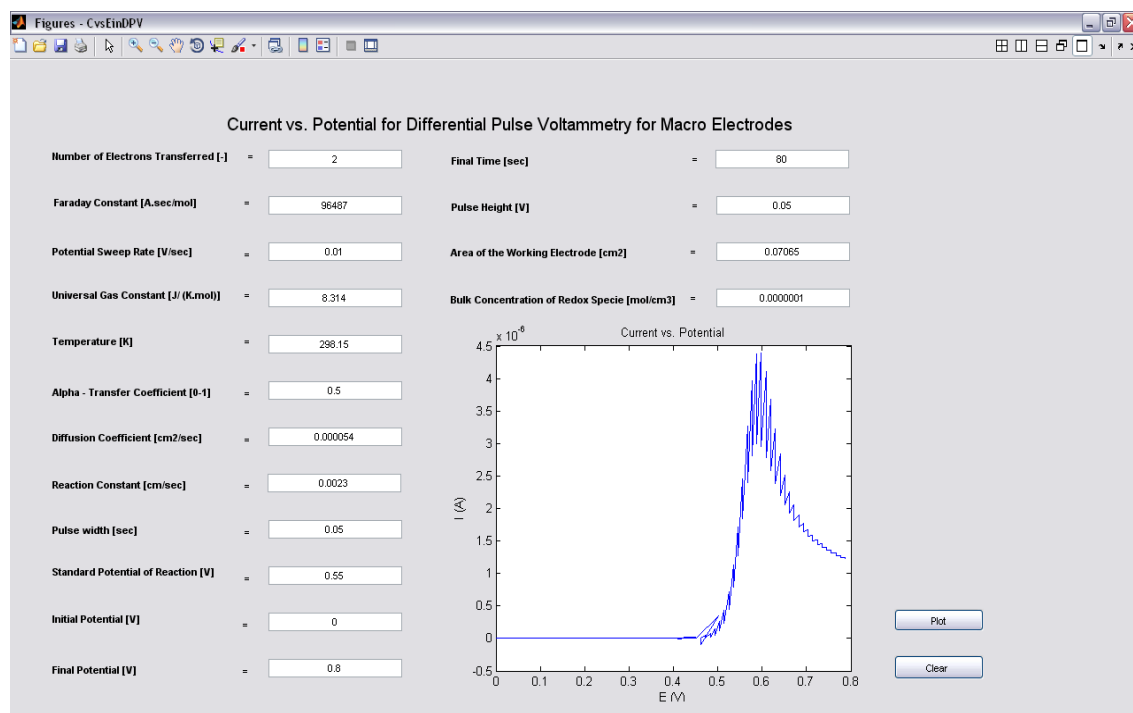


Figure 3.4. Graphical user interface (GUI) for current vs. potential diagram with the parameters taken from the study of (Fan et al., 2000) for DPV.

CHAPTER 4

DESIGN AND FABRICATION OF MICRO ELECTROCHEMICAL SENSOR

The design and fabrication procedures developed in this study for a micro electrochemical sensor are explained below. First, the proposed micro electrochemical sensor is introduced and then the design and preparation of mask layouts for the sensor is presented. Lastly, the details of MEMS based fabrication of the sensor are given.

4.1. Design of Micro Electrochemical Sensor

Proposed DNA electrochemical sensor has inlet, outlet, and a detection zone, which comprises Ag as reference electrode, Au as working electrode, and Pt as counter electrode. The inlet and outlet reservoirs are in connection with the detection zone by using micro channels. Figure 4.1 demonstrates a schematic view of the sensor designed in this study.

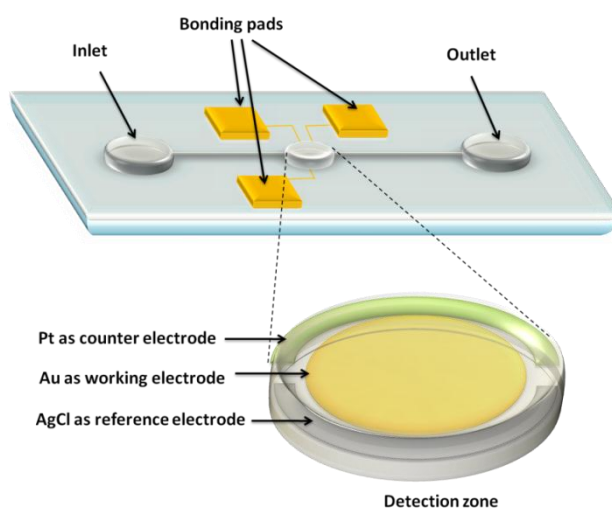


Figure 4.1. A schematic view of micro electrochemical sensor.

In Table 4.1, materials used in the fabrication of the sensor are given (Ceylan Koydemir et al., 2010a). Issues considered in design are as follows:

1. **Geometry of electrodes:** A symmetrical geometry was used for the counter and the reference electrodes to have a valid assumption of equivalent current paths on the working electrode, which minimizes the potential drop due to cell resistance (Wang, 2006), and a disk-shaped working electrode was used to decrease signal to noise ratio (Yue et al., 2006).
2. **Elimination of nonspecific binding of biological analytes to the substrate:** It was prevented by coating the area remaining around the metal sites with Parylene C. Diffusion in mass transport was enhanced by using micro channels and micro reservoirs made out of Parylene C with a height 50 μm at maximum. Parylene C was preferred to have the same coating material at each side of the channel and due to the Parylene C's transparency property for visualization of the electrochemical sensor under microscope.
3. **Contact pads' material:** Gold was used in the fabrication of contact pads that are used for the connection with macro-scaled equipments.

4. **Surface area of the electrodes:** Area increase of working electrodes was achieved by forming Au pillars on the working electrodes.
5. **Size of the sensor:** In order to decrease size of the chip, electrical connections were placed symmetric to each other between inlet and outlet.
6. **Alignment marks:** Circular shapes were placed at the bottom of the micro reservoirs to align nano ports.

Table 4.1. Materials used in the fabrication of the sensor.

Region	Material	Reason of usage
Contact Pads	Au	<ul style="list-style-type: none"> - Ease of deposition, - High electrical conductivity.
Micro Channels Inlet / Outlet Reservoirs	Parylene C	<ul style="list-style-type: none"> - Ease of deposition, - Biocompatibility, - Chemical inertness, - Low water permeability.
Working Electrodes	Au	<ul style="list-style-type: none"> - Chemically resistant, - Biocompatibility, - Electrical conductivity, - Selective adsorption of thiol-DNA, - Not oxidized easily.
Reference Electrodes	Ag	<ul style="list-style-type: none"> - Toxic to biological compounds, - Common reference electrode in electrochemistry.
Counter Electrodes	Pt	<ul style="list-style-type: none"> - Chemical inertness, - High sheet resistance.

Dimensions of micro electrochemical sensor are shown in Figure 4.2 and their values are given in Table 4.2.

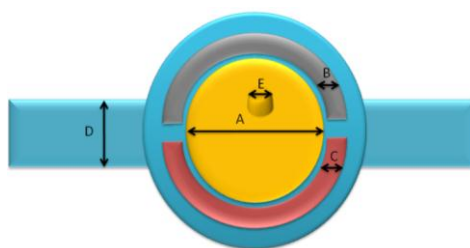


Figure 4.2. The structures of micro electrochemical sensor with electrodes and channels.

Table 4.2. Dimensions of structures of different micro electrochemical sensors.

Sensor #	A	B	C	D	E
1	500 μm	150 μm	150 μm	50 μm	10 μm
2	500 μm	150 μm	150 μm	30 μm	10 μm
3	300 μm	150 μm	150 μm	50 μm	10 μm
4	200 μm	150 μm	150 μm	50 μm	10 μm
5	150 μm	150 μm	150 μm	50 μm	10 μm
6	100 μm	150 μm	150 μm	50 μm	10 μm

4.2. Mask Layouts

Mask layout is a schematic drawing of each layer (e.g., metals, or polymer) of the sensor and composed of geometric shapes to form patterns of the layers in the fabrication. In standard MEMS fabrication processes, sensitivity, and selectivity of a sensor are determined with the geometric shapes fabricated with many chemical, thermal, and photographic steps. Therefore, its preparation is a critical issue to meet the design criteria.

Mask layouts of the electrochemical sensor were prepared by using Cadence® Virtuoso® Layout Editor. A list of layer names and their numbers are given in Table 4.3.

Table 4.3. Layers used, their trade names and numbers.

Layer	Name	Number
Ti	MET1	35
Au	MET2	37
Ag	PAD	40
Parylene	POLY1	20
Openings for Parylene	CAPDEF	55
Au layer electroplated	DIFF	10
Frame	text	230

In preparation of mask layouts, the four steps were taken into consideration as given below:

1. $50\ \mu\text{m} \times 50\ \mu\text{m}$ square parts were placed to obtain uniform thickness in Ag electroplating (Figure 4.3).

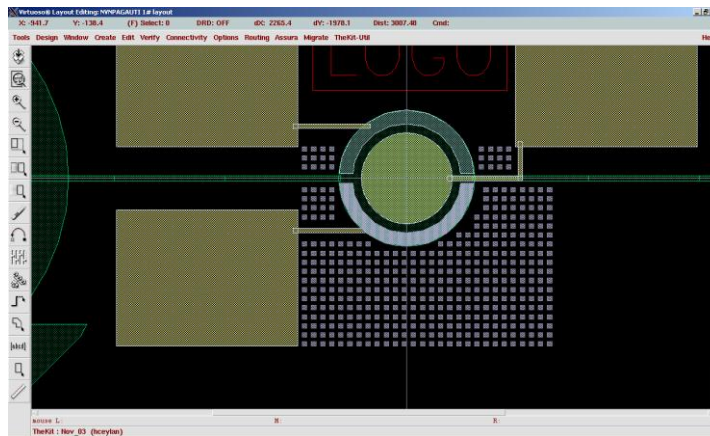


Figure 4.3. Ag electroplating region of the sensor.

2. The bottom of reservoirs was signed with titanium circles to align nano ports easily (Figure 4.4).
3. The contact pads fabricated from gold were placed outside of the detection zone to prevent adsorption of thiol-DNA on these surfaces (Figure 4.5). Only electrical connection of working electrode was placed in the reservoir.
4. Micropillars ($10\ \mu\text{m}$ in height) were placed on an isosceles triangle with the dimensions shown in Figure 4.6 in order to increase the area of working electrode. The results of working electrode with increased area were compared with the area of flat working electrode (Table 4.4).

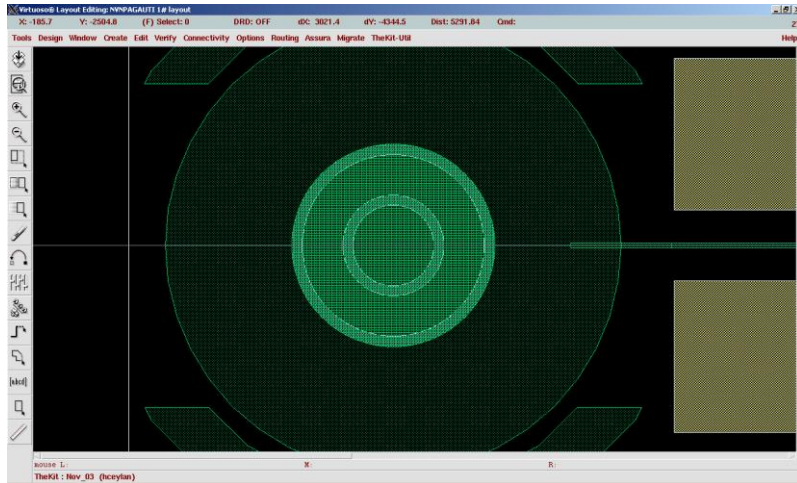


Figure 4.4. Titanium circles in the reservoir.

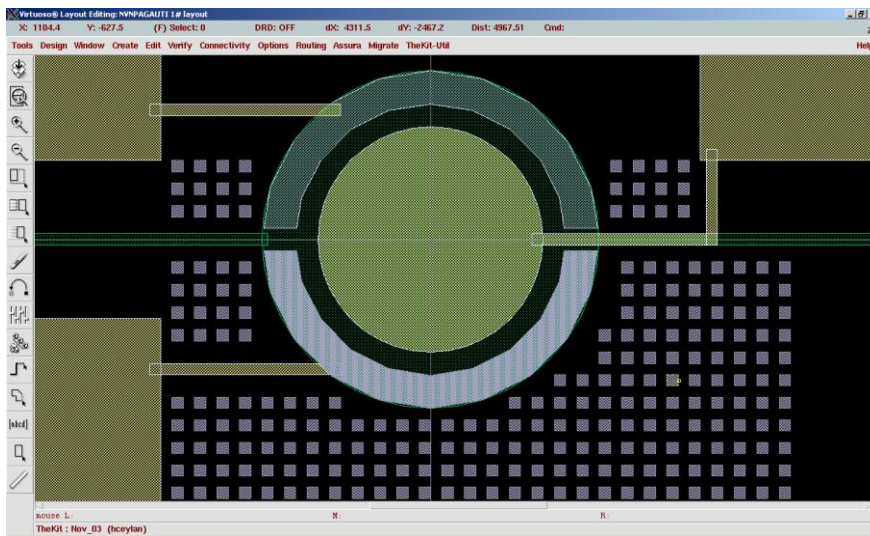


Figure 4.5. Upside view of detection zone.

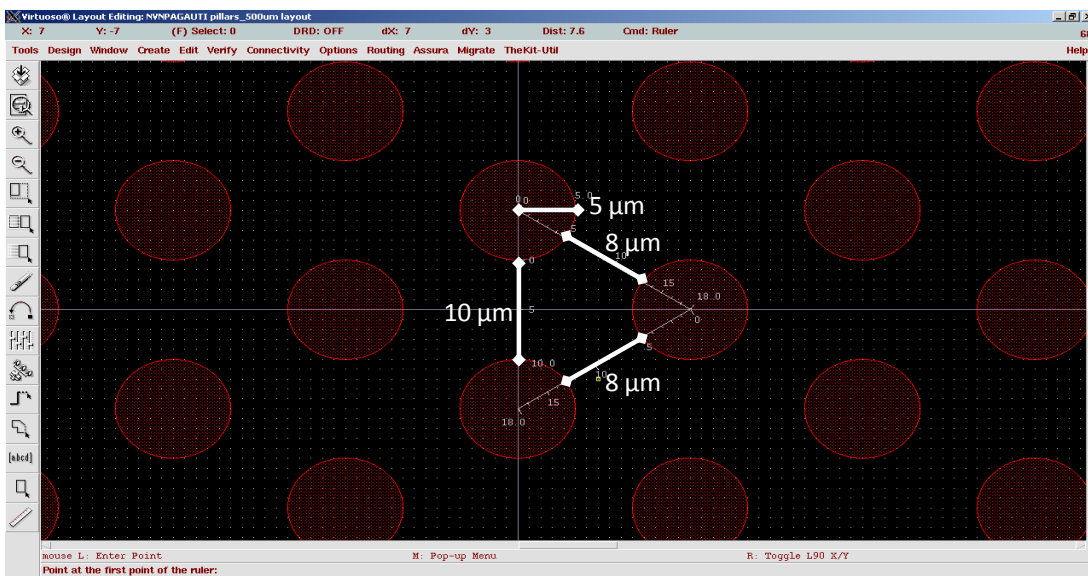


Figure 4.6. Pillars on Au electrode and their dimensions.

Table 4.4. Pillar numbers and area increase.

Au electrode size (μm)	Pillar number	Area increase percentage (with respect to flat electrode area)
500	2358	94
300	813	91
200	334	84
150	172	76
100	110	110

The mask layouts for a device, the proposed micro electrochemical sensor, and for the whole wafer are given in Figure 4.7 and 4.8, and the distribution of devices on wafer is given in Figure 4.9. Total number of devices that can be obtained from a wafer is 27. Seven masks are necessary for the fabrication of the sensors with different sizes. Three of them are dark-field and the others are clear-field masks.

4.3. Fabrication of the Sensor

Standard MEMS fabrication processes were used in the fabrication of the sensor. These processes allow batch fabrication of miniaturized devices. Thus, integration of the devices with circuits provides portability to the devices and enables their usage in point of care diagnosis.

In the following sections, reproducible coating of Ag layer on Au surfaces, which is one of the most important limitations in the fabrication of the sensor, and the fabrication steps of the sensor are given in detail.

4.3.1. Ag Layer Deposition

There are three ways to deposit Ag layer on a surface: electroplating, electroless deposition and sputtering (Ceylan Koydemir et al., 2010b).

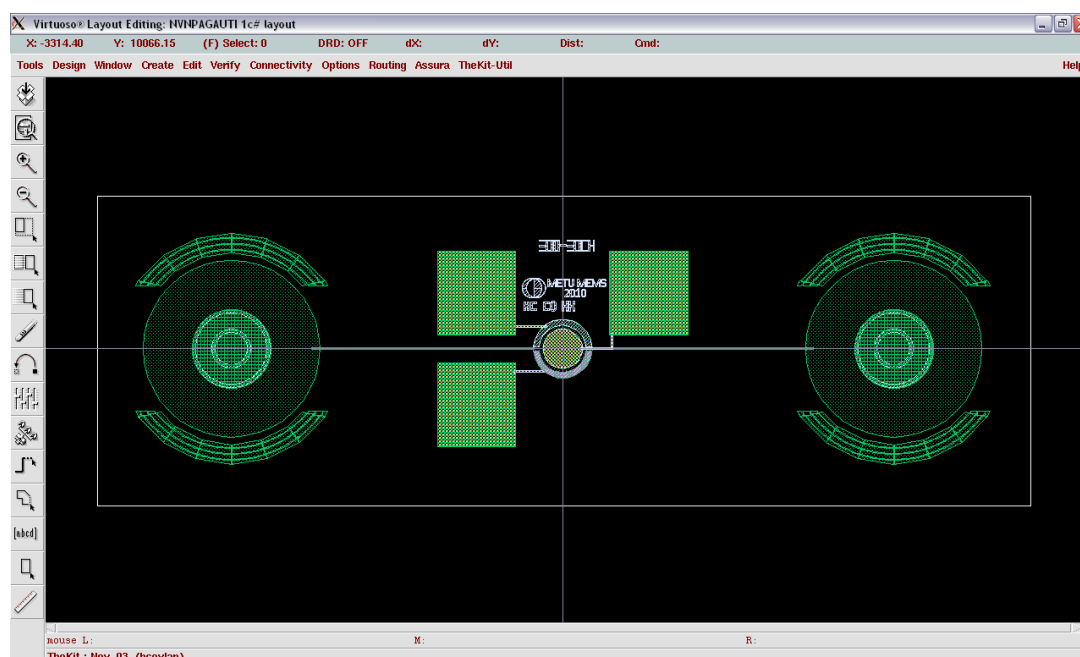


Figure 4.7. Mask layout for a device whose working electrode has the radius of 500 μm .

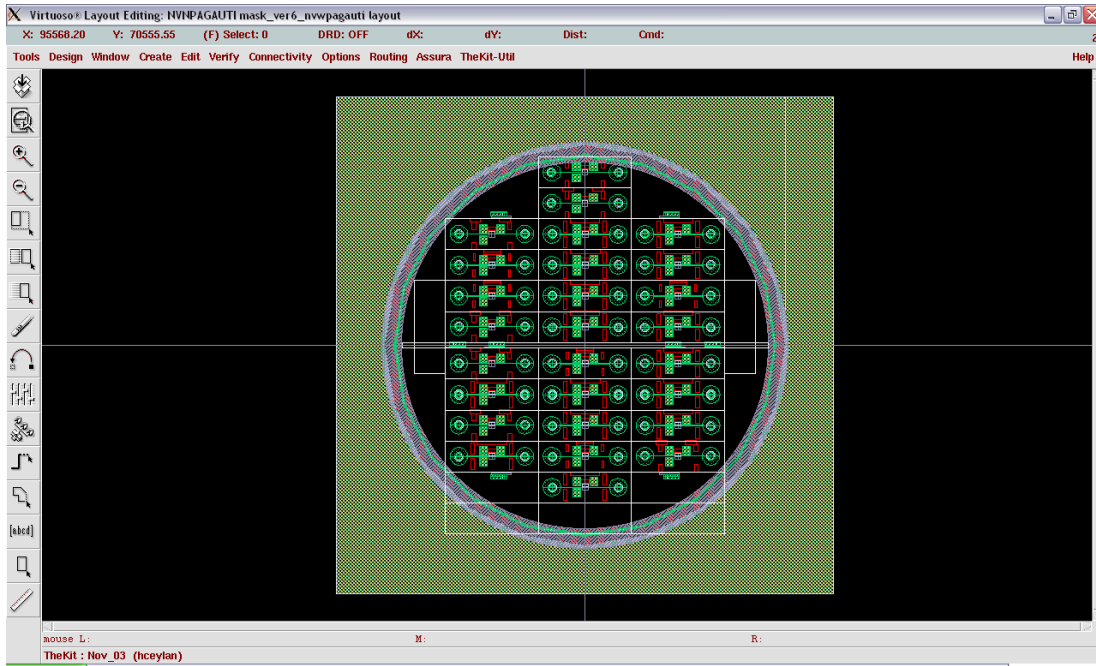


Figure 4.8. Overall view of mask layouts for the whole wafer.

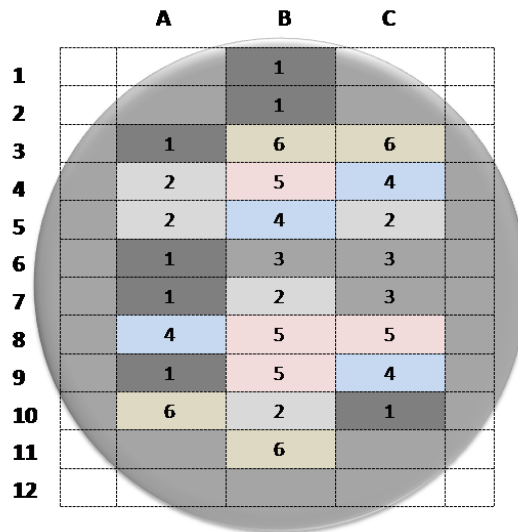


Figure 4.9. Distribution of devices on wafer.

Electroplating: This process is used first because it can be done as a batch process since the batch processes are preferable for high-throughput applications. The desired uniform thickness at Ag electroplating process was 5 μm or larger. Thus, Ti/Au layers as seed layer were coated by sputtering on a 4" Si wafer and a photo resist, AZ[®]9260, which is durable to electroplating applications was spin coated and patterned to have electroplated openings. The areas of electroplated openings and dark mask ring were calculated with the help of Tanner EDA Software Tool - L-Edit and determined as 0.789 cm^2 and 15.543 cm^2 , respectively, in total 16.332 cm^2 . The trial runs done for this process are given below:

- I. The process was performed in a solution of 0.3 M AgNO_3 in 1 M NH_3OH .
 1. Oxidative pre-treatment was performed for 30 s by applying 0.95 V with the use of Autolab PGSTAT 101 (Eco Chemie, The Netherlands) potentiostat, which was connected to the computer using the Nova 1.5 software.

2. 2.4 mA/cm^2 current was applied galvanostatically by using three electrodes, which are rod type Ag/AgCl as reference electrode, rod type Pt as counter electrode, and Ti/Au coated wafer as working electrode.
3. After electroplating process, AZ[®]100 remover was used at 353.15 K for 30 min for complete removal of photo resist. Veeco Wyko Surface Profiler NT1100 was used in the analysis of the surface profile of the wafer (Figure 4.10).

The results showed that the Ag layer could not be formed. These square areas demonstrated in Figure 4.10 were due to removal of Au and Ti from the surface. This may be due to the polarization.

- II. To solve this problem, a second trial was performed by applying -2.4 mA/cm^2 for 20 min. The results of the second trial showed that Ag layer was formed and its thickness changed from $0.7 \text{ }\mu\text{m}$ to $1.3 \text{ }\mu\text{m}$ on the wafer with a high surface roughness (Figure 4.11).
- III. The reproducibility of Ag electroplating was checked with another two Ti/Au coated wafers by using -2.4 mA/cm^2 for 120 min by using 0.3 M and 0.1 M AgNO_3 in 1 M $\text{NH}_3(\text{aq})$ galvanostatically. Although the procedure was the same with the previous experiment, coating could not be observed.

Since electroplating of silver layer with the specified solution resulted in nonreproducible results, another deposition process was used to have reproducible recipe, which can be applied for potential high-throughput applications.

Electroless deposition: A glass slide and Au coated wafer was coated with Ag layer with the recipe given in the study of (Ebina et al., 2009) with some minor changes (Figure 4.12). The experimental steps followed were as follows:

- Concentrated NH_3OH was added drop wise to 40 ml of 0.1 M $\text{AgNO}_{3(\text{aq})}$ until the initial precipitate dissolved.
- Then, 20 ml of 0.8 M NaOH solution was added to form a dark precipitate.

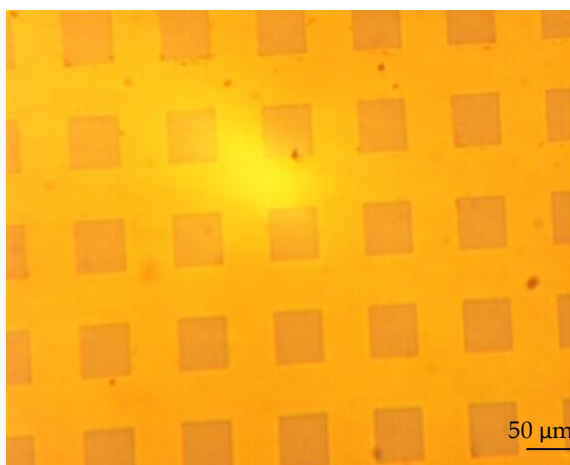


Figure 4.10. $50 \text{ }\mu\text{m} \times 50 \text{ }\mu\text{m}$ regions on Au seed layer after Ag electroplating.

- Enough additional NH_3OH was added to dissolve the precipitate. The resulting solution was colorless.
- The glass slide and Au coated wafer were cleaned by 2-propanol and dried in air (Figure 4.12a).
- The silver solution was placed drop-by-drop onto the slide to form a puddle covers the entire surface at 343.15 K.

- 0.5 M glucose solution was added drop wise to reduce the soluble silver ammonia complex $[Ag(NH_3)_2]^+$ (Figure 4.12b).
- The solution on the slide was mixed for one minute. It was allowed to form Ag layer for two minutes.
- The slide and wafer were washed with distilled water.

The process has to be performed at least twice to have uniform coating. In this experiment, coating was performed three times for glass slide and five times for the wafer. The silver was coated on any surface where the solution contacts (Figure 4.13). Etching of Ag layer is necessary to form patterns, i.e. electrodes, since electroless deposition does not necessitate any seed layer. There are seven types of wet Ag etchant (Table 4.5). However, the ratios can be altered for specific purposes. The selection of the accurate etchant solution was important since the aim was to etch only Ag layer. Therefore, $NH_4OH:H_2O_2(1:1)$ mixture was chosen as Ag etchant, which does not etch Au layer and H_2O was added in the ratio of (1:1:30) in order to decrease etch rate. The silver etchant etched the Ag layer on glass slide in two minutes (Figure 4.14).

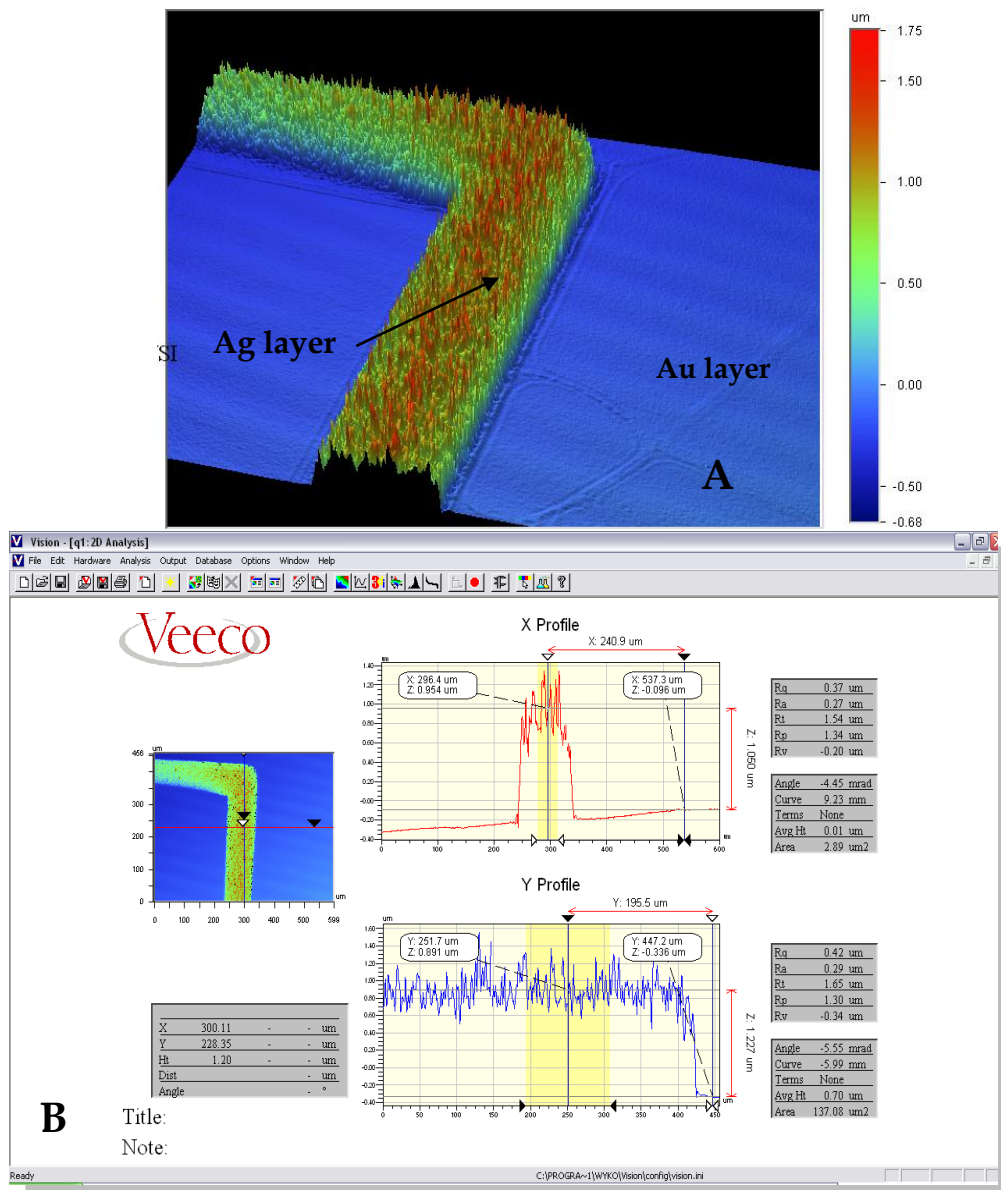


Figure 4.11. Surface profile of electrical connections of diamond structure at quarter one of wafer (A) 3-D view (B) 2-D analysis.



Figure 4.12. (a) Before (b) during (c) after silver deposition.



Figure 4.13. Silver mirror on Au coated wafer.

Table 4.5. Ag and Au etchants (Microchemicals, 2007).

Metal	Etching Mixture	Etch Rate
Ag	$\text{H}_3\text{PO}_4 : \text{HNO}_3 : \text{CH}_3\text{COOH} : \text{H}_2\text{O} = 3 : 3 : 23 : 1$	~100 A/10 min
	Chromium etchant	--
	$\text{NH}_4\text{OH} : \text{H}_2\text{O}_2 = 1 : 1$	--
	$\text{NH}_4\text{OH} : \text{H}_2\text{O}_2 : \text{H}_2\text{O} = 1 : 1 : 4$	360 nm/min
	$\text{HCl} : \text{H}_2\text{O}_2 : \text{H}_2\text{O}$	--
	$\text{HCl} : \text{HNO}_3 : \text{H}_2\text{O} = 1 : 1 : 1$	--
Au	$\text{KI} : \text{I}_2 : \text{H}_2\text{O} = 4 \text{ g} : 1 \text{ g} : 40 \text{ ml}$	--
	NFE 26-12-39 (HF+HNO ₃)	
	$\text{KI} : \text{I}_2 : \text{H}_2\text{O} = 4 \text{ g} : 1 \text{ g} : 40 \text{ ml}$	1 $\mu\text{m}/\text{min}$
	Aqua regia ($\text{HNO}_3 : \text{HCl} = 1 : 3$)	10 $\mu\text{m}/\text{min}$

Contents of solutions: NH_4OH : 29% NH_3 in H_2O , H_2O_2 : 30% in H_2O , HCl : 37% HCl in H_2O , HNO_3 : 70% HNO_3 in H_2O



Figure 4.14. Glass slide (A) before (B) after etching.

The Ag coated wafer was coated with AZ[®]5214E photo resist at 2000 rpm to obtain ~2 μm thickness of photo resist with the procedure indicated at datasheet and patterned. Then, the Ag layer was etched with the prepared Ag etchant. It took two minutes to etch silver layer (Figure 4.15).

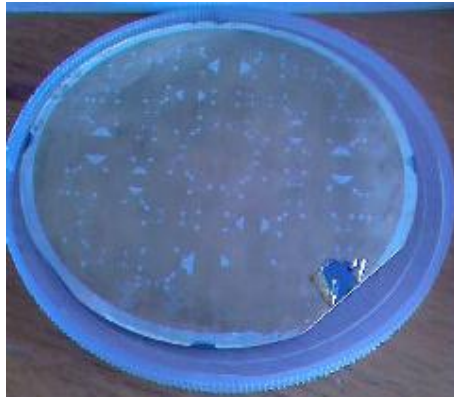


Figure 4.15. Photograph of the wafer after Ag etching process.

Surface profile of the Ag layer was analyzed by coating another wafer with Ag layer and using Veeco Wyko Surface Profiler NT1100 in VSI mode with 10X objective. The results demonstrated that the thickness of Ag layer changed between 0.23 μm to 0.47 μm from one point to another point on the wafer. The results demonstrated that Ag layer was not continuous (Figure 4.16). This may be due to the drop wise deposition of Ag layer. There were empty sides, limiting the usage of this electrode as reference electrode.

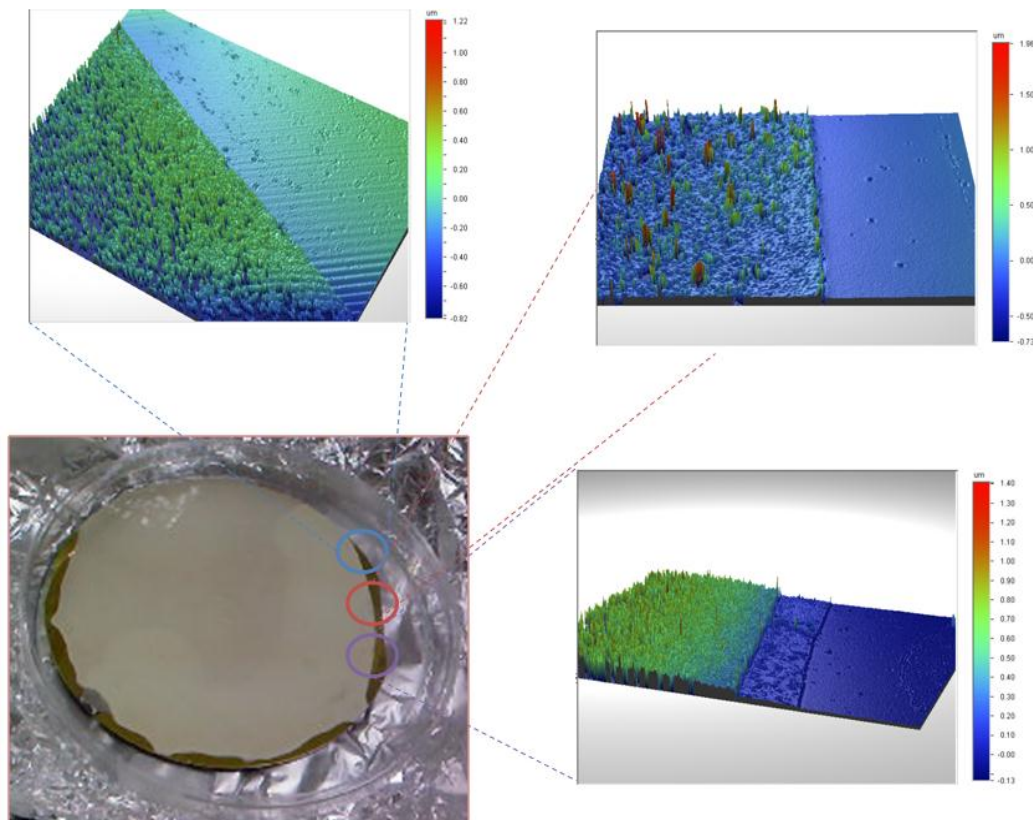


Figure 4.16. 3D surface profile of electroless Ag deposited wafer.

Sputtering: In this procedure, silver layer was deposited by sputtering. For the process, silver source was purchased from AJA Inc. (USA) and its purity was 99.99%. To obtain a desired thickness of silver layer, optimization of the recipe was essential. As a starting point, the process conditions developed by (Sant et al., 1999) (Table 4.6) were analyzed and the recipe (99% Ar, 10 mTorr pressure, 0.5 kW power), except changing the power to 0.3 kW to have smooth surface was selected

as a first trial to obtain ~300 nm thickness of silver layer. The other details of the recipe were a target distance of 28 cm and 99% Ar (23 sccm). Ag layers with different thicknesses were obtained with different sputtering times at process conditions as given in Figure 4.17. The thicknesses were measured by using Dektak 150 Stylus Profiler (Bruker). The process time to obtain ~320 nm Ag layer thickness was determined as 510 s by using a linear interpolation given in Figure 4.17. After this point, the recipe with 510 s was applied for the formation of Ag layer with the desired thickness and measurements of thickness profiles were performed as given in Figure 4.28.

Table 4.6. Process conditions for Ag layer formation (Sant et al., 1999).

Gas composition	Pressure (mTorr)	Power (kW)	Film thickness (nm)
99%Ar-1%O ₂	40	0.05	90
99%Ar-1%O ₂	40	0.05	300
99%Ar-1%O ₂	40	0.1	900
99%Ar-1%O ₂	40	0.15	90
99%Ar-1%O ₂	40	0.15	300
99%Ar-1%O ₂	40	0.15	900
99%Ar-1%O ₂	40	0.3	900
100%Ar	40	0.1	300
99%Ar-1%O₂	10	0.5	300
99%Ar-1%O ₂	40	0.1	300

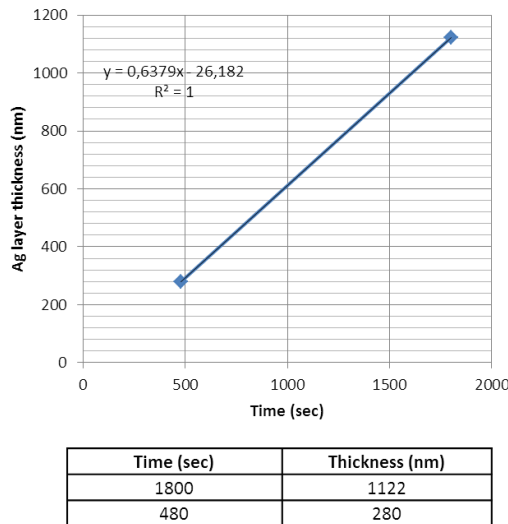
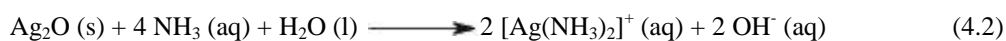


Figure 4.17. Ag layer thickness profile as a function of time [300 W, 10 mTorr, and 100 Ar % (23 sccm)].

An etchant, NH₃OH: H₂O₂: H₂O (1:1:30), which was used before for etching Ag layer deposited by electroless coating was prepared to etch Ag layer deposited by sputtering. When the wafer was immersed into the etchant, the Ag layer turned to black color because of formation of Ag₂O. The complete etch of Ag layer could not be observed. The possible reactions that can take place are given below (Greenwood and Earnshaw, 1997):

- Ammonia precipitating Ag⁺ and forming silver oxide:

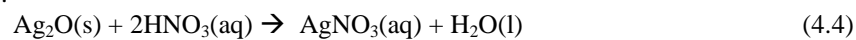
$$2 \text{Ag}^+ (\text{aq}) + 2 \text{NH}_3 (\text{aq}) + \text{H}_2\text{O} (\text{l}) \rightarrow \text{Ag}_2\text{O} (\text{s}) [\text{brown/black}] + 2 \text{NH}_4^+ (\text{aq}) \quad (4.1)$$
- In excess amount of ammonia in the solution, ammonia dissolves the silver oxide and forms diamine silver complex:



- On the other hand, hydroxide ions can form silver oxide by precipitating Ag^+ :

$$2 \text{Ag}^+ \text{(aq)} + 2 \text{OH}^- \text{(aq)} \longrightarrow \text{Ag}_2\text{O (s) [brown/black]} + \text{H}_2\text{O (l)} \quad (4.3)$$

Considering the above reactions, a solution with $\text{HNO}_3:\text{H}_2\text{O}$ (1:1) was prepared in glass petri dish to react with Ag_2O . The Ag layer was etched by immersing it into the solution by the reaction given as follows (Equation 4.4):



However, extensive etch of Ag layer was observed as given in Figure 4.18.

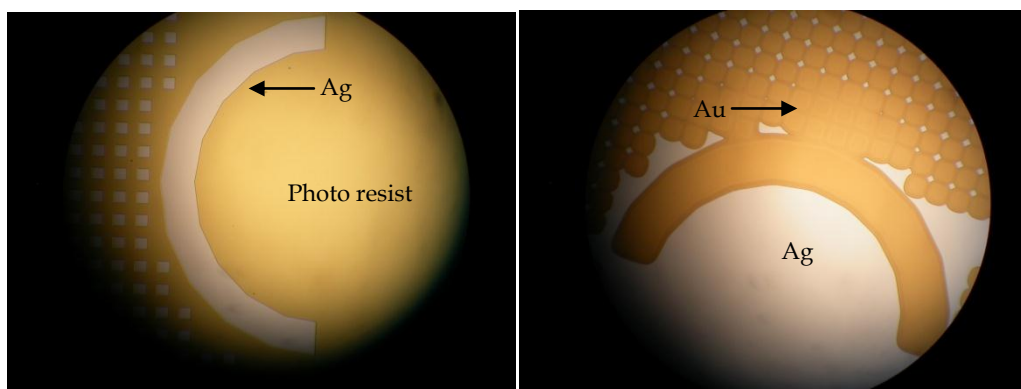


Figure 4.18. (A) Before (B) After Ag etching.

Therefore, three types of etchant solution were prepared by using $\text{HNO}_3:\text{H}_2\text{O}$ in the ratios of (3:100), (18:100), and (40:80) in glass Petri dish to analyze the effect of dilution on etch rate. Three wafers Ag layer coated was diced into four pieces to try different Ag etch scenarios (Table 4.7).

Table 4.7. Different etchants and etch times for Ag etch.

Etch run #	Wafer	Piece	Time (min)	Etchant	Mass transport in chemical etch		Result		Post etch process
					Diffusion	Convection	Pr removal	Ag etch	
1	1	1	4	Cr etchant	+	+	+	Overover	-
2	1	2	2.30	Cr etchant	+	+	+	Overover	-
3	1	3	1.40	Cr etchant	+	+	-	Overover	-
4	1	4	2.30	Cr etchant	+	+	+	Overover	-
5	2	1	3	Cr etchant	+	-	+	Over	-
6	2	2	3	Cr etchant	+	-	+	Over	-
7	2	3	12	NH ₃ OH:H ₂ O ₂ :H ₂ O 1:1:32	+	+	-	-	Immersed into 1:1 HNO ₃ :H ₂ O (etch in seconds)
8	2	4	1/6	HNO ₃ :H ₂ O 1:1	+	-	-	O.K.	-
9	3	1	15	HNO ₃ :H ₂ O 1:15	+	+	-	-	-
10	3	2	1/10	HNO ₃ :H ₂ O 1:1	+	-	-	O.K.	-
11	3	3	(13 + 3)/60	HNO ₃ :H ₂ O 1:1	+	-	-	Over	-
12	3	4	1/6	HNO ₃ :H ₂ O 1:1	+	-	-	O.K.	-

It was clear that sputtered Ag layer can be etched in either the chromium etchant or the nitric acid solution (Figures 4.19 and 4.20). Among them, the use of $\text{HNO}_3:\text{H}_2\text{O}$ (1:1) as silver etchant was preferred for further fabrication, since it could be prepared fresh at each etching process.

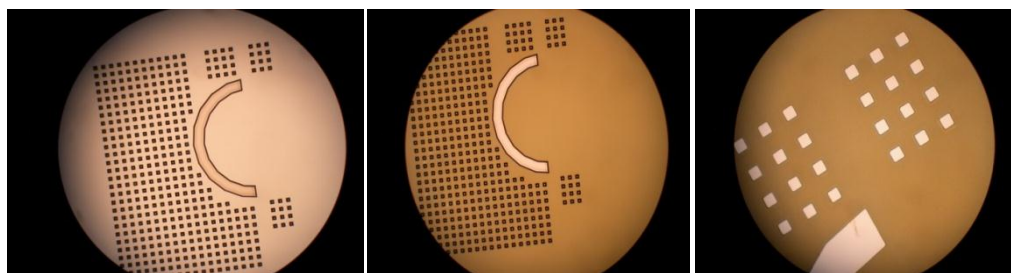


Figure 4.19. $\text{HNO}_3:\text{H}_2\text{O}$ (1:1, 6 s) (A) Before (B) After (with no pr strip) (C) After (with pr strip)

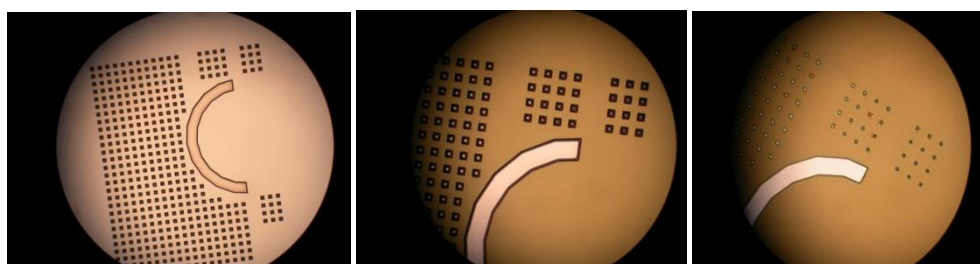


Figure 4.20. $\text{HNO}_3:\text{H}_2\text{O}$ (1:1, 13+3 s) (A) Before (B) After (with no pr strip) (C) After (with pr strip)

4.3.2. Details of Fabrication Steps of the Electrochemical Sensor

Integration of micro fluidics to the fabrication flow is a challenging task due to usage of various materials and the possibility of cross interaction with each other in either etching process or deposition process. Three different fabrication flows were used to fabricate the sensor. The final process flow of the sensor was achieved at the third generation process flow. In the fabrication of the electrochemical sensor, 100 mm (4") Si wafer was used at each generation and the fabrication of the sensor has different steps. The details of process flow for the fabrication of electrochemical sensor for each generation is given in Appendix B.

The first generation: The steps for the fabrication of the first generation devices are as follows:

1. Dehydration step was performed at 383.15 K for 20 min in N_2 purged oven.
2. Silicon nitride (Si_3N_4) with a thickness of 300 nm was deposited to form an insulation layer on Si wafer by using low-pressure chemical vapor deposition (LPCVD).
- 3., 4., 5., Ti, Pt, and Au layers were sputtered to have about 50 nm, 200 nm, and 180 nm thicknesses, respectively.
6. Dehydration step was performed at 383.15 K for 20 min in N_2 purged oven.
7. Lithography step to pattern Au layer was performed by using a positive photo resist, Microposit® S-1813 with a thickness of 1.3 μm . The photo resist was coated at 4000 rpm for 30 s, exposed to UV, developed by using Microposit MIF 319 Developer, and hard baked at 393.15 K for 40 min (Figure 4.21).
8. The potassium iodide chemistry based gold etchant was used to etch Au layer.
9. The photo resist was stripped by using O_2 plasma for 90 minutes.
10. Another lithography process with Microposit® S-1813 photo resist was performed to pattern Pt layer as in the seventh step.
11. Since holders of reactive ion etching (RIE) machine, at which metal etching processes have been done, was for 150 mm (6") wafers, 100 mm (4") process wafers were bonded on 150 mm (6") wafer by using Crystalbond™ adhesive (Figure 4.22).

12. Etching Pt layer was performed by using Cl_2/Ar plasma (5 sccm Ar, 15 sccm Cl_2) in the inductively coupled plasma. Different plasma exposure times were used to find the optimal one: 2 min + 2 min, 2 min + 1 min 5 s, and 2 min + 1 min 3 s. The optimal time was determined as 2 min + 1 min 5 s according to the type of the metal at the field (Figures 4.23 - 4.25).

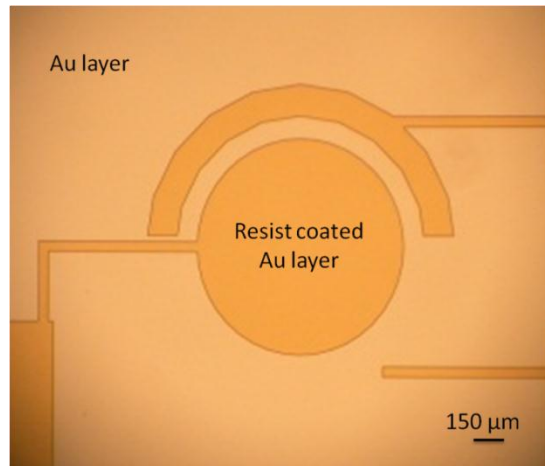


Figure 4. 21. A picture demonstrating detection zone after lithography step for Au etch.

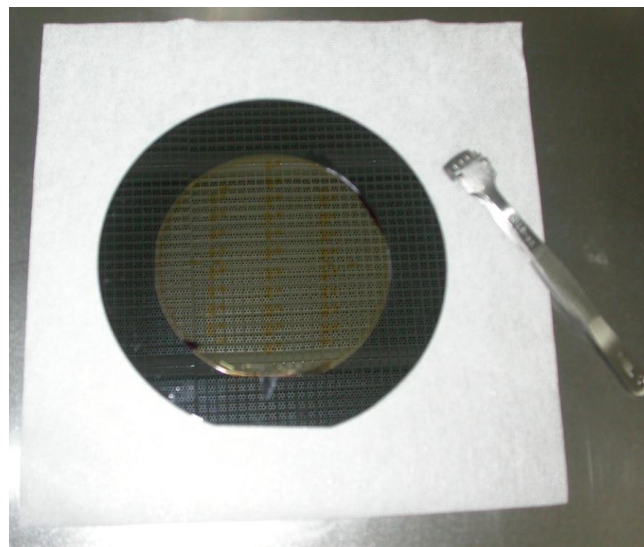


Figure 4.22. A picture demonstrating a CrystalbondTM bonded wafer.

13. Four inch wafer was slipped over 150 mm (6") wafer by heating the bonded wafer on a hot plate at 343.15 K, and backside of wafer was cleaned up with methanol.
14. Since the time necessary to strip photo resist in acetone (5 min) is much lesser than the time necessary for stripping photo resist at oxygen plasma (90 min), the photoresist strip after Pt etch process was performed by immersing wafer into acetone and then, into PRS 1000 photo resist stripper solution. However, complete removal of the photoresist could not be achieved. Wafer was exposed to O_2 plasma for 30 min to strip photo resist residues. Although it was observed that the photoresist residues were completely removed by examining the surface at the optical microscope, SEM pictures of the wafer demonstrated the photo resist residues (Figures 4.26 and 4.27). It was concluded that it was necessary to strip photo resist, which was exposed to any reactive ion etching processes, totally in O_2 plasma.
15. The lithography step for Ti etch was performed by using Microposit® S-1813 with a thickness of 1.3 μm.

16. Since holders of reactive ion etching (RIE) machine, at which metal etching processes have been done, was for 150 mm (6") wafers, 100 mm (4") process wafers were bonded on 150 mm (6") wafer by using Crystalbond™ adhesive.

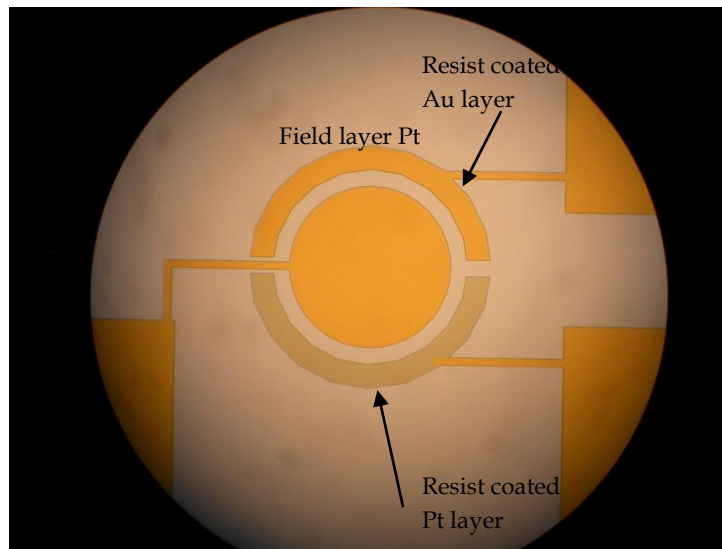


Figure 4.23. A photograph demonstrating electrodes before Pt etch.

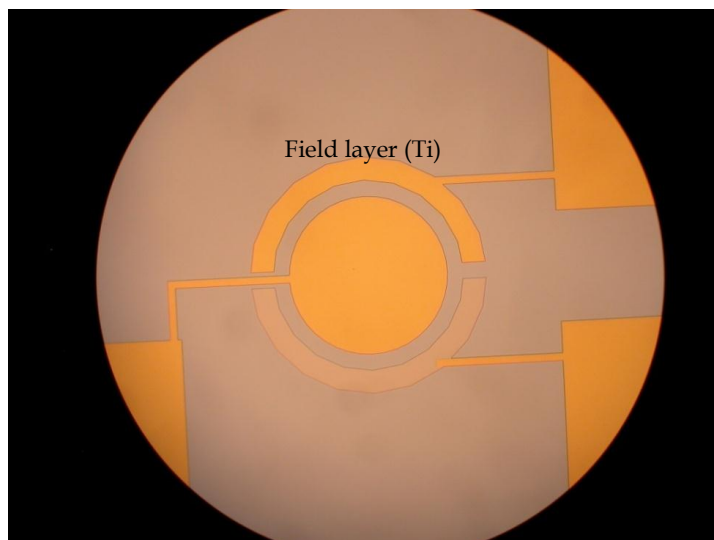


Figure 4.24. A photograph demonstrating electrodes after Pt etch on metal RIE (2 min + 1 min 5 s).

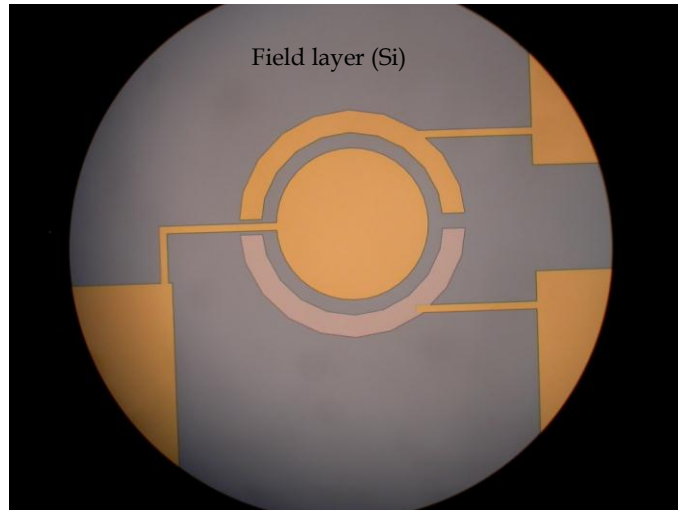


Figure 4.25. A photograph demonstrating detection zone after Pt etch on metal RIE (2 min + 2 min).

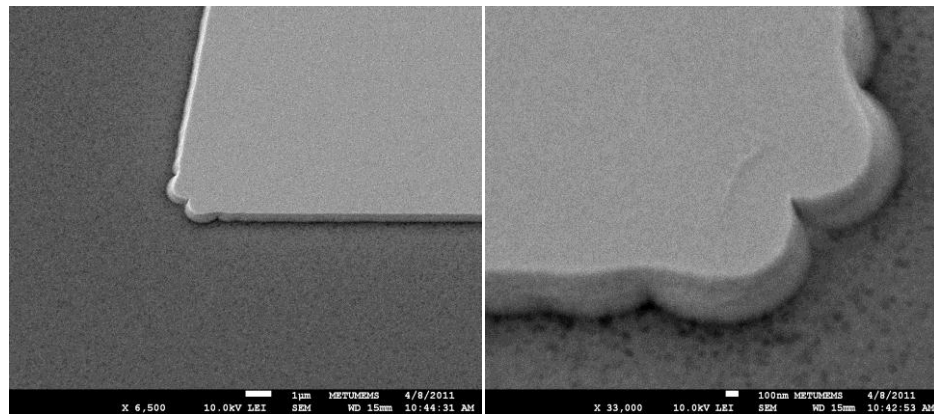


Figure 4.26. The corners of Pt electrode (Pt etch at metal RIE (2 min + 1 min + 10 s + 10 s)).

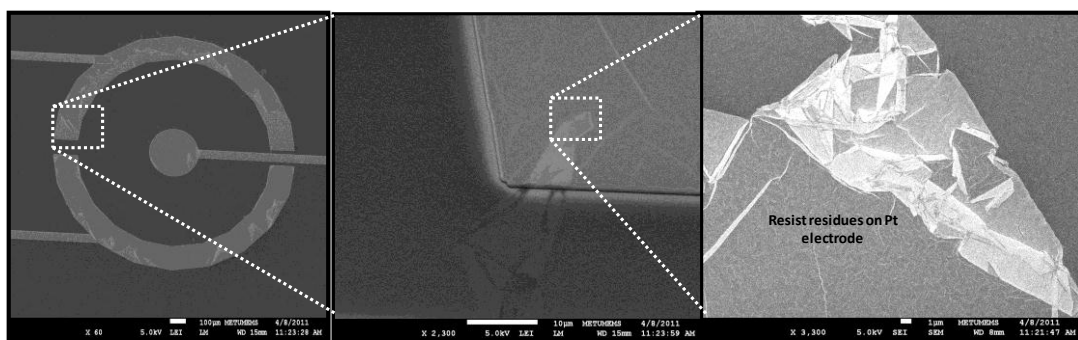


Figure 4.27. SEM pictures taken from the #8 wafer (Pt etch at metal RIE (2min + 2min)).

17. Ti etch was performed in HBr/Ar plasma in an inductively coupled plasma.
18. Four inch wafer was slipped over 6" wafer by heating the bonded wafer on a hot plate at 343.15 K, and backside of wafer was cleaned up with methanol.
19. The photo resist was stripped of in O₂ plasma.

20. Ag layer was coated in sputtering with the developed recipe to obtain ~320 nm thickness.
21. AgCl layer formation can be performed at this step with the use of chloride containing solution.
22. The lithography step for Ag etch was performed by using an image reversal photo resist, TI 35E with a thickness of 3.5 μm .
23. Ag layer was etched in a nitric acid solution. At this step, the thickness measurements of Au, Pt, and Ag layers were performed at Dektak 150 Stylus Profiler (Bruker). The thicknesses of electrodes were measured as 180 nm, 200 nm, and 320 nm respectively, as expected (Figure 4.28).
24. The photo resist was stripped with acetone in 30 minutes.
25. After forming the electrodes, lithography step was performed by using a positive photo resist, AZ[®]9260, to have a thickness of 15 μm . The resist was coated at 1000 rpm, exposed to UV, developed by using AZ 826 MIF Developer, and hard baked at 393.15 K for 40 min.
26. The wafers were coated with 40 g of Parylene C to obtain a thickness of ~20 μm .
27. Another lithography step was performed by double spinning AZ[®]9260.
28. Parylene C film layer was etched with the use of O₂/CF₄ inductively coupled plasma for 40 min to form openings.
29. Wafers were diced to have individual sensors
30. Lastly, wafers were immersed into acetone to strip photo resist inside the channels and micro reservoirs.

After the individual dies immersed into acetone for about one week, it was observed that the photo resist could not be stripped of. It might be due to long baking step at last lithography step. In order to solve the problem, another lithography recipe was used.

The second generation: In this generation, the fabrication steps were same with the first generation fabrication steps up to 25th step. The lithography recipe at 25th step was changed as given in the Appendix A. Subsequently, Parylene C film layer was deposited. However, it was observed that the resist inside the parylene micro channels was spread out in the Parylene C film coating chamber. It might be due to cross contamination of photo resist with silane, which is adhesion promoter of Parylene C. In order to solve the problem, the fabrication flow was changed as given in the third generation so that silane does not meet with photo resist at any step of the process.

The third generation: The fabrication steps were same with the first generation fabrication steps up to 20th step. The next steps of the fabrication were as follows:

20. 2 μm -thick Parylene film layer was deposited after silanization.
21. Lithography step was performed to etch Parylene C film layer on the electrodes and contact pads.
22. Parylene C film layer was etched with the use of O₂/CF₄ inductively coupled plasma for five minutes to form openings.
23. Photo resist layer was stripped in acetone.
24. Ag layer was coated in sputtering with the developed recipe to obtain ~320 nm thickness.
25. AgCl layer formation could be performed at this step with the use of chloride containing solution.
26. The lithography step for Ag etch was performed by using an image reversal photo resist, TI 35E with a thickness of 3.5 μm .
27. Ag layer was etched in a nitric acid solution.
28. The photo resist was stripped with acetone in 30 minutes.
29. After forming the electrodes, lithography step was performed by using a positive photo resist, AZ[®]9260, to have a thickness of 15 μm .
30. The wafers were coated with 40 g of Parylene C to obtain a thickness of ~20 μm .
31. Another lithography step was performed by double spinning AZ[®]9260 (This step is same with 27th step of the first generation fabrication).
32. Parylene C film layer was etched with the use of O₂/CF₄ inductively coupled plasma for 40 min to form openings.
33. Wafers were diced to have individual sensors
34. Lastly, wafers were immersed into acetone to strip photo resist inside the channels and micro reservoirs.

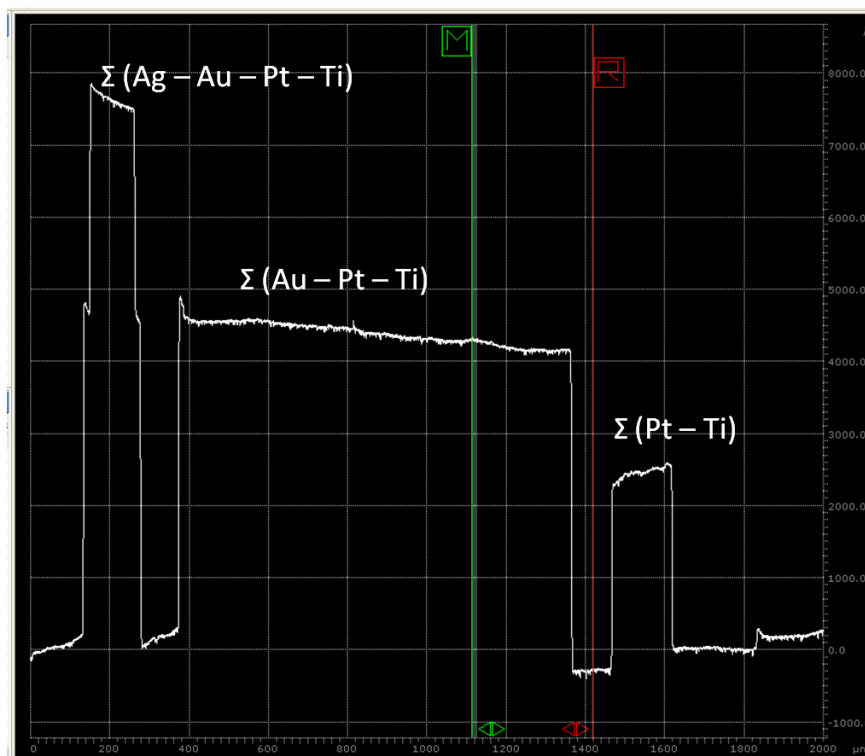


Figure 4.28. Thickness profile of electrode layers.

The third generation of the fabrication flow was successful for integration of electrodes with micro channels and reservoirs. Figure 4.29 demonstrates the process flow of the μ ECS in short. The first step was the insulation of the substrate, which could be of any material such as silicon, glass, or quartz, by coating the surface with silicon nitride (Si_3N_4) (Figure 4.29A). Then, titanium (Ti), platinum (Pt) and gold (Au) layers were sputtered, respectively (Figure 4.29B). Photo resist layer was spin-coated and patterned to form openings for gold etch. The gold layer was etched and the resist was stripped (Figure 4.29C). Then, platinum was etched by patterning it with a plasma durable photo resist layer and using chlorine-based gases in inductively coupled plasma (Figure 4.29D). After that, titanium layer was patterned with a photo resist layer and etched in HBr/Ar based plasma to form separate electrodes and alignment marks (Figure 4.29E). Then, Parylene C was deposited after silanization of the wafer, patterned with photo resist, and etched by using O_2/CF_4 plasma (Figure 4.29F). As shown in Figure 4.29G, silver layer was sputtered, patterned, and etched to form reference electrode. After forming the micro channel and reservoirs, Parylene C was deposited by using chemical vapor deposition (CVD) and etched to form openings of micro reservoirs (Figure 4.29H). Lastly, wafers were diced to have individual sensors and were immersed into acetone to strip photo resist inside the channels and micro reservoirs.

Figures 4.30 and 4.31 demonstrate the fabricated prototype of the sensor (Ceylan Koydemir et al., 2012a; Ceylan Koydemir et al., 2012b). After the complete dissolution of the photo resist inside the microchannels and microreservoirs, nanoports (LabSmith, USA) were adhered to the inlet and outlet reservoirs according to the manufacturer's instructions. Each electrode of the electrochemical sensor was composed of an electrode in the detection zone and a contact pad, which was connected to the potentiostat for electrochemical detection.

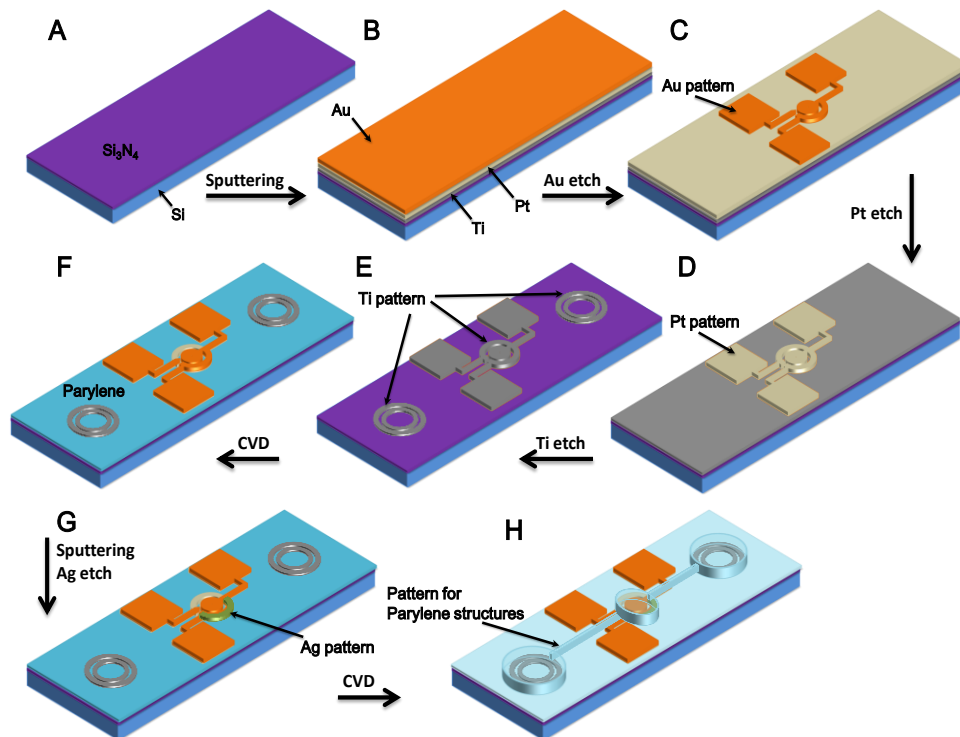


Figure 4.29. Process flow of the micro electrochemical sensor (A) Insulation layer deposition (B) Metallization (C) Formation of working electrode (Au patterning) (D) Formation of counter electrode (Pt patterning) (E) Isolation of electrodes and formation of alignment marks (Ti patterning) (F) Protective layer deposition to prevent non specific adsorption (Parylene C deposition) (G) Formation of reference electrode (Ag sputtering and patterning) (H) Formation of micro channels and micro reservoirs (Parylene C deposition).

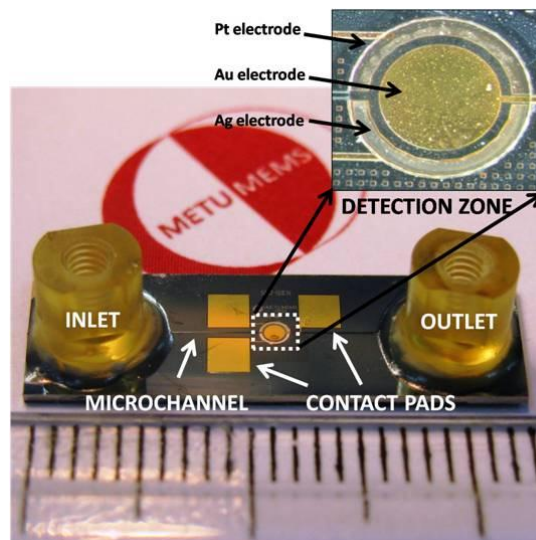


Figure 4.30. A photograph demonstrating fabricated prototype integrated with microchannels ($r = 500 \mu\text{m}$).



Figure 4.31. A photograph demonstrating fabricated prototypes (a) $r = 100 \mu\text{m}$, (b) $r = 150 \mu\text{m}$, (c) $r = 200 \mu\text{m}$, (d) $r = 300 \mu\text{m}$.

CHAPTER 5

EXPERIMENTAL STUDIES

The electrochemical detection of nucleic acids can be classified into two major topics: direct detection and indirect detection. In the former, the oxidation of nucleobases (adenine, guanine, etc.) and sugars, and photoelectroactivity of nucleic acids are detected without making any further modification on the sequence of nucleic acid. Since the selectivity of the direct detection is low, the more specific detections like detection of single nucleotide polymorphisms could not be performed. To increase selectivity and specificity, types of indirect detection are studied mostly. Indirect detections are based on the usage of covalently and non-covalently bound markers, and changes in electronic properties of surface. Among them, usage of covalently bound markers has high stability, density of packing, binding capacity, and specific adsorption.

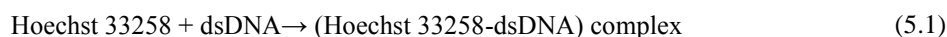
In this study, electrochemical detection of *mecA* gene was done by using two types of indirect detection: (i) redox marker based detection using Hoechst 33258 as redox marker, and (ii) enzyme based detection using horseradish peroxidase as signal amplifying non-electroactive marker. This chapter presents experimental studies in detail for detection of *mecA* gene. First, a brief introduction for each type of detection was given. Then, materials and methods for surface modification procedures and detection of hybridization of DNA with voltammetric methods (i.e., cyclic voltammetry (CV) and differential pulse voltammetry (DPV)) was explained.

5.1. Redox Marker Based Detection

Hoechst 33258, which is an electroactive marker, is used to enhance specificity and selectivity for indirect detection. Hoechst 33258 [2'-(4-hydroxyphenyl)-5-[5-(4-methylpiperazine-1-yl)-benzimidazo-2-yl]-benzimidazole] is a fluorescent cytological stain (350nm/461nm) of DNA with high affinity for dsDNA in fluorescence microscopy (Figure 5.1) (Banerjee and Pal, 2006). Hoechst 33258, which is a bisbenzimidazole derivative, is an irreversible redox compound and it oxidizes approximately at 550 mV (Sufen et al., 2002). Hoechst 33258 selectively binds to minor groove of dsDNA and covers 5(±1) base pairs (Breusegem et al., 2002) especially A-T rich region of DNA double helix (Sufen et al., 2002). The binding scheme is given in Figure 5.2. The A/T sequence specific and minor groove binding of Hoechst 33258 can be due to either a change in slide of the pairs to make wider the floor of minor groove for the dye or an additional movement of sugar phosphate backbone to insert the dye between the walls of minor groove. The AATT sequence has a very narrow groove. This groove has a zero base pair roll and highly ordered spine of hydration (Breusegem et al., 2002).

The affinity of Hoechst 33258 is, in decreasing manner, (5' → 3' sequence) AATT»TAAT≈ATAT>TATA≈TTAA with association constants, K_a , $5.2±0.2×10^8$, $0.277±0.004×10^8$, $0.241±0.004×10^8$, $0.027±0.001×10^8$, and $0.031±0.002×10^8$, respectively. Only one dye molecule bound at one given time for AATT, i.e. it is independent of Hoechst 33258 concentration. The highest affinity for AATT site is due to a large entropic contribution to the binding energy from the release of water molecules from the spine of hydration at the AATT site (Breusegem et al., 2002).

The adsorption of Hoechst 33258 on minor grooves of dsDNA is as follows:



In redox labeling with Hoechst 33258, Hoechst 33258 is oxidized irreversibly on a gold electrode at 550 mV. The number of electrons transferred per molecule is two (Sufen et al., 2002). The schematic view displaying electron transfer is given in Figure 5.3.

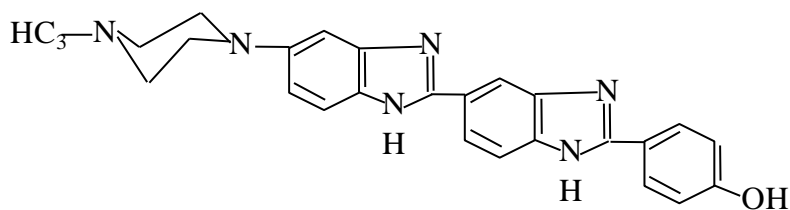


Figure 5.1. Chemical structure of Hoechst 33258.

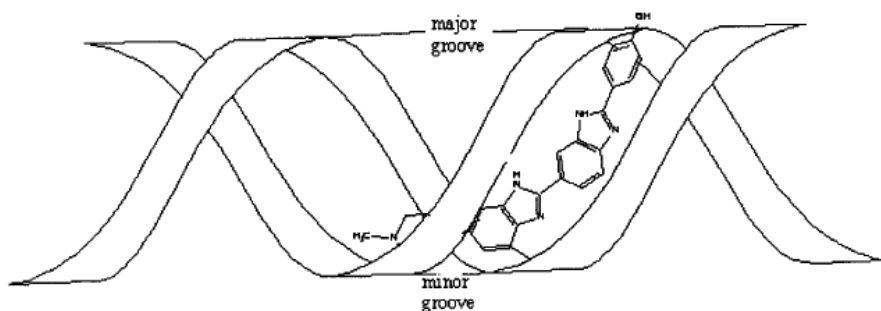


Figure 5.2. The binding of Hoechst 33258 to minor grooves of dsDNA (Sufen et al., 2002).

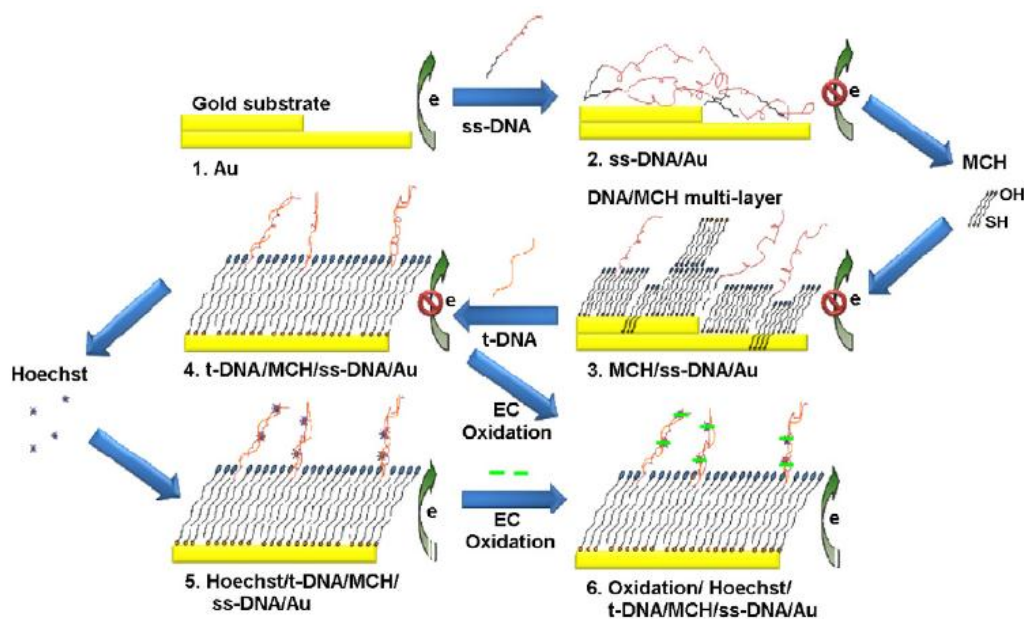


Figure 5.3. Schematic view of mechanism for modification of Au electrode surface (McEwen et al., 2009).

In literature, there are many studies related to the electrochemical analysis of effect of Hoechst 33258 binding on double stranded nucleic acids (Ahmed et al., 2010; Ahmed et al., 2007; Ahmed et al., 2009; Chaumluk et al., 2007; Choi et al., 2005; Fan et al., 2000; Hashimoto and Ishimori, 2001; Kobayashi et al., 2004; Lee and Hsing, 2002; McEwen et al., 2009; Sufen et al., 2002; Takahashi et al., 2005; Wang et al., 2003). In these studies, either gold or carbon paste electrode is used as working electrode with varying areas from 3.14 mm² to 0.04 mm². In the studies in which Au had been used as working electrode, the surface had been activated firstly by using thiol modified DNA sequences or thiol containing chemicals (e.g. cysteine) and then the surface had been immersed into the solution containing at least 10 μM Hoechst 33258 dye. On the other hand, in the studies in which carbon had been used as working electrode, the nucleic acid aggregation property of Hoechst 33258

had been studied mostly, and for this purpose, the electrodes had been immersed firstly into dye and then to the solution containing a certain amount of concentration of nucleic acid. After that, the electrochemical analysis had been performed by using Linear Sweep Voltammetry (LSV), CV, or DPV.

5.1.1. Materials

Acetone, isopropanol, sulfuric acid (H_2SO_4) and ethanol were purchased from J.T. Baker® (USA) in VLSI grade. Hoechst 33258, Pentahydrate (bis-Benzimide) was purchased from Invitrogen (Turkey). The Hoechst solution with a concentration of 100 μM was prepared and kept in dark at 4 °C. HEPES (4-(2-Hydroxyethyl) piperazine-1-ethanesulfonic acid N-(2-Hydroxyethyl)piperazine-N'-(2-ethanesulfonic acid)), sodium chloride (NaCl), TWEEN® 20, potassium chloride (KCl), potassium phosphate dibasic (K_2HPO_4) and potassium phosphate monobasic (KH_2PO_4) were purchased from Sigma Aldrich (Turkey). Autoclaved ultra pure water was used in the experiments. Phosphate buffer saline (PBS) was prepared with 0.04 mol K_2HPO_4 and 0.01 mol KH_2PO_4 . TWEEN® 20 (0.3% (v/v)) with PBS including 10 mM NaCl was prepared for rinsing solution and it was used to reduce background staining and increase specificity of staining (Kerman et al., 2008).

The DNA fragment encompassing 23 nucleotides (between 1680th and 1703rd) of the *mecA* gene belonging to *Staphylococcus aureus* subspecie. aureus MRSA 252 was used in the experiments as target probe. Single stranded complementary of target DNA (modified and lyophilized) was purchased from Alpha DNA (Germany). Lyophilized target and *femA* (Francois et al., 2003) synthetic DNA sequences were purchased from Iontek (Turkey). DNA stock solutions with a concentration of 100 μM were prepared in sterilized water and stored at 253.15 K.

The sequences used in the experiments were as follows

Capture probe: 5'-thiol-AAA CAA ACT ACG GTA ACA TTG AT-3'

mecA: 5'-ATC AAT GTT ACC GTA GTT TGT TT-3'

femA S. aureus: 5'-CAT AGT GGC CAA CAG TTT GCG TGA AAT GA-3'

femA S. epidermis: 5'-CGA TAA CGA TTT GAA GTT CCA CCA GCG TAG TA-3'

5.1.2. Methods

An illustration of surface modification on Au electrode is given in Figure 5.4. Different steps used in the preparation of the sensor are explained below.

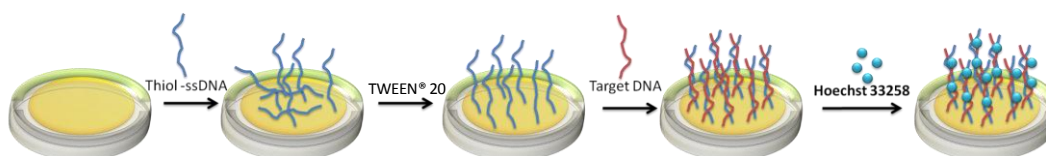


Figure 5.4. Schematic view of mechanism for modification of Au electrode surface.

5.1.2.1. Selection of Capture Probe

The sequence of capture probe DNA plays an important role in determination of sensitivity. Therefore, it is important to have non-folding capture probe DNA on the Au surface to increase hybridization with target DNA sequence. In this study, capture probe DNA was selected analyzing the possible folding structures of it on using mFold Web server.

5.1.2.2. Self-Assembled Monolayer (SAM) Formation

The sensors were immersed into acetone, isopropanol, and ethanol, respectively, in order to remove organic residues (Ceylan Koydemir et al., 2009). After warming up sensors on hot plate to evaporate ethanol, 70 μM capture probe DNA solution in 1 M HEPES was introduced to the sensor, and waited

for 24 hours for adsorption of thiol molecules on Au surface. Then, the sensor was rinsed with TWEEN® 20 solution to remove excess DNA.

5.1.2.3. dsDNA Hybridization and Adsorption of Hoechst 33258

Target DNA, which is complementary to capture probe, was introduced for three hours of hybridization in PBS including 10 mM NaCl at 310.15 K. Then, 100 μ M Hoechst 33258 were prepared with 50 mM PBS including 100 mM NaCl and it was incubated on the electrodes for five minutes. Then, the sensor was rinsed with ultra pure water.

5.1.2.4. Electrochemical Detection

Electrochemical experiments were performed by using Autolab PGSTAT 101 (Eco Chemie, The Netherlands), which was connected to the computer using the Nova 1.5 software. In the experiments of redox marker based detection, the electrochemical sensors with Ag (semi circle in shape with 150 μ m wide), Pt (semi circle in shape with 150 μ m wide), and Au (disc shape with 500 μ m in radius) as reference, counter, and working electrodes, respectively were used. The fabricated sensors were used once for each experiment and disposed after each measurement. A photograph of experimental set-up for electrochemical detection is given in Figure 5.5.

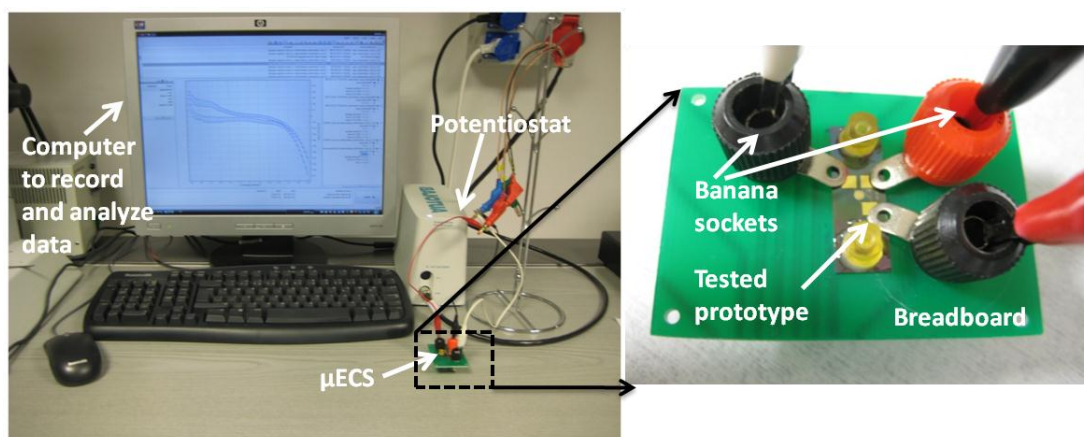


Figure 5.5. Experimental set-up for electrochemical detection.

Cyclic voltammetry was utilized by applying potential between -0.6 V and 0.6 V with a scan rate of 50 mV/s to test the stability of Ag electrode at different Cl⁻ concentrations (Cao et al., 2006). Au characterization in 0.5 M H₂SO₄ was performed by applying potential between 0 V and 1.7 V with cyclic voltammetry. Differential pulse voltammetry was used to detect the presence of DNA in PBS and the potential was scanned between 0 V and 0.9 V with step potential of 4 mV, modulation amplitude as 0.050 V, modulation time as 0.05 s, and interval time as 0.08 s.

5.2. Enzyme Based Detection

Horseshoe peroxidase (HRP) is one of the most commonly used enzymes in immunoassays because of its stability and availability. The general reaction performed by HRP is oxidation of a reversible substrate in the presence of hydrogen peroxide, H₂O₂. The schematic view of enzymatic cycle for HRP is given in Figure 5.6 where H₂O₂ is converted to water and an O atom takes the part in the enzyme to form the oxyferryl π -cation radical heme intermediate ([Fe^{IV}=O]^{•+}) (Dequaire et al., 2002). Formed product is reduced to the oxyferryl intermediate and to reversible product. Finally, enzyme is converted to its original state by forming reversible product and water.

This reversible substrate can be hydroquinone, ferrocene derivatives, 3,3',5,5', tetramethylbenzidine (TMB), or Osmium complex (Volpe et al., 1998). Among them, TMB is used mostly in determination of HRP due to its high sensitivity, availability, non-carcinogenicity, and limited

reaction with H_2O_2 , which gives product visible at 450nm after H_2SO_4 blockage (Figure 5.7) (Frey et al., 2000; Volpe et al., 1998). The oxidation reaction of TMB with HRP in the presence of H_2O_2 results to a blue-colored product (i.e., charge transfer complex, CTC). CTC is electroactive and shows a voltammetric peak in the electrochemical detection. The product becomes yellow due to formation of TMB^{2+} with the addition of sulfuric acid to the reaction solution to stop enzymatic reaction (Fanjul-Bolado et al., 2005; Josephy et al., 1982). The reaction of TMB^0 under acidic conditions presents two-electron redox wave because of formation of TMB^{2+} (Baldrich et al., 2009). As demonstrated in Figure 5.6, the radical intermediate, TMB^+ , is in equilibrium with CTC.

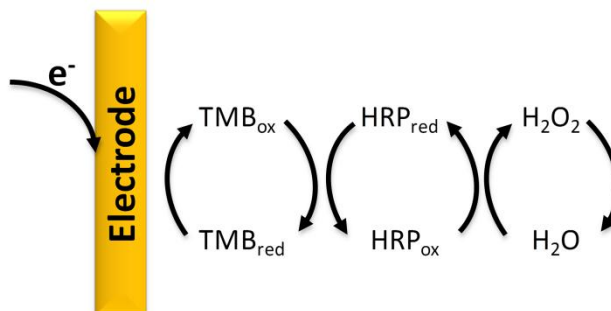


Figure 5.6. Enzymatic cycle of TMB in the presence of H_2O_2 .

However, TMB^0 is not fully soluble and decays rapidly in water based solutions. The solubility can be increased by lowering the pH of the solution (i.e., pH 4.0 – pH 7.0) (Baldrich et al., 2009). Thus, it is necessary to consider the other effects that determine the limit of detection. The rapid decay of the TMB can be overcome with preparing fresh samples for electrochemical detection. In this study, a commercial solution of TMB was used. This solution contains H_2O_2 and TMB such that it is optimized to have reaction kinetics approximately 60% slower than the conventional solutions. The studies related to the electrochemical detection of DNA by using HRP as non-electroactive marker found in the literature are given in Table 5.1 (Azek et al., 2000; Dominguez et al., 2004; Liu et al., 2008; Pan, 2007; Song et al., 2006; Zhang et al., 2002). It is seen from Table 5.1 that the highest detection limit was obtained in the studies, in which TMB with H_2O_2 were used as substrate in amperometric detection.

5.2.1. Materials

Sodium chloride (NaCl), potassium phosphate dibasic (K_2HPO_4), potassium phosphate monobasic (KH_2PO_4), Sodium tetraborate decahydrate ($\text{Na}_2\text{B}_4\text{O}_7 \cdot 10\text{H}_2\text{O}$), hydrochloric acid (HCl), streptavidin from *Streptomyces avidinii*, sodium borohydride (NaBH_4), sodium hydroxide (NaOH), ethanolamine, albumin from bovine serum, 3,3',5,5'-tetramethylbenzidine liquid substrate, (super slow), horseradish peroxidase were purchased from Sigma Aldrich. Disposable Sephadex PD-10 desalting columns were purchased from GE Healthcare and used according to the manufacturer's instructions.

Phosphate buffer saline (PBS) was prepared with 0.04 mol K_2HPO_4 and 0.01 mol KH_2PO_4 . Washing buffer and hybridization buffer were prepared with PBS including 0.1 M NaCl (pH 7.4) and 0.3 M NaCl (pH 7.4), respectively, while immobilization buffer was prepared with 10 mM Tris-HCl, 1mM EDTA, and 10 mM TCEP (pH 7.4).

Throughout the studies, specific sequences of *mecA* gene belonging to *Staphylococcus aureus* subspecies *aureus* MRSA 252 were used as target DNA. DNA stock solutions with a concentration of 100 μM were prepared in sterilized water and stored at 253.15 K. Single-stranded and modified capture and reporter probes were purchased from Alpha DNA. In enzyme-based detection, PCR product of *mecA* gene was used as target sequence.

The sequences used in the experiments were as follows:

Primer-1: 5'-TAG AAA TGA CTG AAC GTC CG

Primer-2: 5'-TTG CGA TCA ATG TTA CCG TAG

Capture probe: 5'-thiol ATT CAG GAT CGT AAA ATA AAA AAA GT
 Reporter probe: 5'-biotin TCG CAA CGT TCA ATT TAA TTT

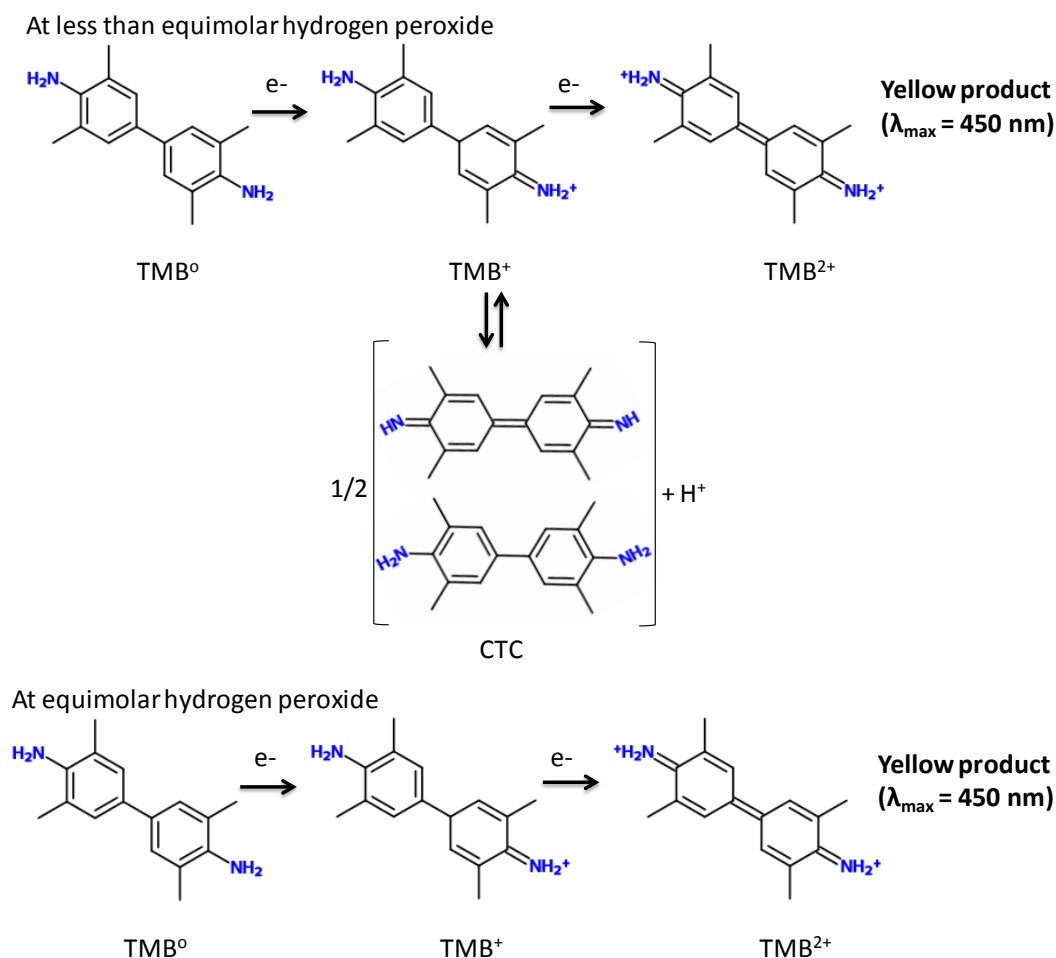


Figure 5.7. Redox reactions of TMB with HRP in the presence of less than equimolar and equimolar concentrations of H₂O₂ (Baldrich et al., 2009; Josephy et al., 1982).

Table 5.1. List of the some studies related to DNA detection by using HRP as non-electroactive marker.

Used electrode	Used substrate	Detection technique	Detection limit	Ref
Au	H ₂ O ₂ with redox probe Fe(CN) ₆ ³⁻	Faradaic impedance spectroscopy	20 ng/l	(Patolsky et al., 1999)
Au	H ₂ O ₂	CV	0.5 μM	(Song et al., 2006)
Au	TMB and H ₂ O ₂	Amperometric	10 fM	(Liu et al., 2008)
Au	TMB and H ₂ O ₂	Amperometric	0.3fM	(Liao et al., 2006)
Pt	H ₂ O ₂ /o-aminophenol	Electrophoresis automatic sequencing	8 pM	(Cao et al., 2010)
Glassy carbon electrode	o-aminophenol and H ₂ O ₂	Faradaic impedance spectroscopy	0.1 pM	(Li et al., 2010)
Carbon paste electrode	H ₂ O ₂	CV	50 pM	(Pan, 2007)

5.2.2. Methods

An illustration of surface modification on Au electrode for enzyme-based detection is given in Figure 5.8. Different steps used in the preparation of the sensor are explained below.

5.2.2.1. Selection of PCR Primers and Probe Design

The amplification of clinical isolates of MRSA was performed with the use of aforementioned primers by using polymerase chain reaction (PCR). The presence of nucleotide sequences on MRSA *mecA* gene was analyzed by using NCBI Blast (Medicine, 2012). For PCR, the bacteria cell was lysed and the DNA was isolated (Figure 5.9). Then, the isolated DNA, primers, and the contents of PCR kit (Qiagen, 201223) were placed in cycling heat machine to perform amplification cycles. Capture probe DNA was selected analyzing the possible folding structures of it on using mFold Web server.

5.2.2.2. Streptavidin-HRP Enzyme Conjugation

The streptavidin-HRP enzyme conjugation was performed by using the Schiff Base formation and reduction of amines (Figure 5.10) (Greg T, 2008). Streptavidin (i.e., amine containing molecule) was dissolved in a borate buffer having a pH 9.5. Then, the enzyme (horseradish peroxidase (HRP)) (i.e., aldehyde containing molecule) was added to the solution to have a typical molar ratio of reaction 3 moles of HRP per mole of protein. 10 μ l of 5M NaBH₄ in 1 M NaOH per ml of conjugation solution volume was added and let to react for four hours at room temperature. To block unreacted sites, 20 μ l of 3 M ethanolamine per ml of the conjugation solution volume was added and reacted for 15 minutes at room temperature. The conjugate was purified by using desalting column (GE-Healthcare, Sephadex PD-10) using borate buffer, which is a suitable buffer for the proteins being crosslinked.

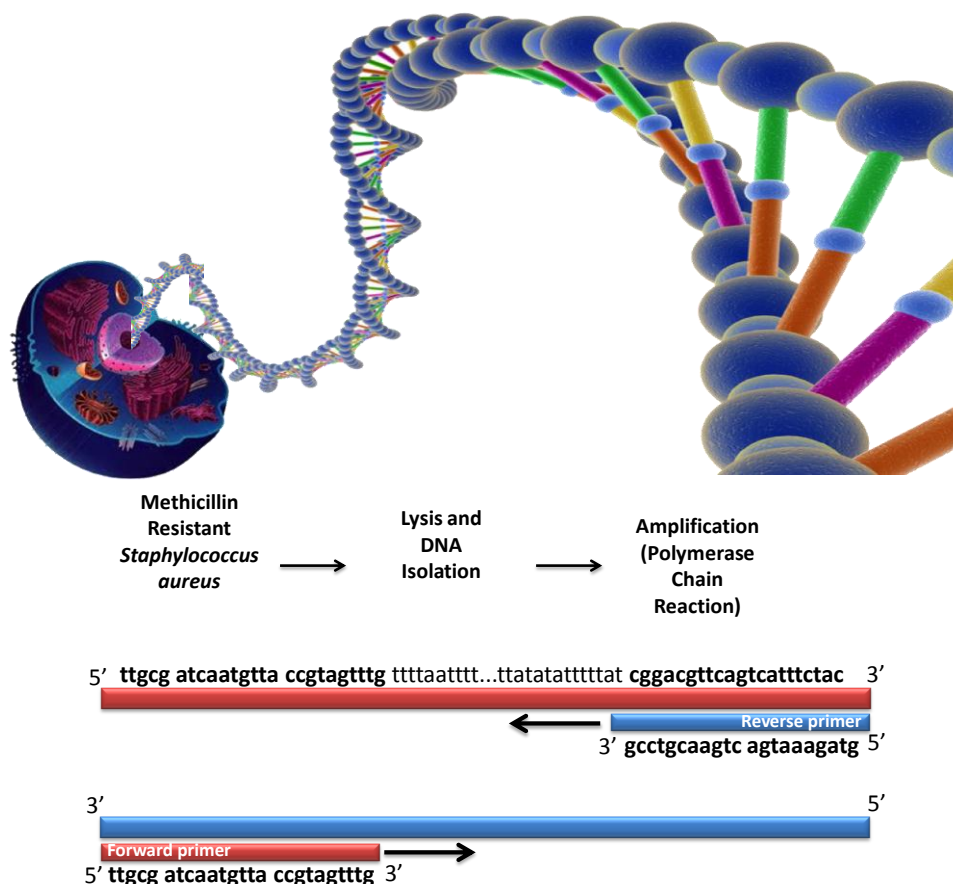


Figure 5.8. Isolation and amplification of DNA.

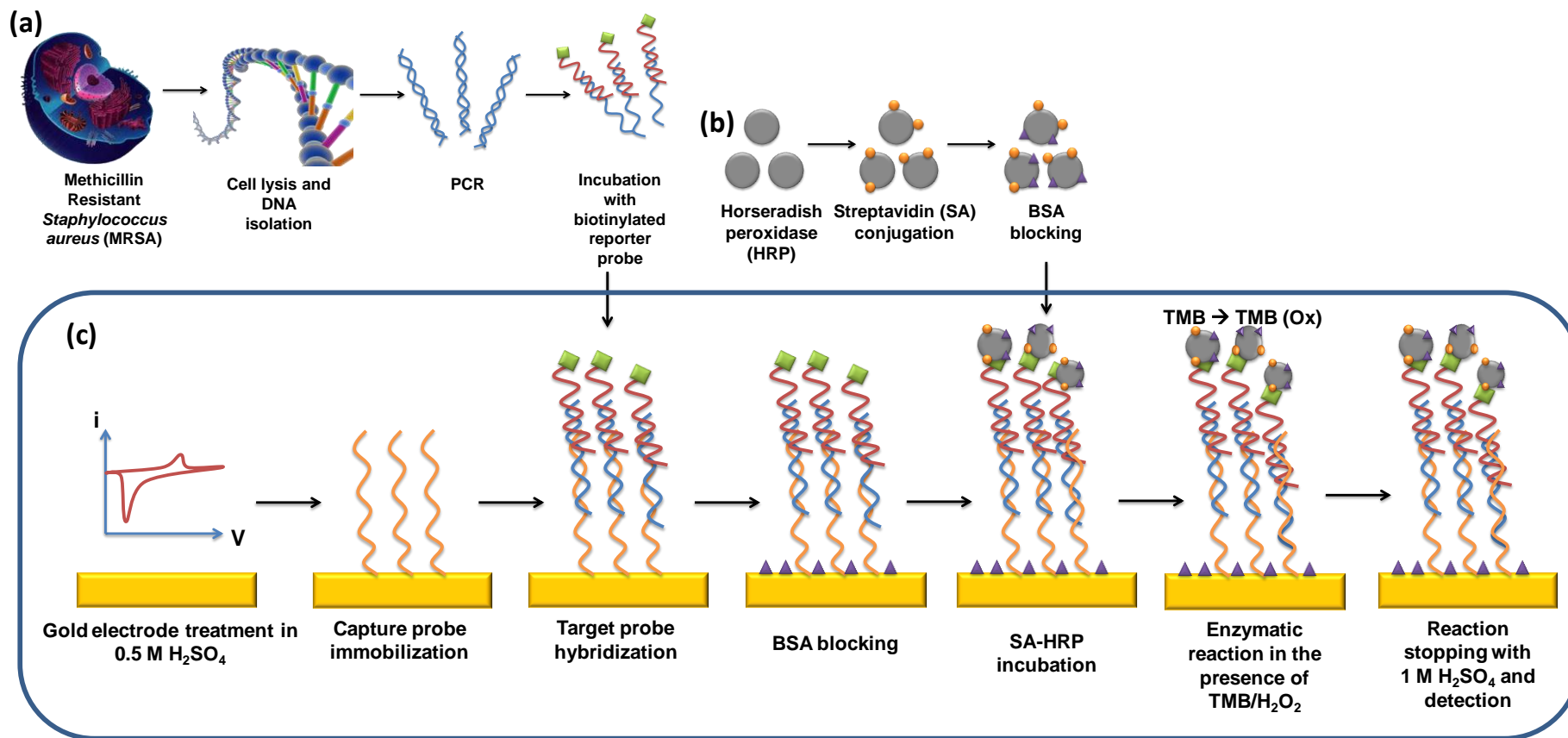


Figure 5.9. A schematic illustration of sandwich-enzyme immunoassay.

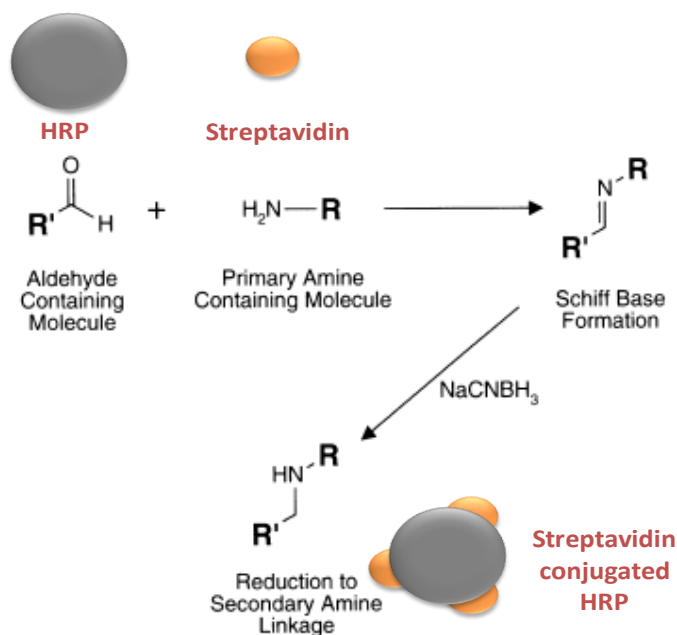


Figure 5.10. A schematic illustration of protein-enzyme conjugation (Adapted from the study of (Greg T, 2008)).

5.2.2.3. Surface Modification

The protocol used in the experiments for enzyme-based detection is as follows:

- Gold electrodes were immersed into ethanol overnight.
- The electrodes were treated electrochemically in fresh 0.5 M H_2SO_4 until stable cyclic voltammogram obtained.
- The electrodes were rinsed with ultra pure water and dried under N_2 .
- The electrodes were used immediately for immobilization of 10 μM capture DNA (prepared in immobilization buffer) for overnight.
- PCR products were diluted 10 times with hybridization buffer prior to hybridization.
- Targets (diluted PCR products) were mixed with biotinylated reporter probe (100 nM) in the hybridization buffer and heated to 353.15 K for five minutes. Mixture was cooled to room temperature.
- Droplet of the solution-containing target DNA (2 μl volume) was placed on the sensor surface for two hours at room temperature.
- After incubation, the sensor was rinsed with washing buffer.
- 1% BSA solution (prepared in hybridization buffer) was incubated on the electrode to react for one hour to block active sites.
- Then, the electrodes were incubated with 2 μl of streptavidin-HRP conjugate for five minutes at room temperature.
- After being rinsed with washing buffer, TMB/ H_2O_2 substrate was spotted and reacted for 15 minutes.
- Then, the reaction was stopped by using 1 M H_2SO_4 and electrochemical detection was performed.

5.2.2.4. Electrochemical Detection

Electrochemical experiments were performed by using Autolab PGSTAT 101 (Eco Chemie, The Netherlands), which was connected to the computer using the Nova 1.5 software. In the experiments of redox marker based detection, the electrochemical sensors with Ag (semi circle in shape with 150 μm wide), Pt (semi circle in shape with 150 μm wide), and Au (disc shape with 100 μm in radius and disc shape with 300 μm in radius) as reference, counter, and working electrodes, respectively were

used. The fabricated sensors were used once for each experiment and disposed after each measurement.

Au characterization in 0.5 M H₂SO₄ was performed by applying potential between 0 V and 1.2 V with cyclic voltammetry. Cyclic voltammetry was used to detect the oxidation of TMB.

5.3. Solvent Compatibility of Parylene C Film Layer

Since 1950s, there has been tremendous effort in realizing miniaturized devices with improved sensitivity, ease of use, and reduced overall cost and weight. Portable devices having such features were recognized first to be applicable in electronics. Later, increasing demand in precise detection of biological analytes at point of care diagnosis has enabled the use of this approach in biomedical field (Sia and Kricka, 2008). Nowadays, these intelligent systems or sensors have applications in several fields ranging from space exploration to consumer electronics (Kralj et al., 2012; Mavandadi et al., 2012; Moon et al., 2006; Shamaï et al., 2008; Siegel et al., 2009). In all of these fields, durability of the entire system with its ideal behavior in its working environment, especially in extreme conditions (e.g., mechanical shock, extreme temperatures, and harsh chemical media), for long-term exposures is essential (Gong et al., 2012; Nightingale et al., 2011). Therefore, selection of materials that are used in design, fabrication, and packaging from a large collection, while preserving the aforementioned benefits of the miniaturization, offers a great challenge to researchers for an end-user product. In this account, a substantial effort has been made by researchers in order to develop the product in a balance between cost and performance (Chung et al., 2012; Hashimoto et al., 2000).

Polymers and plastics have been preferably used in micro fabrication compared to traditional materials, to reduce the fabrication cost (Lu et al., 2010). There are different commercially available polymers, and among these, poly(methyl methacrylate) (PMMA) (Josse et al., 2001), poly(dimethyl)siloxane (PDMS) (Sokolov et al., 2011), and polycarbonate (Delvaux and Demoustier-Champagne, 2003) are some of the most commonly used ones in the design and in the first prototyping of sensors. Although the fabrication of devices based on these polymers is relatively easy with soft lithography, manufacturing process is not compatible with integrated circuit (IC) fabrication, which limits their usage in industry (Becker and Gartner, 2008).

Poly(monochloro-*p*-xylylene) (Parylene C) has been widely used in microfluidic applications in the formation of channels and reservoirs, and packaging of sensors (i.e., insulation of electronics) (Eydelnant et al., 2012; Wright et al., 2007). Its distinctive advantages can be listed as transparency, pinhole-free conformal coating at room temperature, biocompatibility (Lu et al., 2010), and compatibility with standard micro fabrication processes. A simple chemical vapor deposition method is used in forming Parylene C layers on a substrate (Davis et al., 2011). Its adhesion on any surface can be enhanced with silanization of the target surface before coating. It can be patterned with any type of photoresist and mask, and generally, dry processes are used to etch Parylene C film layer. It is also possible to have optically clear devices by either using glass as the substrate or peeling off Parylene C from the substrate.

Parylene deposition starts with solid source material, dimer di-*p*-xylylene (Kumar, 2000). It is heated up to 448.15 K and then 963.15 K subsequently for sublimation and formation of monomer *p*-xylylene, respectively. The monomer is deposited on the surface at room temperature to form poly(*p*-xylylene) (Williams et al., 2003). The chemical structure can be envisioned as a polymer of benzene rings having -CH₂ groups at *p*- positions and a chlorine atom instead of hydrogen in the benzene rings (Williams et al., 2003). This backbone has crystalline structure with no hydrogen bonding groups, which makes it stable against chemical attacks (Kim and Najafi, 2005; Small, 1953). Hence, wet chemical etching of the layer is difficult to achieve (Williams et al., 2003). However, plasma processes enable its etching with a precise pattern definition (Meng et al., 2008). Although its short-term exposure to chemicals does not demonstrate any solubility, solvent diffusion through the Parylene C film layer is an important issue to consider, due to its various microfluidic and packaging applications. However, only a few investigations have been reported in literature on the solvent compatibility of Parylene C. Miller et al. (Miller and Leighton, 1990) and Kumar et al. (Kumar, 2000) studied the swelling of Parylene C with seven selected solvents (chlorobenzene, trichloroethylene, xylene, *o*-dichlorobenzene, bromobenzene, chloroform, and tetrahydrofuran) to determine the cohesive density energy of the polymer. On the other hand, the efficiency of Parylene

C in insulation of electronics was monitored only after exposure to moisture (Davis et al., 2011; Seymour et al., 2009; Simeone et al., 2009; Zhuang et al., 2007). Additionally, Kim et al. (Kim and Najafi, 2005) studied the effects of some chemicals (acetone, 2-propanol (IPA), AZ400K developer, MF319 developer, and buffered hydrofluoric acid (BHF)) on Parylene C bonding strength at different bonding temperatures and reported that prolonged exposure to chemicals decreases bonding strength significantly, especially for strong acids and bases. Although previous studies provide some information related to the effects of solvents on Parylene C, there is not such a detailed report available on the solvent compatibility of Parylene C film layer.

The aim of this study is to present the compatibility of Parylene C to different types of solvents that may eventually affect its long-term use in microfluidic or packaging applications. In this aspect, we analyzed the behavior of Parylene C with 24 different solvents, commonly used in different chemical processes. Swelling ratios and effect of solvents on surface roughness were also investigated with an indication of how such data may be used. The results were compared with the data reported for another common polymer, PDMS, to determine the feasibility of Parylene C as a chemical barrier in the applications. Diffusions of solvents through Parylene C film layer were also studied by means of an encapsulated photoresist structure to infer possible effects of long-term solvent exposure on the Parylene C packaged material.

5.3.1. Materials

Parylene C dimer and its adhesion promoter (A - 174 Silane (3-Methacryloxy propyltrimethoxysilane)) were purchased from Specialty Coating Systems (Indianapolis, IN). Solvents were purchased from Merck, Sigma Aldrich, and J.T. Baker. All chemicals were used as received from commercial vendors.

Two different test structures were fabricated to analyze polymer swelling and penetration of solvents through 4- μm thick Parylene C film layer by using standard micro-electro-mechanical systems (MEMS) fabrication processes. The process of the first test structure requires only one mask to pattern Parylene C at the lithography process (Figure 5.11 A-B). Silicon wafers were dehydrated in an oven at 383.15 K for 30 minutes. After cooling the wafers down to the room temperature and following silanization, Parylene C coating was carried out with PDS-2010 (Specialty Coating Systems, U.S.), by using 10 grams of the dimer. This process resulted in a Parylene C film layer with $\sim 4\text{-}\mu\text{m}$ thickness. Then, AZ@9260 (520 mPa.s) photoresist was spin coated on the Parylene C film layer according to the manufacturer's instructions and patterned with a mask. The Parylene C film layer was etched in O_2/CF_4 inductively coupled plasma and the wafers were diced to have individual test structures. All test structures were immersed into acetone first, then IPA to strip of the photo resist, and then rinsed with DI water, and dried under nitrogen. The test structure was composed of three-square structures of Parylene C film layer with a side length of two millimeters. The Parylene C-square-layers adhered to the Si surfaces were used to prevent curling of the Parylene C film layer. For fabrication of the second type of test structures, glass wafer was used as a substrate since its transparency enables optical analysis of any change upon diffusion of solvents through the Parylene C film layer (Figure 5.11 C-D). After BHF treatment, Parylene C coating was performed as stated previously. AZ@9260 (520 cp) photo resist was spin coated to have 15 μm thickness on the Parylene C film layer according to the manufacturer's instructions and patterned with a mask. Afterwards, another Parylene C layer was coated and the wafer was diced.

5.3.2. Measurements

The estimation of the degree of polymer swelling is a critical issue and the change in the state of a polymer can be measured using different approaches, which are mainly based on optical and mechanical detection methods (Du et al., 1996). A charge-coupled device (CCD) camera connected to a stereoscope (Lee et al., 2003) or an optical microscope (Miller and Leighton, 1990) can be used in optical detection, and the degree of swelling is determined by calculating the difference in dimensions of the polymer structure before and after immersing into the solvent of interest. In mechanical detection, gravimetric methods are commonly used, and the degree of swelling is determined by making a ratio of the mass of swollen polymer to the mass of dry polymer (Hedden et al., 2000; Hedden et al., 1999). In literature, the thicknesses of polymer layers under investigation

were generally larger than 300 μm , and hence the thickness change could be easily detected with both of these techniques (Hedden et al., 2000; Hedden et al., 1999; Lee et al., 2003; Miller and Leighton, 1990). However, in this study, change in the thickness of Parylene C film layer was measured precisely by using a stylus profiler since it is hard to detect any change in such a small thickness accurately by using either optical methods or gravimetric methods.

Parylene C swelling measurements were performed in a clean room environment, which had controlled air circulation with a room temperature of 294.15 K and humidity of 49%. The measurements were based on the comparison of changes in step height of the Parylene C film layer and the surface roughness of this layer for each test structure before and after immersion into a specified solvent for 24 hours at 298.15 K in order to make sure that swelling is finished and stability is attained. The volume of each solvent was about 60 ml, which was much higher than that of the test structure. Step height measurements were performed by using Dektak 8 Advanced Development Profiler. The scan length was 2700 μm with a scan speed of 50 seconds, which results in horizontal resolution of 0.180 $\mu\text{m}/\text{sample}$ for step height measurements.

Surface roughness measurements were performed by using Wyko NT1100 Optical Surface Profiler in phase shifting interferometry (PSI) mode with high magnification filter and 50 X optical zoom. For each solvent, nine different square structures of Parylene C were analyzed for the step height measurements and three different square structures of Parylene C for the surface roughness measurements. The values that are given in Table 6.12 and in the figures were calculated by taking average of these measurements for each solvent. Standard deviation for each data was calculated as $\pm 0.5\%$. While evaluating the experimental data, Si etch rate in the solvents were not taken into consideration, since it's etch rate is zero or too slow (Williams et al., 2003).

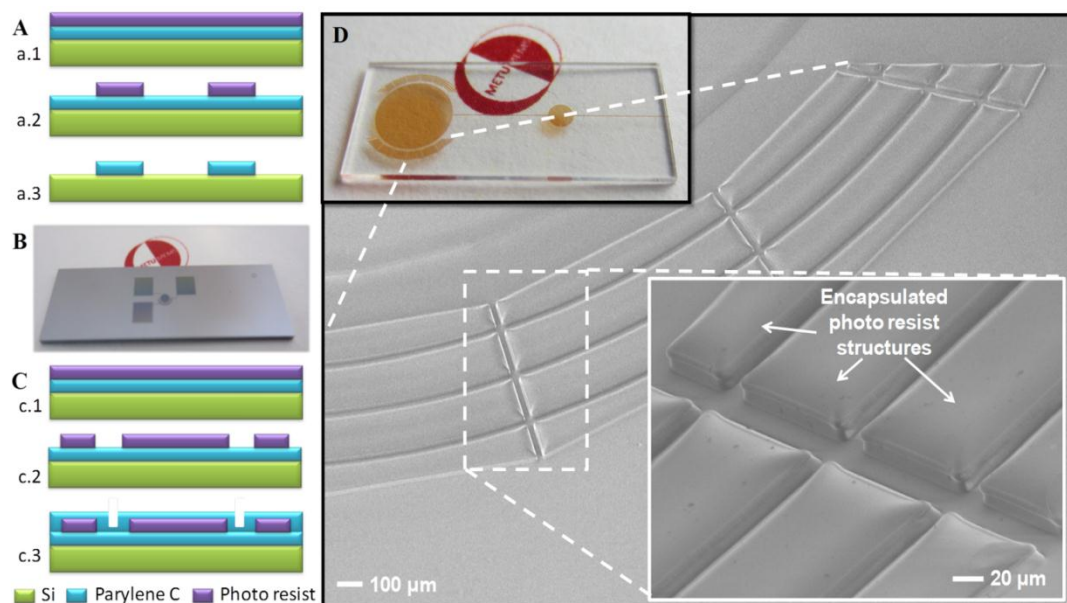


Figure 5.11. (A) Illustration of the process flow for fabrication of the test structures used in the experiments of Parylene C swelling: (a.1) Parylene C deposition, (a.2) Photo resist coating and patterning, (a.3) Parylene C etching and photo resist stripping. (B) A photograph of the fabricated test structure for the Parylene C swelling experiments. (C) Illustration of the process flow for the fabrication of the test structures used in the solvent diffusion experiments: (c.1) Parylene C deposition, (c.2) Photo resist coating and patterning, (c.3) Parylene C layer deposition and dicing. (D) A photograph of fabricated prototype for the solvent diffusion experiments and SEM picture of encapsulated photo resist structures.

5.4. Effects of Solvents on Dissolution of Photo Resist Encapsulated in Parylene Microchannels

Micro channels are the essential parts of lab-on-a-chip systems due to their capabilities in fluid directing and controlling at various fields, such as heat exchangers (Ceylan Koydemir et al., 2012c). (Khan and Fartaj, 2011; Koyuncuoğlu et al., 2012) and diagnosis assays (Beech et al., 2012; Ceylan Koydemir et al., 2011; Choi et al., 2012).

The micro fabrication of channels with desired length and dimension is a critical issue and it necessitates good knowledge about the materials and the fabrication processes. In the prototyping of lab-on-a-chip systems, polydimethylsiloxane (PDMS) is preferred due to its simplicity and rapid prototyping fabrication process (Huh et al., 2010). However, it is not compatible with batch fabrication processes, such as micro-electro-mechanical systems (MEMS) and integrated circuit (IC) technology. Parylene C is a good alternative as a polymer in forming channels due to its several properties, such as biocompatibility, compatibility with mass production processes and conformal coating (Sukas et al., 2008; Tan and Craighhead, 2010; Yildirim and Kulah, 2011). There are many different techniques for fabricating parylene microfluidic channels utilizing different materials. One of the most common techniques is based on the encapsulation of photo resist between a substrate (glass, silicon, etc.) and the parylene. Photo resist is used as a sacrificial layer to form patterns, such as reservoirs, channels, and junction points. After deposition of Parylene C on top of photo resist, the inlet and outlet reservoirs of the channels are opened by using plasma-etching processes and the dies are immersed into a solvent to allow flow in micro channels. However, the removal of photo resist from micro channels is a time consuming process and the complete removal of the photo resist may take days, depending on the length and dimensions of the channel. There are several commercial products as photo resist strippers. However, their usage in the removal of encapsulated photo resist is limited because of low dissolution rates and possibility to attack metals in long time. As an alternative, acetone which is commonly found in each clean room and/or laboratory was studied by Tai's group due to its selectivity (Walsh et al., 2001).

5.4.1. Theory for Dissolution of Photoresist inside the Microchannels

When the photoresist (A) encounters with the liquid (B), the molecules of A penetrate into the solution and undergo an irreversible first-order chemical reaction with a rate constant, k as demonstrated in Figure 5.2. The concentrations of reaction products do not interfere with the diffusion A through B, i.e., pseudo-binary behavior. When $\frac{D_{AB}t}{L^2}$ becomes much higher than one, the system can be treated as at pseudo-steady state.

The governing equation describing the dissolution process is given in Equation (5.1),

$$\frac{d}{dx} \left(D_{AB} \frac{dC_A}{dx} \right) - kC_A = 0 \quad (5.1)$$

Equation (5.1) has to be solved with boundary conditions:

- (1) The concentration of the photo resist at the photo resist surface where it encounters with solvent is equal to the saturation concentration of photo resist in the solvent (C_{A0}),
- (2) The concentration of photo resist in the bulk solvent is equal to zero.

Finally, Equation (5.2) can be obtained as,

$$\cosh(L\sqrt{k/D_{AB}}) = \exp\left(\frac{C_{A0}M_A}{\rho_A}kt\right) \quad (5.2)$$

Then, a quasi-steady state model for the diffusion and chemical reaction of photo resist in solvent can be developed to derive an expression for the length of cleared region inside the channel with time, for small and large values of $L\sqrt{k/D_{AB}}$ (Equations (5.3) and (5.4), respectively) and to figure out the parameters that influence the dissolution rate.

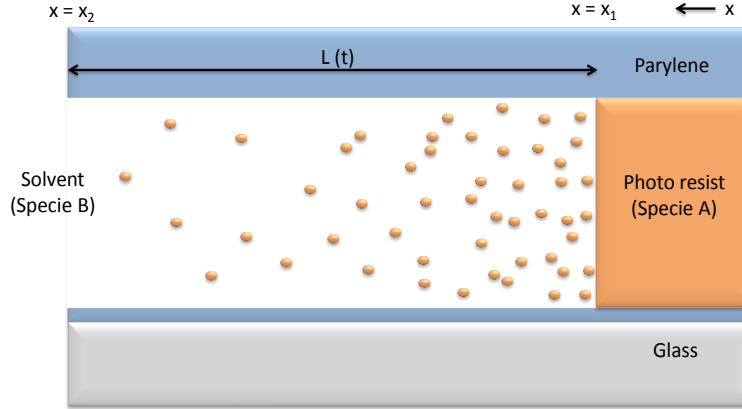


Figure 5.12. Schematic view of dissolution of photo resist in Parylene C microchannel.

$$L^2 = \frac{2}{k/D_{AB}} \exp\left(\frac{C_{A0}M_A}{\rho_A}kt\right) - 1 \quad (5.3)$$

$$L = \frac{1}{\sqrt{k/D_{AB}}} \left(\ln 2 + \ln \frac{C_{A0}M_A}{\rho_A}k \right) + \frac{1}{\sqrt{k/D_{AB}}} \ln t \quad (5.4)$$

where, L is the length of cleared region [m], k is the reaction rate constant [s^{-1}], D_{AB} is the diffusion coefficient [m^2s^{-1}], M_A is molecular weight [$kgkmol^{-1}$], ρ_A is the density of photo resist [kgm^{-3}], and t is the time [s]. The parameters affecting the dissolution rate of photo resist are obtained as k , D_{AB} , and C_{A0} from the Equations (5.3) and (5.4). The effects of these parameters on the dissolution rate can only be analyzed experimentally.

5.4.2. Fabrication of Test Structure and Measurements

The test structures with Parylene C micro-channels, which have a channel cross-section of $15 \mu m \times 50 \mu m$ and length of one centimeter, were fabricated by using surface micromachining processes.

Figure 5.13 shows the process flow diagram for the fabrication of micro-channels. The process requires only one mask for lithography process. Glass wafer was used as substrate to enable the visualization of photo resist inside the micro channels.

- The glass wafer was cleaned with piranha solution and buffered hydrofluoric acid to remove organic residues and to increase the surface roughness for better adhesion of Parylene C (Figure 5.13a).
- Then, Parylene C was coated to have two-micrometer thickness using PDS-2010 (Specialty Coating Systems, US).
- The adhesion promoter, A-174 silane was used to have better adhesion between glass wafer and Parylene C (Figure 5.13b).
- Then, AZ@9260 (520 mPa.s) with $15 \mu m$ thickness was patterned according to the instructions of the manufacturer (Figure 5.13c).
- Next, five-micrometer thickness of Parylene C was coated to form channels (Figure 5.13d).
- Lastly, wafer was diced to have individual dies.

The solvents used in the experiments are given in Table 5.2. The physical properties of solvents affect the diffusion coefficient. Thus, solvents were selected such that the effect of physical properties to be recognizable. In addition, the parameters that affect the photo resist characteristics, such as UV exposure and temperature that change the physical properties of chemicals were also taken into account. The experiments were performed at room temperature (293 K). A die was placed in a glass dish with a cover to decrease evaporation of solvent. The change in the length of the cleared region of microchannel was recorded by taking colored photos with the digital camera of the microscope for a time of 100 minutes with one-minute time intervals.

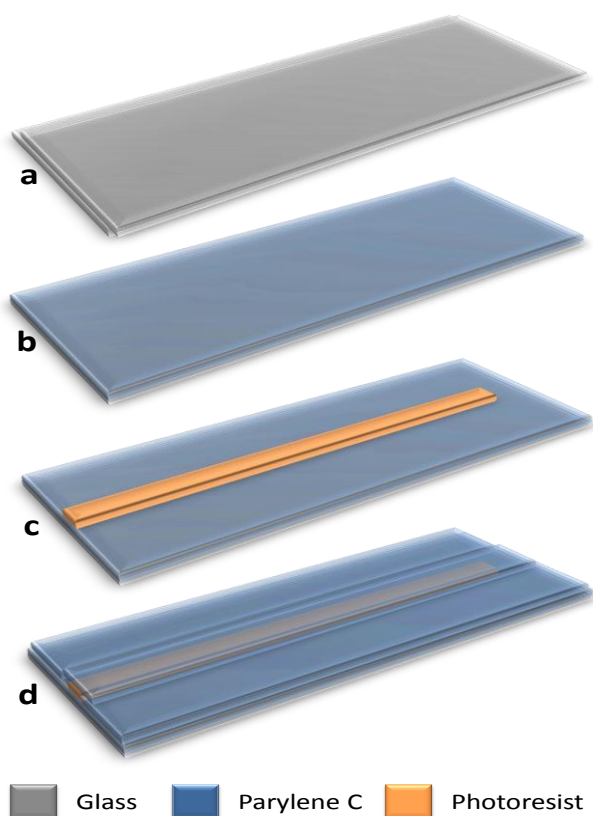


Figure 5.13. Fabrication flow: (a) Wafer cleaning, (b) Parylene C deposition, (c) Patterning with photo resist, (d) Parylene C deposition and dicing.

Table 5.2. Solvents and their physical properties.

	Solvent	ρ (kg/m^3)	BP* (K)	MP** (K)
Organic solvents	N-heptane	679	371	182
	Cyclohexane	774	354	280
Dipolar aprotic solvents	Acetonitrile	776	355	227
	Acetone	784	329	178
	Ethyl acetate	895	350	189
	N-butyl acetate	876	399	195
	Dimethylsulfoxide (DMSO)	1095	462	291.5
	Dimethylformamide (DMF)	944	426	212
	N-methyl-2-pyrrolidone (NMP)	1026	475	249

*BP: Boiling point, **MP: Melting point

CHAPTER 6

RESULTS AND DISCUSSION

In this chapter, characterization of the sensor, the experimental findings for the detection of antimicrobial resistance using two different electrochemical detection methods (i.e., redox marker based detection and enzyme based detection), and experimental findings for the studies on solvent compatibility of Parylene C layer and dissolution of photoresist enclosed in a microchannel are given in detail.

6.1. Characterization of the Sensor

Before starting experiments related to the detection of *mecA* gene, the stability of the electrodes were analyzed. In the analysis, the focus was especially on Ag and Au electrodes, which are reference and working electrodes of the sensors, respectively, and the Parylene C layer. The stability of Pt electrode was not studied due to its high stability.

6.1.1. Ag Electrode

The characterization of Ag reference electrode was analyzed by immersing into different KCl concentrations (i.e., 5 mM, 50 mM, 100 mM, and 500 mM) and PBS concentrations to check the stability of the electrode (Figures 6.1 and 6.2) (Cao et al., 2006). The trend of voltammogram and the forward peak current were stable for KCl, while there was a slight change in reverse peak current with increasing Cl⁻ concentration. At all concentrations, an oxidation peak current and a reduction peak were observed at near 0 V and -0.1 V, respectively. The peaks observed at near 0 V is due to formation of hydrogen bubbles over the surface of the counter electrode while the peak observed at near -0.1 V is probably due to reduction of oxygen (Beni et al., 2004). Moreover, another oxidation peak observed at a potential of near 0.4 V for the cyclic voltammogram of 100 mM KCl concentration may be due to formation of OH⁻ ions. In addition, the dissolution of silver layer and its adsorption on Au and Pt surfaces were observed when the potential range was changed from -0.2 V to 1.5 V. This was due to the formation of silver chloride (AgCl) from Ag in the presence of Cl⁻ ions and dissolution of Cl⁻ ions in the aqueous solution with the equilibrium reaction (Cao et al., 2006). Then, 50 mM PBS (0.04 mol K₂HPO₄ and 0.01 mol KH₂PO₄) was chosen to use in the electrochemical measurements to prevent the dissolution of silver.

6.1.2. Au Electrode

Characterization of Au layer was performed analyzing surface roughness of bare gold electrode and cyclic voltammograms of acid treatment.

Measurement of Au surface roughness was performed by using non contact 3D surface profiler (Wyko NT1100, Veeco Instrument Inc., USA) in PSI mode with Low Mag filter (50X objective) by analyzing 121 μm x 92 μm using WYKO Vision32 software (WYKO Corporation, USA). The average and root mean surface roughnesses of the electrode, which affects the value of effective area of the electrode, are 0.65±0.06 and 0.83±0.07, respectively (Table 6.1). The degree of surface roughness plays an important role in the formation of monolayer on the gold electrode since surface roughness increases effective area of the electrode. Figure 6.3 displays the surface morphology of a bare gold electrode.

In order to determine the effective area of the gold electrode, electrodes were treated electrochemically in fresh 0.5 M H₂SO₄ until stable cyclic voltammogram obtained (Figures 6.4 and 6.5) (Kerman et al., 2008). In this step, since the density of sulfuric acid is higher than the density of water ($\rho_{\text{H}_2\text{SO}_4} = 1.84 \text{ g/cm}^3$, $\rho_{\text{H}_2\text{O}} = 1 \text{ g/cm}^3$), it was very important to mix the acidic solution while

taking a sample from it. Otherwise, the acid would condense at the bottom of the container. The algorithm used for Au layer characterization is given in Appendix C. This cyclic voltammogram represents generation of a gold oxide monolayer with an oxidation peak near 1.1 V and its reduction near at 0.6 V. The area under the reduction peak is comparative to the effective surface area of gold electrode and can be estimated by the following formula (Kudo et al., 2010):

$$\text{Area} = \frac{\text{Intensity of Reduction Peak}}{\text{Scan Rate} * \text{Amount of the charge needed to reduce layer}} \quad (6.1)$$

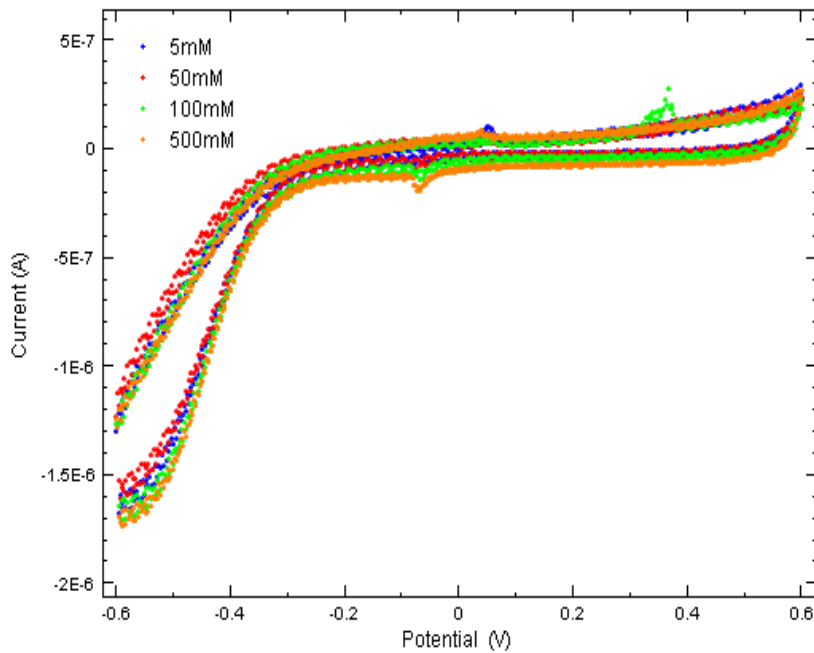


Figure 6.1. Cyclic voltammograms for different KCl concentrations.

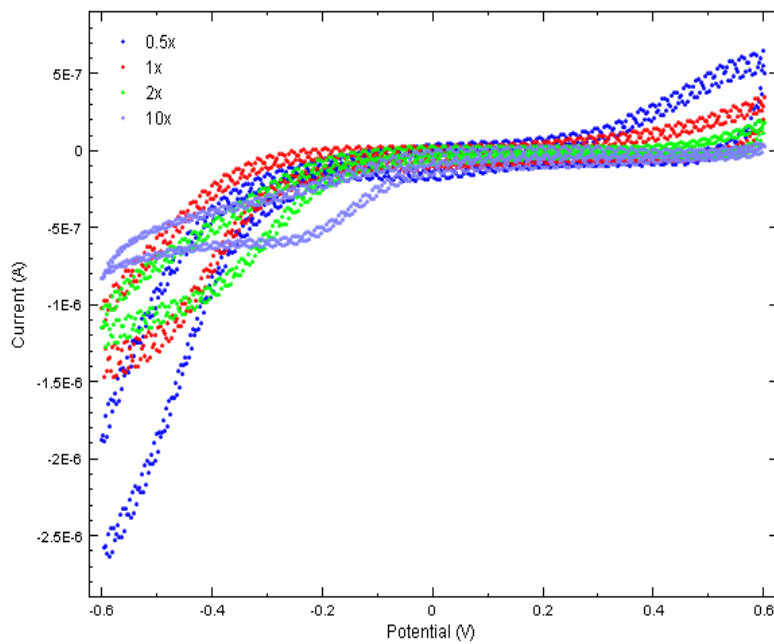


Figure 6.2. Cyclic voltammograms for different PBS concentrations.

Table 6.1. Data for surface roughness measurement.

Measurement No	R _a (nm)	R _q (nm)
1	0.70	0.94
2	0.66	0.83
3	0.92	1.14
4	0.43	0.53
5	0.50	0.62
6	0.55	0.76
7	0.58	0.75
8	0.90	1.17
9	0.57	0.74

R_a: Average roughness.

R_q: Root mean square roughness.

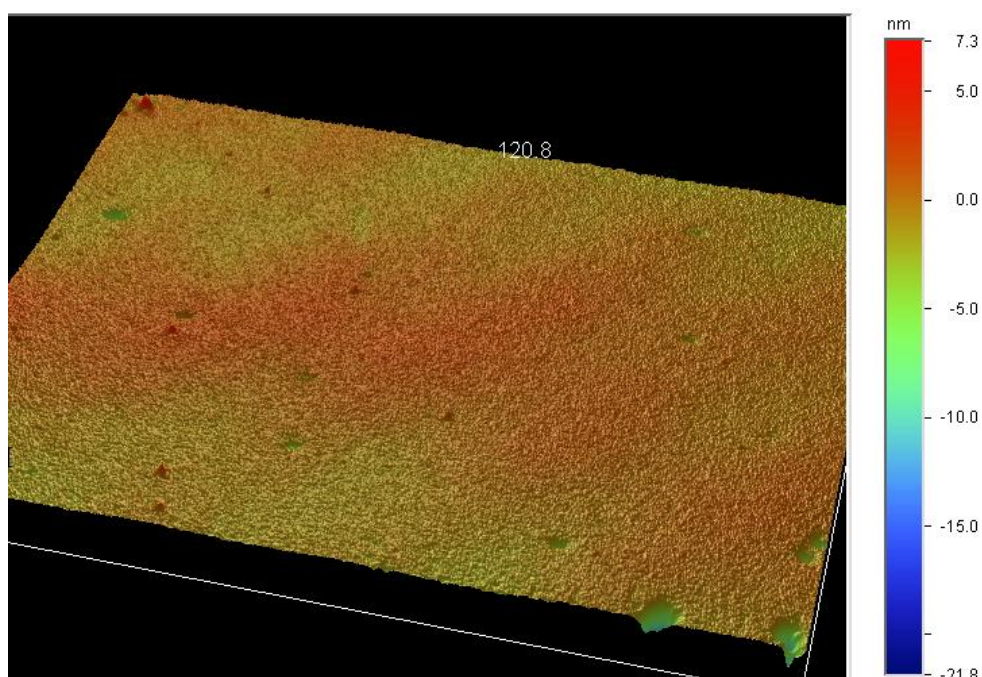


Figure 6.3. 3D plot of a bare gold surface.

The amount of the charge needed to reduce gold layer is $386 \mu\text{C}/\text{cm}^2$ (Kudo et al., 2010). The curve fitting toolbox of MATLAB was used to calculate intensity, and the real surface area of $100 \mu\text{m}$ radius working electrodes which was predicted from the oxide reduction peak was $1.365 \times 10^{-3} \text{ cm}^2$ intensity (Appendix C). The roughness factor can be determined by dividing the real surface area to geometric surface area of the electrode (Yang et al., 2012). Since the geometric surface area of the electrode is $3.14 \times 10^{-4} \text{ cm}^2$, the roughness factor is 4.35, which means that the roughness of gold layer is low.

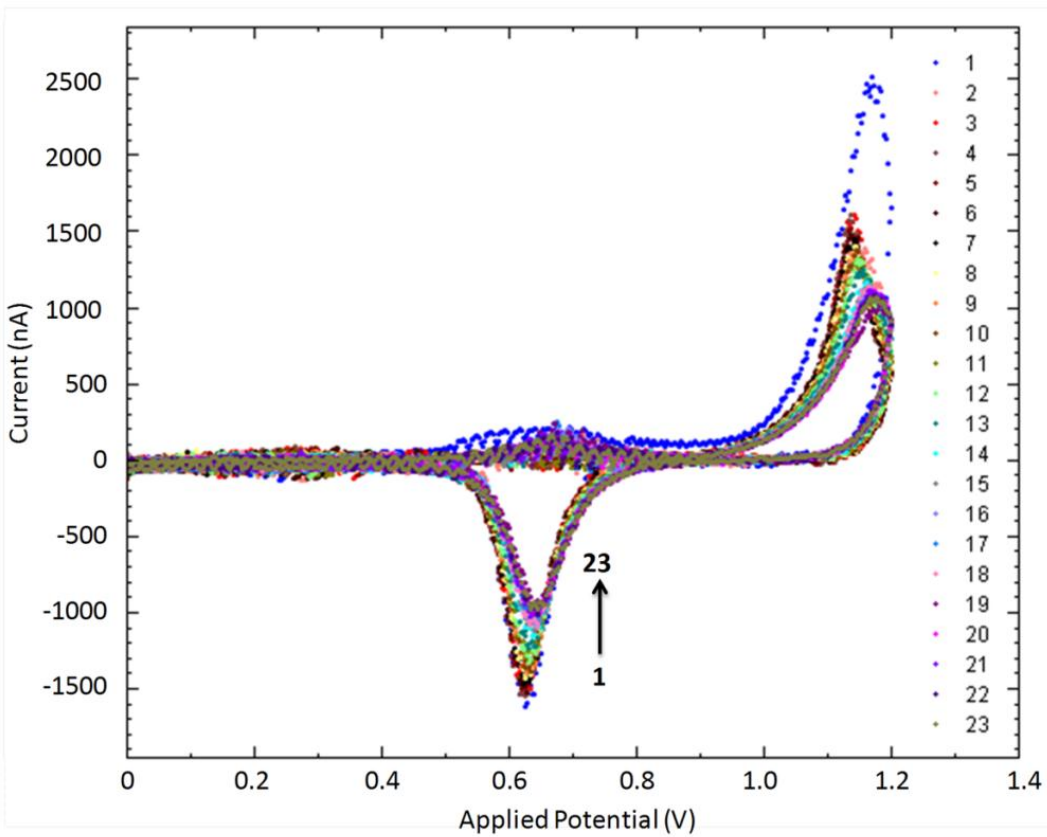
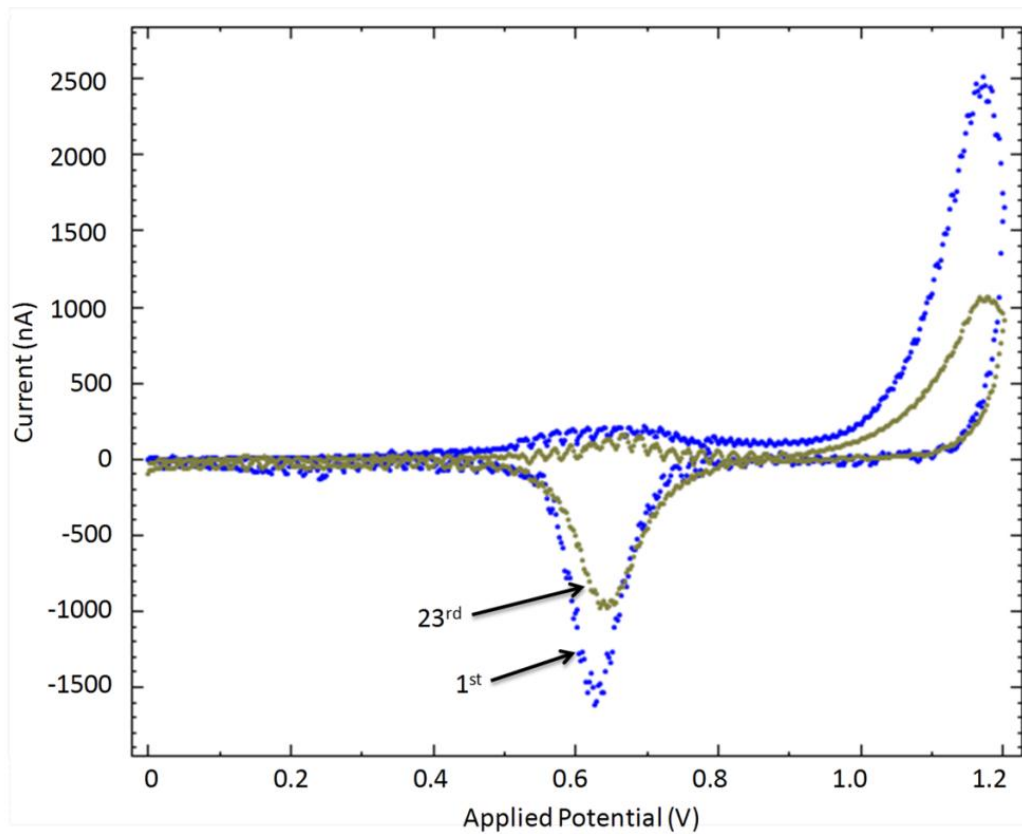


Figure 6.4. Cyclic voltammograms of Au oxidation (a) for the first and the last crossings of cyclic voltammetry (b) for each crossings of cyclic voltammetry ($r = 300 \mu\text{m}$).

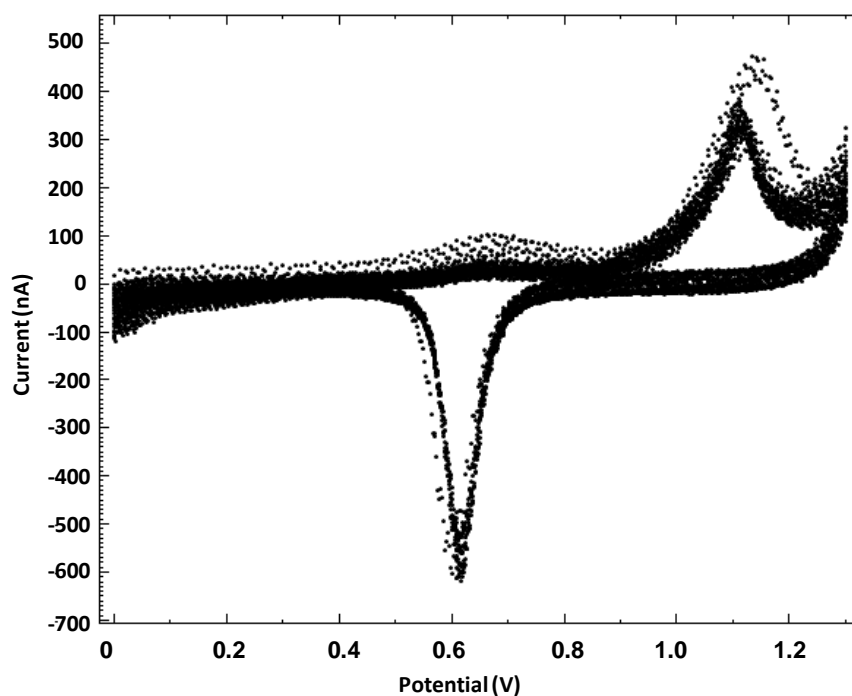


Figure 6.5. Cyclic voltammograms of Au redox cycle ($r = 100 \mu\text{m}$).

6.2. Redox Marker Based Detection

6.2.1. Capture Probe Selection

OligoWiz and mfold servers were used in the selection of capture probe (Ermini et al., 2011). The complete genome of *Staphylococcus aureus* subsp. *aureus* strain MRSA 252 (GenBank ID: BX571856.1) was gathered from GenBank (U.S. Department of Health and Human Services, National Institute of Health, National Center for Biotechnology Information (NCBI)). The analysis was performed according to the protocol given in the study of (Wernersson et al., 2007). In short, the target sequence was prepared in TAB format using the FeatureExtract software (Wernersson, 2005) loaded into OligoWiz 2.0 client, short-mers (24-26) prokaryotic was selected as a predefined parameter set, and a query was submitted to the OligoWiz server. The generated OligoWiz data file was analyzed and *mecA* was selected from the entries part. The parameters were selected as follows: “Cross-hybridization” was set to 0.0, “Delta T_m ” was set to 5.0, “Folding” was set to 0.3, “Position” set to 0 to enlarge the effect of T_m on probe score, and “Low complexity” was set to 1.0. After that, the possible secondary structures of capture probe and the thermodynamic details of folding structures were investigated with the Mfold Web Server (Table 6.2) (Zuker et al., 1999). There were four structures, and among them structure 1 has the highest possibility to form since its T_m value, $25.9 \text{ }^\circ\text{C} \pm 2 \text{ }^\circ\text{C}$ is the near at room temperature. The others could not be observed at the experimental conditions since their T_m values are much lower than the room temperature. Therefore, the hybridization was performed at $37 \text{ }^\circ\text{C}$.

6.2.2 Detection of Hybridization

The detection of biological analyte with high sensitivity was necessary for accurate diagnosis. For this purpose, the changes in the peak currents for different concentrations of *mecA* gene were analyzed by DPV (Figure 6. and Table 6.3). Thiol-modified DNA with Hoechst 33258 marker was used as negative control in the experiments. In the Figure 6.6A, each bar demonstrates arithmetic mean and standard errors of the peak current values acquired from three different samples of DNA sequences. The mean and standard errors were calculated by using equations below:

$$\text{Mean} = \bar{x} = \frac{\sum_{k=1}^n i_{pk}}{n} \quad (6.2)$$

$$\text{Standard error} = \frac{\sigma}{\sqrt{n}} \quad (6.3)$$

where n is the number of measurements, i_p is the peak current value of each measurement, \bar{x} is mean, and σ is standard deviation. The standard deviation was calculated by using the following equation:

$$\sigma = \sqrt{\frac{\sum(i_p - \bar{x})^2}{(n-1)}} \quad (6.4)$$

It was found that as the concentration of target DNA increased, the peak current increased due to the increase in coverage of surface with hybridized target DNA and Hoechst 33258 molecules. Moreover, Figure 6.6B shows the increase in peak current was leveled off at high concentrations. This was due to the saturation of monolayer molecular adsorption on the Au electrode. The monolayer adsorption on the gold surface of micro electrochemical sensor can be modeled by using Langmuir adsorption theory. According to this theory, there are four main assumptions that satisfy the chemisorption of the adsorbate on the adsorbent:

- The surface is homogeneous so that there is not any defects on the surface,
- The adsorption type is chemisorption,
- All adsorption sites are identical to each other,
- Each adsorption site is capable of holding one molecule,
- The adsorbates do not have any interactions with each other.

The equation for the monolayer coverage, θ is as follows:

$$\theta = \frac{K_{eq}C}{1+K_{eq}C} \quad (6.5)$$

where K_{eq} is the adsorption coefficient [M^{-1}] and C is the concentration of adsorbate [M]. The magnitude of monolayer coverage is between zero and one and, it can be expressed as the ratio of the amount of adsorption, Y to maximum adsorption, Y_{max} in units of moles adsorbate per mass adsorbent and it is given as:

$$\theta = \frac{Y}{Y_{max}} \quad (6.6)$$

The Equation 6.5 was rewritten as indicated in Equation 6.6, C/Y vs C graph was plotted (Figure 6.7), and Y_{max} and K_{eq} for the adsorption on gold surface for redox marker based detection were determined as 1428.57 nA and 700 μM^{-1} .

$$\frac{C}{Y} = \frac{1}{K_{eq}Y_{max}} + \frac{C}{Y_{max}} \quad (6.7)$$

Table 6.2. Folding structures and thermodynamic details of the capture probe (0.01 M Na⁺, 310.15 K).

	Structure type			
	1	2	3	4
Structure				
Thermodynamic Details of Folding				
ΔG (kcal/mol) at 37°C	1.03	1.26	1.94	1.96
ΔH (kcal/mol)	-28.00	-12.80	-11.30	-11.30
ΔS (cal/K.mol)	-93.5	-45.3	-42.6	-42.7
T_m (K)	299.05	282.35	264.75	265.35
Standard Errors	$\pm 5, \pm 10, \pm 11, 2-4$ K, respectively			

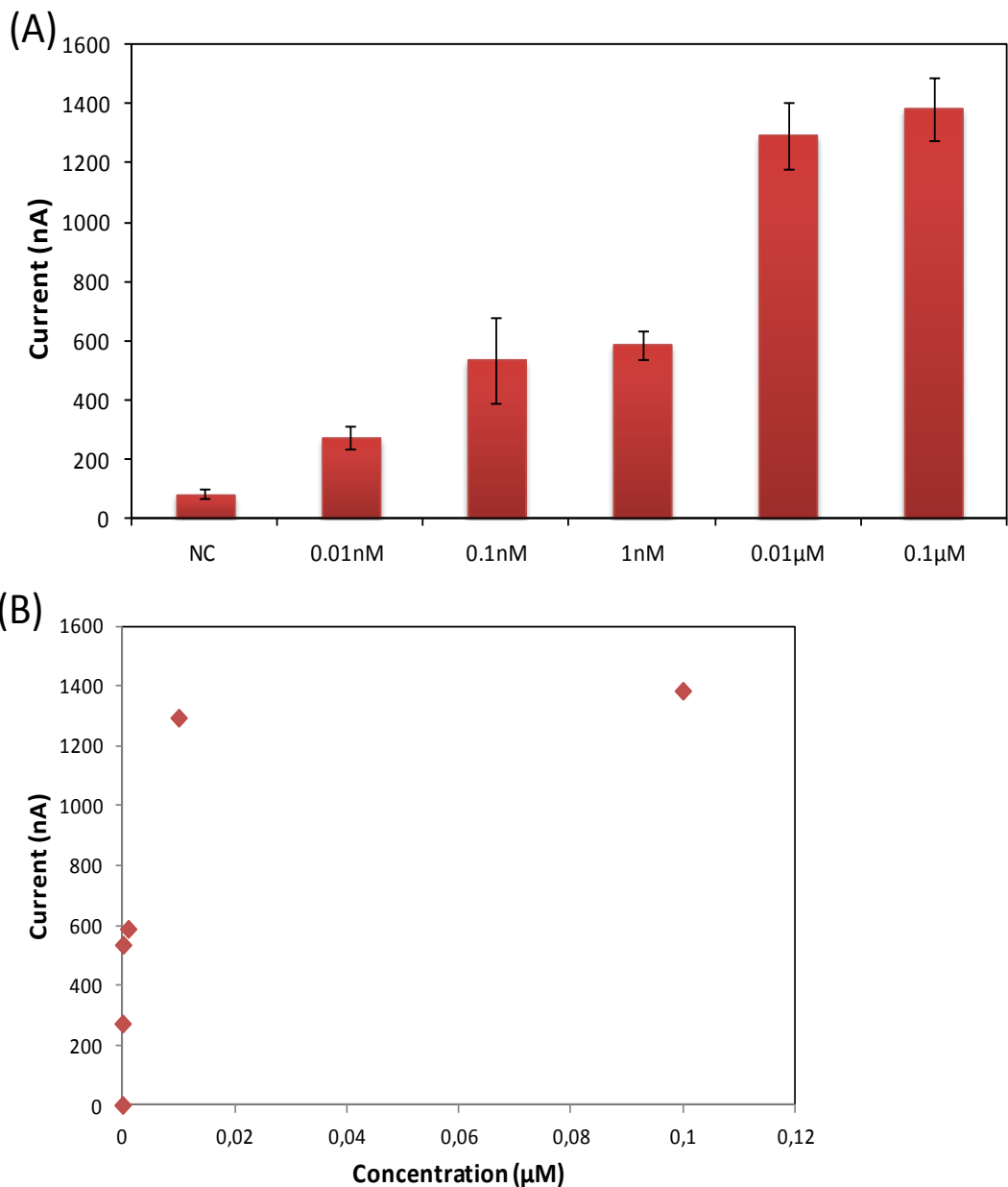


Figure 6.6. Electrochemical detection of methicillin resistance with different concentrations of mecA gene (A) The maximum peak currents obtained by DPV (B) The mean of the peak current values demonstrating the monolayer adsorption isotherm.

Table 6.3. Peak current values for a set of measurements for the electrochemical detection of mecA gene using Hoechst 33258 as redox marker.

Measurement no	Target DNA Concentrations						
	Negative control Thiol DNA	0.01 nM	0.1nM	1 nM	0.01μM	0.1 μM	1 μM
1	117	195,9	505,2	600,0	1500	1600	1720
2	65	319,6	297,0	500,0	1120	1250	1240
3	65	300,9	802,9	665,0	1260	1300	1480
Standard error of the mean	17,27	38,47	146,80	47,99	110,96	109,29	138,56
Mean	82,29	272,12	535,04	588,33	1293,33	1383,33	1480

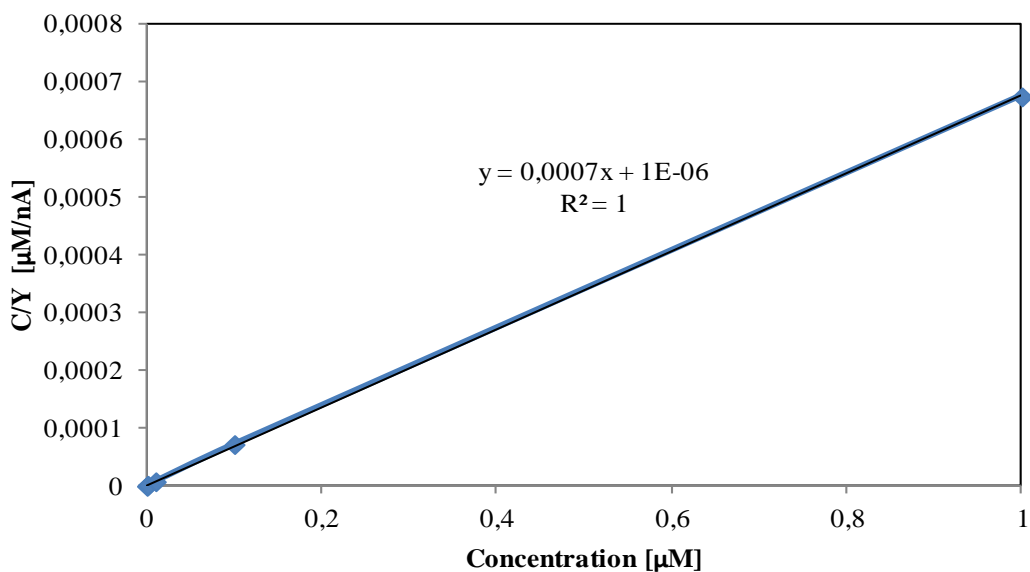


Figure 6.7. C/Y vs. C graph to determine adsorption constants.

6.2.3. Cross-reactivity Tests

The high specificity of the μ ECS was demonstrated with three DNA sequences, which are commonly used in the commercial assays: *mecA* gene, common in *S. aureus* and *S. epidermis*, *femA* gene from *S. aureus* and *femA* gene from *S. epidermis* (Figure 6. 8). *femA* gene was the first discovered gene which encodes proteins that have an effect on the level of methicillin resistance (Li et al., 2012).

After the self-assembled monolayer formation on the surface with thiol modified capture probe, 1 μ M of each sample was introduced and three hours of hybridization step was performed at 310.15 K. Then, Hoechst 33258 was adsorbed and the electrochemical analysis was performed by DPV (Table 6.4). In the Figure 6.8, each bar demonstrates the mean and the standard errors of the peak current values acquired from three different samples of DNA sequences. It was clearly observed that only the *mecA* gene samples was hybridized successfully and resulted to high peak currents.

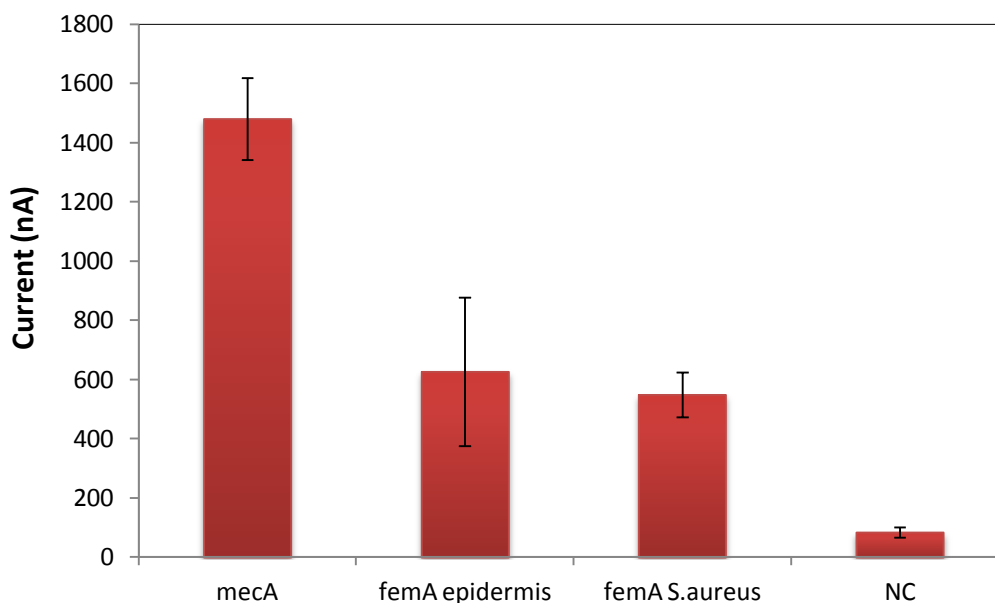


Figure 6.8. Cross reactivity test results for the specificity of the chip.

Table 6.4. Peak current values for cross reactivity tests of 1 µM DNA samples.

Measurement no	DNA sample types			
	Negative control Thiol DNA	<i>femA</i> <i>S. epidermis</i>	<i>femA</i> <i>S. aureus</i>	<i>mecA</i>
1	117	150	400	1720
2	65	730	607	1240
3	65	999	638	1480
Standard error of the mean	17,27	250,70	74,75	138,56
Mean	82,29	626,6	548,41	1480

6.3. Enzyme Based Detection

6.3.1. Capture Probe Selection

The amplification of clinical isolates of MRSA was performed with the use of primers indicated in Table 6.5 by using polymerase chain reaction (PCR)(Murakami et al., 1991). The presence of nucleotide sequences on MRSA *mecA* gene was analyzed by using NCBI Blast (Delvecchio et al., 1995; Medicine, 2012) (Figures 6.9 and 6.10).

Table 6.5. Oligonucleotide primers used for *mecA* amplification.

Primer <i>mecA</i>	Primer Sequence (5'-3')	Amplicon size (bp)	Nucleotide position
MR1	TAGAAATGACTGAACGTCGG	154	179-198
MR2	TTGCGATCAATGTTACCGTAG		332-312

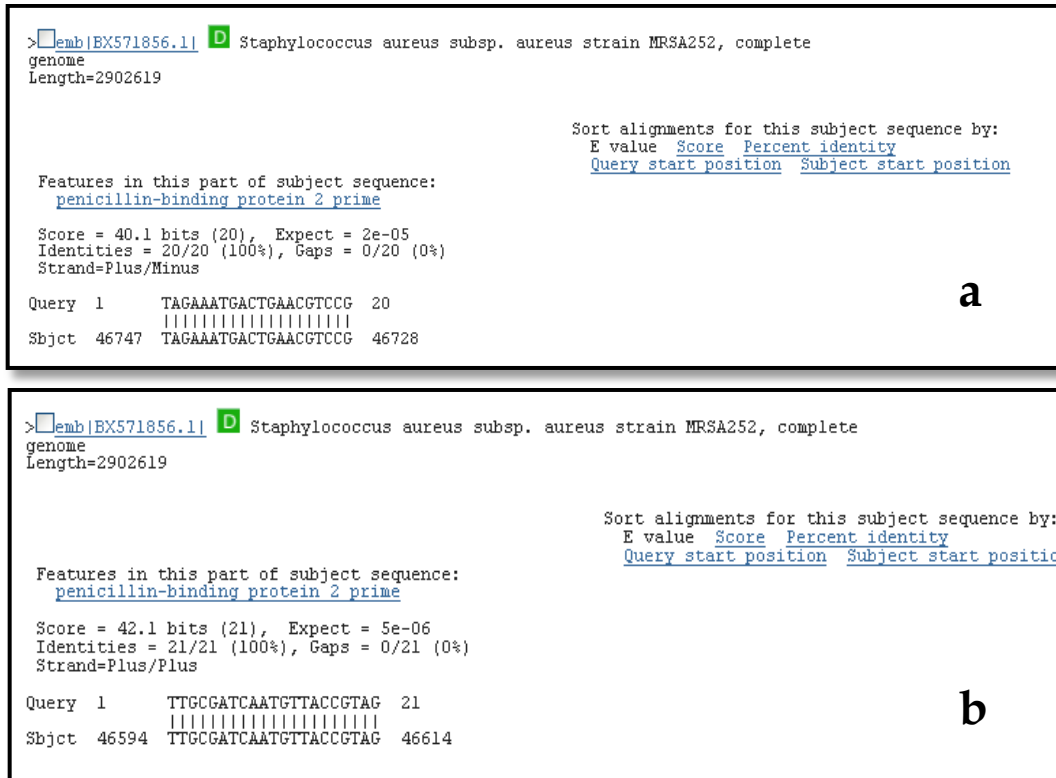


Figure 6.9. NCBI Blast results for the primer sequences (a) MR1 and (b) MR2 (Medicine, 2012).


```

1 ttattcatct atactgtatt ttttattacc gttctcatat agctcatcat acactttacc
61 tgagattttg gcattgtagc tagccattcc tttatcttgt acatctttaa cattaatagc
121 catcatcatg tttggattat ctttatcata tgatataaac cacccaattt gtctgccagt
181 ttctccttgt ttcattttga gttctgcagt accggatttg ccaattaagt ttgcataaga
241 tctataaata tcttctttat gtgttttatt tacgacttgt tgcataccat cagttaatag
301 attgatattt tctttggaaa taatattttt cttccaaact ttgtttttcg tgtcttttaa
361 taagtgaggt gcgtaatat tgccattatt ttctaatacg ctatagattg aaaggatctg
421 tactgggtta atcagtattt caccttgccc gtaacctgaa tcagctaata atatttcatt
481 atctaattt ttgtttgaaa tttgagcatt ataaaatgga taatcacttg gtatatcttc
541 accaacacct agttttttca tgccttttcc aaatttctta ctgcctaatt cgagtgctac
601 tctagcaaag aaaatgttat ctgatgatcc tattgcttgt ttaagtctga tattaccatt
661 taccacttca tatcttgtaa cgttgtaacc accccaagat ttatcttttt gccaaccttt
721 accatcgatt ttataacttg ttttatcgtc taatgttttg ttatttaacc caatcattgc
781 tgtaaatatt ttttgagttg aacctgggga agttgtaatc tggaaacttg tgagcagagg
841 ttctttttta tcttcgggta atttattata ttcttcgtta tctcatgccat acataaatgg
901 atagacgtca tatgaagggt tgcttacaag tgctaataat tcacctgttt gagggtggat
961 agcagacct gagccataat ctttttccat gttgttataa atactctttt gaactttagc
1021 atcaatagtt agttgaaat ctttgccatc ttttttcttt ttctctatta atgtatgtgc
1081 gattgtattg ctattatcgt caacgattgt gacacgatag ccatcttcat gttggagctt
1141 tttatcgtaa agtttttctga gtcccttttt accaataact gcatcatctt tatagccttt
1201 atattctttt tgttttaatt cttcagagtt aatgggacca acataaccta atagatgtga
1261 agtcgctttt cctagaggat agttacgact ttctgtttca ttagtgttaa gatgaaattt
1321 ttttgcgaaa tcaactaaat attcatccat ttttttaacg gttttaagtg gaacgaaggt
1381 atcatcttgt acccaatttt gatccatttg ttgtttgata tagtcttcag aaatacttag
1441 ttctttagcg attgctttat aatctttttt agatacattc tttggaacga tgcctatctc
1501 atatgctggt cctgtattgg ccaattccac attgtttcgg tctaaaattt taccacgttc
1561 tgattttaaa ttttcaatat gtatgctttg gtctttctgc attcctggaa taatgacgct
1621 atgatcccaa tctaacttcc acataaccatc ttctttaaca aaattaatgt gaacggttggc
1681 atcaatgtta ccgtagtttg ttttaatttt atattgagca tctactcgtt ttttattttt
1741 agatactttt tttattttac gatcctgaat gtttatactt ttaacgccta aactattata
1801 tatttttatc ggacggttcag tcattttctac ttcaccatta tcgcttttag aaatataact
1861 gctatcttta taaacttggt tgaaaatttt atcttcaatt gcatcaatag tattattaat
1921 ttctttatct tttgaagcat aaaaatatat accaaaccgg acaactacaa ctattaaaaa
1981 aagtggaaca atttttatct ttttcat

```

Figure 6.10. Nucleotide sequence of mecA gene indicating the primers selected (Medicine, 2012).

The amplified product with the use of MR1 and MR2 primers has the sequence as,
5' – TTGCG ATCAATGTTA CCGTAGTTG TTTTAATTTT ATATTGAGCA TCTACTCGTT
TTTTATTTT TAGATACTTT TTTTATTTTA AGATACTTTT TTTATTTTAC GATCCTGAAT
GTTTATATCT TTAACGCCTA AACTATTATA TATTTTATC GGACGTTTCAG TCATTTCTA
– 3'

The folding structure of amplified product was examined with the use of mfold server by taking into consideration 300mM Na⁺ in the solution and the program was resulted with possible five structures whose thermodynamic details are given in Table 6.6.

Table 6.6. The thermodynamic details of folding structures of amplified product.

Thermodynamic parameters*	Structure Number				
	1	2	3	4	5
ΔG at 310.15 K [kcal/mol]	-1.70	-1.49	-1.10	-1.06	-0.86
ΔH [kcal/mol]	-120.10	-150.20	-121	-93.10	-104.20
ΔS [cal/(K·mol)]	-381.7	-479.4	-386.5	-296.7	-333.1
T _m [K]	314.55	313.25	312.95	313.65	312.65

*Standard errors are roughly ±5%, ±10%, ±11% and 2-4 K for free energy, enthalpy, entropy and T_m, respectively.

Afterwards, the region of capture probe was selected by crossing all structures of amplified product and by finding non-folding region. The reverse complement of the selected region was searched for folding by using mfold server (Figure 6.11).

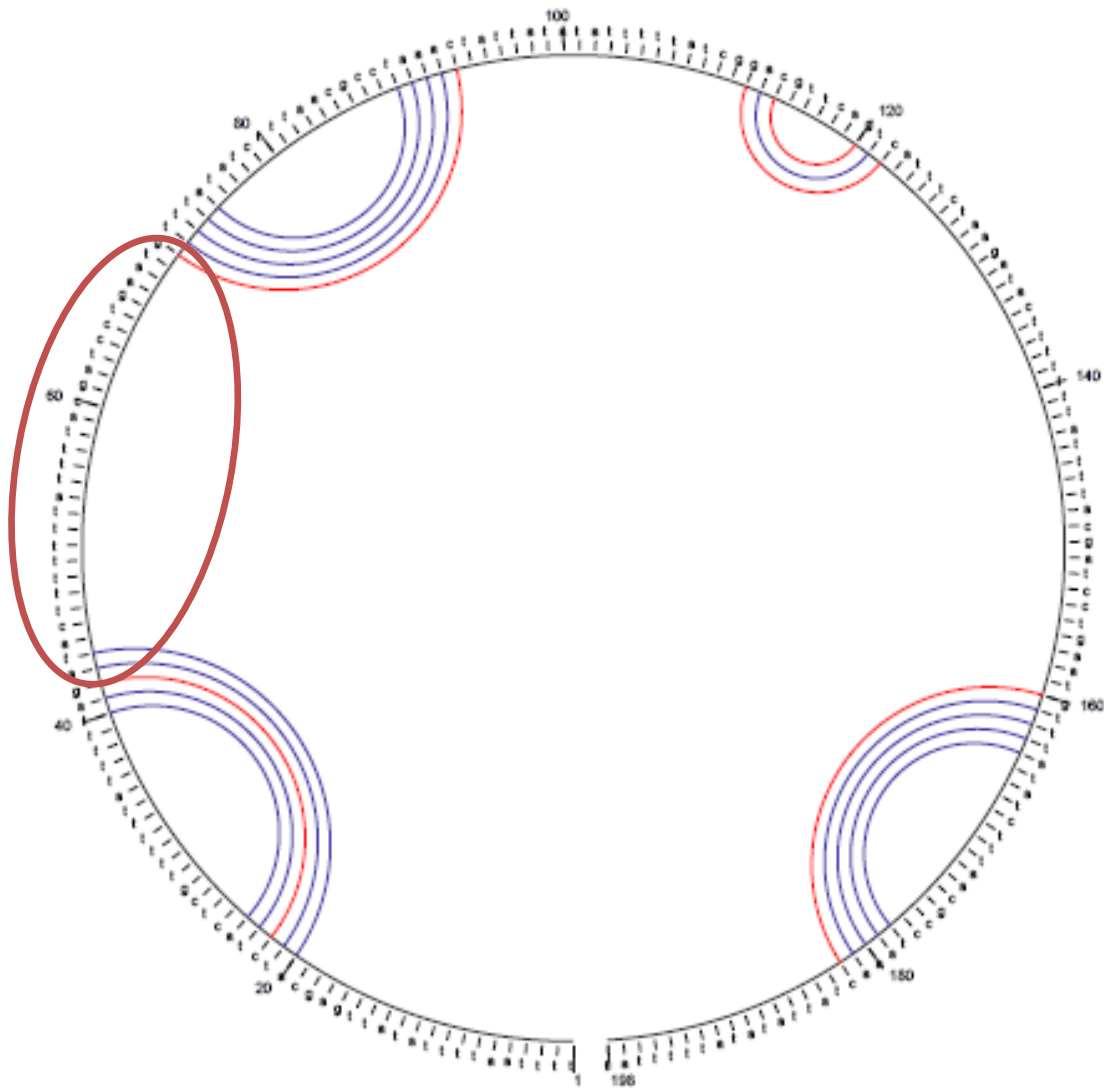


Figure 6.11 Circular diagram for the reverse complement of amplified product.

Capture probe was selected as the nucleotide sequence encompassing between 45th and 70th bases and it is as follows,

5' – thiol-ATT CAG GAT CGT AAA ATA AAA AAA GT- 3'

The results of mfold server with loading capture probe showed that there are nine different possible folding structures. Table 6.7 gives the thermodynamic details of the structures. The DNA sequence will be most probably linear without any folding at the room temperature when the melting temperatures of the structures were analyzed.

Table 6.7. The thermodynamic details of folding structures of capture probe DNA.

Structure number	ΔG at 310.15 K [kcal/mol]	ΔH [kcal/mol]	ΔS [cal/(K·mol)]	T_m [K]
1	1.85	-9.40	-36.27	259.15
2	1.89	-8.70	-34.14	254.75
3	1.94	-16.20	-58.49	276.95
4	2.51	-11.80	-46.14	255.75
5	2.51	-11.70	-45.82	255.35
6	2.55	-3.20	-18.54	172.65
7	2.69	-1.60	-13.83	115.65
8	2.70	-7.50	-32.89	228.05
9	2.81	-11.80	-47.11	250.45

6.3.2. Cyclic Voltammetry

The oxidation reaction of TMB with HRP in the presence of H_2O_2 results to a blue-colored product. The product becomes yellow due to formation of TMB^{2+} (Fanjul-Bolado et al., 2005; Josephy et al., 1982). The peaks observed due to TMB oxidation and reduction reactions are shown in Figure 6.12. The oxidation peak was observed at near 0.7 V and the reduction peak was observed at near 0.55 V. As it is seen from the cyclic voltammogram it is quasi reversible reaction since the voltammogram is not symmetric and the peaks are in a shift position (Wang, 2006).

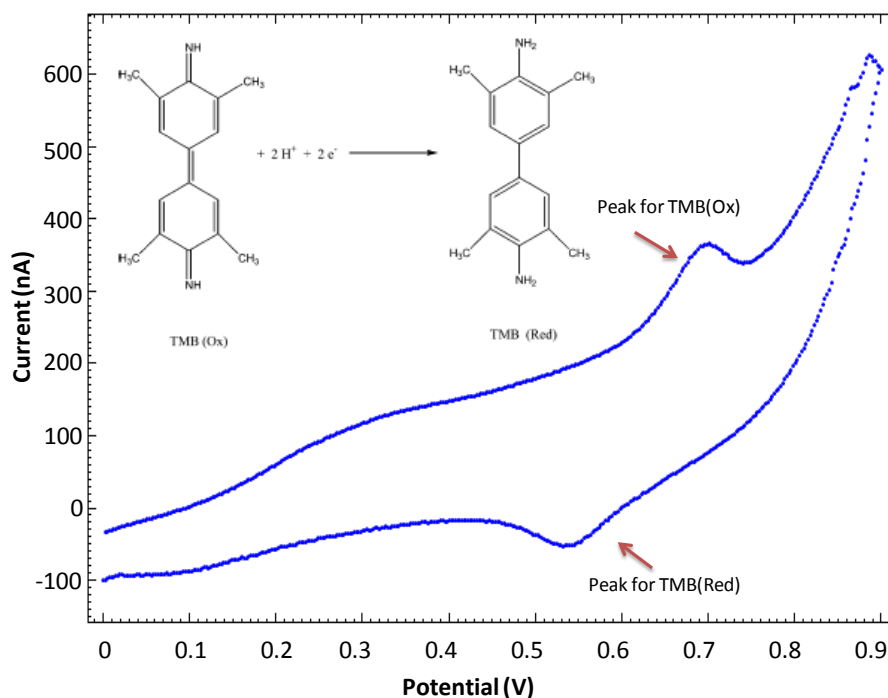


Figure 6.12. Cyclic voltammogram for TMB solution on HRP activated gold microdisc electrode.

6.3.3. Microdisk Chronoamperometry

The activity of HRP was demonstrated at a fixed potential, $E = 0.15$ V. This potential was selected so that the background current is nearly zero and there is not any substrate reaction occurred on the surface of the working electrode at this stable potential (Fanjul-Bolado et al., 2005). The chronoamperometry algorithm of the potentiostat is given in Appendix C and current-time response curve for 2- μ l TMB solution is shown in Figure 6.13. As shown in the figure, the TMB solution put

on the gold electrode after the effect of washing buffer was passed away. A comparison of current-time response curves of surfaces in the absence and presence of target DNA is given in Figure 6.14. These figures indicate that the diffusion layer over the surface of the electrode is so thin that diffusion to the electrode surface is linear for short times. As time passes, radial diffusion has contribution to the current as the diffusion layer thickens, and the value of current reaches a steady state (Compton and Banks, 2011).

Microdisc Chronoamperometry enables to measure diffusion coefficient, D , and the number of electrons, n transferred to an electroactive species of interest if there is not any reaction on the surface at the beginning of the experiment. In a chronoamperometry experiment, time dependent current response of the reaction on the surface was measured upon an applied potential step. The time dependent current response, I for a potential step, which results to a diffusion-controlled reductive current, can be calculated from the following equation:

$$I = -4nFD\text{Crf}(\tau) \quad (6.8)$$

The function of $f(\tau)$ is determined using the following expression developed by Shoup and Szabo (Shoup and Szabo, 1982);

$$f(\tau) = 0.7854 + 0.8862\tau^{-1/2} + 0.2146e^{-0.7823\tau^{-1/2}} \quad (6.9)$$

where $\tau = \frac{4Dt}{r^2}$, F is Faraday constant, 96485.34 s.A/mol, r is the radius of working electrode, and t is the time in seconds (Paddon et al., 2006).

The chronoamperometric experiment has two periods: (1) short time, at which I is proportional to $D^{1/2}$, (2) long time, at which I is proportional to D . The diffusion coefficient, D was determined as $9.43 \pm 0.74 \times 10^{-6} \text{ cm}^2/\text{s}$ by fitting the experimental data to the Equations (6.8) to (6.9) with Curve Fitting Toolbox of MATLAB R2010b (Figure 6.15). The details of calculations are given in Appendix C.

The estimation of diffusion coefficient was also studied and estimated as $3.11 \times 10^{-6} \text{ cm}^2\text{s}^{-1}$ by (Baldrich et al., 2009) using the following semiempirical formula developed by (Wilke and Chang, 1955):

$$D = 7.4 \times 10^{-8} \frac{(xM)^{1/2}T}{\eta V^{0.6}} \quad (6.10)$$

where x is the association parameter and it is 2.6 for water, D is the diffusion coefficient, molecular weight of the solvent, molar volume of solute at normal boiling point (cm^3/mole), T is the temperature (K), and η is the viscosity of solution (cp). The diffusion coefficient estimated in this study is threefold larger than that of literature. This difference may be due to the differences in the estimation methods.

6.3.4. Optimization of Detection Method

Incubation times of each step of the detection procedure were changed to optimize the performance of the detection procedure. These steps are (1) hybridization time of target DNA with the capture probe, (2) binding of streptavidin – conjugated HRP, and (3) TMB incubation time. The effect of each step is given in detail in the following text. Efficient capture probe immobilization is important to form monolayer coverage on working electrode for sensitive detection. It mainly depends on immobilization time and the amount of thiol modified capture probe DNA. The solution of capture probe was incubated on the surface for overnight at room temperature to maximize surface coverage of self-assembled monolayers while keeping the amount of capture probe in the solution constant at $10 \mu\text{M}$. 10 times diluted PCR product was biotinylated with reporter probe and this biotinylated PCR product was used in the hybridization of target DNA with the capture probe. Then, the following steps of sandwich immunoassay were completed to analyze the effect of incubation time for hybridization (Figure 6.16 and Figure 6.17).

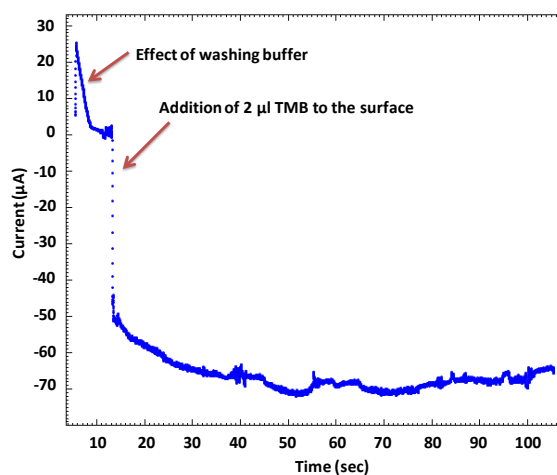


Figure 6.13. Current-time response curve of TMB solution on HRP activated gold microdisc electrode.

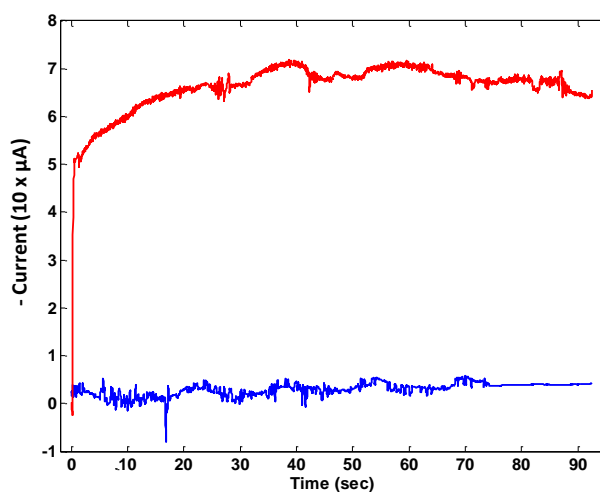


Figure 6.14. Current-time (*i-t*) response curves for working electrodes in the absence (blue line) and in the presence (red line) of target DNA (hybridized for one hour at room temperature) in the TMB substrate solution. $E = 0.15$ V.

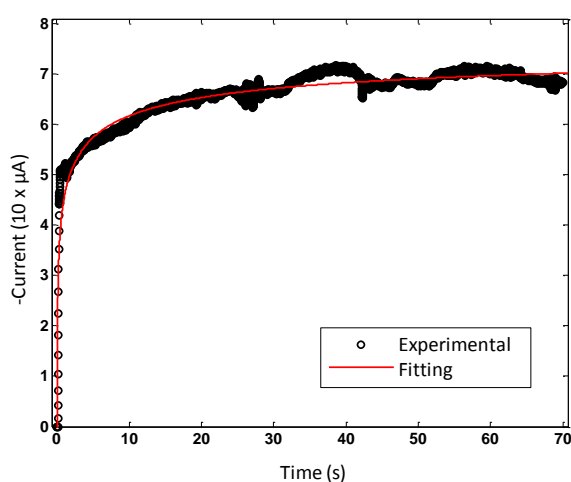


Figure 6.15. Experimental (circles) and fitted (red line) chronoamperometric curve for the two-electron reduction of TMB on a 300- μm gold microdisc electrode for a fixed potential of 0.15 V. Fitting was performed by MATLAB software and Diffusion coefficient, D was determined as $9.43 \pm 0.74 \times 10^{-6} \text{ cm}^2/\text{s}$.

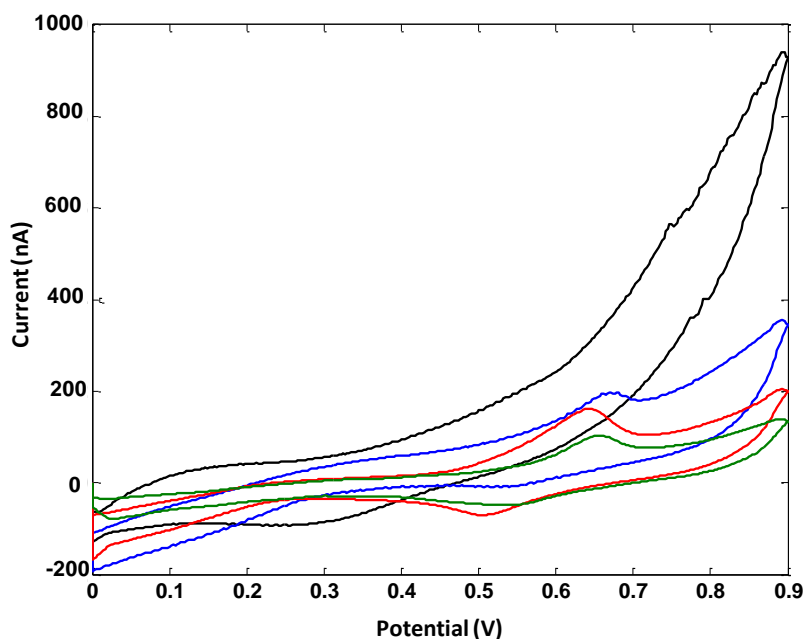


Figure 6.16. Cyclic voltammograms for the optimization of hybridization time for 100 μm working electrode (black line (30 min), blue line (1 hour), red line (2 hours), green line (3 hours)).

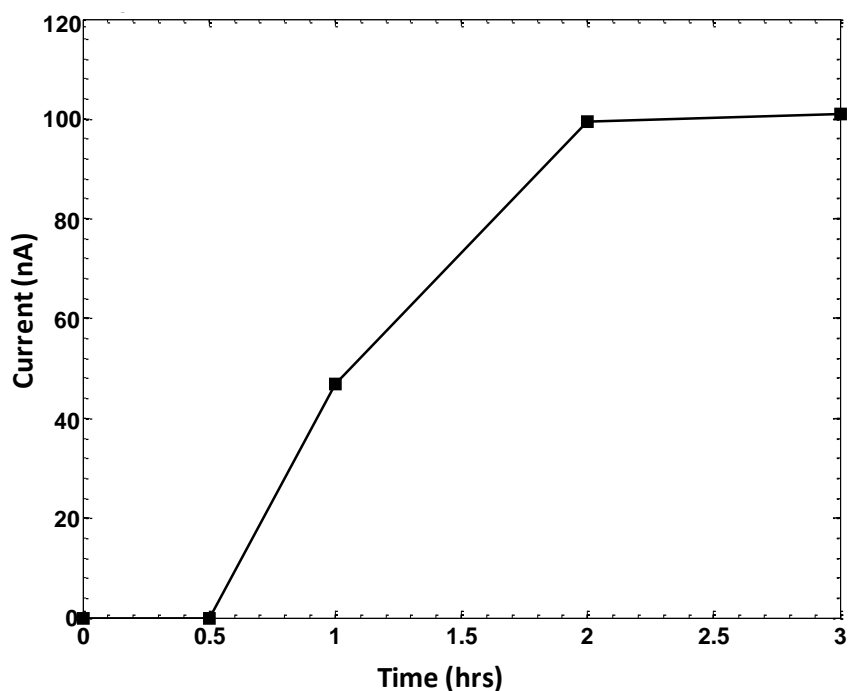


Figure 6.17. Optimization of hybridization time. Operating conditions: capture probe, 10 μM ; target probe, 10 times diluted PCR product; capture probe immobilization time, 24 hrs; streptavidin conjugated HRP incubation time, 15 min; TMB/ H_2O_2 incubation time, 15 min. Other conditions: wait time, 5s; lower vertex potential, 0 V; upper vertex potential, 0.9 V; step potential, 2.44 mV; scan rate, 0.1 V/s.

To analyze the binding performance of streptavidin conjugated HRP to biotin molecules, incubation times were varied as 5 min, 10 min, 15 min, and 60 min. In this analysis, the incubation time for

immobilization of capture probe on Au surface was selected as 24 hours to eliminate its effect and target probe was immobilized on the surface for two hours. The incubation time of BSA solution used for reducing nonspecific binding was one hour. Figure 6.18 shows cyclic voltammogram of TMB oxidation for different HRP incubation times ranging from 5 min to 60 min. Although the obtained signal for peak current is slightly changing with time, the signal limit, which is near 215 nA for 300 μm -radius working electrode, is reached in five minutes. This fast reaction is due to the affinity between the biotin and the streptavidin molecules, which is among the highest covalent contributions.

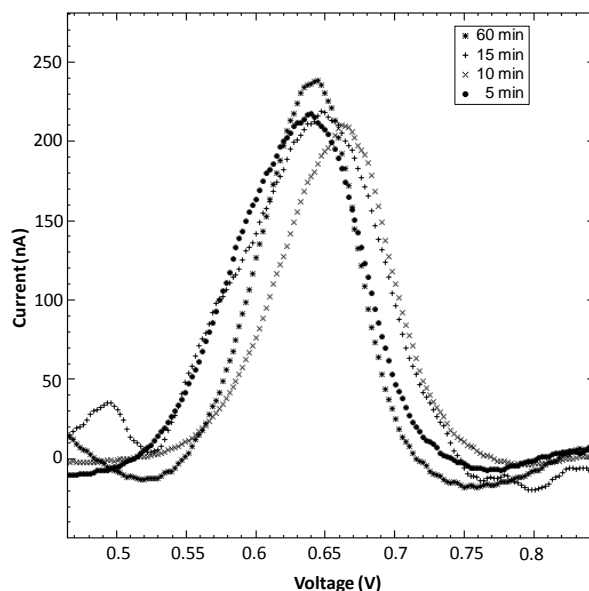


Figure 6.18. The effect of increasing incubation time on binding of streptavidin-conjugated HRP. Operating conditions: capture probe, 10 μM ; target probe, 10 times diluted PCR product; capture probe immobilization time, 24 hrs; target probe incubation time, 2 hrs; TMB/ H_2O_2 incubation time, 15 min. Other conditions: wait time, 5s; lower vertex potential, 0 V; upper vertex potential, 0.9 V; step potential, 2.44 mV; scan rate, 0.1 V/s.

Moreover, electrochemical detections were performed by using cyclic voltammetry to analyze the behavior of TMB oxidation with changing time. Figure 6.19 shows cyclic voltammograms of the substrate mixture, TMB/ H_2O_2 , for an applied potential scan ranging from 0 V to 0.9 V, for different times (5 min, 15 min, and 30 min) just after facing to enzyme-adsorbed surface. As displayed in Figures 6.19, the shape of voltammogram reaches steady state in five minutes due to rapid reaction of the TMB substrate. Figure 6.20 shows the change in peak current with different incubation time of the TMB substrate. The peak current increases as the incubation time increases, it levels off after 15 minutes and reaches a value near 130 nA after 30 minutes. To reduce detection time, TMB incubation time was selected as 15 minutes.

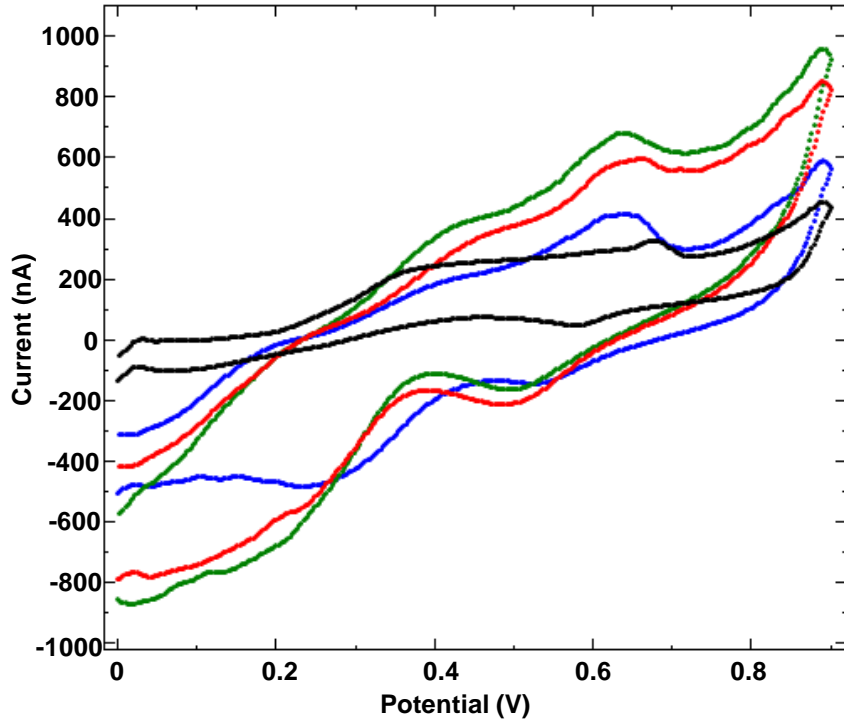


Figure 6.19. Cyclic voltammograms showing TMB oxidation with different incubation times (black line, no HRP; blue line, 5 min; red line, 15min; green line, 30 min). Operating conditions: capture probe, 10 μ M; target probe, 10 times diluted PCR product; capture probe immobilization time, 24 hrs; target probe incubation time, 2 hrs; streptavidin conjugated HRP incubation time 5 min. Other conditions: wait time, 5s; lower vertex potential, 0 V; upper vertex potential, 0.9 V; step potential, 2.44 mV; scan rate, 0.1 V/s.

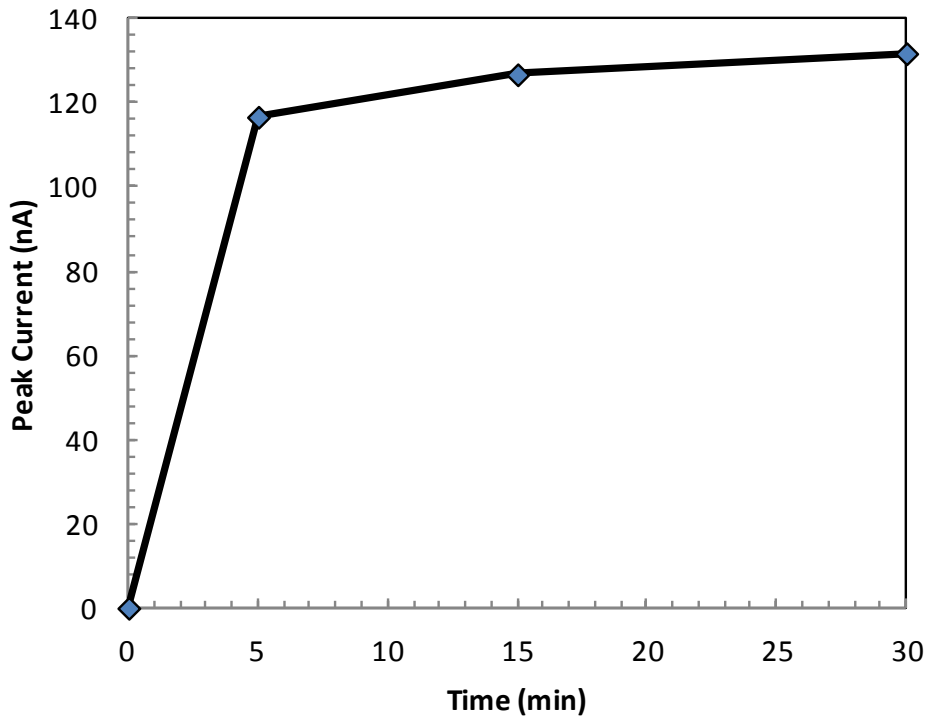


Figure 6.20. Peak current vs incubation time graph for TMB oxidation reaction.

6.3.5. Analysis of Effect of Scan Rate on Peak Current

As the potential is swept from an initial potential to a final potential, the diffusion layer surrounding the electrode becomes thinner. As the time to scan the potential increases, the thickness of diffusion layer increases. On the contrary, as the time to scan potential decreases, the thickness decreases. It is also shown by Fick's first law that the thickness of diffusion layer decreases as the flux increases for a constant concentration drop. This increase in the scan rate can also be observed from the change in peak current, i_p . In both reversible and irreversible reactions, there is a square root dependence of scan rate on the acquired peak current as indicated in the following equations, respectively:

$$i_p = (2.69 \times 10^5) n^{3/2} A C D^{1/2} \nu^{1/2} \quad (6.11)$$

$$i_p = (2.99 \times 10^5) n (\alpha n_a)^{1/2} A C D^{1/2} \nu^{1/2} \quad (6.12)$$

where n is the number of electrons, A is the electrode area [cm^2], C is the concentration [mol/cm^3], D is the diffusion coefficient [cm^2/s], α is the transfer coefficient (generally taken as 0.5), n_a is the number of electrons involved in charge transfer step and ν is the potential scan rate [V/s]. Equation (6.11) is also known as Randles-Sevcik equation. Cyclic voltammograms of TMB oxidation in the presence of H_2O_2 for different scan rates are displayed in Figures 6.21 and 6.22, and the data are given in Table 6.8.

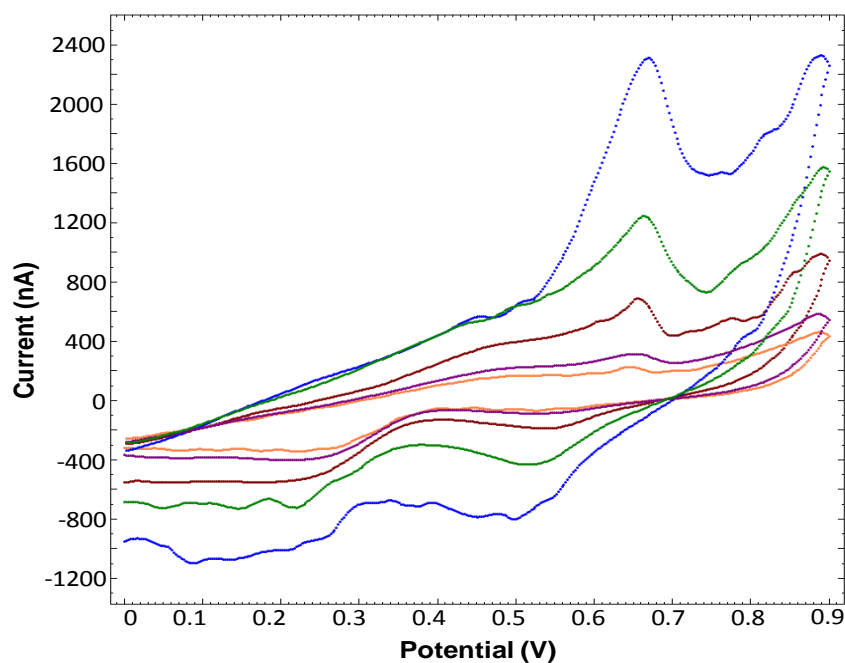


Figure 6.21. Cyclic voltammograms of TMB oxidation for different scan rates (blue line: 1 V/s, green line: 0.5625 V/s, red line: 0.25 V/s, purple line: 0.1 V/s, orange line: 0.0625 V/s).

As shown in Figure 6.21, the square root of scan rate is linearly proportional to the peak current, and it is quasi-reversible, which means that it is diffusion-controlled process. By using Equation (6.12), the concentration of TMB in the bulk solution is estimated to be around 0.326 ± 0.057 mM. In the calculation, the diffusion coefficient determined with aforementioned method is used for working electrode with radius $100 \mu\text{m}$ ($n = 2$). The data obtained from the calculations are tabulated in Table 6.8.

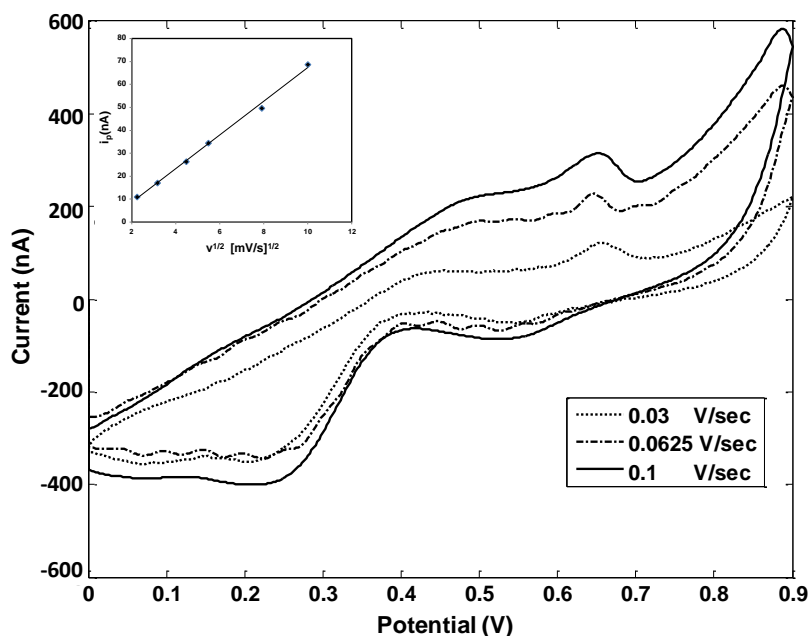


Figure 6.22. Cyclic voltammograms of TMB oxidation for different scan rates. Inset: Linear proportionality of peak current to the square root of scan rate.

Table 6.8. The data of TMB oxidation peak for each scan rate.

Scan rate [V/s]	E_p [V]	i_p [nA]
0.005	0.65964	10.9
0.01	0.65964	10.7
0.02	0.64941	26.4
0.03	0.65674	34.8
0.0625	0.64697	49.7
0.1	0.64941	68.7

Table 6.9. The concentration of TMB for each scan rate.

Scan rate [V/s]	[TMB] [mM]
0.005	0.269
0.01	0.296
0.02	0.323
0.03	0.345
0.0625	0.345
0.1	0.377

6.3.6. Different concentrations of target DNA

Different concentrations of biotinylated PCR product were detected using the derived optimal parameters of enzyme based detection protocol. The concentrations of PCR products were measured using Thermo Scientific NanoDrop™ ND-2000c Spectrophotometer. The acquired data and the solution contents are given in Table 6.10. Increasing concentrations of PCR product resulted in an increase in current as it was expected (Figure 6.23). As can be seen from Figure 6.23, it is possible to

detect biotinylated PCR product with a concentration of as low as 20.8 ng/ μ l using micro electrochemical sensor, which has 100 μ m radius working electrode.

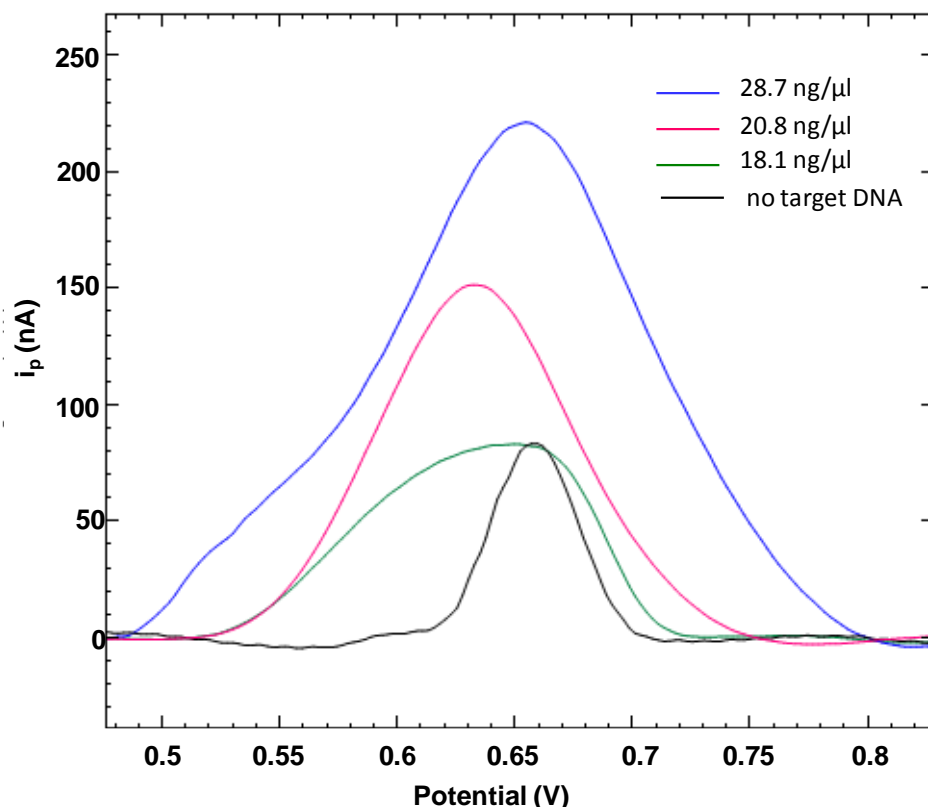


Figure 6.23. Concentration dependence for biotinylated PCR product: (blue line) 28.7 ng/ μ l, (red line) 20.8 ng/ μ l, (green line) 18.1 ng/ μ l, (black line) no target DNA. Operating conditions: capture probe, 10 μ M; capture probe immobilization time, 24 hrs; target probe incubation time, 2 hrs; streptavidin conjugated HRP incubation time 5 min. TMB incubation time, 15 min; Other conditions: wait time, 5s; lower vertex potential, 0 V; upper vertex potential, 0.9 V; step potential, 2.44 mV; scan rate, 0.1 V/s.

Table 6.10. Concentrations of prepared solutions for the analysis of change in concentration of target DNA.

Prepared solution	Estimated Concentration [ng/ μ l]
2 μ l hybridization buffer + 8 μ l [(10-times diluted) PCR product + biotinylated probe]	28.7
4 μ l hybridization buffer + 6 μ l [(10-times diluted) PCR product + biotinylated probe]	20.8
5 μ l hybridization buffer + 5 μ l [(10-times diluted) PCR product + biotinylated probe]	18.1

6.3.7. Analysis of Effect of Addition of Acid

TMB^o substrate, which is a ready to use solution of TMB/H₂O₂, is a colorless solution. When the substrate reacted with HRP enzyme, it develops a blue substrate in mildly acidic solutions and a yellow product in acidic solutions (Figure 6.24).

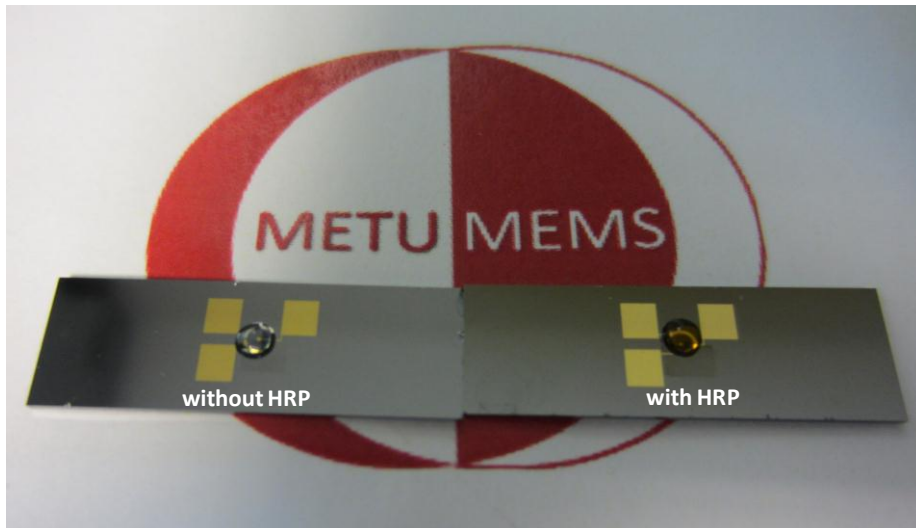


Figure 6.24. A photo demonstrating the color change due to enzymatic activity of HRP.

In order to observe the effect of acid on HRP enzymatic activity, chronoamperometry was applied at a fixed potential of 0.15 V (Figure 6.25). Consequently, the surface was modified as mentioned before. After rinsing the surface with washing buffer to remove unbound HRP, recording of current vs. time was started; TMB solution was incubated on the surface and waited for reaching of current to steady state. After the system reached to steady state, 2 μl of 1M H_2SO_4 solution was added to the surface to inhibit the enzyme. Then, the surface was rinsed with washing buffer and another droplet of TMB was incubated on the surface. Since the enzyme was degraded, TMB oxidation could not be observed as expected. The enzymatic activity observed for the sample without target DNA at the beginning of the experiment can be due to non-specific adsorption of HRP enzyme to Si surface.

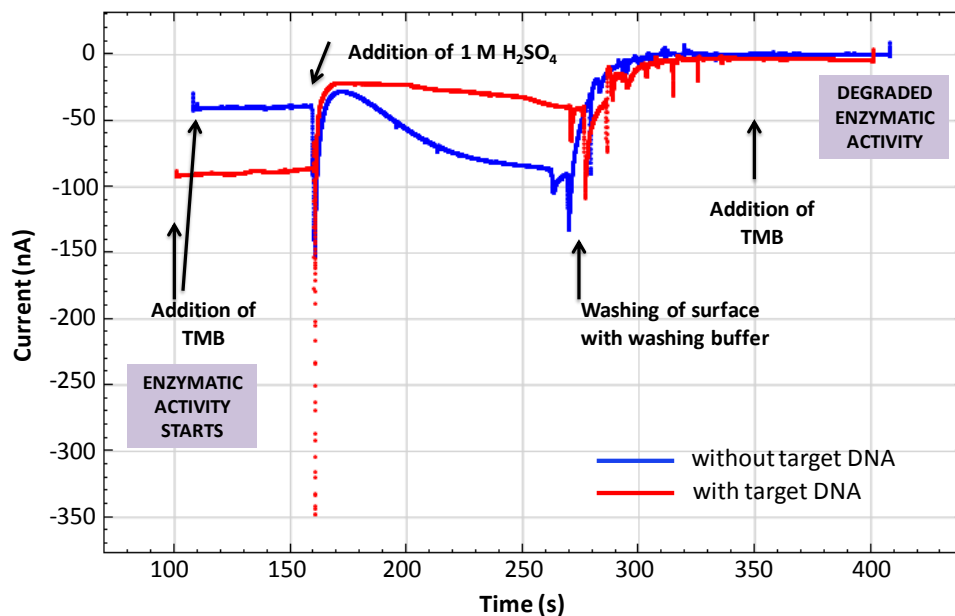


Figure 6.25. Time course of enzymatic activity and the effect of addition of acid.

6.4. Comparison with Other Studies in Literature

In the literature, there are different detection strategies reported to detect MRSA with the use of different biological analytes such as cells and nucleic acids (Table 6.11). The first study on the on-

Table 6.11. A summary of some reported MEMS biosensors in the literature and their comparison with this work.

Reference	Culturing	Target analyte	Time to reach result	Volume of detection chamber or Size of electrode	On-Chip detection method	Detection limit / Sensitivity
(Lagally et al., 2004)		219 bp of <i>femA</i> 310 bp part of <i>mecA</i>	<20 min for 30 cycles of PCR	200 nl	PCR amplification and capillary electrophoresis	
(Dutta et al., 2005)	Necessary	Volatile organic compounds (odor) produced by MRSA			Electronic Nose	96 - 99.69%
(Tombelli et al., 2006)	Not necessary	<i>mecA</i>		42.6 mm ²	Piezoelectric biosensor	0.015 μM
(Boedicker et al., 2008)	Not necessary	Cell (<i>S. aureus</i> ATCC# 43300 (MRSA))	Two hours	1 nl	Confinement of single cell, fluorescent dye, and antibiotics in a nanoliter droplet and optical detection	10 ⁵ CFU/ml
(Guntupalli et al., 2008)	Not necessary	Cell			Bacteriophage as a probe and optical detection	10 ⁶ CFU/ml
(Sista et al., 2008)	Not necessary		10 min for immunoassay protocols 12 min for 40 cycles of real time PCR	300 nl	PCR and optical detection	1 copy per reaction well
(Lindsey et al., 2008)	Necessary	<i>mecA</i> , <i>femB</i> , and <i>tuf</i>	90 min	6 mm x 6 mm	Enzyme based optical detection	5 × 10 ⁷ CFU/mL
(Naikare et al., 2009)	Not necessary	<i>femA</i> and <i>mecA</i>	Three hours		Cycling probe reaction and capillary electrophoresis	10 ⁴ colony forming unit of bacteria /ml of blood
(House et al., 2010)	Not necessary	a 306 bp fragment of the 791 bp regions of the 16S rRNA genes shared solely among Staphylococci		3 μl	Real time PCR and optical detection	11.2 pg DNA
(Lutz et al., 2010)	Not necessary	420 bp of <i>mecA</i> gene of <i>S.aureus</i>	< 20 min	10 μl	Isothermal Recombinase Polymerase Amplification (RPA)	10 copies per reaction well
(Focke et al., 2010a)	Not necessary	<i>ExfA</i> gene of MRSA	110 min	9.8 μl	Real time PCR	10 copies per reaction well
(Focke et al., 2010b)	Not necessary	<i>ExfA</i> gene of MRSA	30 min + 110 min	12.8 μl	Primary amplification and real time PCR	7 copies per reaction well
(Klonoski et al., 2010)	Necessary	<i>mecA</i> , <i>femB</i> , and <i>tuf</i>	25-35 min		Enzyme based optical detection	1 fmol/L
(Gebala et al., 2011)	Not necessary			70 μm x 70 μm	Redox marker and enzyme based electrochemical detection	100 pM
(Wang et al., 2011a)	Not necessary	<i>spa</i> gene (GenBank Accession No. BX571856) <i>mecA</i> (EU929079)	60 min	15 μl	Magnetic bead based detection with loop mediated amplification (LAMP) process	10 fg/ μl
(Wang et al., 2011b)	Not necessary			1.5 mm in diameter	Label-free electrochemical detection	100 fM
This study	Not necessary	mecA	2-3 hours for PCR 3 hours for hybridization and detection	10 μl / 500 μm in radius	Redox marker based electrochemical detection	0.01 nM
This study	Not necessary	mecA	2-3 hours for PCR 3.5 hours for hybridization and detection	2 μl / 100 μm in radius	Enzyme based electrochemical detection	10 times diluted PCR product (as low as 21 ng/μl).

chip detection of MRSA was performed by (Lagally et al., 2004) and it was based on combination of PCR and capillary electrophoresis. This approach had been improved by eliminating purification of lysed cell sample (Naikare et al., 2009). Then, odor-based detection was studied in order to decrease size of system of detection and detect MRSA directly from culture (Dutta et al., 2005). This method offers high sensitivity with 96% accuracy but it necessitates a detailed analysis of acquired complex signals; therefore, it was time consuming. The isothermal PCR and microfluidics were combined by (Lutz et al., 2010) in order to eliminate heating and cooling cycles of PCR in a miniaturized system. Since the developed system based on optical detection, portability of device is limited. Then, electrochemical detection was performed successfully to detect MRSA by (Wang et al., 2011b) with the use of macro scale electrodes with 3 mm diameter. This study presents, for the first time in the literature, a micro electrochemical sensor (μ ECS) for detection of *mecA* gene, utilizing microfluidic channels with on-chip silver (Ag), gold (Au), and platinum (Pt) electrodes.

When compared with other biosensors studied, the micro electrochemical sensor proposed in this study offers high sensitivity with respect to sizes of the working electrodes and their detection methods (Table 6.11). The level of sensitivity may be attributed to the ability of capture probe, which was optimized to have non-folding structures, dominancy of mass transport diffusion since the analytes are very close to the electrodes (Ehrfeld et al., 2000), The dependency on diffusion results to have long hybridization time. However, it is acceptable since total time to result, including amplification of nucleic acid, is around six hours, which is less than the time to result obtained by conventional culture methods for the detection of MRSA. Moreover, fabrication of the developed system with the use of standard MEMS fabrication processes enables integration of the sensor with circuits (i.e., potentiostat) and other parts of lab-on-a-chip system to have a complete system for hand-held devices.

6.5 Solvent Compatibility of Parylene C Film Layer

6.5.1. Swelling of Parylene C in Solvents

Solubility parameter, δ , enables to predict cohesive and adhesive properties of materials by only knowing the properties of compounds (Du et al., 1996; Small, 1953). Molar heat of vaporization, which is the amount of energy required to break all interactions in the condensed phase, is commonly used to predict the solubility parameters of solvents (Small, 1953). According to Hansen solubility parameter (HSP) approach, the total energy of vaporization is composed of three main interactions: (1) nonpolar atomic interactions (dispersion forces), (2) inherent molecular interactions (polar forces), and (3) attractions among the molecules due to hydrogen bonds (hydrogen-bonding forces) (Hansen, 2007b; Lee et al., 2003); and δ can be predicted as given below (Hansen, 2007b; Lee et al., 2003):

$$\delta = \sqrt{\delta_d^2 + \delta_p^2 + \delta_h^2} \quad (6.13)$$

where δ_d , δ_p , and δ_h are the solubility parameters of dispersion forces, polar forces, and hydrogen bonding forces, respectively.

Solubility parameter can be used in analyzing polymer-solvent interactions, especially swelling of a polymer in a solvent. From the thermodynamics point of view, polymer swelling in a solvent is observed when the free energy of mixing is less than zero, ($\Delta G_m < 0$) (Du et al., 1996; Lee et al., 2003). ΔG_m is defined as (Hansen, 2007b):

$$\Delta G_m = \Delta H_m - T\Delta S_m \quad (6.14)$$

where ΔH_m and ΔS_m are the enthalpy change and the entropy change in the mixing process, respectively, T is the absolute temperature (Hansen, 2007b). Enthalpy difference can further be written as:

$$\Delta H_m = V_m \phi_p \phi_s (\delta^p - \delta^s)^2 \quad (6.15)$$

where V_m is the volume of the mixture, ϕ is the volume fraction of the material in the mixture, and the superscripts p and s denote polymer and solvent (Du et al., 1996). $T\Delta S_m$ is always greater than zero in mixing operations. Thus, ΔG_m can be less than zero if ΔH_m is smaller than $T\Delta S_m$. In other words, the value of $(\delta^p - \delta^s)^2$ has to be very small, (i.e., close to zero) (Lee et al., 2003). Thus, maximum swelling can be obtained in a solvent whose solubility parameter is close to that of the polymer.

Degree of swelling of Parylene C was predicted by using swelling ratio, S_{Parylene} , which was determined as H/H_0 , where H and H_0 are the heights of Parylene C layer after and before immersing into solvent, respectively. When S_{Parylene} is equal to one it means that there is no swelling, but a value greater than one indicates the presence of swelling. In Table 6.12, a list of solubility parameters for different solvents are given in comparison to their swelling ratios. Ranks of the solvents were assigned to the values of S_{Parylene} in descending order (Lee et al., 2003). Figure D.2 shows the change of S_{Parylene} as a function of the solubility parameters of the solvents (Lee et al., 2003). Experimental data of this analysis revealed a peak in the degree of swelling when the solubility parameter is about $9.2 \text{ (cal/cm}^3)^{1/2}$ rather than that obtained by Miller et al. (Miller and Leighton, 1990) as $9.6 \text{ (cal/cm}^3)^{1/2}$. This can be due to the differences (e.g., thickness of Parylene C film layer and detection method for the degree of swelling) between this study and the study of Miller et al. (Miller and Leighton, 1990).

As can be seen in Figure 6.26, the degree of swelling increases, as the difference between the solubility parameter of a solvent and that of Parylene C approaches zero (Kumar, 2000). This is due to high affinity of materials that have similar HSP for each other (Hansen, 2007b). For example, the solubility parameter of EtOAc ($\delta = 8.9 \text{ (cal/cm}^3)^{1/2}$), which is ranked as 7, is very close to the solubility parameter of Parylene C ($\delta = 9.6 \text{ (cal/cm}^3)^{1/2}$), hence Parylene C swells in that solvent. This means that the value of $(\delta^p - \delta^s)^2$ is very close to zero, and the degree of swelling is high ($\text{Log}(S_{\text{EtOAc}}) = 0.013$). On the other hand, the solubility parameter of water, whose ranking number is 22, is $23.4 \text{ (cal/cm}^3)^{1/2}$. So, the value of $(\delta^p - \delta^s)^2$ is large and the degree of swelling is low ($\text{Log}(S_{\text{Water}}) = 0$) in water. However, the relationship between the solubility parameter and the degree of swelling is not always linear, since contributions of the forces on the solubility parameter differ (Hansen, 2007b).

Table 6.12. Parylene C swelling ratios in different solvents.

Solvent	δ_d^*	δ_p^*	δ_h^*	δ^*	S_{Parylene}	Rank	Ref
pentane	7.1	0.0	0.0	7.1	1.01	16	(Hansen, 2007a)
hexane	7.3	0.0	0.0	7.3	1.02	9	(Hansen, 2007a)
PDMS				7.3			(Du et al., 1996; Lee et al., 2003)
n-heptane	7.5	0.0	0.0	7.5	1.00	24	(Hansen, 2007a)
cyclohexane	8.2	0.0	0.1	8.2	1.00	23	(Hansen, 2007a)
n-butylacetate	7.7	1.8	3.1	8.5	1.01	11	(Hansen, 2007a)
toluene	8.6	0.5	1.5	8.8	1.05	4	(Hansen, 2007a)
ethyl acetate (EtOAc)	7.7	2.6	3.5	8.9	1.03	7	(Hansen, 2007a)
xylene	8.8	0.7	1.0	8.9	1.01	18	(Hansen, 2007a)
chloroform	9.0	0.0	1.0	9.0	1.06	2	(Hansen, 2007a)
N-methylpyrrolidone (NMP)	8.3	1.4	3.4	9.1	1.01	14	(Hansen, 2007a)
trichloroethylene	8.7	1.5	2.8	9.3	1.05	3	(Hansen, 2007a)
benzene	8.8	1.5	2.6	9.3	1.07	1	(Hansen, 2007a)
2-butanone (MEK)	7.8	4.4	2.5	9.3	1.04	5	(Hansen, 2007a)
Parylene C	8.8	3.9	0.0	9.6			(Miller and Leighton, 1990)
acetone	7.6	5.1	3.4	9.7	1.03	6	(Hansen, 2007a)
<i>o</i> -dichlorobenzene	9.4	3.1	1.6	10.0	1.02	10	(Hansen, 2007a)
2-propanol (IPA)	7.7	3.0	8.0	11.5	1.00	20	(Hansen, 2007a)
1-propanol	7.5	8.8	3.0	11.9	1.01	15	(Hansen, 2007a)
acetonitrile	7.8	3.3	8.5	12.0	1.01	12	(Hansen, 2007a)
dimethylformamide (DMF)	8.5	6.7	5.5	12.2	1.02	8	(Hansen, 2007a)
ethanol	7.7	4.3	9.5	13.0	1.01	13	(Hansen, 2007a)
dimethyl sulfoxide (DMSO)	9.0	8.0	5.0	13.0	1.01	17	(Hansen, 2007a)
methanol (MeOH)	7.4	6.0	10.9	14.5	1.00	19	(Hansen, 2007a)
ethylene glycol	8.3	5.4	12.7	16.1	1.00	21	(Hansen, 2007a)
water	7.6	7.8	20.7	23.4	1.00	22	(Hansen, 2007a)

* δ_d , δ_p , δ_h , and δ are in the units of $(\text{cal/cm}^3)^{1/2}$.

Degree of swelling of Parylene C was analyzed by dividing the solvents into two groups: solvents in which Parylene C has no solubility ($S = 1.00$), and solvents in which Parylene C has solubility ($1.00 < S < 1.08$).

Solvents in which Parylene C has no solubility: Solvents with no solubility include alcohols (methanol (MeOH), IPA, and ethylene glycol) and water. Their solubility parameters are in the range of $11.5\text{-}23.4 \text{ (cal/cm}^3)^{1/2}$. These solvents generally have highest contribution of hydrogen-bonding forces ($\delta_h > 8 \text{ (cal/cm}^3)^{1/2}$) and moderate to high contribution of polar forces to their solubility parameters. On the other hand, the contribution of dispersion forces to the solubility parameter of the solvents is slightly smaller than that of Parylene C (e.g., $\delta_d = 7.7 \text{ (cal/cm}^3)^{1/2}$ for IPA).

Cyclic and acyclic hydrocarbons (cyclohexane and n-heptane) also do not have any effect on the Parylene C swelling although the contributions of their hydrogen-bonding forces are similar to that of Parylene C. It can be due to the differences in their other partitions of the solubility parameters compared to the solubility parameter of Parylene C. As a result, Parylene C can be exposed to these solvents with no solubility for long-term exposures and it can serve as a good barrier polymer for these solvents since they would not swell.

Solvents in which Parylene C has solubility: These solvents extend over a relatively large collection of solvents including cyclic and acyclic hydrocarbons (pentane and hexane), aromatic hydrocarbons

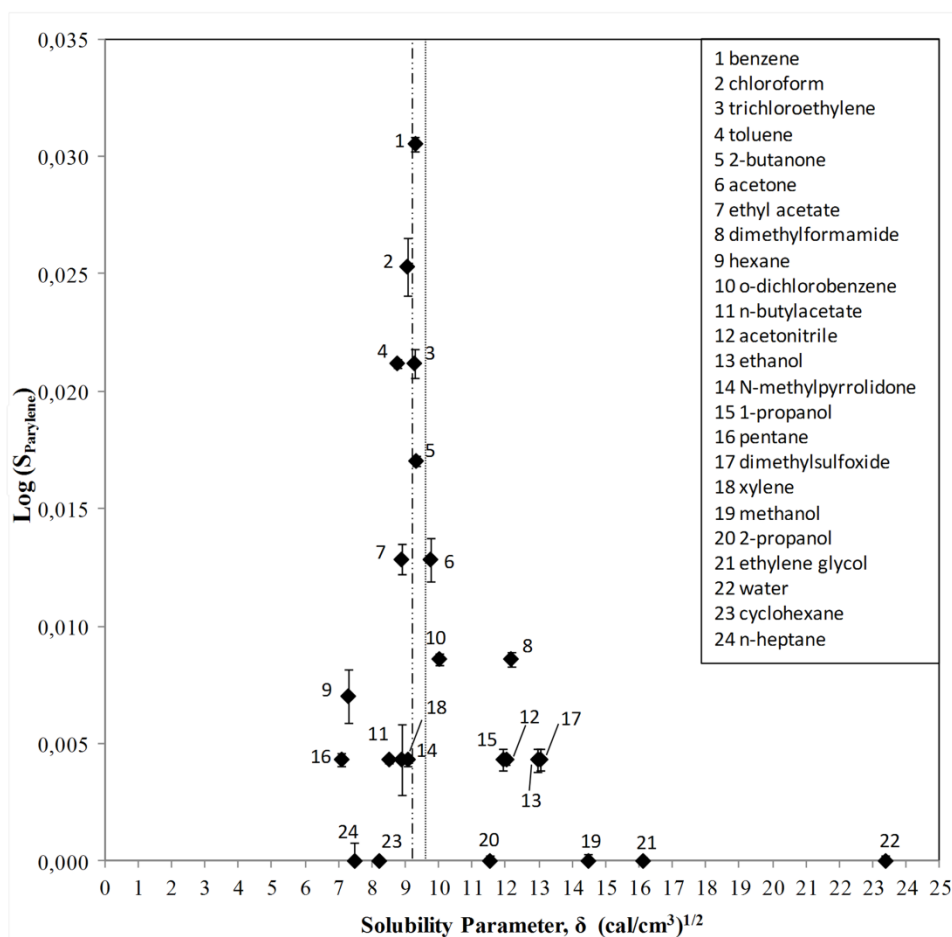


Figure 6.26. The change of the swelling ratio of Parylene C (S_{Parylene}) with the solubility parameter (δ). Error bars demonstrate an error of $\pm 0.5\%$ standard deviation (number of samples = 9). The line (.....) designates the place of solubility parameter of Parylene C ($\delta = 9.6 \text{ (cal/cm}^3)^{1/2}$), calculated from the study of Miller et al. (Miller and Leighton, 1990) while the line (- . - .) indicates the place of solubility parameter of Parylene C ($\delta = 9.2 \text{ (cal/cm}^3)^{1/2}$) proposed in this study.

(toluene, xylene, and benzene), halogenated compounds (trichloroethylene, o-dichlorobenzene), nitriles (acetonitrile), acyl compounds (acetone, 2-butanone (MEK), ethyl acetate (EtOAc), and n-butyl acetate), disubstituted amides (dimethylformamide (DMF) and N-methylpyrrolidone (NMP)), sulfoxides (dimethylsulfoxide (DMSO)), weak hydrogen-bonding donors (chloroform), and alcohols (ethanol and 1-propanol). Their solubility parameters are in the range of 7.1-13.0 (cal/cm³)^{1/2}.

The solvents that lead to the highest swelling are benzene, chloroform, trichloroethylene, and toluene. They have almost the same contribution of dispersion forces to their solubility parameters which are ranging from 8.8-9.3 (cal/cm³)^{1/2}. Although benzene and trichloroethylene have similar contributions of HSPs on the solubility parameter of the solvents (i.e., $\delta = 8.9$ (cal/cm³)^{1/2}), the swelling ratio in benzene is higher than that of trichloroethylene. It may be due to the effect of molecular size of the solvents ($V_{\text{benzene}} = 89.4$ cm³/mol and $V_{\text{trichloroethylene}} = 90.2$ cm³/mol) on polymer swelling, since the small molecules can diffuse more readily than the larger ones (Hansen and Tim, 2007). Moreover, EtOAc has a considerably higher effect on solubility than xylene, although their solubility parameters are the same ($\delta = 8.9$ (cal/cm³)^{1/2}). This may be due to high contributions of polar forces and hydrogen-bonding forces in EtOAc.

In case of acyl compounds, all of the four solvents have almost the same atomic interactions (i.e., δ_d of all four solvents are nearly equal to each other). Among them, we observed the highest swelling of Parylene C in MEK. Experimental findings indicate that the degree of swelling of Parylene C in acyl compounds increases as the contribution of hydrogen-bonding forces decreases and the contribution of polarity increases. The increase in the contribution of hydrogen-bonding forces has the opposite effect on swelling when DMF and NMP were used as solvent.

The solvents that result in swelling of Parylene C can be used in the microfluidic systems only for short-term micro total analysis systems (μ TAS) applications. In the long-term, Parylene C film layer swells and the molecules of solvent penetrate through the film layer. If the solvent is inside the micro channels or structures made out of Parylene C, the total amount of solvent, or the concentration of the solvent in a mixture in the micro channels can change with time. If Parylene C film layer is used as a chemical barrier to insulate electronics, the long-term exposure to the above-listed solvents may lead to device failure.

6.5.2. Prediction of Solvent Compatibility

In the Hansen's approach, those solvents swelling the polymer have HSPs that are closer to those of polymer than the solvents with no solubility (Hansen, 2007b). However, it is necessary to determine the degree of proximity to the HSPs of the polymer so that the interaction of any solvent with the polymer can be predicted and taken into consideration for the progress of a study (Williams, 2007).

The degree of proximity was estimated using interaction radius, R_o , which is considered as the fourth parameter of HSP approach in the analysis of solvent solubility (Hansen, 2007b; Williams, 2007). It indicates the radius of a sphere obtained from the solubility sphere approach, which is based on two-dimensional plots of δ_p vs. δ_d , δ_h vs. δ_d , and δ_p vs. δ_h . A circle with a radius of R_o is adjusted on each plot by trial and error method in order to include all solvents that result in swelling/solubility in a sphere on a three dimensional plot of HSPs (Williams, 2007). Figures 6.27 to 6.30 show the 2D and 3D plots of these parameters of the solvents used in this study. As can be seen from these plots, an interaction radius $R_o = 4.8$ incorporates mostly the solvents that results in swelling. Four of the solvents in which Parylene C has no solubility (MeOH, IPA, ethylene glycol, and water) were at the outer region of the sphere while two of them (cyclohexane and n-heptane) were in the inner region of the sphere in the analysis of solubility sphere approach. Occurrences of solvents with no solubility in the sphere is due to the large molecular size of the solvents, which makes them less effective solvents than the solvents with small molecules (Hansen, 2007b; Williams, 2007). In the same manner, although some solvents (e.g., DMF, IPA, and DMSO) have HSPs at the outer region of the solubility sphere, they swelled the Parylene C film layer because of their small molecular size (Hansen, 2007b; Williams, 2007).

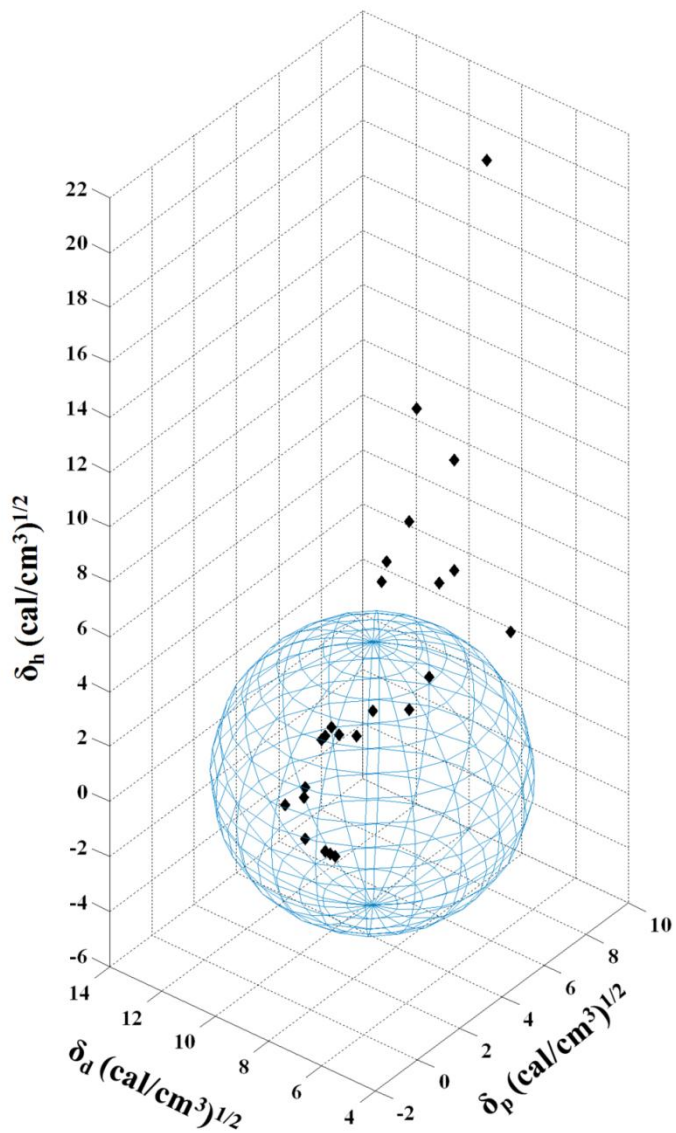


Figure 6.27. 3D solubility sphere of Parylene C created in MATLAB.

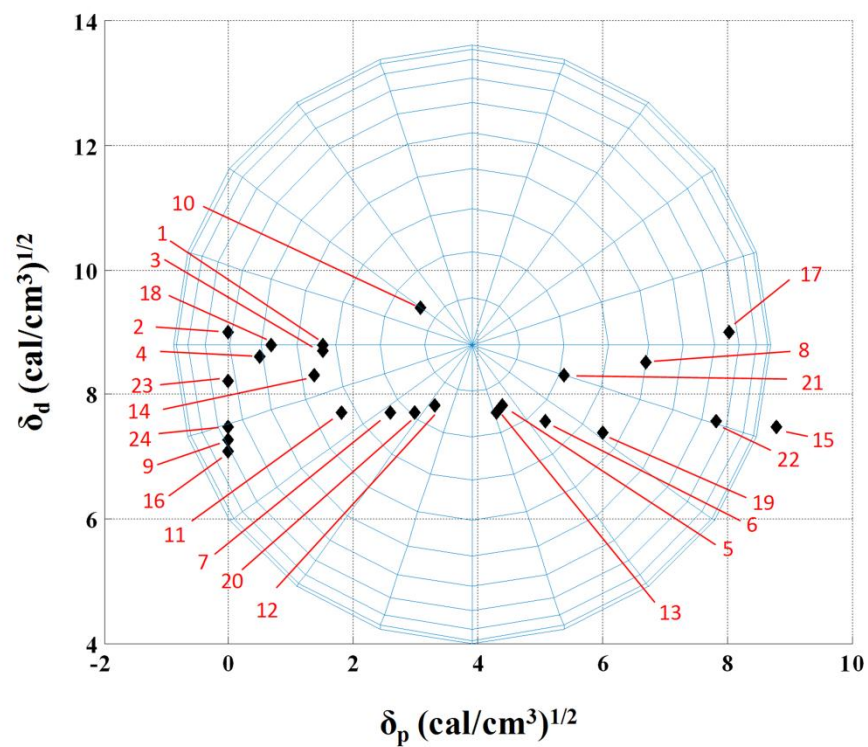


Figure 6.28. δ_d vs. δ_p two dimensional plot of Parylene C in the solvents specified in Table 6.12. The solvents are indicated using their ranking numbers.

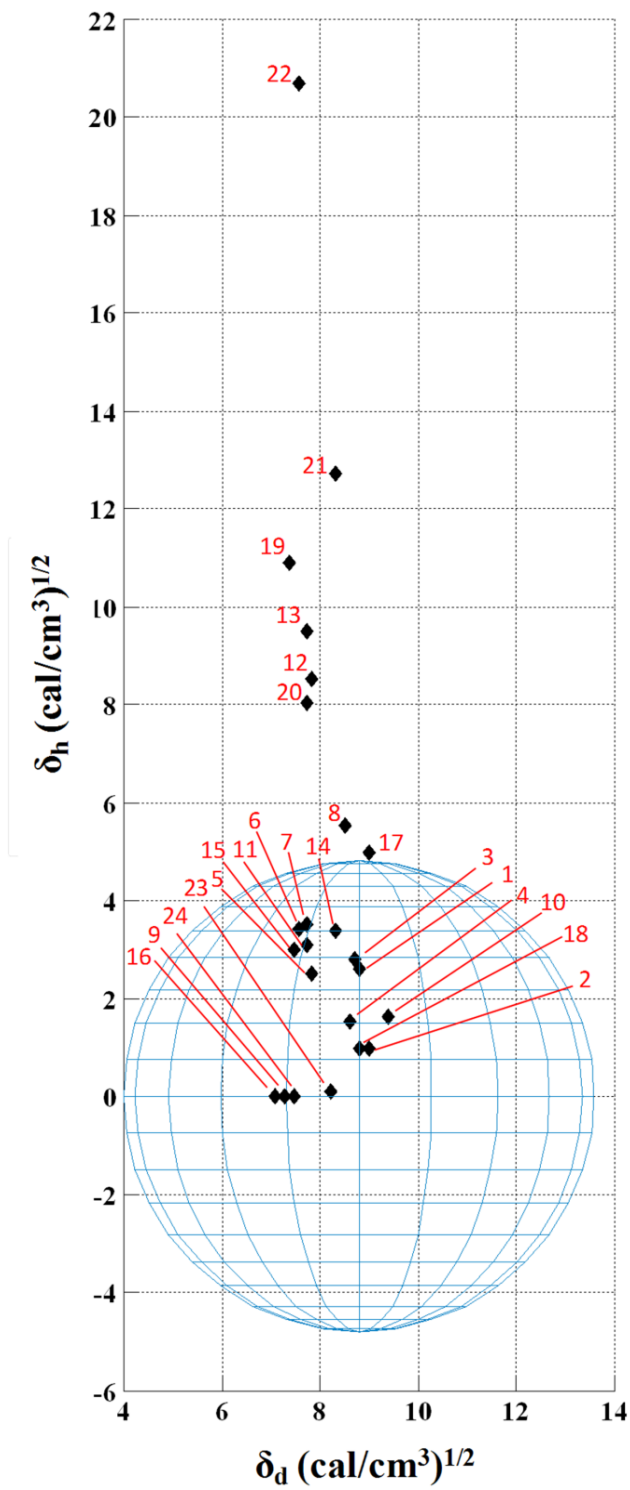


Figure 6.29. δ_h vs. δ_d two dimensional plot of Parylene C in the solvents specified in Table 6.12. The solvents are indicated using their ranking numbers.

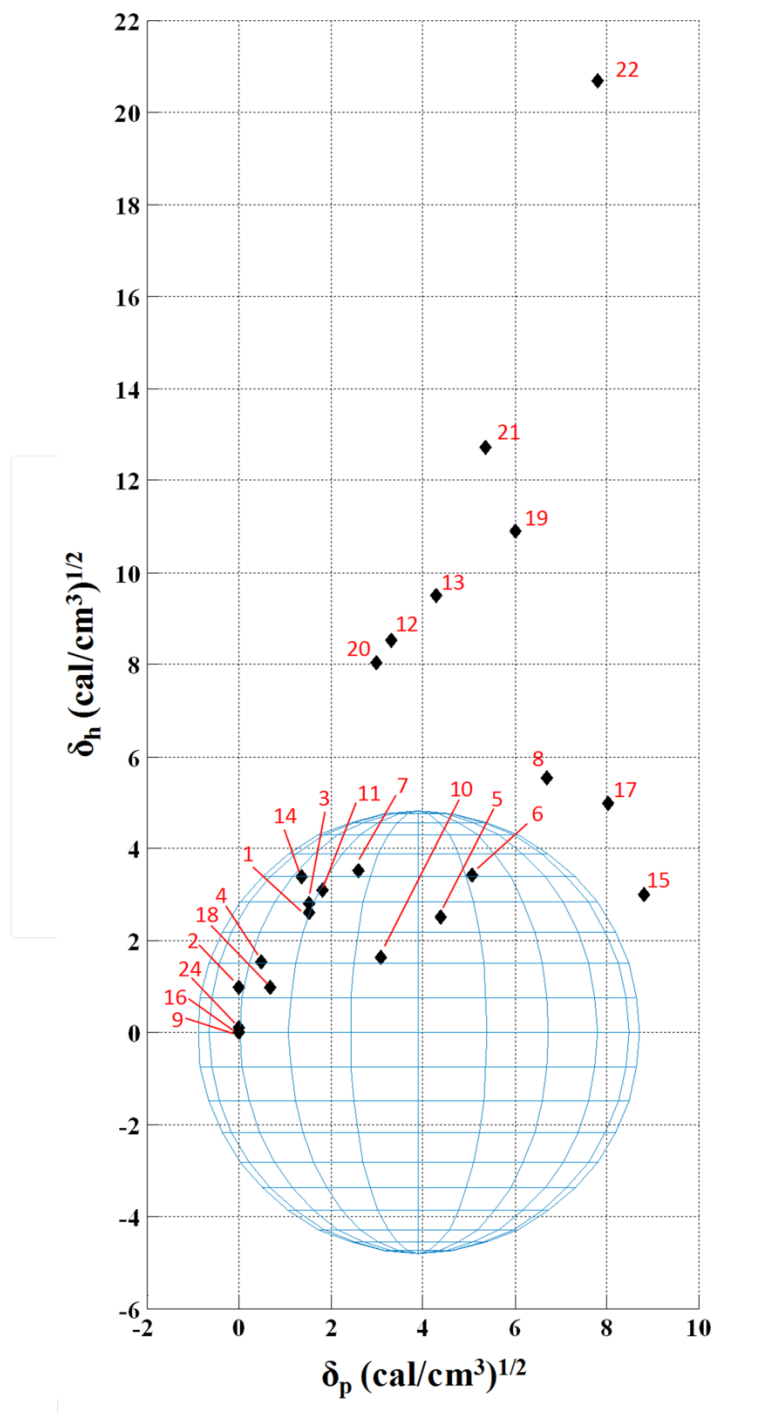


Figure 6.30. δ_h vs. δ_p two dimensional plot of Parylene C in the solvents specified in Table 6.12. The solvents are indicated using their ranking numbers.

In the analysis of solvents that have not been tested experimentally, another parameter is required additionally, known as solubility parameter distance, Ra (Hansen, 2007b). It is necessary to evaluate interaction between solvent and polymer by using the ratio Ra/Ro, which is known as relative energy difference (RED) number. Ra of a solvent can be calculated using δ_d , δ_p , and δ_h with the following formula:

$$(Ra)^2 = 4(\delta_d^p - \delta_d^s)^2 + (\delta_p^p - \delta_p^s)^2 + (\delta_h^p - \delta_h^s)^2 \quad (6.16)$$

Table 6.13 presents values of Ra and RED numbers of each specified solvent for the Parylene C swelling. There are three cases in the evaluation of RED number for a solvent:

- 1 RED < 1,
- 2 RED ~ 1, and
- 3 RED > 1.

A value of RED < 1 indicates that the molecules of the mixture have high affinity for each other and the solvent can swell the polymer. A value of RED < 1 indicates that the molecules of the mixture have high affinity for each other and the solvent can swell the polymer. As given in Table 6.13, solvents that swelled Parylene C film layer mostly have RED number smaller than one. For example, MEK whose ranking number is 5 has high affinity with Parylene C and it has a RED number of 0.67. Other than the value of the RED number, there is another indicatory parameter, molecular size of the solvent, which has an effect on possibility of swelling. Thus, although cyclohexane and n-heptane did not swell the film layer, their RED numbers are smaller than one. This is due to large size of the solvent molecules ($V_{\text{cyclohexane}} = 108.7 \text{ cm}^3/\text{mole}$, $V_{\text{n-heptane}} = 147.4 \text{ cm}^3/\text{mole}$), which limits swelling of the polymer. Among the studied solvents, only pentane and hexane has a value of RED number that is almost equal to one. This indicates a transition between the solvents in which Parylene C swells and the solvents with no solubility. As the affinity between the solvent and Parylene C decreases, value of RED number increases. For example, water whose ranking number is 22 has low affinity with Parylene C and a RED number of 4.41, which is higher than one.

Table 6.13. Molar volumes, values of Ra, and RED numbers of each specified solvent with their Parylene C swelling ranks.

Solvent	Molar Volume (Hansen, 2007a) [cm ³ /mole]	Ra	RED (Ra/Ro)	Rank
water	18.0	21.19	4.41	22
methanol	40.7	11.46	2.39	19
acetonitrile	52.6	8.75	1.82	12
ethylene glycol	55.8	12.83	2.67	21
ethanol	58.5	9.73	2.03	13
dimethyl sulfoxide	71.3	6.47	1.35	17
acetone	74.0	4.37	0.91	6
1-propanol	75.2	6.31	1.31	15
2-propanol	76.8	8.35	1.74	20
dimethylformamide	77.0	6.22	1.29	8
chloroform	80.7	4.05	0.84	2
benzene	89.4	3.53	0.74	1
2-butanone	90.1	3.21	0.67	5
trichloroethylene	90.2	3.68	0.77	3
ethyl acetate	98.5	4.33	0.90	7
N-methylpyrrolidone	104.0	4.34	0.90	14
toluene	106.8	3.76	0.78	4
cyclohexane	108.7	4.08	0.85	23
o-dichlorobenzene	112.8	2.16	0.45	10
pentane	116.2	5.20	1.08	16
xylene	123.3	3.37	0.70	18
hexane	131.6	4.95	1.03	9
n-butylacetate	132.5	4.30	0.90	11
n-heptane	147.4	4.72	0.98	24

In this part, the functionality of solubility parameter in solvent selection is demonstrated. The behaviors of solvents that are not included in this experimental work can be predicted by analyzing not only solubility parameter of the solvents but also the contributions of dispersion, polar, and hydrogen-bonding forces on the solubility parameter (Hansen and Tim, 2007). In this analysis, the generally used statement, “Like Dissolves Like”, can be considered as a starting point (Hansen and Tim, 2007).

6.5.3. Deswelling of Parylene C

Swelling can occur by immersing Parylene C into a solvent whereas swollen Parylene C can deswell and return to its initial dry state after evaporation of the solvent. We used acetone as a solvent to analyze the deswelling behavior of Parylene C since acetone is commonly used in removal of photoresist, which is encapsulated in micro channels made out of Parylene C (Ryu et al., 2004). After exposing the Parylene C film layer to the solvent (i.e., acetone) for 24 hours at room temperature, the test structure was taken out from the solvent and was kept in air for 24 hours to achieve solvent evaporation. It was observed that the swollen Parylene C structure shrank and went back to its original dimensions after totally dried. Deswelling of the Parylene C film layer do not have any effect on the mechanical and the electrical properties of the polymer (Yildirim et al., 2012).

6.5.4. Surface Roughness Measurements

Surface roughness is used to detect variations in surface height characteristics. There are several formulations to determine the surface roughness. Among them, average roughness (R_a) and root mean square roughness (R_q) are commonly used to characterize surface roughness in practical work and theoretical studies, respectively (Chandrasekaran and Sundararajan, 2004). R_a is obtained by the arithmetic mean of the absolute values of the surface variations while R_q is calculated by squaring each height value in dataset and then taking the square root of the mean (John Lee and Sundararajan, 2010).

In Figure 6.31, percent changes in the roughness of the film layer upon immersion into different solvents are shown for both parameters. Pentane changed the surface roughness to the greatest (149.7% R_a , 280.6% R_q) extent, while ethylene glycol had the least or no effect at all (0.65% R_a , 1.04% R_q). The percent changes of R_a and R_q in nonaromatic hydrocarbons increased, as the solubility parameters of the solvents decreased. However, there was no such relation similar to those in aromatic hydrocarbons, as well as among the ranking of swelling ratios. For the studied acyl compounds, only n-butyl acetate had a positive percent change on both surface roughness parameters. Acetone, EtOAc, and MEK decreased the surface roughness of Parylene C layer upon exposure for 24 hours. Halogenated compounds (i.e., trichloroethylene and o-dichlorobenzene) increased the surface roughness. The change in R_a value (3%) of trichloroethylene was not similar to that in R_q value (9.6%), which could be due to the presence of large deviations from the mean surface roughness. Among the alcohols studied, MeOH and 1-propanol decreased the surface roughness contrary to the effects of ethyl alcohol and IPA. Although there was only a slight change in the percentage of surface roughness after the film layer was exposed to 1-propanol (4% R_a , 4.3% R_q), IPA resulted in a very rough surface (37.1% R_a , 38.8% R_q).

It is certain that solvents have an effect on the surface roughness of Parylene C film layer upon long-time exposure. This is important since surface roughness is a critical parameter for both micro- and nano-sized devices. Roughness affects the flow characteristics in the micro fluidic devices, especially in gas flows (Girardo et al., 2012), and can also be used for the manipulation of droplets in micro or nano channels (Kwon et al., 2009). The roughness can affect bonding strength (Kim and Najafi, 2005) and optical quality (Dean et al., 2010) of layers as well. In microscale devices at which surface chemistry plays an important role surface area or biological analyte attachment sites can be enhanced by increasing surface roughness.

6.5.5. Comparison with Swelling of PDMS

PDMS has an important place in the research of μ TAS applications due to its transparency, inertness to chemicals, and suitability for easy and rapid prototyping (Lee et al., 2003). However, soft lithography method, which is used in its fabrication, is the rate-limiting step and makes the use of

PDMS unsuitable for mass production. In contrast, the compatibility of Parylene C with integrated circuit fabrication processes enables its usage in industry. Thus, the effect of solvents on these polymers can be compared to derive further information.

Figure 6.32 demonstrates the relationship between the swelling ratios and the solubility parameters of solvents for Parylene C and PDMS (Lee et al., 2003). The degree of swelling of Parylene C is generally less than that of PDMS. It may be due to pinhole free conformal coating of Parylene C, which can effectively limit penetration of the solvents through the film layer. Among the solvents of interest, the solvent that results in the greatest swelling of PDMS is pentane, while it is benzene for that of Parylene C. NMP, acetonitrile, DMF, DMSO, MeOH, ethylene glycol, and water have approximately the same effect considering the swelling of both polymers. Parylene C is more compatible than PDMS in microfluidic applications, especially for high solubility solvents, which result in only a low level of swelling of Parylene C (Lee et al., 2003). The use of Parylene C in high solubility solvents can increase the time that is required for saturation of the polymer with the solvent.

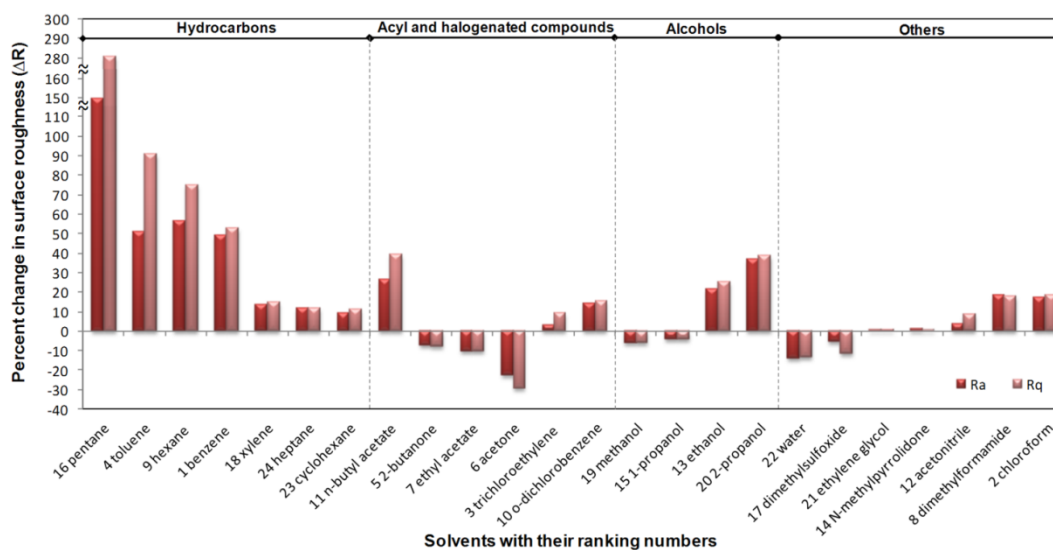


Figure 6.31. Percent changes in the average roughness (R_a) and root mean square roughness (R_q) of Parylene C surfaces after being immersed into the specified solvents for 24 hours at room temperature. The dashed lines are used to group the solvents as hydrocarbons, acyl and halogenated compounds, alcohols, and the others.

6.5.6. Application

Parylene C is known as a barrier to all chemical attacks at temperatures below its melting point of 290 °C, except with chloronaphthalene, which can dissolve Parylene C at 175 °C (Kumar, 2000). However, upon exposure of Parylene C film to a solvent, the molecules of the solvent may penetrate through the film, react with the underlying material or substrate, and result in the failure of proper functionality of the material or the substrate. This is important especially for the applications at which Parylene C is used as a chemical barrier. Tire pressure monitoring sensors (Liu, 2007), implants (Malvadkar et al., 2009), heads up display units (Zara and Smith, 2002), integrated circuits and printed circuit boards (PCB) (Mao et al., 2012) are some examples of these applications.

We employed an encapsulated photoresist structure to emulate solvent diffusivity through the Parylene C film layer of an insulated electronics (Figure 5.11 C-D). Six different solvents which can dissolve the photoresist were selected to demonstrate color change upon reaction as a result of diffusion of the solvents through the film layer (Ceylan Koydemir et al., 2012c). For this purpose, the structures were immersed into the solvents for four days at room temperature. Photographs of each structure were taken to visualize the state of diffusion after one hour, four hours, one day, and four days of exposure (Figure 6.33).

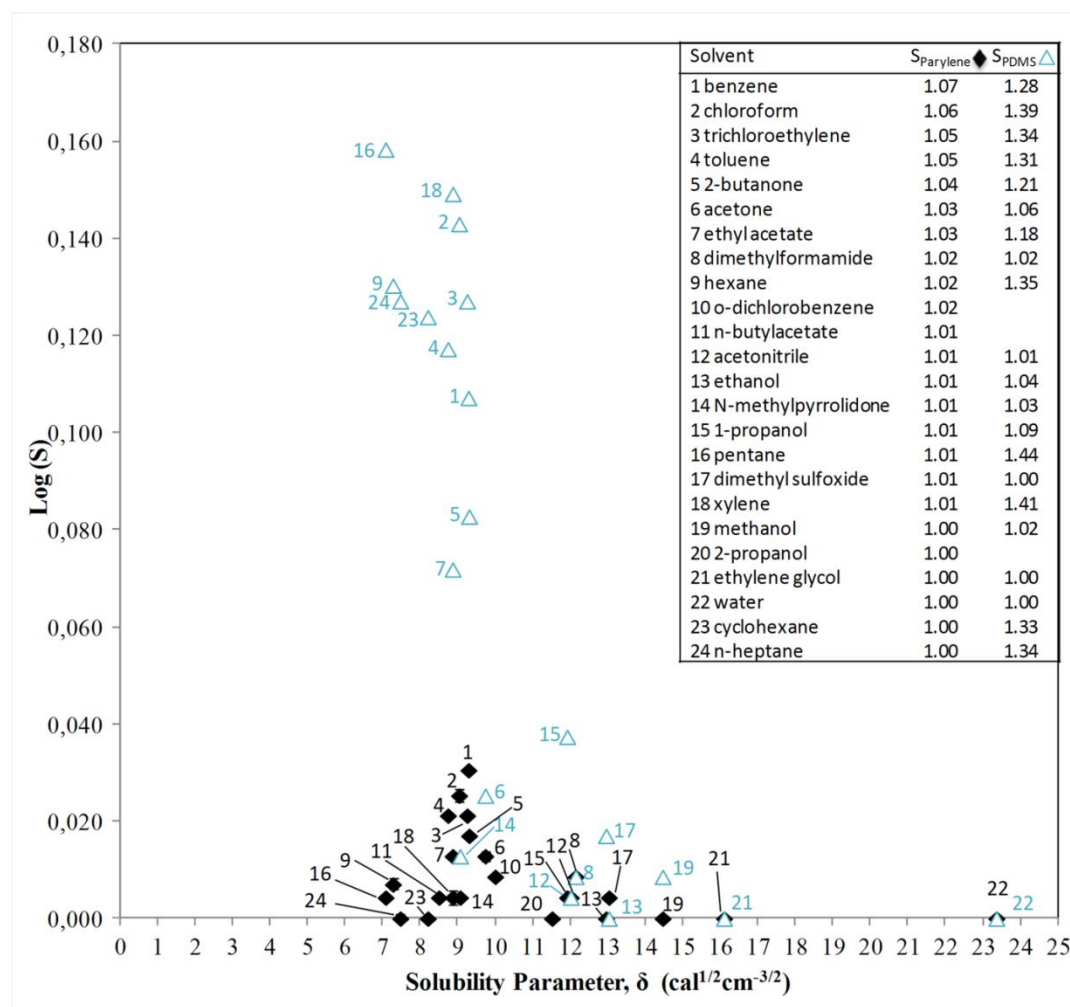


Figure 6.32. The change of the swelling ratios of Parylene C (S_{Parylene}) and PDMS (S_{PDMS})(Lee et al., 2003) with solubility parameter (δ). Ranking of solvents was made with respect to the degree of swelling ratio of Parylene C.

The Parylene C structures decolorized upon reaction with the solvents. It was observed that penetration of MEK through the Parylene C layer and its reaction with photoresist were much more rapid than that of the other solvents. Among the solvents, DMSO has the minimum color change. This indicates the existence of only little diffusivity of solvent through the Parylene C at room temperature. Descending order for the diffusion of solvents through the Parylene C film is as MEK > NMP > n-butyl acetate > acetone > DMF > and DMSO. However, this order is not the same with the ranking order of the degree of Parylene C swelling. It may be due to differences in reaction rate of photoresist removal at each solvent (Ceylan Koydemir et al., 2012c). Moreover, deformations (i.e., merging) on the structures were observed after four hours of exposure to the solvents. This can be due to low diffusivity of gaseous products from the reaction of photoresist with the solvent (Kumar, 2000).

Experimental results indicated that the degree of Parylene C swelling is mainly related to three variables:

- 1 Solvent type,
- 2 Molecular size of solvent, and
- 3 Thickness of Parylene C film layer.

Solvent type is the determining factor for the duration of the Parylene C usage.

Solvents with solubility can be used in microfluidic applications for only short-term exposures since they may result in leaks, significantly impairing its usefulness, while solvents with no solubility extend the time in the applications. For example, in the study of Li et al. (Li et al., 2011), electrodes of a retinal implant were insulated with a 10 μm -thick-Parylene C film layer and its performance tests in the saline environment (0.9% NaCl) were resulted in the durability of the implant over 20 years. Other than the solvent type, the size of the solvent molecules affects the degree of polymer swelling because small molecules have more tendency to solubilize than solvents with large molecular size (Hansen, 2007b). Thickness of Parylene C film layer is also very important. Since diffusion is related with the thickness of the layer, the swelling of Parylene C and its saturation with solvents over time can take longer in thick film layers. However, the degree of swelling in thin films can offer an advantage to the possible applications of Parylene C, since it behaves as a membrane (Lu et al., 2012).

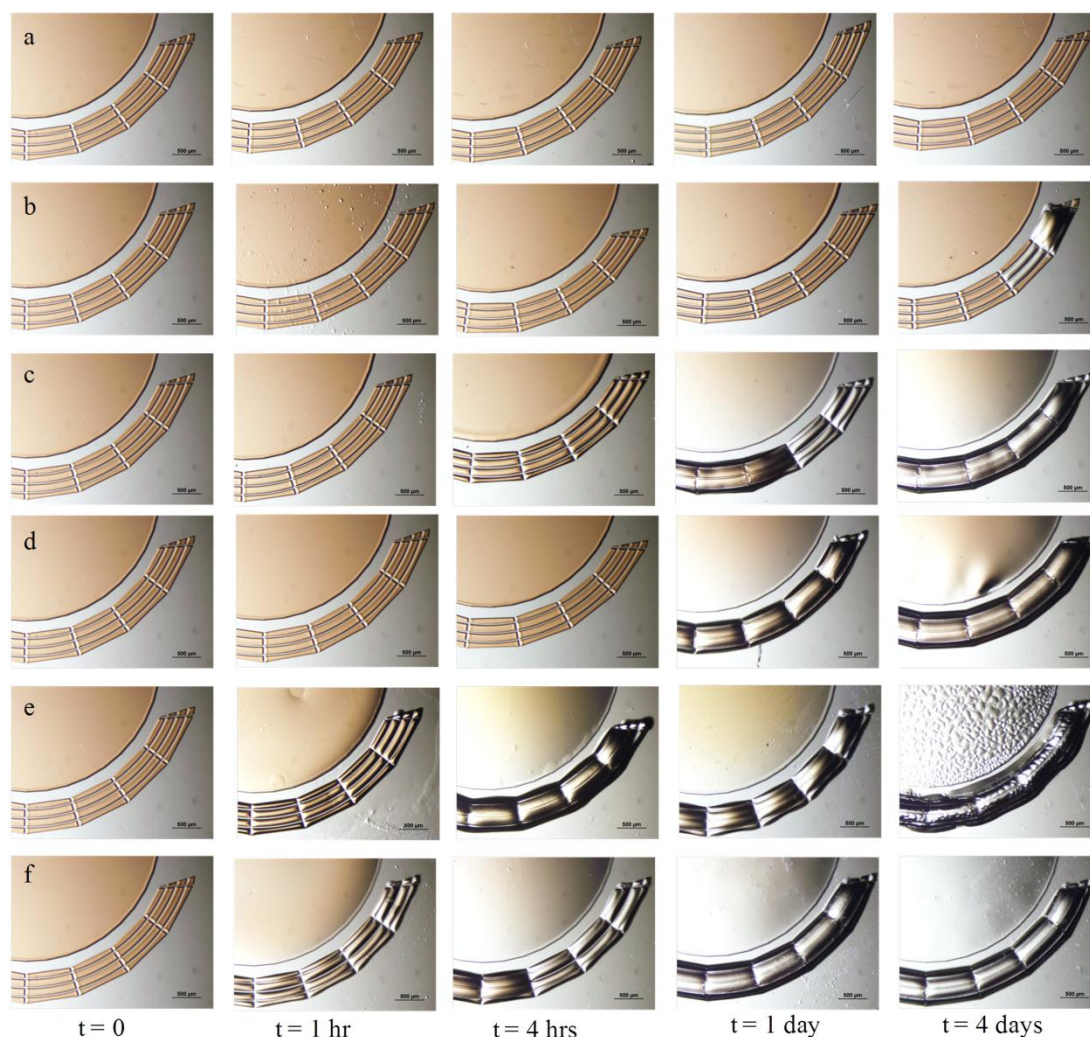


Figure 6.33. Time course of solvent penetration through 4 μm -thick Parylene C film layer. Solvents: (a) DMSO, (b) DMF, (c) acetone, (d) n-butyl acetate (e) NMP, and (f) MEK

6.6 Effects of Solvents on Dissolution of Photo Resist Encapsulated in Parylene Microchannels

In the experiments that were carried out by using organic solvents (i.e., n-heptane and cyclohexane) it was seen that, the dissolution rates of n-heptane and cyclohexane were too low. Thus, there was no change inside the channels after one hour (data not shown).

The dissolution rates with the immersion of individual dies into dipolar aprotic solvents showed that there was an increase in the length of cleared region with time as given in Figure 6.34.

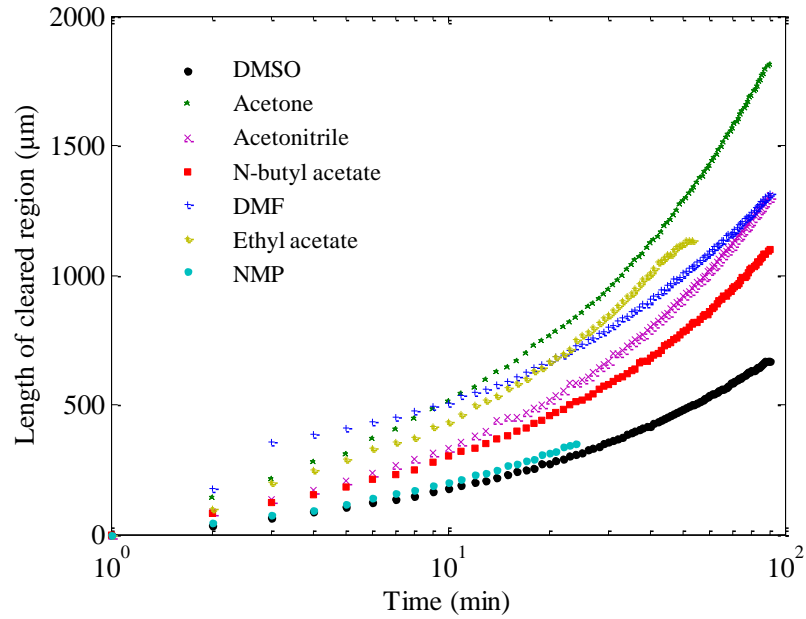


Figure 6.34. Dissolution data for dipolar aprotic solvents.

The rate of photo resist dissolution for the first 10 minutes was higher than the one for the last 10 minutes. Among the polar aprotic solvents studied, acetone had the highest dissolution rate while, DMSO had the lowest dissolution rate. This could be due to the low boiling temperature and low viscosity of the acetone compared to DMSO. The dissolution rate of solvents in increasing order was as follows: DMSO < NMP < n-butyl acetate < acetonitrile < ethyl acetate < DMF < acetone. There was no boundary region, which separates the photo resist from the cleared region after about 25 and 55 minutes for n-methyl-2-pyrrolidone and ethyl acetate, respectively. Therefore, further data could not be taken.

Also, the effect of UV exposure was studied experimentally by exposing the dies to 100, 300, and 999.9 mJ/cm² via using CL – 1000 UV Crosslinker (UVP LLC, US) before immersing the die into solvent. Figure 6.35 demonstrates that there is a slight effect of UV exposure (i.e., 3% difference between the final lengths of cleared regions) in release rate as it was expected.

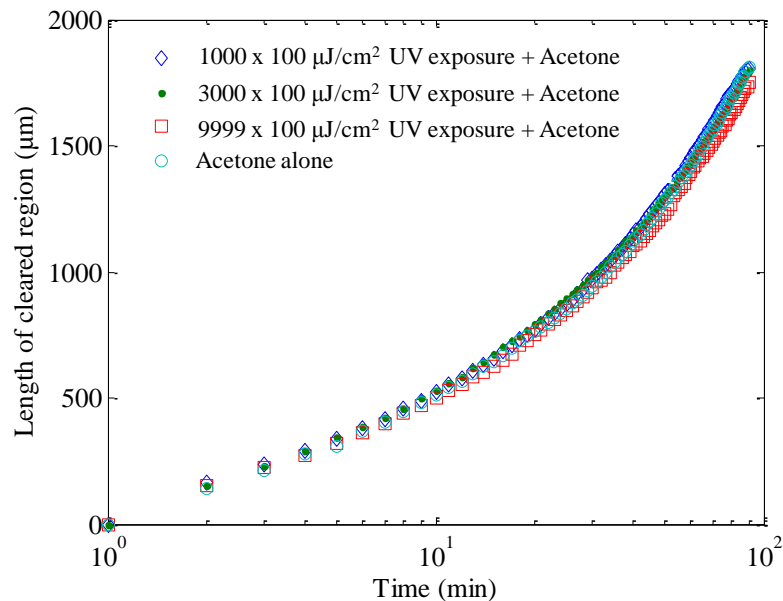


Figure 6.35. Dissolution data for different UV exposure values.

The three different mixtures of acetone and DMSO (20% acetone, 40% acetone, and 60% acetone [v/v]) were prepared to see the effect of mixing on dissolution rate at room temperature. As shown in Figure 6.36, dissolution rate of acetone alone was higher than the others although the mixing percentage with acetone increases the dissolution rate. The increase in dissolution rate in mixtures is due to the decrease in boiling point temperature and density.

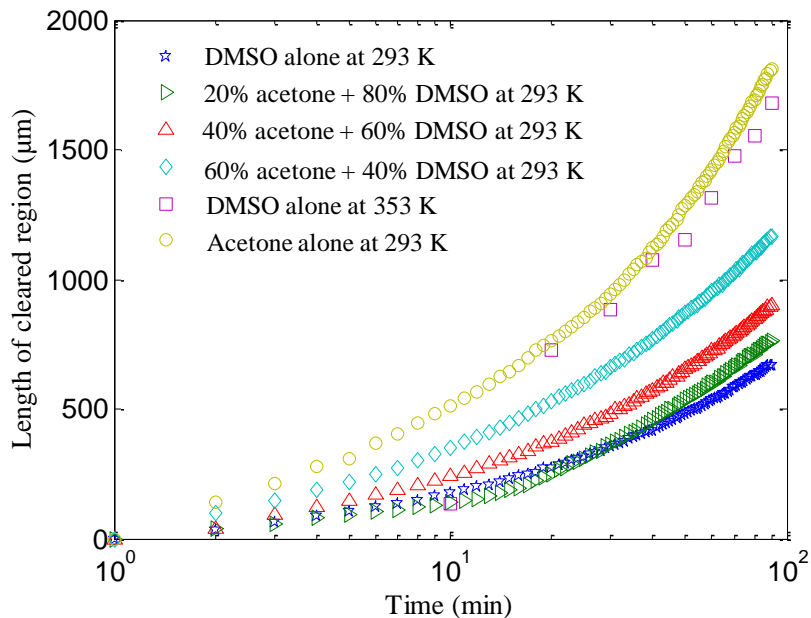


Figure 6.36. Dissolution data for DMSO at different temperatures and percentages [v/v] with acetone.

As a further study, the effect of temperature on the dissolution rate was studied. Increase in temperature, decreased viscosity, and density of the solvent. Thus, DMSO with high boiling temperature (462 K) was heated up to 353 K. Since the glass transition temperature of Parylene C is between 353 K and 373 K, maximum temperature was selected as 353 K so that the Parylene C layer will not be damaged with temperature (Dahmardeh et al., 2011). It was found that, the dissolution rate at 353 K with DMSO was 2.4 fold greater than the one at 293 K (Figure 6.36). The use of DMSO as an alternative to acetone can be preferred since the evaporation rate of DMSO even at 353 K is too low and that renewal of the solvent is not necessary. The increase of temperature further will also increase the dissolution rate since the boiling point temperature of photo resist is around 413 K.

CHAPTER 7

CONCLUSIONS AND RECOMMENDATIONS

The objective of this study was to design, fabricate, and test MEMS based electrochemical DNA biosensor to detect *mecA*, *vanA*, and *vanB* genes. As a result of the tasks accomplished, the followings were obtained:

- SAMs were formed on gold electrodes and detected optically using nucleic acid stains. The covalent attachment of ssDNA probes on gold layer was selectively accomplished using thiol (-SH) linkers on ssDNA probes since sulfur has strong affinity to gold. The chemisorption of DNA molecules is important not to lose formed layers during rinsing steps of surface modification protocols.
- A complete system with its micro reservoirs (inlet and outlet ports, and detection zone), microelectrodes, and micro channels was designed by taking into account several design features. This system with its on-chip reference (Ag), counter (Pt), and working (Au) electrodes and microfluidic structures is proposed for the first time in the literature and its fabrication steps are completely compatible to MEMS fabrication processes and IC technology.
- The designed sensor was fabricated using standard MEMS fabrication processes and integrated with microchannels using Parylene C as insulation layer. During fabrication, formation of Ag layer was accomplished by using electroplating, electroless deposition, and sputtering. The experimental findings showed that, Ag layer coated using the non-cyanide electroplating solution was not reproducible, which limits its usage in fabrication of test structures for potential high-throughput applications. Ag layer formed using electroless deposition resulted in non-continuous layer that limits its usage as an electrode. This type of coating of Ag layer can be used to form non-uniformly distributed Ag pillar structures on any substrate including and not limited to paper, silicon, and glass. On the contrary, Ag layer formed using sputtering technique is reproducible and uniform throughout the wafer.
- The amount of current obtained at macro electrodes using differential pulse voltammetry was predicted by a simulation code written. However, there are some limitations of the code since geometries of the electrodes and the presence of SAMs on gold electrode were not included in the formulations.
- As a result of the characterization of the sensor, Ag electrode, Au electrode, and Parylene C layer were analyzed as listed below:
 - The effect of buffer solutions used throughout the steps of electrochemical detection on Ag layer dissolution was studied. The experimental findings showed that Ag layer reacts with Cl^- in the buffer solution when the potential is above 1 V, and forms AgCl. This phenomenon was eliminated by using buffer solutions that do not contain Cl^- during the measurement using the electrochemical detection.
 - The stability of the Au electrode was demonstrated electrochemically in 0.5 M H_2SO_4 solution. It was concluded that at most 25 cycles of potential scan between 0 – 1.3 V was enough for the fabricated gold microelectrodes although at least 70 cycles of potential scan for the treatment were necessary for macro scale electrodes. The effect of surface roughness on effective electroactive area was studied and it was correlated with surface roughness of the gold layer.

- The effects of solvents on dissolution of photoresist encapsulated in Parylene C microchannels were analyzed using polar aprotic solvents and organic solvents and the dissolution of the photoresist was observed only in polar aprotic solvents in the increasing order of dissolution rate as DMSO < NMP < n-butyl acetate < acetonitrile < ethyl acetate < DMF < acetone. The effects of temperature of the solution and the UV exposure before immersing the test structure into a specified solvent were investigated and found that there was no effect of UV exposure on dissolution rate although the increase in temperature of the solution increases dissolution rate. These polar aprotic solvents can be used as an alternative to acetone in the dissolution of the photoresist in the fabrication of any test structure.
- The solvent compatibility of Parylene C layer was investigated and radius of solubility sphere for Parylene C layer was predicted as 4.8 using solubility sphere approach. The compatibility of Parylene C layer to any solvent which were not used in the experiments and whose Hansen solubility parameters are known can be predicted by using RED number. Moreover, the swelling ratios of Parylene C in different solvents were compared with those of PDMS and it was concluded that Parylene C film layer is more durable to the solvents than PDMS and Parylene C film layer can be used as a chemical barrier for insulation of electronics in short term exposures to the solvents that has solubility. In addition, the experimental findings showed that the swelling of a polymer layer mainly depends on molecular size of the solvent, solvent type, and thickness of Parylene C film layer.
- Specific parts of *mecA* gene belonging to *Staphylococcus aureus* subsp. *aureus* strain MRSA 252 (GenBank ID: BX571856.1) were detected using synthetic target probes and bacterial PCR product and found that:
 - Sensor functionality can be found by using redox marker based detection method utilizing Hoechst 33258 as redox marker. The design of capture probe selection was performed to enhance adsorption of target DNA. Thus, folding structures of the capture probe was analyzed using mfold Web server and found that after modification of the surface of working electrode with thiol-DNA, target DNA, and Hoechst 33258, electrochemical detection can be achieved by analyzing the oxidation peak of Hoechst 33258 near at 0.55 V using differential pulse voltammetry. The specificity of the capture probe was also demonstrated with the use of two different *femA* genes, i.e., one of them is belonging to *S.aureus* and the other one is belonging to *S. epidermis*. The experimental findings showed that it is possible to detect as low as 0.01 nM *mecA* gene using the sensor with its designed capture probe sequences.
 - The detection of bacterial PCR product was demonstrated using enzyme based detection method utilizing horseradish peroxidase as non-electroactive marker. Thus, the design of capture probe selection was performed to enhance adsorption of target DNA and folding structures of the capture probe was analyzed. HRP was conjugated with streptavidin molecules using Schiff-Base formation to enhance specificity and selectivity of the enzyme for rapid reactivity with biotin molecules. The enzymatic activity of HRP was demonstrated using microchronoamperometry and diffusion coefficient was predicted as $9.43 \pm 0.74 \times 10^{-6} \text{ cm}^2/\text{s}$. The detection of the nucleic acid was done by modifying the surface of working electrode with thiol-DNA and 10-times diluted PCR product hybridized with the capture probe. Subsequently, adsorption of streptavidin-conjugated HRP on modified surface was performed and the oxidation and reduction current peaks of TMB/H₂O₂ substrate were detected electrochemically using cyclic voltammetry. Moreover, the effect of addition of acid on HRP-modified surface was investigated to demonstrate the degradation of enzymatic activity of HRP in 1 M H₂SO₄. It was shown that it is possible to detect the presence of 10-times diluted PCR product in a solution by using HRP as enzyme both optically and electrochemically, since the product of HRP reaction with TMB/H₂O₂ substrate is yellow and it is visible at 450 nm.

In conclusion, the sensor designed with its compatibility to MEMS fabrication processes and IC technology has a promising potential to be a part of hand-held device for POC with the integration of micropotentiostat. Although all major objectives planned to be carried out were achieved in this thesis, there are still some issues that can be enhanced or done as a future work for the ultimate goal, as follows:

- The sample preparation part of this study was carried out in macro scale equipments, with more handling times and large volume of chemicals. This sample preparation approach is not convenient for a user-friendly and portable diagnostic system. Therefore, the sample preparation part belonging to cell separation, cell lyses, and PCR can be on-chip and can be integrated to the inlet reservoir of the sensor.
- The area of the working electrode is one of the major parameters for the adsorption of capture probes, which plays a major role in determination of the sensitivity of the sensor. Therefore, the effect of increasing electroactive area with pillars can be analyzed in order to enhance obtained peak current value.
- The time for detecting *mecA* gene using both redox marker based detection and enzyme based detection is about six hours including sample preparation in macro scale equipments. However, if the sample preparation part is integrated to the sensor, then it is necessary to optimize the surface modification protocols for the sample prepared on-chip in order to decrease time to result, decrease cross-reactivity of the chemicals used in sample preparation, and enhance sensitivity.
- The time for detecting *mecA* gene using both redox marker based detection and enzyme based detection is about six hours including sample preparation in macro scale equipments. The time to result can be decreased further by characterizing the DNA modified surface in more detail to enhance specificity and selectivity by using characterization methods like ToF-SIMS.
- In this study, the functionality of the sensor was demonstrated using *mecA* gene. The sensor can be used to detect *vanA* and *vanB* genes to detect the presence of VRE or any other DNA sequence to detect the presence of a specific nucleic acid sequence for diagnosis of diseases.
- The sensor can be expanded with parallelized microchannels in order to detect multiple analytes at the same time.
- The design of the sensor can be changed to an inlet, an outlet, and more than one detection zone in a microfluidic channel in order to detect the same type of biological analyte for averaging the results.
- The sensor can be modified to detect toxin (e.g., SEB toxin), cell, and protein other than the nucleic acid by using different surface immobilization protocols.
- The sensor can be used to detect volatile organic compounds by using Parylene C microchannels as a chemical barrier to prevent the diffusion of gas through the layer.
- Zero-cost diagnostic tools using electrochemical detection can be designed and fabricated in order to decrease cost of the sensor. For example,
 - A handheld device with its own reference and counter electrodes and micropotentiostat can be designed and fabricated so that the disposable sensor has only working electrode and its contact pads,
 - Printed electrodes on paper or Parylene C film layer can be used,
 - Graphene can be used as the working electrode in order to increase sensitivity.

REFERENCES

- Ahmed, M.U., Hasan, Q., Hossain, M.M., Saito, M., Tamiya, E., 2010. *Food Control* 21(5), 599-605.
- Ahmed, M.U., Idegami, K., Chikae, M., Kerman, K., Chaumpluk, P., Yamamura, S., Tamiya, E., 2007. *Analyst* 132(5), 431-438.
- Ahmed, M.U., Saito, M., Hossain, M.M., Rao, S.R., Furui, S., Hino, A., Takamura, Y., Takagi, M., Tamiya, E., 2009. *Analyst* 134(5), 966-972.
- Aoki, K., Tokuda, K., Matsuda, H., 1984. *Journal of Electroanalytical Chemistry* 175(1-2), 1-13.
- Aryan, E., Makvandi, M., Farajzadeh, A., Huygen, K., Bifani, P., Mousavi, S.L., Fateh, A., Jelodar, A., Gouya, M.M., Romano, M., 2010. *Microbiological Research* 165(3), 211-220.
- Azek, F., Grossiord, C., Joannes, M., Limoges, B., Brossier, P., 2000. *Analytical Biochemistry* 284(1), 107-113.
- Baldrich, E., del Campo, F.J., Munoz, F.X., 2009. *Biosensors & Bioelectronics* 25(4), 920-926.
- Bally, M., Halter, M., Voros, J., Grandin, H.M., 2006. *Surface and Interface Analysis* 38(11), 1442-1458.
- Banerjee, D., Pal, S.K., 2006. *Chemical Physics Letters* 432(1-3), 257-262.
- Becker, H., Gartner, C., 2008. *Analytical and Bioanalytical Chemistry* 390(1), 89-111.
- Beech, J.P., Holm, S.H., Adolfsson, K., Tegenfeldt, J.O., 2012. *Lab on a Chip* 12(6), 1048-1051.
- Beni, V., Newton, H.V., Arrigan, D.W.M., Hill, M., Lane, W.A., Mathewson, A., 2004. *Analytica Chimica Acta* 502(2), 195-206.
- Berger-Bächli, B., 2002. *International Journal of Medical Microbiology* 292(1), 27-35.
- Berger-Bächli, B., Rohrer, S., 2002. *Archives of Microbiology* 178(3), 165-171.
- Bhattacharya, S., Jang, J.S., Yang, L.J., Akin, D., Bashir, R., 2007. *Journal of Rapid Methods and Automation in Microbiology* 15(1), 1-32.
- Bischof, L.J., Lapsley, L., Fontecchio, K., Jacosalem, D., Young, C., Hankerd, R., Newton, D.W., 2009. *Journal of Clinical Microbiology* 47(7), 2281-2283.
- Boedicker, J.Q., Li, L., Kline, T.R., Ismagilov, R.F., 2008. *Lab on a Chip* 8(8), 1265-1272.
- Bordon, J., Master, R.N., Clark, R.B., Duvvuri, P., Karlowsky, J.A., Ayesu, K., Klotchko, A., Kapoor, R., Ramirez, J., 2010. *Diagnostic Microbiology and Infectious Disease* 67(4), 395-398.
- Breusegem, S.Y., Clegg, R.M., Loontjens, F.G., 2002. *Journal of Molecular Biology* 315(5), 1049-1061.
- Brown, D.F.J., 2001. *Journal of Antimicrobial Chemotherapy* 48, 65-70.
- Brown, D.F.J., Edwards, D.I., Hawkey, P.M., Morrison, D., Ridgway, G.L., Towner, K.J., Wren, M.W.D., Joint Working Party British Soc, A., 2005. *Journal of Antimicrobial Chemotherapy* 56(6), 1000-1018.
- Bugg, T.D.H., Walsh, C.T., 1992. *Natural Product Reports* 9(3).
- Cao, F., Grewe, D.W., Oppenheim, I.J., VanBriesen, J., , 2006. *Meet. Abstr. - Electrochem. Soc.* 602(2119), 1- 8.
- Cao, W., Su, M.M., Zhang, S.S., 2010. *Electrophoresis* 31(4), 659-665.
- Ceylan Koydemir, H., Kulah, H., Alp, A., Hascelik, G., Ozgen, C., 2010a. Design and Fabrication of MEMS Based Electrochemical Biosensor. 9th National Chemical Engineering Congress, Ankara.
- Ceylan Koydemir, H., Kulah, H., Alp, A., Ozgen, C., Hascelik, G., 2010b. A Disposable MEMS DNA Biosensor for Antibiotic Resistant Gene Detection in *Staphylococcus aureus*. 15th National Biomedical Engineering Meeting, Antalya.

- Ceylan Koydemir, H., Kulah, H., Ozgen, C., 2012a. A micro electrochemical sensor for the detection of methicillin resistance in *Staphylococcus aureus*. *Biosensors 2012 - 22nd Anniversary World Congress on Biosensors*, Cancun, Mexico.
- Ceylan Koydemir, H., Kulah, H., Ozgen, C., Alp, A., Hascelik, G., 2009. Detection of Bacterial DNA using MEMS Based DNA Biosensor. *Turkish National Committee of Automatic Control*, Istanbul.
- Ceylan Koydemir, H., Kulah, H., Ozgen, C., Alp, A., Hascelik, G., 2011. *Biosensors and Bioelectronics* 29(1), 1-12.
- Ceylan Koydemir, H., Kulah, H., Ozgen, C., Alp, A., Hascelik, G., 2012b. MEMS Based Micro Electrochemical Sensor for Detection of MRSA. *7th National Molecular and Diagnostic Microbiology Congress*, Ankara.
- Ceylan Koydemir, H., K ulah, H.,  zgen, C., Tosun,  ., 2012c. Effects of Solvents on Dissolution of Photoresist in Parylene Microchannels *NSTI TechConnect World 2012 Joint Conferences, Expo & Innovation Showcase*, pp. 372-375. *TechConnect World*, Santa Clara, California.
- Chandrasekaran, S., Sundararajan, S., 2004. *Surface and Coatings Technology* 188(0), 581-587.
- Chaumpluk, P., Kerman, K., Takamura, Y., Tamiya, E., 2007. *Science and Technology of Advanced Materials* 8(4), 323-330.
- Choi, K., Kim, J.-Y., Ahn, J.-H., Choi, J.-M., Im, M., Choi, Y.-K., 2012. *Lab on a Chip* 12, 1533-1539.
- Choi, Y.S., Lee, K.S., Park, D.H., 2005. *Journal of Micromechanics and Microengineering* 15(10), 1938-1946.
- Chung, M.G., Kim, D.H., Lee, H.M., Kim, T., Choi, J.H., Seo, D.K., Yoo, J.B., Hong, S.H., Kang, T.J., Kim, Y.H., 2012. *Sensors and Actuators B-Chemical* 166, 172-176.
- Compton, J., 1991. *Nature* 350(6313), 91-92.
- Compton, R.G., Banks, C.E., 2011. *Understanding Voltammetry*, 2nd Edition ed. *World Scientific Printers*, Singapore.
-  etinkaya, Y., Falk, P., Mayhall, C.G., 2000. *Clinical Microbiology Reviews* 13(4), 686-707.
- Dahmardeh, M., Khalid, W., Mohamed Ali, M.S., 2011. *MEMS 2011*, 272-275.
- Davis, E.M., Benetatos, N.M., Regnault, W.F., Winey, K.I., Elabd, Y.A., 2011. *Polymer* 52(23), 5378-5386.
- Dean, C.R., Young, A.F., Meric, I., Lee, C., Wang, L., Sorgenfrei, S., Watanabe, K., Taniguchi, T., Kim, P., Shepard, K.L., Hone, J., 2010. *Nature Nanotechnology* 5(10), 722-726.
- Deisingh, A.K., Thompson, M., 2002. *Analyst* 127(5), 567-581.
- Delvaux, M., Demoustier-Champagne, S., 2003. *Biosensors & Bioelectronics* 18(7), 943-951.
- Delvecchio, V.G., Petroziello, J.M., Gress, M.J., McCleskey, F.K., Melcher, G.P., Crouch, H.K., Lupski, J.R., 1995. *Journal of Clinical Microbiology* 33(8), 2141-2144.
- Delves, L.M., Mohamed, J.L., 1992. *Computational Methods for Integral Equations*, 1st ed. *Cambridge University Press*.
- Dequaire, M., Limoges, B., Moiroux, J., Saveant, J.M., 2002. *Journal of the American Chemical Society* 124(2), 240-253.
- Deurenberg, R.H., Stobberingh, E.E., 2008. *Infection Genetics and Evolution* 8(6), 747-763.
- Dodgson, K.J., 2004. *Clinical Microbiology Newsletter* 26(4), 25-30.
- Dominguez, E., Rincon, O., Narvaez, A., 2004. *Analytical Chemistry* 76(11), 3132-3138.
- Du, Y., Xue, Y., Frisch, H.L., 1996. *Solubility Parameters. Physical Properties of Polymers Handbook*, pp. 227-239. *AIP Press*, Woodbury, NY.
- Dutta, R., Morgan, D., Baker, N., Gardner, J.W., Hines, E.L., 2005. *Sensors and Actuators B-Chemical* 109(2), 355-362.
- Dworkin, M., Falkow, S., Rosenberg, E., Schleifer, K.-H., Stackebrandt, E., 2006. *The Prokaryotes: A Handbook on the Biology of Bacteria Bacteria: Firmicutes, Cyanobacteria*, 3rd ed. *Springer*.
- Ebina, W., Rowat, A.C., Weitz, D.A., 2009. *Biomicrofluidics* 3(3).

- ECDC, 2010. Antimicrobial resistance surveillance in Europe: Annual report of the European Antimicrobial Resistance Surveillance Network (EARS-Net). Surveillance Report. European Centre for Disease Prevention and Control, Stockholm: ECDC.
- Ehrfeld, W., Hessel, V., Haverkamp, V., 2000. Microreactors. Ullmann's Encyclopedia of Industrial Chemistry. Wiley-VCH Verlag GmbH & Co. KGaA.
- Ermini, M.L., Scarano, S., Bini, R., Banchelli, M., Berti, D., Mascini, M., Minunni, M., 2011. Biosensors and Bioelectronics 26(12), 4785-4790.
- ETAG, 2006. Antibiotic Resistance. European Parliament.
- Eydelnant, I.A., Uddayasankar, U., Li, B.B., Liao, M.W., Wheeler, A.R., 2012. Lab on a Chip 12(4), 750-757.
- Fan, C.H., Li, G.X., Gu, Q.R., Zhu, J.Q., Zhu, D.X., 2000. Analytical Letters 33(8), 1479-1490.
- Fanjul-Bolado, P., Gonzalez-Garia, M.B., Costa-Garcia, A., 2005. Analytical and Bioanalytical Chemistry 382(2), 297-302.
- Felten, A., Grandry, B., Lagrange, P.H., Casin, I., 2002. Journal of Clinical Microbiology 40(8), 2766-2771.
- Focke, M., Stumpf, F., Faltin, B., Reith, P., Bamarni, D., Wadle, S., Muller, C., Reinecke, H., Schrenzel, J., Francois, P., Mark, D., Roth, G., Zengerle, R., von Stetten, F., 2010a. Lab on a Chip 10(19), 2519-2526.
- Focke, M., Stumpf, F., Roth, G., Zengerle, R., von Stetten, F., 2010b. Lab on a Chip 10(23), 3210-3212.
- Francois, P., Pittet, D., Bento, M., Pepey, B., Vaudaux, P., Lew, D., Schrenzel, J., 2003. Journal of Clinical Microbiology 41(1), 254-260.
- Franz, C.M.A.P., Holzapfel, W.H., Stiles, M.E., 1999. International Journal of Food Microbiology 47(1), 1-24.
- Freeman-Cook, L., Freeman-Cook, K.D., 2006. *Staphylococcus aureus* infections, 1st ed. Chelsea House Publishers.
- Frey, A., Meckelein, B., Externest, D., Schmidt, M.A., 2000. Journal of Immunological Methods 233(1-2), 47-56.
- Fritz, J., Baller, M.K., Lang, H.P., Rothuizen, H., Vettiger, P., Meyer, E., Guntherodt, H.J., Gerber, C., Gimzewski, J.K., 2000. Science 288(5464), 316-318.
- Garcia-Lara, J., Masalha, M., Foster, S.J., 2005. Drug Discovery Today 10(9), 643-651.
- Gebala, M., Hartwich, G., Schuhmann, W., 2011. Faraday Discussions 149, 11-22.
- Girardo, S., Palpacelli, S., De Maio, A., Cingolani, R., Succi, S., Pisignano, D., 2012. Langmuir 28(5), 2596-2603.
- Gong, G., Wu, J., Liu, J., Sun, N., Zhao, Y., Jiang, L., 2012. Journal of Materials Chemistry 22(17), 8257-8262.
- Gould, I.M., 2005. Journal of Hospital Infection 61(4), 277-282.
- Graves, S.F., Kobayashi, S.D., DeLeo, F.R., 2010. Journal of Molecular Medicine-Jmm 88(2), 109-114.
- Greenwood, N.N., Earnshaw, A., 1997. Copper, Silver and Gold. Chemistry of Materials, pp. 117-1186, 2nd ed. Elsevier.
- Greg T, H., 2008. Chapter 3 - Zero-Length Crosslinkers. Bioconjugate Techniques (Second Edition), pp. 234-275. Academic Press, New York.
- Gu, H.W., Ho, P.L., Tsang, K.W.T., Wang, L., Xu, B., 2003. Journal of the American Chemical Society 125(51), 15702-15703.
- Guntupalli, R., Sorokulova, I., Krumnow, A., Pustovyy, O., Olsen, E., Vodyanoy, V., 2008. Biosensors & Bioelectronics 24(1), 151-154.
- Hansen, C.M., 2007a. Appendix A: Table A.1. Hansen Solubility Parameters: A User's Handbook pp. 345-483, 2nd ed. Taylor & Francis Group, LLC, Florida.
- Hansen, C.M., 2007b. Solubility Parameters - An Introduction. Hansen Solubility Parameters: A User's Handbook pp. 1-19, 2nd ed. Taylor & Francis Group, LLC, Florida.

- Hansen, C.M., Tim, P.S., 2007. Hansen Solubility Parameters - Biological Materials. Hansen Solubility Parameters: A User's Handbook pp. 270-292, 2nd ed. Taylor & Francis Group, LLC, Florida.
- Hashimoto, K., Ishimori, Y., 2001. Lab on a Chip 1(1), 61-63.
- Hashimoto, K., Tsuruta, T., Morinaka, K., Yoshiike, N., 2000. Sensors and Actuators a-Physical 79(1), 46-52.
- Hedden, R.C., Saxena, H., Cohen, C., 2000. Macromolecules 33(23), 8676-8684.
- Hedden, R.C., Wong, C., Cohen, C., 1999. Macromolecules 32(15), 5154-5158.
- Heinze, J., 1984. Angewandte Chemie International Edition in English 23(11), 831-847.
- Heinze, J., 1993. Angewandte Chemie International Edition in English 32(9), 1268-1288.
- Hiramatsu, K., Cui, L., Kuroda, M., Ito, T., 2001. Trends in Microbiology 9(10), 486-493.
- House, D.L., Chon, C.H., Creech, C.B., Skaar, E.P., Li, D.Q., 2010. Journal of Biotechnology 146(3), 93-99.
- Huh, D., Matthews, B.D., Mammoto, A., Montoya-Zavala, M., Hsin, H.Y., Ingber, D.E., 2010. Science 328(5986), 1662-1668.
- Jeljaszewicz, J., Mlynarczyk, G., Mlynarczyk, A., 2000. International Journal of Antimicrobial Agents 16(4), 473-478.
- Jenison, R., Yang, S., Haeberli, A., Polisky, B., 2001. Nature Biotechnology 19(1), 62-65.
- John Lee, S.-J., Sundararajan, N., 2010. Microfabrication for Microfluidics. Artech House Inc. , Norwood, MA.
- Joseph, P.D., Eling, T., Mason, R.P., 1982. Journal of Biological Chemistry 257(7), 3669-3675.
- Josse, F., Bender, F., Cernosek, R.W., 2001. Analytical Chemistry 73(24), 5937-5944.
- Kerman, K., Vestergaard, M.d., Tamiya, E., 2008. Electrochemical DNA Biosensors: Protocols for Intercalator-Based Detection of Hybridization in Solution and at the Surface. pp. 99-113.
- Khan, M.G., Fartaj, A., 2011. International Journal of Energy Research 35(7), 553-582.
- Kim, H., Najafi, K., 2005. J. Microelectromech. Syst. 14(6), 1347-1355.
- Klonoski, J., Mondesire, R., Rea, L., Ward, D.C., Jenison, R.D., 2010. Analytical Biochemistry 396(2), 284-289.
- Knapp, C.C., Ludwig, M.D., Washington, J.A., 1994. Journal of Clinical Microbiology 32(10), 2588-2589.
- Kobayashi, M., Takashi, K.B., Saito, M., Kaji, S., Oomura, M., Iwabuchi, S., Morita, Y., Hasan, Q., Tamiya, E., 2004. Electrochemistry Communications 6(4), 337-343.
- Koyuncuoğlu, A., Jafari, R., Okutucu-Özyurt, T., Kūlah, H., 2012. International Journal of Thermal Sciences 56(0), 77-85.
- Kralj, J.G., Arya, C., Tona, A., Forbes, T.P., Munson, M.S., Sorbara, L., Srivastava, S., Forry, S.P., 2012. Lab on a Chip 12(23), 4972-4975.
- Kudo, A., Fujita, T., Lang, X.Y., Chen, L.Y., Chen, M.W., 2010. Materials Transactions 51(9), 1566-1569.
- Kumar, R., 2000. Xylylene polymers. Kirk-Othmer Encyclopedia of Chemical Technology. John Wiley & Sons, Inc.
- Kunishima, H., Yamamoto, N., Kobayashi, T., Minegishi, M., Nakajima, S., Chiba, J., Kitagawa, M., Hirakata, Y., Honda, Y., Kaku, M., 2010. Journal of Infection and Chemotherapy 16(6), 414-417.
- Kwon, Y., Patankar, N., Choi, J., Lee, J., 2009. Langmuir 25(11), 6129-6136.
- Lagally, E.T., Scherer, J.R., Blazej, R.G., Toriello, N.M., Diep, B.A., Ramchandani, M., Sensabaugh, G.F., Riley, L.W., Mathies, R.A., 2004. Analytical Chemistry 76(11), 3162-3170.
- Lee, J.N., Park, C., Whitesides, G.M., 2003. Analytical Chemistry 75(23), 6544-6554.
- Lee, S.J., Lee, S.Y., 2004. Applied Microbiology and Biotechnology 64(3), 289-299.
- Lee, T.M.H., Hsing, I.M., 2002. Analytical Chemistry 74(19), 5057-5062.
- Li, W., Rodger, D.C., Pinto, A., Meng, E., Weiland, J.D., Humayun, M.S., Tai, Y.-C., 2011. Sensors and Actuators A: Physical 166(2), 193-200.

- Li, X., Xiong, Y., Fan, X., Feng, P., Tang, H., Zhou, T., 2012. *Medecine Et Maladies Infectieuses* 42(5), 218-225.
- Li, X.M., Fu, P.Y., Liu, J.M., Zhang, S.S., 2010. *Analytica Chimica Acta* 673(2), 133-138.
- Liao, J.C., Mastali, M., Gau, V., Suchard, M.A., Moller, A.K., Bruckner, D.A., Babbitt, J.T., Li, Y., Gornbein, J., Landaw, E.M., McCabe, E.R.B., Churchill, B.M., Haake, D.A., 2006. *Journal of Clinical Microbiology* 44(2), 561-570.
- Lindsey, W.C., Woodruff, E.S., Weed, D., Ward, D.C., Jenison, R.D., 2008. *Diagnostic Microbiology and Infectious Disease* 61(3), 273-279.
- Liu, C., 2007. *Adv. Mater.* 19(22), 3783-3790.
- Liu, G., Wan, Y., Gau, V., Zhang, J., Wang, L.H., Song, S.P., Fan, C.H., 2008. *Journal of the American Chemical Society* 130(21), 6820-6825.
- Lizardi, P.M., Huang, X.H., Zhu, Z.R., Bray-Ward, P., Thomas, D.C., Ward, D.C., 1998. *Nature Genetics* 19(3), 225-232.
- Lowy, F.D., 2003. *Journal of Clinical Investigation* 111(9), 1265-1273.
- Lu, B., Zheng, S., Quach, B.Q., Tai, Y.-C., 2010. *Lab on a Chip* 10(14), 1826-1834.
- Lu, B., Zhu, D.H., Hinton, D., Humayun, M.S., Tai, Y.C., 2012. *Biomed. Microdevices* 14(4), 659-667.
- Lutz, S., Weber, P., Focke, M., Faltin, B., Hoffmann, J., Muller, C., Mark, D., Roth, G., Munday, P., Armes, N., Piepenburg, O., Zengerle, R., von Stetten, F., 2010. *Lab on a Chip* 10(7), 887-893.
- Madigan, M.T., Martinko, J.M., Parker, J., 2000. *Brock Biology of Microorganisms*, 9th ed. Prentice Hall.
- Malhotra-Kumar, S., Abrahantes, J.C., Sabiiti, W., Lammens, C., Vercauteren, G., Ieven, M., Molenberghs, G., Aerts, M., Goossens, H., Team, M.W.S., 2010. *Journal of Clinical Microbiology* 48(4), 1040-1046.
- Malvadkar, N., Dressick, W.J., Demirel, M.C., 2009. *Journal of Materials Chemistry* 19(27), 4796-4804.
- Mao, F., Lindeberg, M., Hjort, K., Klintberg, L., 2012. *Sensors and Actuators A: Physical* 179, 56-61.
- Mavandadi, S., Dimitrov, S., Feng, S., Yu, F., Yu, R., Sikora, U., Ozcan, A., 2012. *Lab on a Chip* 12(20), 4102-4106.
- McEwen, G.D., Chen, F., Zhou, A.H., 2009. *Analytica Chimica Acta* 643(1-2), 26-37.
- Medicine, N.N.L.o., 2012. *BLAST: Basic Local Alignment Search Tool*. Maryland, US.
- Meng, E., Li, P.Y., Tai, Y.C., 2008. *Journal of Micromechanics and Microengineering* 18(4), 1-13.
- Microchemicals, 2007. *Lithography, Theory and Application of Photoresists, Developers, Solvents and Etchants*.
- Miller, E., Leighton, E., 1990. *Journal of Elastomers and Plastics* 22(1), 46-57.
- Modrusan, Z., Marlowe, C., Wheeler, D., Pirseyedi, M., Bryan, R.N., 1999. *Molecular and Cellular Probes* 13(3), 223-231.
- Moller, J.K., Pedersen, L.N., Persson, K., 2008. *Journal of Clinical Microbiology* 46(12), 3892-3895.
- Moon, H., Wheeler, A.R., Garrell, R.L., Loo, J.A., Kim, C.J., 2006. *Lab on a Chip* 6(9), 1213-1219.
- Murakami, K., Minamide, W., Wada, K., Nakamura, E., Teraoka, H., Watanabe, S., 1991. *Journal of Clinical Microbiology* 29(10), 2240-2244.
- Naikare, H., Ramachandran, A., Goad, D., Clarke, J., Clarke, C., 2009. *Electrophoresis* 30(3), 472-478.
- Nichol, K.A., Sill, M., Laing, N.M., Johnson, J.L., Hoban, D.J., Zhanel, G.G., Grp, N., 2006. *International Journal of Antimicrobial Agents* 27(5), 392-396.
- Nightingale, A.M., Krishnasadan, S.H., Berhanu, D., Niu, X., Drury, C., McIntyre, R., Valsami-Jones, E., deMello, J.C., 2011. *Lab on a Chip* 11(7), 1221-1227.
- Nordberg, P., Monnet, L.D., Cars, O., 2005. *Antibacterial Drug Resistance WHO project: Priority Medicines for Europe and the World "A Public Health Approach to Innovation."*, p. 40. World Health Organization.

- Okeke, I.N., Laxminarayan, R., Bhutta, Z.A., Duse, A.G., Jenkins, P., O'Brien, T.F., Pablos-Mendez, A., Klugman, K.P., 2005. *Lancet Infectious Diseases* 5(8), 481-493.
- Paddon, C.A., Bhatti, F.L., Donohoe, T.J., Compton, R.G., 2006. *Journal of Electroanalytical Chemistry* 589(2), 187-194.
- Palecek, E., Fojta, M., 2007. *Talanta* 74(3), 276-290.
- Pan, J., 2007. *Biochemical Engineering Journal* 35(2), 183-190.
- Pantosti, A., Sanchini, A., Monaco, M., 2007. *Future Microbiology* 2(3), 323-334.
- Patolsky, F., Katz, E., Bardea, A., Willner, I., 1999. *Langmuir* 15(11), 3703-3706.
- Peterson, L.R., Liesenfeld, O., Woods, C.W., Allen, S.D., Pombo, D., Patel, P.A., Mehta, M.S., Nicholson, B., Fuller, D., Onderdonk, A., 2010. *Journal of Clinical Microbiology* 48(5), 1661-1666.
- Piepenburg, O., Williams, C.H., Stemple, D.L., Armes, N.A., 2006. *Plos Biology* 4(7), 1115-1121.
- Prere, M.F., Baron, O., Bacrie, S.C., Fayet, O., 2006. *Pathologie Biologie* 54(8-9), 502-505.
- Rajan, L., Smyth, E., Humphreys, H., 2007. *Journal of Infection* 55(4), 353-357.
- Reinert, R.R., Low, D.E., Rossi, F., Zhang, X., Wattal, C., Dowzicky, M.J., 2007. *Journal of Antimicrobial Chemotherapy* 60(5), 1018-1029.
- Ryu, K.S., Shaikh, K., Goluch, E., Fan, Z.F., Liu, C., 2004. *Lab on a Chip* 4(6), 608-613.
- Salminen, S., von Wright, A., Morelli, L., Marteau, P., Brassart, D., de Vos, W.M., Fondén, R., Saxelin, M., Collins, K., Mogensen, G., Birkeland, S.-E., Mattila-Sandholm, T., 1998. *International Journal of Food Microbiology* 44(1-2), 93-106.
- Sant, S.B., Gill, K.S., Burrell, R.E., 1999. *Scripta Materialia* 41(12), 1333-1339.
- Schouten, M.A., Hoogkamp-Korstanje, J.A.A., Meis, J.F.G., Voss, A., the European, V.R.E.S.G., 2000. *European Journal of Clinical Microbiology & Infectious Diseases* 19(11), 816-822.
- Seymour, J.P., Elkasabi, Y.M., Chen, H.Y., Lahann, J., Kipke, D.R., 2009. *Biomaterials* 30(31), 6158-6167.
- Shamai, R., Andelman, D., Berge, B., Hayes, R., 2008. *Soft Matter* 4(1), 38-45.
- Shen, F., Du, W.B., Davydova, E.K., Karymov, M.A., Pandey, J., Ismagilov, R.F., 2010. *Analytical Chemistry* 82(11), 4606-4612.
- Shoup, D., Szabo, A., 1982. *Journal of Electroanalytical Chemistry* 140(2), 237-245.
- Sia, S.K., Kricka, L.J., 2008. *Lab on a Chip* 8(12), 1982-1983.
- Siegel, A.C., Phillips, S.T., Wiley, B.J., Whitesides, G.M., 2009. *Lab on a Chip* 9(19), 2775-2781.
- Simeone, D., Cipolloni, S., Mariucci, L., Rapisarda, M., Minotti, A., Pecora, A., Cuscunà, M., Maiolo, L., Fortunato, G., 2009. *Thin Solid Films* 517(23), 6283-6286.
- Sista, R., Hua, Z.S., Thwar, P., Sudarsan, A., Srinivasan, V., Eckhardt, A., Pollack, M., Pamula, V., 2008. *Lab on a Chip* 8(12), 2091-2104.
- Small, P.A., 1953. *Journal of Applied Chemistry* 3(2), 71-80.
- Smith, T.L., Jarvis, W.R., 1999. *Microbes and Infection* 1(10), 795-805.
- Sokolov, A.N., Tee, B.C.K., Bettinger, C.J., Tok, J.B.H., Bao, Z., 2011. *Accounts of Chemical Research* 45(3), 361-371.
- Solutions, N., 2012. *Enterococcus* sp., Bacteria, gram-positive cocci. California.
- Song, Y.H., Wang, L., Ren, C.B., Zhu, G.Y., Li, Z., 2006. *Sensors and Actuators B-Chemical* 114(2), 1001-1006.
- Struelens, M.J., Hawkey, P.M., French, G.L., Witte, W., Tacconelli, E., 2009. *Clinical Microbiology and Infection* 15(2), 112-119.
- Sufen, W., Tuzhi, P., Yang, C.F., 2002. *Electroanalysis* 14(23), 1648-1653.
- Sukas, S., Erson, A.E., Sert, C., Kulah, H., 2008. *Electrophoresis* 29(18), 3752-3758.
- Tacconelli, E., Cataldo, M.A., 2008. *International Journal of Antimicrobial Agents* 31(2), 99-106.
- Takahashi, M., Okada, J., Ito, K., Hashimoto, M., Hashimoto, K., Yoshida, Y., Furuichi, Y., Ohta, Y., Mishiro, S., Gemma, N., 2005. *Analyst* 130(5), 687-693.
- Tan, C.P., Craighead, H.G., 2010. *Mater.* 3(3), 1803-1832.

- Taylor-Robinson, D., Bebear, C., 1997. *Journal of Antimicrobial Chemotherapy* 40(5), 622-630.
- Tombelli, S., Minunni, M., Santucci, A., Spiriti, M.M., Mascini, M., 2006. *Talanta* 68(3), 806-812.
- Uttley, A.H.C., Woodford, N., Johnson, A.P., Cookson, B., George, R.C., Wilcox, M., Spencer, R., Weeks, G., Frieden, T., Munsiff, S., Low, D., Kreiswirth, B., Manso, E., De Sio, G., Biavasco, F., Varaldo, P., Sambo, G., Maffei, C., 1993. *The Lancet* 342(8871), 615-617.
- van Hal, S.J., Stark, D., Lockwood, B., Marriott, D., Harkness, J., 2007. *Journal of Clinical Microbiology* 45(8), 2486-2490.
- Verpoorte, E., De Rooij, N.F., 2003. *Proceedings of the Ieee* 91(6), 930-953.
- Volpe, G., Compagnone, D., Draisci, R., Palleschi, G., 1998. *Analyst* 123(6), 1303-1307.
- Walsh, K., Norville, J., Tai, Y.C., 2001. Photoresist as a sacrificial layer by dissolution in acetone. 14th IEEE International Conference on Micro Electro Mechanical Systems, Technical Digest, pp. 114-117.
- Wang, C.H., Lien, K.Y., Wu, J.J., Lee, G.B., 2011a. *Lab on a Chip* 11(8), 1521-1531.
- Wang, J., 2006. *Analytical Electrochemistry*. Wiley-VCH.
- Wang, S., Peng, T., Yang, C.F., 2003. *Journal of Biochemical and Biophysical Methods* 55(3), 191-204.
- Wang, Z., Zhang, J., Chen, P., Zhou, X., Yang, Y., Wu, S., Niu, L., Han, Y., Wang, L., Boey, F., Zhang, Q., Liedberg, B., Zhang, H., 2011b. *Biosensors and Bioelectronics* 26(9), 3881-3886.
- Wernersson, R., 2005. *Nucleic Acids Research* 33, W567-W569.
- Wernersson, R., Juncker, A.S., Nielsen, H.B., 2007. *Nature Protocols* 2(11), 2677-2691.
- WHO, 2012. WHO/Europe | Antimicrobial resistance - Frequently asked questions.
- Wilke, C.R., Chang, P., 1955. *AIChE Journal* 1(2), 264-270.
- Williams, K.R., Gupta, K., Wasilik, M., 2003. *J. Microelectromech. Syst.* 12(6), 761-778.
- Williams, L., 2007. Determination of Hansen Solubility Parameter Values for Carbon Dioxide. *Hansen Solubility Parameters: A User's Handbook* pp. 177-201, 2nd ed. Taylor & Francis Group, LLC, Florida.
- Woodford, N., Livermore, D.M., 2009. *Journal of Infection* 59, Supplement 1(0), S4-S16.
- Wright, D., Rajalingam, B., Selvarasah, S., Dokmeci, M.R., Khademhosseini, A., 2007. *Lab on a Chip* 7(10), 1272-1279.
- Yang, Y.C., Xia, Y., Huang, W., Zheng, J.F., Li, Z.L., 2012. *Journal of Solid State Electrochemistry* 16(4), 1733-1739.
- Yildirim, E., Arikan, M.A.S., Kulah, H., 2012. *Sensors and Actuators a-Physical* 181, 81-86.
- Yildirim, E., Kulah, H., 2011. *Journal of Micromechanics and Microengineering* 21(10), 105009.
- Yoon, Y.K., Sim, H.S., Kim, J.Y., Park, D.W., Sohn, J.W., Roh, K.H., Lee, S.E., Kim, M.J., 2009. *Yonsei Medical Journal* 50(5), 637-643.
- Yue, H., Mason, A., Greiner, A.J., Ofoli, R.Y., Worden, R.M., 2006. Post-CMOS Compatible Microfabrication of a Multi-Analyte Bioelectrochemical Sensor Array Microsystem. *Sensors*, 2006. 5th IEEE Conference on, pp. 612-615.
- Zara, J.M., Smith, S.W., 2002. *Sensors and Actuators a-Physical* 102(1-2), 176-184.
- Zhang, Y.C., Kim, H.H., Mano, N., Dequaire, M., Heller, A., 2002. *Analytical and Bioanalytical Chemistry* 374(6), 1050-1055.
- Zhuang, X., Nikoozadeh, A., Beasley, M.A., Yaralioglu, G.G., Khuri-Yakub, B.T., Pruitt, B.L., 2007. *Journal of Micromechanics and Microengineering* 17(5), 994-1001.
- Zuker, M., Mathews, D.H., Turner, D.H., 1999. *Rna Biochemistry and Biotechnology* 70, 11-43.

APPENDIX A

SIMULATION CODE

The simulation code prepared in MATLAB is given as follows:

```
function varargout = CvsEinDPV(varargin)
% CVSEINDPV MATLAB code for CvsEinDPV.fig
%   CVSEINDPV, by itself, creates a new CVSEINDPV or raises the existing
%   singleton*.
%
%   H = CVSEINDPV returns the handle to a new CVSEINDPV or the handle to
%   the existing singleton*.
%
%   CVSEINDPV('CALLBACK',hObject,eventData,handles,...) calls the local
%   function named CALLBACK in CVSEINDPV.M with the given input arguments.
%
%   CVSEINDPV('Property','Value',...) creates a new CVSEINDPV or raises the
%   existing singleton*. Starting from the left, property value pairs are
%   applied to the GUI before CvsEinDPV_OpeningFcn gets called. An
%   unrecognized property name or invalid value makes property application
%   stop. All inputs are passed to CvsEinDPV_OpeningFcn via varargin.
%
%   *See GUI Options on GUIDE's Tools menu. Choose "GUI allows only one
%   instance to run (singleton)".
%
% See also: GUIDE, GUIDATA, GUIHANDLES

% Edit the above text to modify the response to help CvsEinDPV

% Last Modified by GUIDE v2.5 31-May-2011 15:46:52

% Begin initialization code - DO NOT EDIT
gui_Singleton = 1;
gui_State = struct('gui_Name',    mfilename, ...
                  'gui_Singleton', gui_Singleton, ...
                  'gui_OpeningFcn', @CvsEinDPV_OpeningFcn, ...
                  'gui_OutputFcn', @CvsEinDPV_OutputFcn, ...
                  'gui_LayoutFcn', [] , ...
                  'gui_Callback', []);
if nargin && ischar(varargin{1})
    gui_State.gui_Callback = str2func(varargin{1});
end

if nargout
    [varargout{1:nargout}] = gui_mainfcn(gui_State, varargin(Medicine));
else
    gui_mainfcn(gui_State, varargin(Medicine));
end
% End initialization code - DO NOT EDIT

% --- Executes just before CvsEinDPV is made visible.
function CvsEinDPV_OpeningFcn(hObject, eventdata, handles, varargin)
```

```

% This function has no output args, see OutputFcn.
% hObject handle to figure
% eventdata reserved - to be defined in a future version of MATLAB
% handles structure with handles and user data (see GUIDATA)
% varargin command line arguments to CvsEinDPV (see VARARGIN)

% Choose default command line output for CvsEinDPV
handles.output = hObject;

% Update handles structure
set(hObject,'toolbar','figure');
guidata(hObject, handles);

% UIWAIT makes CvsEinDPV wait for user response (see UIRESUME)
% uiwait(handles.figure1);

% --- Outputs from this function are returned to the command line.
function varargout = CvsEinDPV_OutputFcn(hObject, eventdata, handles)
% varargout cell array for returning output args (see VARARGOUT);
% hObject handle to figure
% eventdata reserved - to be defined in a future version of MATLAB
% handles structure with handles and user data (see GUIDATA)

% Get default command line output from handles structure
varargout{1} = handles.output;

function NE_Callback(hObject, eventdata, handles)
% hObject handle to NE (see GCBO)
% eventdata reserved - to be defined in a future version of MATLAB
% handles structure with handles and user data (see GUIDATA)

% Hints: get(hObject,'String') returns contents of NE as text
% str2double(get(hObject,'String')) returns contents of NE as a double

%store the contents of NE as a string. if the string
%is not a number then input will be empty
input = str2num(get(hObject,'String'));

%checks to see if input is empty. if so, default NE to zero
if (isempty(input))
    set(hObject,'String','0')
end
guidata(hObject, handles);

% --- Executes during object creation, after setting all properties.
function NE_CreateFcn(hObject, eventdata, handles)
% hObject handle to NE (see GCBO)
% eventdata reserved - to be defined in a future version of MATLAB
% handles empty - handles not created until after all CreateFcns called

% Hint: edit controls usually have a white background on Windows.
% See ISPC and COMPUTER.
if ispc && isequal(get(hObject,'BackgroundColor'), get(0,'defaultUicontrolBackgroundColor'))
    set(hObject,'BackgroundColor','white');
end

function F_Callback(hObject, eventdata, handles)
% hObject handle to F (see GCBO)
% eventdata reserved - to be defined in a future version of MATLAB

```

```

% handles  structure with handles and user data (see GUIDATA)

% Hints: get(hObject,'String') returns contents of F as text
%   str2double(get(hObject,'String')) returns contents of F as a double

%Store the contents of F as a string. if the string
%is not a number then input will be empty
input = str2num(get(hObject,'String'));

%checks to see if input is empty. if so, default F to zero
if (isempty(input))
    set(hObject,'String','0')
end
guidata(hObject, handles);

% --- Executes during object creation, after setting all properties.
function F_CreateFcn(hObject, eventdata, handles)
% hObject  handle to F (see GCBO)
% eventdata reserved - to be defined in a future version of MATLAB
% handles  empty - handles not created until after all CreateFcns called

% Hint: edit controls usually have a white background on Windows.
%   See ISPC and COMPUTER.
if ispc && isequal(get(hObject,'BackgroundColor'), get(0,'defaultUicontrolBackgroundColor'))
    set(hObject,'BackgroundColor','white');
end

function v_Callback(hObject, eventdata, handles)
% hObject  handle to v (see GCBO)
% eventdata reserved - to be defined in a future version of MATLAB
% handles  structure with handles and user data (see GUIDATA)

% Hints: get(hObject,'String') returns contents of v as text
%   str2double(get(hObject,'String')) returns contents of v as a double

%store the contents of v as a string. if the string
%is not a number then input will be empty
input = str2num(get(hObject,'String'));

%checks to see if input is empty. if so, default v to zero
if (isempty(input))
    set(hObject,'String','0')
end
guidata(hObject, handles);

% --- Executes during object creation, after setting all properties.
function v_CreateFcn(hObject, eventdata, handles)
% hObject  handle to v (see GCBO)
% eventdata reserved - to be defined in a future version of MATLAB
% handles  empty - handles not created until after all CreateFcns called

% Hint: edit controls usually have a white background on Windows.
%   See ISPC and COMPUTER.
if ispc && isequal(get(hObject,'BackgroundColor'), get(0,'defaultUicontrolBackgroundColor'))
    set(hObject,'BackgroundColor','white');
end

function R_Callback(hObject, eventdata, handles)
% hObject  handle to R (see GCBO)

```

```

% eventdata reserved - to be defined in a future version of MATLAB
% handles structure with handles and user data (see GUIDATA)

% Hints: get(hObject,'String') returns contents of R as text
% str2double(get(hObject,'String')) returns contents of R as a double

%store the contents of R as a string. if the string
%is not a number then input will be empty
input = str2num(get(hObject,'String'));

%checks to see if input is empty. if so, default R to zero
if (isempty(input))
    set(hObject,'String','0')
end
guidata(hObject, handles);

% --- Executes during object creation, after setting all properties.
function R_CreateFcn(hObject, eventdata, handles)
% hObject handle to R (see GCBO)
% eventdata reserved - to be defined in a future version of MATLAB
% handles empty - handles not created until after all CreateFcns called

% Hint: edit controls usually have a white background on Windows.
% See ISPC and COMPUTER.
if ispc && isequal(get(hObject,'BackgroundColor'), get(0,'defaultUicontrolBackgroundColor'))
    set(hObject,'BackgroundColor','white');
end

function Temp_Callback(hObject, eventdata, handles)
% hObject handle to Temp (see GCBO)
% eventdata reserved - to be defined in a future version of MATLAB
% handles structure with handles and user data (see GUIDATA)

% Hints: get(hObject,'String') returns contents of Temp as text
% str2double(get(hObject,'String')) returns contents of Temp as a double

%store the contents of Temp as a string. if the string
%is not a number then input will be empty
input = str2num(get(hObject,'String'));

%checks to see if input is empty. if so, default Temp to zero
if (isempty(input))
    set(hObject,'String','0')
end
guidata(hObject, handles);

% --- Executes during object creation, after setting all properties.
function Temp_CreateFcn(hObject, eventdata, handles)
% hObject handle to Temp (see GCBO)
% eventdata reserved - to be defined in a future version of MATLAB
% handles empty - handles not created until after all CreateFcns called

% Hint: edit controls usually have a white background on Windows.
% See ISPC and COMPUTER.
if ispc && isequal(get(hObject,'BackgroundColor'), get(0,'defaultUicontrolBackgroundColor'))
    set(hObject,'BackgroundColor','white');
end

function Alpha_Callback(hObject, eventdata, handles)

```

```

% hObject handle to Alpha (see GCBO)
% eventdata reserved - to be defined in a future version of MATLAB
% handles structure with handles and user data (see GUIDATA)

% Hints: get(hObject,'String') returns contents of Alpha as text
% str2double(get(hObject,'String')) returns contents of Alpha as a double

%Store the contents of Alpha as a string. if the string
%is not a number then input will be empty
input = str2num(get(hObject,'String'));

%checks to see if input is empty. if so, default Alpha to zero
if (isempty(input))
    set(hObject,'String','0')
end
guidata(hObject, handles);

% --- Executes during object creation, after setting all properties.
function Alpha_CreateFcn(hObject, eventdata, handles)
% hObject handle to Alpha (see GCBO)
% eventdata reserved - to be defined in a future version of MATLAB
% handles empty - handles not created until after all CreateFcns called

% Hint: edit controls usually have a white background on Windows.
% See ISPC and COMPUTER.
if ispc && isequal(get(hObject,'BackgroundColor'), get(0,'defaultUicontrolBackgroundColor'))
    set(hObject,'BackgroundColor','white');
end

function D_Callback(hObject, eventdata, handles)
% hObject handle to D (see GCBO)
% eventdata reserved - to be defined in a future version of MATLAB
% handles structure with handles and user data (see GUIDATA)

% Hints: get(hObject,'String') returns contents of D as text
% str2double(get(hObject,'String')) returns contents of D as a double

%Store the contents of D as a string. if the string
%is not a number then input will be empty
input = str2num(get(hObject,'String'));

%checks to see if input is empty. if so, default D to zero
if (isempty(input))
    set(hObject,'String','0')
end
guidata(hObject, handles);

% --- Executes during object creation, after setting all properties.
function D_CreateFcn(hObject, eventdata, handles)
% hObject handle to D (see GCBO)
% eventdata reserved - to be defined in a future version of MATLAB
% handles empty - handles not created until after all CreateFcns called

% Hint: edit controls usually have a white background on Windows.
% See ISPC and COMPUTER.
if ispc && isequal(get(hObject,'BackgroundColor'), get(0,'defaultUicontrolBackgroundColor'))
    set(hObject,'BackgroundColor','white');
end

```

```

function ko_Callback(hObject, eventdata, handles)
% hObject   handle to ko (see GCBO)
% eventdata reserved - to be defined in a future version of MATLAB
% handles   structure with handles and user data (see GUIDATA)

% Hints: get(hObject,'String') returns contents of ko as text
%       str2double(get(hObject,'String')) returns contents of ko as a double

%store the contents of ko as a string. if the string
%is not a number then input will be empty
input = str2num(get(hObject,'String'));

%checks to see if input is empty. if so, default ko to zero
if (isempty(input))
    set(hObject,'String','0')
end
guidata(hObject, handles);

% --- Executes during object creation, after setting all properties.
function ko_CreateFcn(hObject, eventdata, handles)
% hObject   handle to ko (see GCBO)
% eventdata reserved - to be defined in a future version of MATLAB
% handles   empty - handles not created until after all CreateFcns called

% Hint: edit controls usually have a white background on Windows.
%       See ISPC and COMPUTER.
if ispc && isequal(get(hObject,'BackgroundColor'), get(0,'defaultUicontrolBackgroundColor'))
    set(hObject,'BackgroundColor','white');
end

function Delta_Callback(hObject, eventdata, handles)
% hObject   handle to Delta (see GCBO)
% eventdata reserved - to be defined in a future version of MATLAB
% handles   structure with handles and user data (see GUIDATA)

% Hints: get(hObject,'String') returns contents of Delta as text
%       str2double(get(hObject,'String')) returns contents of Delta as a double

%Store the contents of Delta as a string. if the string
%is not a number then input will be empty
input = str2num(get(hObject,'String'));

%checks to see if input is empty. if so, default Delta to zero
if (isempty(input))
    set(hObject,'String','0')
end
guidata(hObject, handles);

% --- Executes during object creation, after setting all properties.
function Delta_CreateFcn(hObject, eventdata, handles)
% hObject   handle to Delta (see GCBO)
% eventdata reserved - to be defined in a future version of MATLAB
% handles   empty - handles not created until after all CreateFcns called

% Hint: edit controls usually have a white background on Windows.
%       See ISPC and COMPUTER.
if ispc && isequal(get(hObject,'BackgroundColor'), get(0,'defaultUicontrolBackgroundColor'))
    set(hObject,'BackgroundColor','white');
end

```

```

function Eo_Callback(hObject, eventdata, handles)
% hObject handle to Eo (see GCBO)
% eventdata reserved - to be defined in a future version of MATLAB
% handles structure with handles and user data (see GUIDATA)

% Hints: get(hObject,'String') returns contents of Eo as text
% str2double(get(hObject,'String')) returns contents of Eo as a double

%store the contents of Eo as a string. if the string
%is not a number then input will be empty
input = str2num(get(hObject,'String'));

%checks to see if input is empty. if so, default Eo to zero
if (isempty(input))
    set(hObject,'String','0')
end
guidata(hObject, handles);

% --- Executes during object creation, after setting all properties.
function Eo_CreateFcn(hObject, eventdata, handles)
% hObject handle to Eo (see GCBO)
% eventdata reserved - to be defined in a future version of MATLAB
% handles empty - handles not created until after all CreateFcns called

% Hint: edit controls usually have a white background on Windows.
% See ISPC and COMPUTER.
if ispc && isequal(get(hObject,'BackgroundColor'), get(0,'defaultUicontrolBackgroundColor'))
    set(hObject,'BackgroundColor','white');
end

function Ei_Callback(hObject, eventdata, handles)
% hObject handle to Ei (see GCBO)
% eventdata reserved - to be defined in a future version of MATLAB
% handles structure with handles and user data (see GUIDATA)

% Hints: get(hObject,'String') returns contents of Ei as text
% str2double(get(hObject,'String')) returns contents of Ei as a double

%store the contents of Ei as a string. if the string
%is not a number then input will be empty
input = str2num(get(hObject,'String'));

%checks to see if input is empty. if so, default Ei to zero
if (isempty(input))
    set(hObject,'String','0')
end
guidata(hObject, handles);

% --- Executes during object creation, after setting all properties.
function Ei_CreateFcn(hObject, eventdata, handles)
% hObject handle to Ei (see GCBO)
% eventdata reserved - to be defined in a future version of MATLAB
% handles empty - handles not created until after all CreateFcns called

% Hint: edit controls usually have a white background on Windows.
% See ISPC and COMPUTER.
if ispc && isequal(get(hObject,'BackgroundColor'), get(0,'defaultUicontrolBackgroundColor'))
    set(hObject,'BackgroundColor','white');
end

```

```

end

function Ef_Callback(hObject, eventdata, handles)
% hObject   handle to Ef (see GCBO)
% eventdata reserved - to be defined in a future version of MATLAB
% handles   structure with handles and user data (see GUIDATA)

% Hints: get(hObject,'String') returns contents of Ef as text
%   str2double(get(hObject,'String')) returns contents of Ef as a double

%Store the contents of Ef as a string. if the string
%is not a number then input will be empty
input = str2num(get(hObject,'String'));

%checks to see if input is empty. if so, default Ef to zero
if (isempty(input))
    set(hObject,'String','0')
end
guidata(hObject, handles);

% --- Executes during object creation, after setting all properties.
function Ef_CreateFcn(hObject, eventdata, handles)
% hObject   handle to Ef (see GCBO)
% eventdata reserved - to be defined in a future version of MATLAB
% handles   empty - handles not created until after all CreateFcns called

% Hint: edit controls usually have a white background on Windows.
%   See ISPC and COMPUTER.
if ispc && isequal(get(hObject,'BackgroundColor'), get(0,'defaultUicontrolBackgroundColor'))
    set(hObject,'BackgroundColor','white');
end

function tfinal_Callback(hObject, eventdata, handles)
% hObject   handle to tfinal (see GCBO)
% eventdata reserved - to be defined in a future version of MATLAB
% handles   structure with handles and user data (see GUIDATA)

% Hints: get(hObject,'String') returns contents of tfinal as text
%   str2double(get(hObject,'String')) returns contents of tfinal as a double

%store the contents of tfinal as a string. if the string
%is not a number then input will be empty
input = str2num(get(hObject,'String'));

%checks to see if input is empty. if so, default tfinal to zero
if (isempty(input))
    set(hObject,'String','0')
end
guidata(hObject, handles);

% --- Executes during object creation, after setting all properties.
function tfinal_CreateFcn(hObject, eventdata, handles)
% hObject   handle to tfinal (see GCBO)
% eventdata reserved - to be defined in a future version of MATLAB
% handles   empty - handles not created until after all CreateFcns called

% Hint: edit controls usually have a white background on Windows.
%   See ISPC and COMPUTER.
if ispc && isequal(get(hObject,'BackgroundColor'), get(0,'defaultUicontrolBackgroundColor'))

```



```

    set(hObject,'BackgroundColor','white');
end

function D_E_Callback(hObject, eventdata, handles)
% hObject    handle to D_E (see GCBO)
% eventdata reserved - to be defined in a future version of MATLAB
% handles    structure with handles and user data (see GUIDATA)

% Hints: get(hObject,'String') returns contents of D_E as text
%    str2double(get(hObject,'String')) returns contents of D_E as a double

%Store the contents of D_E as a string. if the string
%is not a number then input will be empty
input = str2num(get(hObject,'String'));

%checks to see if input is empty. if so, default D_E to zero
if (isempty(input))
    set(hObject,'String','0')
end
guidata(hObject, handles);

% --- Executes during object creation, after setting all properties.
function D_E_CreateFcn(hObject, eventdata, handles)
% hObject    handle to D_E (see GCBO)
% eventdata reserved - to be defined in a future version of MATLAB
% handles    empty - handles not created until after all CreateFcns called

% Hint: edit controls usually have a white background on Windows.
%    See ISPC and COMPUTER.
if ispc && isequal(get(hObject,'BackgroundColor'), get(0,'defaultUicontrolBackgroundColor'))
    set(hObject,'BackgroundColor','white');
end

function Area_Callback(hObject, eventdata, handles)
% hObject    handle to Area (see GCBO)
% eventdata reserved - to be defined in a future version of MATLAB
% handles    structure with handles and user data (see GUIDATA)

% Hints: get(hObject,'String') returns contents of Area as text
%    str2double(get(hObject,'String')) returns contents of Area as a double

%Store the contents of Area as a string. if the string
%is not a number then input will be empty
input = str2num(get(hObject,'String'));

%checks to see if input is empty. if so, default Area to zero
if (isempty(input))
    set(hObject,'String','0')
end
guidata(hObject, handles);

% --- Executes during object creation, after setting all properties.
function Area_CreateFcn(hObject, eventdata, handles)
% hObject    handle to Area (see GCBO)
% eventdata reserved - to be defined in a future version of MATLAB
% handles    empty - handles not created until after all CreateFcns called

% Hint: edit controls usually have a white background on Windows.
%    See ISPC and COMPUTER.

```

```

if ispc && isequal(get(hObject,'BackgroundColor'), get(0,'defaultUicontrolBackgroundColor'))
    set(hObject,'BackgroundColor','white');
end

```

```

function Conc_Callback(hObject, eventdata, handles)
% hObject    handle to Conc (see GCBO)
% eventdata  reserved - to be defined in a future version of MATLAB
% handles    structure with handles and user data (see GUIDATA)

% Hints: get(hObject,'String') returns contents of Conc as text
%        str2double(get(hObject,'String')) returns contents of Conc as a double

```

```

%Store the contents of Conc as a string. if the string
%is not a number then input will be empty
input = str2num(get(hObject,'String'));

```

```

%checks to see if input is empty. if so, default Conc to zero
if (isempty(input))
    set(hObject,'String','0')
end
guidata(hObject, handles);

```

```

% --- Executes during object creation, after setting all properties.
function Conc_CreateFcn(hObject, eventdata, handles)
% hObject    handle to Conc (see GCBO)
% eventdata  reserved - to be defined in a future version of MATLAB
% handles    empty - handles not created until after all CreateFcns called

```

```

% Hint: edit controls usually have a white background on Windows.
%       See ISPC and COMPUTER.
if ispc && isequal(get(hObject,'BackgroundColor'), get(0,'defaultUicontrolBackgroundColor'))
    set(hObject,'BackgroundColor','white');
end

```

```

% --- Executes on button press in Plot.
function Plot_Callback(hObject, eventdata, handles)
% hObject    handle to Plot (see GCBO)
% eventdata  reserved - to be defined in a future version of MATLAB
% handles    structure with handles and user data (see GUIDATA)

```

```

%selects axes1 as the current axes, so that
%Matlab knows where to plot the data
axes(handles.axes1)
NE = get(handles.NE,'String');
F = get(handles.F,'String');
v = get(handles.v,'String');
R = get(handles.R,'String');
Temp = get(handles.Temp,'String');
Alpha = get(handles.Alpha,'String');
F = get(handles.F,'String');
D = get(handles.D,'String');
ko = get(handles.ko,'String');
Delta = get(handles.Delta,'String')
Eo = get(handles.Eo,'String');
Ei = get(handles.Ei,'String');
Ef = get(handles.Ef,'String');
tfinal = get(handles.tfinal,'String');
D_E = get(handles.D_E,'String');
Area = get(handles.Area,'String');

```

```

Conc = get(handles.Conc,'String');
% These parameters are variables of Strings type, and need to be converted
% to variables of Number type.
tinitial = 0; % Initial time [sec]
Tao = str2num(Delta)*20 % [sec]
N = round ((str2num(tfinal)/str2num(Delta))/21);
NT = N*21;%(tfinal-tinitial)/(Delta); % increment sayýsý
f = zeros(NT,1); % f = zeros (1,k)
Xi = zeros(NT,1);
t = zeros(NT,1);

% Initialization
w = (str2num(NE)*str2num(F)*str2num(v)/(str2num(R)*str2num(Temp)))*str2num(Delta);
% dimensionless
r = Tao/str2num(Delta); % dimensionless
D_Xi = str2num(NE)*str2num(F)*str2num(D_E)/(str2num(R)*str2num(Temp));
% dimensionless
Lambda = str2num(ko)*(str2num(Delta)/str2num(D))^(1/2); %
dimensionless
id =
str2num(NE)*str2num(F)*str2num(Area)*str2num(Conc)*(str2num(D)/(pi*str2num(Delta)))^(1/2);
% [A]
h = (str2num(tfinal)/str2num(Delta))/NT; %
dimensionless

% Weight parameters of Volterra Equation of second kind for the solution
% with product integral method.
W = zeros(NT+1,NT+1);
Current = zeros(NT,1);
Delta_Current = zeros(NT,1);
E = str2num(Ei);
A = zeros(NT,1);
B = zeros(NT,1);
K = zeros(NT,1);
for m =1:N;
    for k = ((m-1)*(r+1)+1):m*(r+1);
        t(k,1) = (k-1)*str2num(Delta) + tinitial;
        % DPV wave
form=====
        if ((t(k,1)>((m-1)*(Tao+str2num(Delta)) + Tao)&& t(k,1)<(m*(Tao+str2num(Delta))))
            Xi(k,1) = (str2num(NE)*str2num(F)*(str2num(Ei)-
str2num(Eo))/(str2num(R)*str2num(Temp)))+(m-1)*w*(1+r)+ D_Xi;
            E(k,1) = str2num(Ei)+(m-1)*str2num(v)*(Tao+ str2num(Delta))+str2num(D_E);
        else
            Xi(k,1) = (str2num(NE)*str2num(F)*(str2num(Ei)-
str2num(Eo))/(str2num(R)*str2num(Temp)))+(m-1)*w*(1+r);
            E(k,1)= str2num(Ei)+(m-1)*str2num(v)*(Tao+str2num(Delta));
        end
        % 3 farklý w deđerinin hesaplanmasý=====
        for j=0:k;
            if (j==0)
                W(k,1)= ((2*h^(1/2))/3)* (3*k^(1/2)+ 2*((k-1)^(3/2)-(k)^(3/2)));
            elseif (j==k)
                W(k,k+1)= ((4*h^(1/2))/3);
            else
                W(k,j+1)= ((4*h^(1/2))/3)* ((k-j-1)^(3/2)+(k-j+1)^(3/2)-2*(k-j)^(3/2));
            end
        end
        % K hesaplama aþamasý=====

```

```

% A hesaplama aşaması
A(k,1) = Lambda * ((pi)^(1/2))*exp(str2num(Alpha)*Xi(k,1));
% B hesaplama aşaması
B(k,1) = (pi^(-1))*(1+exp(-Xi(k,1)));
K(k,1) = 1 + A(k,1)*B(k,1)* W(k,k+1);
% C sum hesaplama aşaması=====
C=0;
f(1,1) = Lambda * (pi)^(1/2)* exp (str2num(Alpha)*str2num(NE)*str2num(F)*(str2num(Ei)-
str2num(Eo))/(str2num(R)*str2num(Temp)));
for j=0:k-1;
    C = W(k,j+1)*f(j+1,1)+ C;
end
% fk hesaplama aşaması=====
f(k,1) = (A(k,1)*(1-B(k,1)*C))/(1+A(k,1)*B(k,1)*W(k,k+1));
Current(k,1) = f(k,1)*id;
if k>=2
    Delta_Current(k,1)=Current(k,1)-Current(k-1,1);
end
end
end

%plots the x and y data
plot(E,Current);
%adds a title, x-axis description, and y-axis description
title('Current vs. Potential');
xlabel('E (V)');
ylabel('I (A)');
guidata(hObject, handles); %updates the handles

% --- Executes on button press in Clear.
function Clear_Callback(hObject, eventdata, handles)
% hObject   handle to Clear (see GCBO)
% eventdata reserved - to be defined in a future version of MATLAB
% handles   structure with handles and user data (see GUIDATA)

%these two lines of code clears both axes
cla(handles.axes1,'reset')
guidata(hObject, handles); %updates the handles

```

APPENDIX B

PROCESS FLOW

The steps for the fabrication of the sensor are given in Table B.1.

Table B.1. Details of the steps for the fabrication of the sensor.

1st generation		2nd generation		3rd generation	
1 Silicon wafer		1 Silicon wafer		1 Silicon wafer	
2 Si₃N₄ coating (LPCVD) :		2 Si₃N₄ coating (LPCVD) :		2 Si₃N₄ coating (LPCVD) :	
550 mTorr, 1960 sccm N ₂ , 40sccm Silane (SiH ₄), 20 sccm NH ₃		550 mTorr, 1960 sccm N ₂ , 40sccm Silane (SiH ₄), 20 sccm NH ₃		550 mTorr, 1960 sccm N ₂ , 40sccm Silane (SiH ₄), 20 sccm NH ₃	
60 W, Low Frequency (380 kHz), 3 min 50 sec		60 W, Low Frequency (380 kHz), 3 min 50 sec		60 W, Low Frequency (380 kHz), 3 min 50 sec	
300 °C = Substrate Temperature		300 °C = Substrate Temperature		300 °C = Substrate Temperature	
250 °C = Gas Inlet Temperature		250 °C = Gas Inlet Temperature		250 °C = Gas Inlet Temperature	
3 Ti sputtering as adhesion layer ~50 nm (AJA)		3 Ti sputtering as adhesion layer ~50 nm (BESTEC)		3 Ti sputtering as adhesion layer ~50 nm (BESTEC)	
Ti 300 W 300 sec ~25 nm 3 mTorr Ar (273 V, 1096 mA) x2		Ti 300 W 120 sec 215 sec 2.5 sccm Ar 135 mm distance		Ti 300 W 120 sec 215 sec 2.5 sccm, 135 mm distance	
4 Pt sputtering ~ 200 nm (AJA)		4 Pt sputtering ~ 200 nm (AJA)		4 Pt sputtering ~ 200 nm (AJA)	
Pt 75 W 3 mTorr Ar 1600 sec (350 V, 214 mA) x2		Pt 75 W 3 mTorr Ar 1600 sec (350 V, 214 mA) x2		Pt 75 W 3 mTorr Ar 1600 sec (350 V, 214 mA) x2	
5 Au sputtering ~ 180 nm (AJA)		5 Au sputtering ~ 180nm (BESTEC)		5 Au sputtering ~ 180nm (BESTEC)	
Au 350 W 3 mTorr Ar 170 sec (413 V, 861 mA) x2		Au 300W 120sec 190 sec 6.2sccm Ar 170 mm distance		Au 300W 120sec 190 sec 6.2sccm Ar 170 mm distance	
6 Dehydration at oven at 110 °C for 20 min		6 Dehydration at oven at 110 °C for 20 min		6 Dehydration at oven at 110 °C for 20 min	
Desiccator for 5 min.		Desiccator for 5 min.		Desiccator for 5 min.	
7 Lithography for Au etch ~1.3 μm	Mask 2	7 Lithography for Au etch ~1.3 um	Mask 2	7 Lithography for Au etch ~1.3 um	Mask 2
HMDS coating - 500 rpm 7 sec + 4000rpm 30sec.		HMDS coating - 500 rpm 7 sec + 4000rpm 30sec.		HMDS coating - 500 rpm 7 sec + 4000rpm 30sec.	
S1813 500 rpm 7sec + @ 4000 rpm for 30s, soft bake 115 oC for 3min.		S1813 500 rpm 7sec + @ 4000 rpm for 30s, soft bake 115 oC for 3min.		S1813 500 rpm 7sec + @ 4000 rpm for 30s, soft bake 115 oC for 3min.	
Expose UV for 4 sec (150 mJ/12. 5mW) vakum + hard contact		Expose UV for 4 sec (150 mJ/12. 5mW) vakum + hard contact		Expose UV for 4 sec (150 mJ/12. 5mW) vakum + hard contact	
Develop in MF 319 for 40 sec.		Develop in MF 319 for 40 sec.		Develop in MF 319 for 40 sec.	
DI water rinse 1.5min +1.5min.		DI water rinse 1.5min +1.5min.		DI water rinse 1.5min +1.5min.	
Dry by N ₂ .		Dry by N ₂ .		Dry by N ₂ .	
Inspection		Inspection.		Inspection.	
Hard bake 120 °C for 40 min		Hard bake 120 °C for 40 min		Hard bake 120 °C for 40 min	
Desiccator for 5 min.		Desiccator for 5 min.		Desiccator for 5 min.	
Inspection.		Inspection.		Inspection.	
Mask cleaning.		Mask cleaning.		Mask cleaning.	
8 Au etch		8 Au etch		8 Au etch	
Au etchant - 40 sec		Au etchant - 40 sec		Au etchant - 40 sec	
DI water rinse 3 cycles		DI water rinse 3 cycles		DI water rinse 3 cycles	
Dry by N ₂ .		Dry by N ₂ .		Dry by N ₂ .	
Inspection.		Inspection.		Inspection.	
9 Strip photoresist.		9 Strip photoresist.		9 Strip photoresist.	
Equipment: NANOPLAS-2 Recipe: PRstrip15 Power: 520W T Chamber: 125C T Substrate: 135C MFC O2: 30 sccm MFC N2: 5 sccm SP Pressure: 0.2 Torr		PRS 1000		Equipment: NANOPLAS-2 Recipe: PRstrip15 Power: 520W T Chamber: 125C T Substrate: 135C MFC O2: 30 sccm MFC N2: 5 sccm SP Pressure: 0.2 Torr	

Table B.1. Details of the steps for the fabrication of the sensor (Continued).

10 Lithography for Pt etch ~1.3 μm	Mask 7	10 Lithography for Pt etch ~1.3 μm	Mask 7	10 Lithography for Pt etch ~1.3 μm	Mask 7
HMDS coating - 500 rpm 7 sec + 4000rpm 30sec.		HMDS coating - 500 rpm 7 sec + 4000rpm 30sec.		HMDS coating - 500 rpm 7 sec + 4000rpm 30sec.	
S1813 500 rpm 7sec + @ 4000 rpm for 30s, soft bake 115 oC for 3min.		S1813 500 rpm 7sec + @ 4000 rpm for 30s, soft bake 115 oC for 3min.		S1813 500 rpm 7sec + @ 4000 rpm for 30s, soft bake 115 oC for 3min.	
Expose UV for 4 sec (150 mJ/12. 5mW) vakum + hard contact		Expose UV for 4 sec (150 mJ/12. 5mW) vakum + hard contact		Expose UV for 4 sec (150 mJ/12. 5mW) vakum + hard contact	
Develop in MF 319 for 40 sec.		Develop in MF 319 for 40 sec.		Develop in MF 319 for 40 sec.	
DI water rinse 1.5min +1.5min.		DI water rinse 1.5min +1.5min.		DI water rinse 1.5min +1.5min.	
Dry by N ₂ .		Dry by N ₂ .		Dry by N ₂ .	
Inspection		Inspection		Inspection.	
Hard bake 120 °C for 40 min		Hard bake 120 °C for 40 min		Hard bake 120 °C for 40 min	
Desiccator for 5 min.		Desiccator for 5 min.		Desiccator for 5 min.	
Inspection.		Inspection.		Inspection.	
Mask cleaning.		Mask cleaning.		Mask cleaning.	
11 Crystal bonding 4" to 6"		11 Crystal bonding 4" to 6"		11 Crystal bonding 4" to 6"	
12 Pt etch – Metal RIE		12 Pt etch – Metal RIE		12 Pt etch – Metal RIE	
5 sccm Ar + 15 sccm Cl ₂ (2 min + 1 min 04 sec)		5 sccm Ar + 15 sccm Cl ₂ (2 min + 1 min 04 sec)		5 sccm Ar + 15 sccm Cl ₂ (2 min + 1 min 04 sec)	
13 Removal of crystal bond		13 Removal of crystal bond		13 Removal of crystal bond	
14 Strip photoresist.		14 Strip photoresist.		14 Strip photoresist.	
Equipment: NANOPLAS-2 Recipe: PRstrip15 Power: 520W T Chamber: 125C T Substrate: 135C MFC O2: 30 sccm MFC N2: 5 sccm SP Pressure: 0.2 Torr		Equipment: NANOPLAS-2 Recipe: PRstrip15 Power: 520W T Chamber: 125C T Substrate: 135C MFC O2: 30 sccm MFC N2: 5 sccm SP Pressure: 0.2 Torr		Equipment: NANOPLAS-2 Recipe: PRstrip15 Power: 520W T Chamber: 125C T Substrate: 135C MFC O2: 30 sccm MFC N2: 5 sccm SP Pressure: 0.2 Torr	
15 Lithography for Ti etch ~1.3 μm	Mask 3	15 Lithography for Ti etch ~1.3 μm	Mask 3	15 Lithography for Ti etch ~1.3 μm	Mask 3
HMDS coating - 500 rpm 7 sec + 4000rpm 30sec.		HMDS coating - 500 rpm 7 sec + 4000rpm 30sec.		HMDS coating - 500 rpm 7 sec + 4000rpm 30sec.	
S1813 500 rpm 7sec + @ 4000 rpm for 30s, soft bake 115 oC for 3min.		S1813 500 rpm 7sec + @ 4000 rpm for 30s, soft bake 115 oC for 3min.		S1813 500 rpm 7sec + @ 4000 rpm for 30s, soft bake 115 oC for 3min.	
Expose UV for 4 sec (150 mJ/12. 5mW) vakum + hard contact		Expose UV for 4 sec (150 mJ/12. 5mW) vakum + hard contact		Expose UV for 4 sec (150 mJ/12. 5mW) vakum + hard contact	
Develop in MF 319 for 40 sec.		Develop in MF 319 for 40 sec.		Develop in MF 319 for 40 sec.	
DI water rinse 1.5min +1.5min.		DI water rinse 1.5min +1.5min.		DI water rinse 1.5min +1.5min.	
Dry by N ₂ .		Dry by N ₂ .		Dry by N ₂ .	
Inspection		Inspection		Inspection.	
Hard bake 120 °C for 40 min		Hard bake 120 °C for 40 min		Hard bake 120 °C for 40 min	
Desiccator for 5 min.		Desiccator for 5 min.		Desiccator for 5 min.	
Inspection.		Inspection.		Inspection.	
Mask cleaning.		Mask cleaning.		Mask cleaning.	
16 Crystal bonding 4" to 6"		16 Crystal bonding 4" to 6"		16 Crystal bonding 4" to 6"	
17 Ti etch – Metal RIE		17 Ti etch – Metal RIE		17 Ti etch – Metal RIE	
HBr 30 sccm , Ar 20 sccm (60 sec)		HBr 30 sccm , Ar 20 sccm (60 sec)		HBr 30 sccm , Ar 20 sccm (60 sec)	
18 Removal of crystal bond		18 Removal of crystal bond		18 Removal of crystal bond	
19 Strip photoresist.		19 Strip photoresist.		19 Strip photoresist.	
O ₂ plasma treatment		O ₂ plasma treatment		O ₂ plasma treatment	

Table B.1. Details of the steps for the fabrication of the sensor (Continued).

20 Ag sputtering (AJA)		20 Ag sputtering (AJA)		20 Parylene deposition	
Ag Gun1 300W 510sec 10mTorr		Ag Gun1 300W 510sec 10mTorr		Dimer: 3 gr	
21 AgCl formation		21 AgCl formation		Use silane	
Chloride içeren bir kimyasal (HCl vb.) ile yapılacak.		Chloride içeren bir kimyasal (HCl vb.) ile yapılacak.		Set Point: 15	
22 Lithography for Ag etch	Mask 1	22 Lithography for Ag etch	Mask 1	PLA_I: 10	
Primer (HMDS), 500 rpm 7sec + 3000 rpm 35 sec.		Primer (HMDS), 500 rpm 7sec + 3000 rpm 35 sec.		Meas: ~1.5 µm	
TI35E, 500 rpm 7sec +3000 rpm 35 sec		TI35E, 500 rpm 7sec +3000 rpm 35 sec		21 Lithography to etch parylene on electrode surfaces	Mask 3
Softbake 95 °C,2min, hotplate		Softbake 95 °C,2min, hotplate		Primer (HMDS), 500 rpm 7 sec + 3000rpm 35 sec.	
Align and expose 10 sec		Align and expose 10 sec		TI35ES 500 rpm 7sec + 3000 rpm 35 sec	
Post bake 120°C, 2min hotplate		Post bake 120°C, 2min hotplate		Softbake 95 °C, 2min, hotplate	
Flood Expose 45 sec		Flood Expose 45 sec		Align and expose 10 sec	
Develop, AZ 826 MIF (1.40 min + 1.40 min)		Develop, AZ 826 MIF (1.40 min + 1.40 min)		Post bake 120 °C, 2min hotplate	
DI water rinse 1.5 min + 1.5 min.		DI water rinse 1.5 min + 1.5 min.		Flood expose 45 sec	
Dry by N ₂		Dry by N ₂		Develop, AZ 826 MIF (1.40 min + 1.40 min)	
Inspection.		Inspection.		DI water rinse 1.5 min + 1.5min.	
Hard bake 110 °C for 10 min on hotplate		Hard bake 110 °C for 10 min on hotplate		Dry by N ₂	
Mask cleaning.		Mask cleaning.		Inspection.	
23 Ag etch		23 Ag etch		Hard bake 110 °C for 10 min on hotplate	
HNO ₃ :H ₂ O (1:1)		HNO ₃ :H ₂ O (1:1)		Mask cleaning.	
Mix the solution, dip for 5 sec.		Mix the solution, dip for 5 sec.		22 Parylene etching	
DI water rinse 3 cycles.		DI water rinse 3 cycles.		Etch parylene in RIE	
Dry by N ₂ .		Dry by N ₂ .		Inspection.	
Inspection.		Inspection.		23 Strip photoresist.	
24 Strip photoresist.		24 Strip photoresist.		Immerse into the acetone	
Immerse into the acetone		Immerse into the acetone		24 Ag sputtering (AJA)	
25 Channel Lithography	Mask 4	25 Channel Lithography	Mask 4	Ag Gun1 300W 510sec 10mTorr	
Primer (HMDS), 300 rpm 5 sec + 1000 rpm 60 sec		Primer (HMDS), 300 rpm 5 sec + 900 rpm 20 sec		25 AgCl formation (Optional)	
AZ 9260 300 rpm 5 sec + 1000 rpm 60 sec		AZ 9260 300 rpm 5 sec + 900 rpm 20 sec		Immerse into the Chloride containing solution	
Edge bead removal		Wait for 15 min.		26 Lithography for Ag etch	Mask 1
Softbake 110 °C for 140 sec.		Prebake 95 °C, 90 sec, hotplate		Primer (HMDS), 500 rpm 7sec + 3000 rpm 35 sec.	
Align and expose 45 sec.		Edge bead removal		TI35E, 500 rpm 7sec +3000 rpm 35 sec	
Develop AZ 826 MIF, 10min		Softbake start at room temperature, raise the temperature to 95 °C, 30 min at 95 °C.		Softbake 95 °C,2min, hotplate	
DI water rinse, 1.5min + 1.5 min		Rehydration (3 pipettes of DI water in blue box,1hrs)		Align and expose 10 sec	
Dry by N ₂		Align and expose 45 sec		Post bake 120°C, 2min hotplate	
Inspection.		Develop AZ 826 MIF, 10 min		Flood Expose 45 sec	
Hard bake 120 °C for 40min		DI water rinse, 1.5min + 1.5 min		Develop, AZ 826 MIF (1.40 min + 1.40 min)	
Desiccator for 5 min.		Inspection.		DI water rinse 1.5 min + 1.5 min.	
Inspection.		Mask cleaning.		Dry by N ₂	
Mask cleaning.				Inspection.	
26 Parylene deposition		26 Parylene deposition		Hard bake 110 °C for 10 min on hotplate	
Dimer: 40 gr		Dimer: 40 gr		Mask cleaning.	
Use silane		Use silane		27 Ag etch	
Set Point: 15		Set Point: 15		HNO ₃ :H ₂ O (1:1)	
PLA_I: 10		PLA_I: 10		Mix the solution, dip for 5 sec.	
Meas: ~20um		Meas: ~20um		DI water rinse 3 cycles.	
27 Lithography	Mask 5			Dry by N ₂ .	
Primer (HMDS), 500 rpm 10 sec + 750 rpm 20sec.				Inspection.	
AZ9260 PR, 500 rpm 10 sec + 750 rpm 20 sec.				28 Strip photoresist.	
Wait for 15 min.				acetone	
Pre bake 90 °C, 3 min, hotplate					

Table B.1. Details of the steps for the fabrication of the sensor (Continued).

	Edge bead removal, 500 rpm 10 sec + 750 rpm 20 sec.			29 Channel Lithography	Mask 4
	AZ9260 PR, 500 rpm 10 sec + 750 rpm 20 sec.			Primer (HMDS), 300 rpm (300,30,50,900,50,200)	
	Wait for 15 min.			AZ 9260 300 rpm (300,30,50,900,50,200)	
	Pre bake 90 °C, 5 min, hotplate			Wait for 15 min.	
	Edge bead removal, 500 rpm 10 sec + 750 rpm 20 sec.			Prebake 95oC, 90sec, hotplate	
	Softbake start at room temperature, raise the temperature to 95 °C, 60min at 90			Edge bead removal 300 rpm (300,30,50,900,50,200)	
	Rehydration (4 pipettes of DI water in blue box, 2 hrs)			softbake start at room temperature, raise the temperature to 95oC, 30min at	
	Align and expose 55 sec			Rehydration (3 pipettes of DI water in blue box,1hrs)	
	Develop AZ 826 MIF, 30min			Align and expose 45 sec with AZ9260 900 rpm recipe	
	DI water rinse, 1.5min + 1.5 min			Develop AZ 826 MIF, 10min	
	Dry by N2			DI water rinse, 1.5min + 1.5 min	
	Align and expose 55 sec			Desiccator içine koy soğuması bekle.	
	Develop AZ 826 MIF, 20min			Inspection.	
	DI water rinse, 1.5min + 1.5 min			Mask cleaning.	
	Dry by N2			30 Parylene deposition	
	Inspection			Dimer: 40 gr	
	Mask cleaning			Do not use silane	
28 Parylene etching				Set Point: 15	
	Etch parylene in RIE (20 min+ 20min + 20min)			PLA I: 10	
	Inspection			Meas: ~20um	
29 Dicing				31 Channel Lithography	Mask 5
	Fill the form for dicing request			Primer (HMDS), 500 rpm 10 sec + 750 rpm 20sec.	
30 Strip photoresist.				AZ9260 PR, 500 rpm 10 sec + 750 rpm 20 sec.	
				Wait for 15 min.	
				Pre bake 90 °C, 3 min, hotplate	
				Edge bead removal, 500 rpm 10 sec + 750 rpm 20 sec.	
				AZ9260 PR, 500 rpm 10 sec + 750 rpm 20 sec.	
				Wait for 15 min.	
				Pre bake 90 °C, 5 min, hotplate	
				Edge bead removal, 500 rpm 10 sec + 750 rpm 20 sec.	
				Softbake start at room temperature, raise the temperature to 95 °C, 60min at 90	
				Rehydration (4 pipettes of DI water in blue box, 2 hrs)	
				Align and expose 55 sec	
				Develop AZ 826 MIF, 30min	
				DI water rinse, 1.5min + 1.5 min	
				Dry by N2	
				Align and expose 55 sec	
				Develop AZ 826 MIF, 20min	
				DI water rinse, 1.5min + 1.5 min	
				Dry by N2	
				Inspection	
				Mask cleaning	
				32 Parylene etching	
				Etch parylene in RIE (20 min+ 20min + 20min)	
				Inspection	
				33 Dicing	
				Fill the form for dicing request	
				34 Strip photoresist.	

APPENDIX C

ALGORITHMS AND CALCULATIONS

C.1. Algorithms

The some of the algorithms used in this study were given in the following figures.

Cyclic voltammetry Au layer characterization with sulfuric acid		
Remarks	Cyclic voltammetry potentiostatic: no e...	
End status Autolab	...	
Signal sampler	Time, WE(1).Current	...
Options	1 Options	...
Timed procedure	...	
Autolab control	...	
WE(1).Current range	1 mA	
WE(1).Bandwidth	High stability	
WE(1).Mode	Potentiostatic	
Set potential	0.002	
Potential (V)	0.002	
Set cell	On	
WE(1).Cell	On	
Wait time (s)	5	
Duration (s)	5	
Optimize current range	5	
CV staircase	[0.002, 1.300, 0.000, 0.002, 20, 0.10000]	
Start potential (V)	0.002	
Upper vertex potential (V)	1.300	
Lower vertex potential (V)	0.000	
Stop potential (V)	0.002	
Number of stop crossings	20	
Step potential (V)	0.00244	
Scan rate (V/s)	0.10000	
Total number of points	10670	
Interval time (s)	0.024414	
Signal sampler	Time, WE(1).Current	...
Options	1 Options	...
Potential applied	<..array.> (V)	
Time	<..array.> (s)	
WE(1).Current	<..array.> (A)	
Scan	<..array.>	
Index	<..array.>	
i vs E	...	
X	Potential applied (V)	
Y	WE(1).Current (A)	
Z	WE(1).Current (A)	
Show during measurement	Yes	
Measurement plot number	1	
Set cell	Off	
WE(1).Cell	Off	
<..>		
<..>		

Figure C.1. Algorithm for Nova 1.5 to characterize Au layer using cyclic voltammetry.

Commands	Parameters	
Chrono amperometry ($\Delta t > 1$ ms)		
Remarks	Chrono amperometry ($\Delta t > 1$ ms): no e...	...
End status Autolab		...
Signal sampler	Time, WE(1).Potential, WE(1).Current	...
Options	1 Options	...
Timed procedure		
Autolab control		...
Set potential	0.150	
Potential [V]	0.150	
Set cell	On	...
WE(1).Cell	On	...
Wait time [s]	5	
Duration [s]	5	
Record signals (>1 ms)	[100, 0.01]	
Duration [s]	100	
Interval time [s]	0.01	
Total number of points	10000	
Signal sampler	Time, WE(1).Potential, WE(1).Current	...
Options	1 Options	...
Corrected time	<..array..> [s]	
Time	<..array..> [s]	
WE(1).Potential	<..array..> [V]	
WE(1).Current	<..array..> [A]	
Index	<..array..>	
i vs t		...
Set cell	Off	...
WE(1).Cell	Off	...
<..>		
<..>		

Figure C. 2. Chronoamperometry algorithm for determination of HRP activity.

C.2. Calculations

C.2.1. Curve Fit to Find Effective Surface Area of Gold Electrode

The current intensity for reduction of oxide monolayer on gold electrode was determined by fitting the experimental data to a Gaussian equation (Figure C.3). The equation and its coefficients with 95% confidence bounds ($R^2 = 0.8464$) are as follows:

$$f(x) = a_1 * e^{-\left(\frac{x-b_1}{c_1}\right)^2} + a_2 * e^{-\left(\frac{x-b_2}{c_2}\right)^2} \quad (C.1)$$

$$a_1 = -0.08645 \quad (-0.09049, -0.0824) \quad (C.2)$$

$$b_1 = 0.6453 \quad (0.643, 0.6477) \quad (C.3)$$

$$c_1 = 0.06325 \quad (0.0596, 0.0669) \quad (C.4)$$

$$a_2 = -0.005979 \quad (-0.007563, -0.004395) \quad (C.5)$$

$$b_2 = 0.361 \quad (0.146, 0.5759) \quad (C.6)$$

$$c_2 = 0.6334 \quad (0.2556, 1.011) \quad (C.7)$$

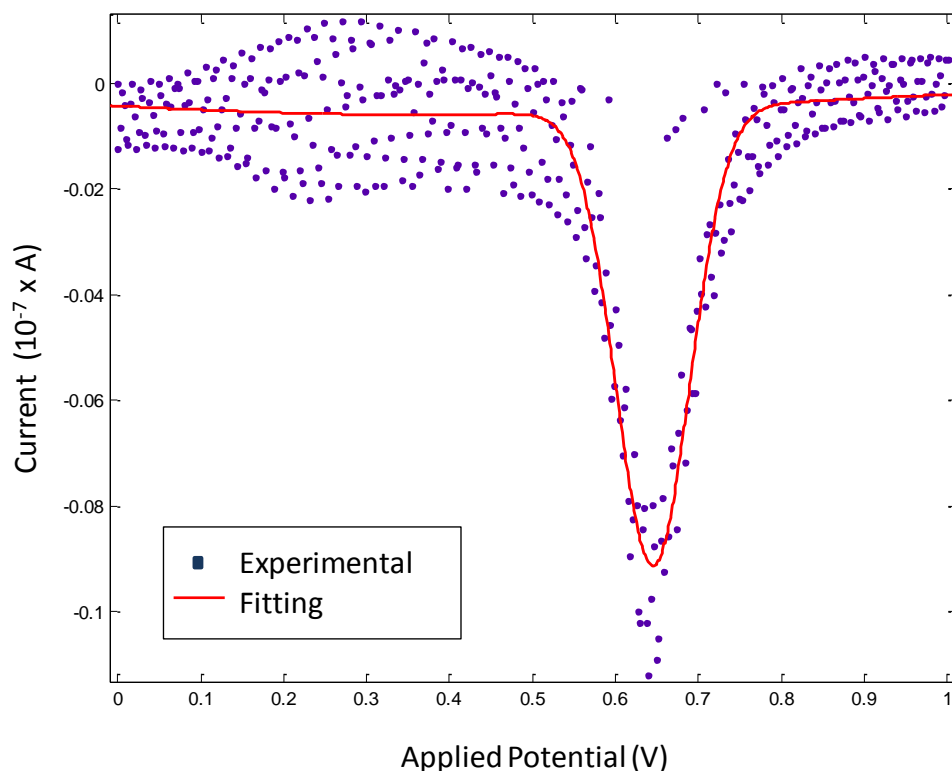


Figure C.3 Experimental (dots) and fitted (red line) cyclic voltammogram for the gold layer characterization in the acid solution for 300 μm electrode.

C.2.2. Curve Fit to Find D and C

The coefficients of Equation C.8 are determined by fitting the experimental data to a custom equation of Curve Fitting Toolbox in MATLAB. The equation and its coefficients with 95% confidence bounds ($R^2 = 0.954$) are as follows:

$$f(x) = c \cdot \exp\left(-d \cdot x^{\frac{1}{2}}\right) + b \cdot x^{-\frac{1}{2}} + a \quad (\text{C.8})$$

$$a = 5.352 \times 10^{-7} \quad (5.297 \times 10^{-7}, 5.406 \times 10^{-7}) \quad (\text{C.9})$$

$$b = -1.081 \times 10^{-7} \quad (-1.101 \times 10^{-7}, -1.061 \times 10^{-7}) \quad (\text{C.10})$$

$$c = 2.346 \times 10^{-7} \quad (2.3 \times 10^{-7}, 2.393 \times 10^{-7}) \quad (\text{C.11})$$

$$d = 2.229 \quad (2.141, 2.317) \quad (\text{C.12})$$

Diffusion coefficient, D can be determined from d term, since it is as follows:

$$d = 0.7823 \cdot \left(\frac{4 \cdot D}{r^2}\right) \quad (\text{C.13})$$

And when the system reaches steady state, the value of current becomes proportional to D value, and concentration of TMB, C can be calculated as follows:

$$a + c = 4 \cdot n \cdot F \cdot C \cdot D \cdot r \quad (\text{C.14})$$

C.2.3. Polymer Preparation and Characterization

C.2.3.1. Polymer Preparation

Aminodextran (500 kDa) (D7144, Invitrogen) was reacted at 1mg/ml with 500 μM sulfo-NHS-biotin (21217, Pierce) in 0.1 M borate buffer (pH 8.5) at room temperature for three hours with constant mixing (Klonoski et al., 2010). The buffer was prepared by weighing 9.5 g of $\text{Na}_2\text{B}_4\text{O}_7 \cdot 10\text{H}_2\text{O}$

(71999, Sigma Aldrich) and adding 200 ml ultra pure water. Then, pH was adjusted to 8.6 by adding droplets of HBO_3 (B6768, Sigma Aldrich) and the solution was filled up to 250 ml, and autoclaved. The sulfo-NHS-biotin was reacted with aminodextran according to the manufacturer's instructions. 2.2 mg of sulfo-NHS-biotin was mixed with 500 μl of ultra pure water. 10 mg of aminodextran was mixed with 10 ml of 0.1 M borate buffer and 40 μl of sulfo-NHS-biotin solution was added and let to react at room temperature with mixing for overnight. The biotinylated dextran was purified and desalted using a PD-10 Column (GE Healthcare) equilibrated in 0.1 M borate buffer (pH 8.6) following the manufacturer's instructions. The polymer solution was diluted to 5 ml in 0.1 M borate buffer and reacted with 100 μM sulfo-NHS-acetate at room temperature for three hours with constant mixing. For this purpose, the solution, which I had 2 fold volume compared to the referred journal protocol, was diluted to 10 ml and the sulfo-NHS-acetate was used according to the manufacturer's instructions, and 50 μl of prepared solution in ultrapure water by adding 2.6 mg of acetate was added to the solution with volume 10 ml. The mixture was mixed by shaking for about half an hour and incubated at room temperature for three hours. Afterwards, the reaction mixture was passed over another PD-10 column equilibrated with 1 X PBS (pH 7.0) and stored at 4°C until further use. For this purpose, PBS buffer solution, consists of 210 mg/L KH_2PO_4 , 9000 mg/L NaCl and 2.71 mM Na_2HPO_4 , was prepared, adjusted to pH 7.0 with HCl solution, and autoclaved. The equilibration of the mixture was made by using the manufacturer's instructions and stored at 4 °C until further use.

C.2.3.2. Characterization

Estimation of mole-to-mole ratio of biotin to protein was done by using HABA (4'-hydroxyazobenzene-2-carboxylic acid) (Thermo Scientific, product no 28010) and avidin (Thermo Scientific, product no 21121). HABA is a reagent that displaces with biotin in a mixture of HABA, avidin, and biotinylated protein and its absorption at 500nm decreases proportional to the concentration of biotin. With this method, it is possible to estimate concentration of biotin in an unknown sample by only measuring absorbances of HABA/avidin and HABA/avidin/biotinylated sample. The instructions of manufacturer were followed. 24.2 mg HABA was dissolved in 9.9 ml of ultrapure water and 0.1 ml of 1 M or 1 N NaOH solution was added to dissolve HABA completely. If HABA is not dissolved, another 0.1 ml of 1 M or 1 N NaOH can be added. 10 mg avidin was dissolved in 19.4 ml PBS and 600 μl HABA solution was added and mixed well. The prepared solutions were stored at 4 °C for two weeks. The absorbance was measured in UV-Spectrophotometer (Shimadzu, UV 1208) by using 1 ml glass cuvette. 900 μl of HABA/Avidin solution was placed into 1 ml cuvette and absorbance was measured at 500 nm. A_{500} of this solution was found as 1.295. Then, 100 μl of biotinylated protein sample was added to the cuvette, mixed, and absorbance was measured as 1.014 at 500 nm. The calculations for estimation of moles of biotin per mole of amino dextran protein are given as follows:

Calculations for moles of biotin per mole of protein were performed at four steps:

- Calculation of concentration of biotinylated protein
- Calculation of change in absorbance at 500nm
- Calculation of concentration of biotin in mmol/ml reaction mixture
- Calculation of mmol of biotin/mmol of protein.

Calculation of concentration of biotinylated protein

$$\text{mmol protein/ml} = \frac{\text{Protein concentration (mg/ml)}}{\text{MW of protein (mg/mmol)}}$$

$$\text{mmol protein/ml} = \frac{1 \text{ mg/ml}}{500000 \text{ mg/mmol}} = 2 \times 10^{-6}$$

Calculation of change in absorbance at 500nm

$$\Delta A_{500} = (0.9 \times A_{500} \text{ HABA} - \text{avidin}) - (A_{500} \text{ HABA} - \text{avidin} - \text{biotin})$$

$$\Delta A_{500} = (0.9 \times 1.295) - (1.014) = 0.1515$$

Calculation of concentration of biotin in mmol/ml reaction mixture

$$\frac{\text{mmol biotin}}{\text{ml reaction mixture}} = \frac{\Delta A_{500}}{34000}$$

$$\frac{\text{mmol biotin}}{\text{ml reaction mixture}} = \frac{\Delta A_{500}}{34000} = \frac{0.1515}{34000} = 4.45 \times 10^{-6}$$

Calculation of mmol of biotin/mmol of protein

$$\begin{aligned} &= \frac{\text{mmol biotin in original sample}}{\text{mmol protein in original sample}} \\ &= \frac{\text{mmol biotin in reaction mixture} \times 10 \times \text{dilution factor}}{\text{mmol protein in original sample}} \\ &= \frac{4.45 \times 10^{-6} \times 10 \times 1}{2 \times 10^{-6}} = 22.25 \text{ biotin molecule per amino dextran protein} \end{aligned}$$

CURRICULUM VITAE

PERSONAL INFORMATION

Surname, Name: Ceylan Koydemir, Hatice
Nationality: Turkish (TC)
Date and Place of Birth: 14 January 1982, Zonguldak
Phone: +90 312 210 6080

EDUCATION

Degree	Institution /Department	Year of Graduation
M.Sc.	METU, Chemical Engineering	2007
B.Sc.	METU, Environmental Engineering	2004
Minor Program	METU, Food Engineering	2004

WORK EXPERIENCE

Enrollment	Institution /Department	Year
Researcher	METU-MEMS Research and Application Center	2010 - Present
Research Assistant	METU, Graduate School of Natural and Applied Sciences	2007 - 2010

FOREIGN LANGUAGES

English, Spanish, Korean.

PUBLICATIONS

Publications in Progress

- H. Ceylan Koydemir, H. K ulah, C.  zgen, A. Alp, G. Has elik, "Fabrication and Characterization of a MicroElectrochemical Sensor and its Implementation for Detection of Methicillin Resistance in *Staphylococcus aureus*", (To be submitted to Biosensors and Bioelectronics, In preparation).
- H. Ceylan Koydemir, C.  zgen, H. K ulah, "Compatibility of Parylene C Film Layer to Harsh Chemical Environments", Submitted to the 17th International Conference on Solid-State Sensors, Actuators and Microsystems, Transducers 2013 & Eurosensors XXVII.
- H. Ceylan Koydemir, H. K ulah, C.  zgen, "A Micro Electrochemical Sensor For Enzyme Based Detection of Methicillin Resistance in *Staphylococcus aureus*", Submitted to the 17th International Conference on Solid-State Sensors, Actuators and Microsystems, Transducers 2013 & Eurosensors XXVII.
- H. Ceylan Koydemir, H. K ulah, C.  zgen, "Solvent Compatibility of Parylene C Film Layer", Submitted.

Patent

- H. Ceylan Koydemir, H. K ulah, C.  zgen, "Micro Electrochemical Sensor", International patent application was filed in 2012.

Articles

- H. Ceylan Koydemir, H. Külâh, C. Özgen, A. Alp, G. Hasçelik, “MEMS Biosensors for Detection of Methicillin Resistant *Staphylococcus aureus*”, *Biosensors and Bioelectronics*, Vol. 29, No. 1, pp. 1-12, October 2011.
(In the list of most downloaded articles between October 2011- February 2012).

Book Chapter

- H. Ceylan Koydemir, H. Külâh, C. Özgen, “Thin Films and Biosensors”, in “Thin Films and Coatings in Biology”, Editors: S. Nazarpour, M. Chaker, Springer, to appear in Jan 2013.

Conference Proceedings

- H. Ceylan Koydemir, H. Külâh, C. Özgen, “Thin Film Biosensor for Electrochemical Detection of Hybridization of DNA”, 10. National Chemical Engineering Congress, İstanbul, 3-6 September 2012.
- H. Ceylan Koydemir, H. Külâh, C. Özgen, İ. Tosun, “Effects of Solvents on Dissolution of Photoresist in Parylene Microchannels”, TechConnect World 2012 (Nanotech), Santa Clara, California, 18-21 June 2012.
- H. Ceylan Koydemir, H. Külâh, C. Özgen, A. Alp, G. Hasçelik, “MEMS Based Micro Electrochemical Sensor for Detection of MRSA”, 7th National Molecular and Diagnostic Microbiology Congress, Ankara, 5-8 June 2012.
- H. Ceylan Koydemir, H. Külâh, C. Özgen, “A Micro Electrochemical Sensor for the Detection of Methicillin Resistance in *Staphylococcus aureus*”, 22nd Anniversary World Congress on Biosensors, Cancun, Mexico, 15-18 May 2012.
- D. Ertürkan, H. Ceylan Koydemir, H. Külâh, and C. Özgen, “Detection of *Candida albicans* with the Use of Protocol Developed for MEMS Based Biosensors”, Turkish National Committee of Automatic Control, 14-16 September 2011.
- H. Ceylan, H. Külâh, A. Alp, G. Hasçelik, C. Özgen, “Design and Fabrication of MEMS Based Electrochemical Biosensor”, 9th National Chemical Engineering Congress, Ankara, 22-25 June 2010.
- H. Ceylan, H. Külâh, A. Alp, C. Özgen and G. Hasçelik, “A Disposable MEMS DNA Biosensor for Antibiotic Resistant Gene Detection in *Staphylococcus aureus*”, 15th National Biomedical Engineering Meeting, 21-24 April 2010.
- H. Ceylan, H. Külâh, C. Özgen, A. Alp, G. Hasçelik, “Detection of Bacterial DNA using MEMS Based DNA Biosensor”, Turkish National Committee of Automatic Control, İstanbul, 13-16 October 2009.
- H. Ceylan, C. Özgen, “Dynamic Modelling and Optimal Control of a Multicomponent Batch Distillation Column”, 17th IFAC World Congress Seoul, Korea, 6-11 July 2008.
- H. Ceylan, C. Özgen, “Dynamic Modeling and Simulation Studies for a Multicomponent Batch Packed Distillation Column”, 8th National Chemical Engineering Congress, Malatya, 26-28 August 2008.
- H. Ceylan, C. Özgen, “Optimal Control of Multicomponent Batch Packed Distillation Column”, Turkish National Committee of Automatic Control, 05-07 September 2007.

HONORS AND AWARDS

- Prof. Dr. Hasan Orbey Ph.D. Thesis Award, given by Department of Chemical Engineering, METU, 2011.
- The Scientific and Technological Research Council of Turkey Incentive Award for the International Scientific Publications, 2011.
- METU Publication Award, 2011.
- The Best Paper Award in the 15th National Biomedical Engineering Conference, 2010.
- The Scientific and Technological Research Council of Turkey Ph.D. Fellowship, 2007 – 2012.
- The Scientific and Technological Research Council of Turkey M. Sc. Fellowship, 2005 – 2007.